TELECONNECTION BETWEEN ANTARCTIC SEA ICE VARIABILITY AND INDIAN SUMMER MONSOON

SITI SYAIRAH ATIQAH BINTI AZHAR

INSTITUTE FOR ADVANCED STUDIES
UNIVERSITI MALAYA
KUALA LUMPUR

2023

TELECONNECTION BETWEEN ANTARCTIC SEA ICE VARIABILITY AND INDIAN SUMMER MONSOON

SITI SYAIRAH ATIQAH BINTI AZHAR

THESIS SUBMITTED IN FULFILMENT OF THE REQUIREMENTS FOR THE DEGREE OF DOCTOR OF PHILOSOPHY

INSTITUTE FOR ADVANCED STUDIES
UNIVERSITI MALAYA
KUALA LUMPUR

2023

UNIVERSITY OF MALAYA

ORIGINAL LITERARY WORK DECLARATION

Name of Candidate: **Siti Syairah Atiqah Azhar**

Matric No: **17041616/3/ HHQ150003**

Name of Degree: **Doctor of Philosophy**

Title of Project Paper/Research Report/Dissertation/Thesis ("this Work"): **Teleconnection between Antarctic sea ice variability and Indian summer monsoon**

Field of Study: **Earth Science (Meteorology)**

I do solemnly and sincerely declare that:

(1) I am the sole author/writer of this Work;
(2) This Work is original;
(3) Any use of any work in which copyright exists was done by way of fair dealing and for permitted purposes and any excerpt or extract from, or reference to or reproduction of any copyright work has been disclosed expressly and sufficiently and the title of the Work and its authorship have been acknowledged in this Work;
(4) I do not have any actual knowledge nor do I ought reasonably to know that the making of this work constitutes an infringement of any copyright work;
(5) I hereby assign all and every rights in the copyright to this Work to the University of Malaya ("UM"), who henceforth shall be owner of the copyright in this Work and that any reproduction or use in any form or by any means whatsoever is prohibited without the written consent of UM having been first had and obtained;
(6) I am fully aware that if in the course of making this Work I have infringed any copyright whether intentionally or otherwise, I may be subject to legal action or any other action as may be determined by UM.

Candidate's Signature Date:

Subscribed and solemnly declared before,

Witness's Signature Date:

Name:

Designation:

[TELECONNECTION BETWEEN ANTARCTIC SEA ICE VARIABILITY AND INDIAN SUMMER MONSOON]

ABSTRACT

Teleconnection between the Antarctic sea ice and the tropical climate has become an important issue in recent years, particularly among scientists and researchers. Further investigating the subject, this study examines the teleconnection between the Antarctic sea ice extent in the Indian Ocean sector and the Indian summer monsoon rainfall. It utilises reanalysis, satellite and in-situ observation data, and model output from the coupled model Intercomparison project phase 5 (CMIP5) from 1979 to 2013. The study is divided into three main parts. Firstly, examining the climatology of the sea ice extent in the Indian Ocean sector and Indian summer monsoon rainfall, both seasonal and monthly. Secondly, examines the relationship between the sea ice extent in the Indian Ocean sector and Indian summer monsoon rainfall variability under the influence of the Mascarene High. Thirdly, offers the mechanism connecting the sea ice extent in the Indian Ocean sector and Indian summer monsoon rainfall regarding atmospheric circulation features and compares it with several CMIP5 models. The long term monthly average of the sea ice extent in the Indian Ocean sector for 35 years shows that the maximum amount of sea ice extent produced is in October while the minimum amount is in February. The highest seasonal month of the sea ice extent during September-October-November (SON), and the lowest was in December-January-February (DJF). Furthermore, the northeastern region of India receives the highest mean annual rainfall during the summer monsoon season, whereas the northwestern region of India receives the lowest mean annual rainfall. The correlation analysis revealed that the April-May-June (AMJ) sea ice extent in the Indian Ocean sector significantly positively correlated with the Indian summer monsoon rainfall, particularly over the Peninsular India region

from 1979 to 2013 ($r = 0.44$, $p < 0.05$). This connection is indicated by the correspondence of the high ice phase (HIP) and low ice phase (LIP) years to the strengthening and weakening of the Mascarene High, resulting in the increase and decrease of Indian summer monsoon rainfall. The empirical orthogonal function (EOF) and correlation analysis show that the first and third modes of principal component (PC1 and PC3) of AMJ sea ice extent in the Indian Ocean sector during are significantly correlated with the second mode of principal component (PC2) of Indian summer monsoon rainfall. The reanalysis data revealed that the changes in the sea ice extent excite meridional wave train responses along the Indian Ocean for both principal component modes. Positive (negative) sea ice extent anomalies based on first and third EOFs (EOF1 and EOF3), contribute to the strengthening (weakening) of the Polar, Ferrel, and Hadley cells, inducing stronger (weaker) convective activity over the Indian latitudes. The stronger (weaker) convective activity over the Indian region leads to more (less) rainfall over the region during high (low) ice phase years. Furthermore, a stronger (weaker) polar jet during the high (low) ice phase is also noted. The AMJ sea ice extent simulated by the NorESM1-M model was significantly positively correlated with Indian summer monsoon rainfall, whereas the IPSL-CM54-LR model showed a negative correlation. Both models were able to captured certain atmospheric teleconnection features found in the reanalysis.

Keywords: *Sea ice extent, Mascarene High, Indian summer monsoon rainfall, convection activity, high/low ice phase*.

[TELESAMBUNGAN ANTARA VARIABILITI AIS LAUT ANTRAKTIK DAN MONSUN MUSIM PANAS INDIA]

ABSTRAK

Telehubungan antara ais laut Antartika dan iklim tropika telah menjadi isu penting dalam beberapa tahun kebelakangan ini, terutamanya dalam kalangan saintis dan penyelidik. Menyiasat lebih lanjut subjek, kajian ini mengkaji telehubungan antara keluasan ais laut Antartika di sektor Lautan Hindi dan hujan monsun musim panas India. Ia menggunakan analisis semula, data pemerhatian satelit dan in-situ, dan output model daripada model berganding Intercomparison project fasa 5 (CMIP5) dari 1979 hingga 2013. Kajian ini dibahagikan kepada tiga bahagian utama. Pertama, mengkaji klimatologi keluasan ais laut di sektor Lautan Hindi dan hujan monsun musim panas India, kedua-dua bermusim dan bulanan. Kedua, mengkaji hubungan antara keluasan ais laut di sektor Lautan Hindi dan kebolehubahan hujan monsun musim panas India di bawah pengaruh Mascarene High. Ketiga, menawarkan mekanisme yang menghubungkan keluasan ais laut di sektor Lautan Hindi dan hujan monsun musim panas India mengenai ciri peredaran atmosfera dan membandingkannya dengan beberapa model CMIP5. Purata bulanan jangka panjang bagi keluasan ais laut di sektor Lautan Hindi selama 35 tahun menunjukkan jumlah maksimum keluasan ais laut yang dihasilkan adalah pada bulan Oktober manakala jumlah minimum adalah pada bulan Februari. Bulan bermusim tertinggi bagi keluasan ais laut pada September-Oktober-November (SON), dan yang terendah ialah pada Disember-Januari-Februari (DJF). Tambahan pula, wilayah timur laut India menerima purata hujan tahunan tertinggi semasa musim monsun musim panas, manakala wilayah barat laut India menerima purata hujan tahunan terendah. Analisis korelasi mendedahkan bahawa keluasan ais laut April-Mei-Jun (AMJ) di sektor Lautan Hindi secara signifikan berkorelasi positif dengan hujan monsun musim panas India, terutamanya di kawasan Semenanjung India dari 1979 hingga 2013 ($r = 0.44$, $p < 0.05$).

). Sambungan ini ditunjukkan oleh koresponden tahun fasa ais tinggi (HIP) dan fasa ais rendah (LIP) kepada pengukuhan dan kelemahan Mascarene High, mengakibatkan peningkatan dan penurunan hujan monsun musim panas India. Fungsi ortogonal empirikal (EOF) dan analisis korelasi menunjukkan bahawa mod pertama dan ketiga bagi komponen utama (PC1 dan PC3) bagi keluasan ais laut AMJ di sektor Lautan Hindi pada masa ini mempunyai korelasi yang ketara dengan mod kedua komponen utama (PC2) bagi Hujan monsun musim panas India. Data analisis semula mendedahkan bahawa perubahan dalam tahap ais laut merangsang tindak balas kereta api meridional di sepanjang Lautan Hindi untuk kedua-dua mod komponen utama. Anomali takat ais laut yang positif (negatif) berdasarkan EOF pertama dan ketiga (EOF1 dan EOF3), menyumbang kepada pengukuhan (melemahkan) sel Polar, Ferrel dan Hadley, mendorong aktiviti perolakan yang lebih kuat (lemah) di atas latitud India. Aktiviti perolakan yang lebih kuat (lemah) di rantau India membawa kepada lebih banyak (kurang) hujan di rantau itu semasa tahun fasa ais yang tinggi (rendah). Tambahan pula, pancutan kutub yang lebih kuat (lemah) semasa fasa ais tinggi (rendah) juga diperhatikan. Tahap ais laut AMJ yang disimulasikan oleh model NorESM1-M secara signifikan berkorelasi positif dengan hujan monsun musim panas India, manakala model IPSL-CM54-LR menunjukkan korelasi negatif. Kedua-dua model dapat menangkap ciri telesambungan atmosfera tertentu yang terdapat dalam analisis semula.

Kata kunci: Tahap ais laut, Mascarene High, hujan monsun musim panas India, aktiviti perolakan, fasa ais tinggi/rendah.

ACKNOWLEDGEMENTS

I would like to thank my supervisors, Professor Dato' Dr. Azizan bin Hj Abu Samah and Dr. Sheeba Nettukandy Chenoli, for their guidance and support throughout my PhD. Despite their busy academic and administrative schedules, I am deeply moved by their patience and enthusiasm in aiding my research outputs and correcting them numerous times before and after submitting them for publication. Words fail to convey my respect and gratitude to them.

I would also like to thank Mr. Ooi See Hai and Dr. Mohd Fadzil Firdzaus Mohd Nor for the help and advice in scripting the analysis. In addition, I would like to thank Dr. Seong Joong Kim of the Korea Polar Research Institute (KOPRI) and Dr. Nuncio Murukesh of the National Centre for Polar and Ocean Research (NCPOR) for their ideas and suggestions on how to improve the analysis and manuscript. I would like to thank Muhammad Yunus bin Ahmad Mazuki for providing help in improving the quality of the figures in the reviewed manuscript during Malaysia's Movement Control Order (MCO) due to the global COVID-19 pandemic. Anonymous reviewers from the Polar Journal are also in my debt for the careful review of the manuscript and valuable suggestions to refining the quality of the paper, which led to further improvement of this dissertation.

I am thankful to the Ministry of Sciences, Technology and Innovation Flagship for funding this research under grant no. FP1213E037. The dissertation is strongly supported by the Academic Sciences of Malaysia, the Sultan Mizan Antarctic Research Foundation, the Malaysian Antarctic Research Program and the Vice Chancellor of the University of Malaya. The Fundamental Research Grant Scheme (FRGS) FP059-2019A and the FIO-UM Joint

Center of Marine Science and Technology Fund are also acknowledged. Dr. Seong-Joong Kim's contribution to the overall progress is supported by the Korean Polar Research Institute (KOPRI) project (PE20070).

My heartiest appreciation to my colleagues at the National Antarctic Research Center (NARC) and the Institute of Ocean and Earth Sciences (IOES); your views and expertise have significantly contributed to this research study.

Finally, I would like to extend my gratitude to my husband and family for their support and encouragement throughout this study.

TABLE OF CONTENTS

LIST OF FIGURES

LIST OF TABLES

LIST OF SYMBOLS AND ABBREVIATIONS

CMIP5	:	Coupled model Intercomparison project phase 5
SON	:	September-October-November
DJF	:	December-January-February
AMJ	:	April-May-June
HIP	:	High ice phase
LIP	:	Low ice phase
NSIDC	:	National Snow and Ice Data Center
IITM	:	Indian Institute of Tropical Meteorology
GPCP	:	Global Precipitation Climatology Project
CMIP	:	Coupled Model Intercomparison Project
WGCM	:	Working Group on Coupled Modelling
WCRP	:	World Climate Research Programme
IGBP's AIMES	:	Analysis, Integration, and Modeling of the Earth System
AR4	:	IPCC Fourth Assessment Report
WGCM	:	Working Group on Coupled Modelling
WCRP	:	World Climate Research Programme
ASL	:	Amundsen Sea Low
AAO	:	Antarctic Oscillation
SAM	:	Southern Ocean Annual Mode

ENSO	:	El Nino-Southern Oscillation
MSLP	:	mean sea level pressure
ACW	:	Antarctic circumpolar wave
ADP	:	Antarctic Dipole
IOD	:	Indian Ocean Dipole
IPO	:	Interdecadal Pacific Oscillation
AMO	:	Atlantic Multidecadal Oscillation
EASM	:	East Asian summer monsoon
NAO	:	North Atlantic Oscillation
ESRL	:	Earth System Research Laboratory
NOAA	:	National Oceanic and Atmospheric Administration
OLR	:	outgoing long radiation
MAM	:	March-April-May
JJA	:	June–July–August
r	:	correlation coefficient
JFM	:	January-February-March
FMA	:	February-March-April
$\bar{X}_m$	:	long term average (35 years) of the variables for the composite months (m)
$X_{n,m}$	:	value of the interested variables for the composite months (m) in year (n)

X_n	:	variables of interest at n years
σ_m	:	long term standard deviation of variables for the composite months (m)
TMH	:	Temporal Mascarene high
$\boldsymbol{W}$	:	Wave activity's flux
WHO	:	World Meteorological Organization
netCDF	:	Network Common Data Form
CDO	:	Climate Data operate
SIOD	:	the southern Indian Ocean Dipole
TMHI+	:	TMH positive index
TMHI-	:	TMH negative index

LIST OF APPENDICES

CHAPTER 1

INTRODUCTION

1.1 Teleconnection

Weather and climate occurrences are found worldwide, and they are often linked to other regions. The climate at one latitude will usually directly or indirectly impact another latitude, either locally or remotely. This interaction process over a very long distance is known as "teleconnection", and it has the persistent characteristic of lasting for 1 to 2 weeks or longer (Feldstein et al., 2017). Teleconnection has been defined variously among the researchers. In atmospheric science, teleconnection implies the correlation of distant regional climates, either contemporaneously or with nonzero lag or lead durations (Mirsa, 2020). Teleconnections are typically characterized as low-frequency variations in the atmosphere and oceans, whereas weather is defined as random high-frequency variability in the atmosphere. A further definition of teleconnections is substantial correlations of climatological data at widely distant locations on the globe, indicating preferred trough/ridge placements. These preferred modes of variability can be quantified using indices for flow patterns linked with the teleconnection. The indices can then be connected with global climatic indicators that show substantial connections. Teleconnections can effect temperature, precipitation, storm tracks, severe weather, and drought over several weeks to several decades. In general, it is a term that refers to a type of climate variability, such as a sea surface temperature or wind pattern, that connects different parts of the planet. For example, changing wind patterns over Hawaii are linked to winds over California, the Middle East, and South Africa. Another example is the change in sea surface temperature in the central equatorial Pacific Ocean, which can have a massive and significant impact on weather patterns around the world. Typically, dry

regions could indeed experience intense flooding, while wet regions could experience extreme drought. Specifically, it can be defined as a relationship between weather or climate in a region that influences one another over a significant distance (Berdon, 2013). It can also be defined as a linkage between high and low latitudes in a long range. According to Wallace and Gutzler (1981), teleconnection is the interaction of physical changes in climate parameters that occur synchronously at points apart. Apart from that, teleconnection also has been describing as a long term climatic linkages providing climate system predictability on timescales ranging from years to decades. It is frequently stated as a single number to reflect various phases of the climate system, which frequently deal with variations in significant modes of atmospheric circulation. Teleconnections and associated climatic changes occur every 1-100 years on interannual to decadal time intervals (Mock, 2014). Similarly defined by Nigam et al. (2015), referred teleconnections to the variability of climate that linked between the discontiguous geographical areas. Feldstein et al. (2017) defined teleconnection as a spatial variability or patterns in the atmosphere that connect climate and weather anomalies over largest distance across the globe. Based on Wang et al. (2021), teleconnections are important components of the climate system that describe the links between climate variability in geographically separated regions. Teleconnections are frequently investigated in their mature phase of variability, with the realization that the teleconnections have a growing spatiotemporal scale. In many cases, the mutual interactions of natural variations can result in noncanonical teleconnection patterns, which frequently create unintended effects of the oscillation on the surrounding climate (Mock, 2014). The interaction between the two climate variability can occur through the atmosphere, the ocean, or both (Leathers et al., 1991; Liu and Alexander, 2007). The term "teleconnection" is employed in the field of atmospheric science to study how global circulation patterns affect climate and weather patterns on continents around the world, both over the course of a year and over the course

of a decade (Liu and Alexander, 2007). The usage of the term itself is widespread amongst meteorologists. It is a very useful tool and is commonly used in forecasting or predicting long-range values and patterns of climate variability over a specific region (Liu and Alexander, 2007), such as rainfall, storm track, snow, extreme weather events, and drought. Furthermore, teleconnections are frequently utilized by seasonal forecasters as a useful tool in anticipating commodity and energy trading markets. While many teleconnections were initially obtained empirically, advances in understanding the physical mechanics behind many of them have helped to enhance their predictability. In addition to weather and climate, teleconnection patterns are connected to numerous fields such as sea ice, the ocean, and other (Feldstein et al., 2017).

In the late 19th century, Sir Gilbert Walker was the first meteorologist to discover teleconnection. He invented this term by correlating the two-time series of temperature, atmospheric pressure, and rainfall. He successfully proved that the relationships between the two-time series of the parameters are casual rather than random (Glantz et al., 1991). In 1935, Swedish physicist Anders Ångström coined the term "teleconnection" to describe patterns of fluctuation in atmospheric pressure along the North Atlantic Ocean. This pattern, now known as the North Atlantic Oscillation (NAO), has a significant impact on weather and climate across the North Atlantic region (Liu and Alexander, 2007). Despite the fact that the term "teleconnection" had been used in the climate field since the middle of 1930s, it was rarely used in research until the 1980s. As time passed, more meteorologists were exposed to this phrase, and many researchers started to take an interest in exploring teleconnection (Wallace and Gutzler, 1981; Simmons et al., 1983; Ogallo et al., 1988). The summary of teleconnection found and used is shown in Figure 1.1. However, according to Feldstein et al. (2017), the Vikings were among the first to notice atmospheric teleconnection. It was written in an anonymous Norwegian book

called "Kings Mirror" around the year 1235, in the context of a conversation between a father and his son, that cold weather in Greenland coincides with warm weather in distant locations, and vice versa. For centuries, people interested in weather have been aware of the remote teleconnection nature of weather.

Teleconnections are receiving much interest these days among researchers because they represent energy transfer and climate dynamics on a global scale. Liu et al. (2007) and Tsonis et al. (2007) suggest that these factors are likely to be of great importance in global climate change and variability. Generally, the majority of teleconnections are caused by wave propagation and energy transport in the ocean and atmosphere. The teleconnections allow the atmosphere to play a role as a "bridge" between distinct ocean areas, while the ocean plays a role as a "tunnel" in connecting different areas of the atmosphere (Liu et al. 2007). Apart from that, it is because they last longer than most other phenomena in the atmosphere and enable scientists to conduct weather forecasts over time. The characteristics that make teleconnection durable are (1) its long wavelength, (2) its slow growth and decay, and (3) its coercive mechanism (Feldstein et al., 2017). Despite the fact that the teleconnection was discovered in recent years, the specific teleconnection mechanisms are still not well understood, as these known patterns describe the maturation phase of variability rather than the developmental phase (Nigam et al., 2015). Therefore, a more in-depth investigation of the evolutionary process is needed in the form of physical and dynamic mechanisms, especially when involving the teleconnection between the polar and the tropic. In the literature review section, the concept of teleconnection will be examined in greater depth. The rest of the chapter will cover an overview of sea ice, monsoon variability, and the Coupled Model Intercomparison Project Phase 5 Model (CMIP5) model. In addition, the problem statement, research questions, study objectives, scope and challenges, significance of the

study, and thesis structure will all be described in this chapter.

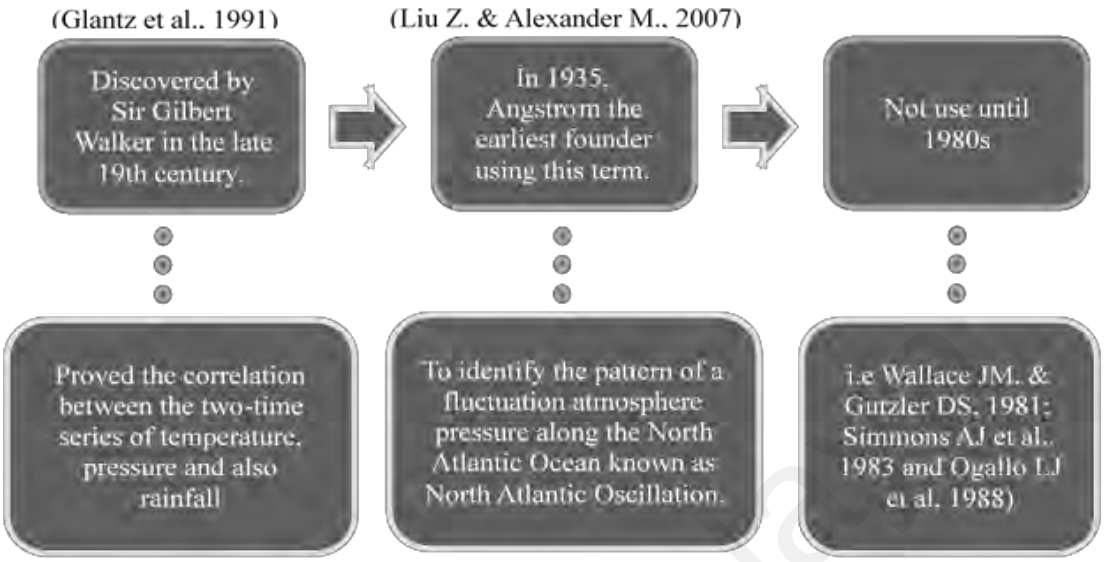

Figure 1.1: Flow chart on how the concept of teleconnection evolved and used

1.2 Sea ice

The polar regions have become a focus of attention in recent years, both in the scientific society and in the public eye. This is due to their high sensitivity to climate change and the dramatic changes that have already occurred there (Karahalil et al., 2021). The polar regions are critical to the Earth's climate system because they reflect a significant amount of heat back into space. Furthermore, it has also been identified as the region that has been most affected by global climate change during the last several decades (IPPC report, 2014). Sea ice, a relatively small part of the Earth's surface, has a surprisingly large impact on the global atmospheric system. It exists as a thin layer at the boundary between the ocean and the atmosphere, and is very responsive to even slight changes in temperature and the amount of energy from the sun (Hunke et al., 2010). A small change in sea ice can alter the way heat and energy are transported around the globe, which can lead to changes in weather patterns and climate. It is also very significant for animal habitats, human activities, and the economy. Sea ice is a unique, fascinating, and complex feature of the polar regions that plays an extremely important role in the Earth's

climate system (Deser et al., 2000; Gao et al., 2013).

Sea ice is a type of ice that forms on the surface of the ocean. It is made up of frozen seawater and is less dense than fresh water ice. This means that sea ice floats on top of the ocean, unlike fresh water ice, which sinks. Sea ice is made up of a combination of salt water, ice crystals, and solid salts. It's different from glaciers, ice shelves, icebergs, and ice sheets, which are formed on land from fresh water and compacted snow. Sea ice typically expands in the winter and shrinks in the summer, but it can remain year round in some areas. It can cover up to 10% of the world's oceans (Hunke et al., 2010). Sea ice might be subdivided into two categories, which are fast ice and ice floes. Fast ice refers to the ice attached to the land, while ice floes are not. It can also be classified according to its drift capacity and age. Sea ice may be quantified and defined in terms of concentration, area, and extent. As stated by the National Snow and Ice Data Centre (NSIDC), the definition of sea ice is explained as follows:

'The region that is 'ice-covered' or 'not covered' with a threshold of 15% ice concentration is described as ***sea ice extent****'*

'The ***concentration of sea ice*** *is measured in percentages (0 to 100), fractions (0 to 1), or tenths (0/10 to 10/10) of the total ice area'*

*'****Sea ice area*** *refers to the area covered by sea ice, measured in kilometers'*

Sea ice does not develop and melt in a predictable pattern; its existence has been tremendously dynamic. The formations of the sea ice can be due to several factors, such as ice floes and ridges, leads, polynyas or open water areas, sensible-heat (open-ocean) polynyas, and latent-heat (coastal) polynyas. For example, ice floes and ridges. The ice

floes or ice sheets floating in the water that were pushed by the wind, ocean current, and other forces collided, causing ice to pile up on the ridge and keel. Furthermore, the change in sea ice is strongly effected by wind, sea surface tilt, Coriolis force, ocean currents, and internal ice stress. Sea ice variability can have a major impact on the amount of sunlight that is reflected back into space (Hall, 2004; Perovich et al., 2007), the amount of heat that is transferred between the atmosphere and the ocean (Heil et al., 1996), and the formation of deep water and deep ocean currents (Pellichero et al., 2018). Sea ice dominates atmospheric-ocean exchange mechanisms in the polar regions, impacting seasonal and interannual oscillations at the ocean-atmosphere interface.

The widely known Antarctic sea ice is an integral part of the world's climate system. It is recognised as one of the most distinctive, intriguing, complicated, and crucial features in the polar regions (Deser et al., 2000; Gao et al., 2014). The Antarctic sea ice is warmer, younger, saltier, thinner, and more movable compared to the sea ice over the Arctic. Thus, the changes in its variabilities will have an impact on the entire global system, regional climate, and ecosystems, encompassing physical, biological, and economic processes, as well as animal habitats (Yuan and Martinson, 2000; Liu et al., 2004; Zhang, 2007; Oza et al., 2011). Usually, the amount of sea ice in Antarctica is at its greatest in September and at its smallest in February (see Figure 1.2) (Parkinson et al., 2012). The annual variations of the Antarctic sea ice are more variable than the Arctic sea ice because it is not surrounded by land. This means that the sea ice is not blocked by landmasses from moving and growing, which can cause large changes in the amount of sea ice from year to year (Dieckmann and Hellmer, 2010). Sea ice can grow and extend to 60 ° S to 70° S latitudes (Maksym et al., 2012). The topography of the Antarctic continent is encircled by water, allowing the ice to move freely and expand above the ocean surface. The amount of sea ice is affected by a variety of Earth's atmosphere and

oceans factors, including the strength of winds near the surface of the ocean, temperature of air, currents of an ocean, temperature, and salinity (Turner et al., 2015; details in Chapter 2). However, as previously stated, the development and degradation of Antarctic sea ice is a multifaceted process. This is due to the fact that they may incorporate a variety of components and conditions, such as physical geography, atmospheric conditions, and biological factors. The sea ice over the Antarctic is also less accessible and not studied very well compared to the Arctic sea ice. Furthermore, the sea ice over the Antarctic region has shown increasing trends since 1979 (details in Chapter 2), unlike the Arctic, which shows opposite trends. However, there is no particular mechanism that can describe the variability in the Antarctic sea ice (Stroeve et al., 2016). To date, research and development on Antarctic sea ice variability are still being pursued by researchers around the world.

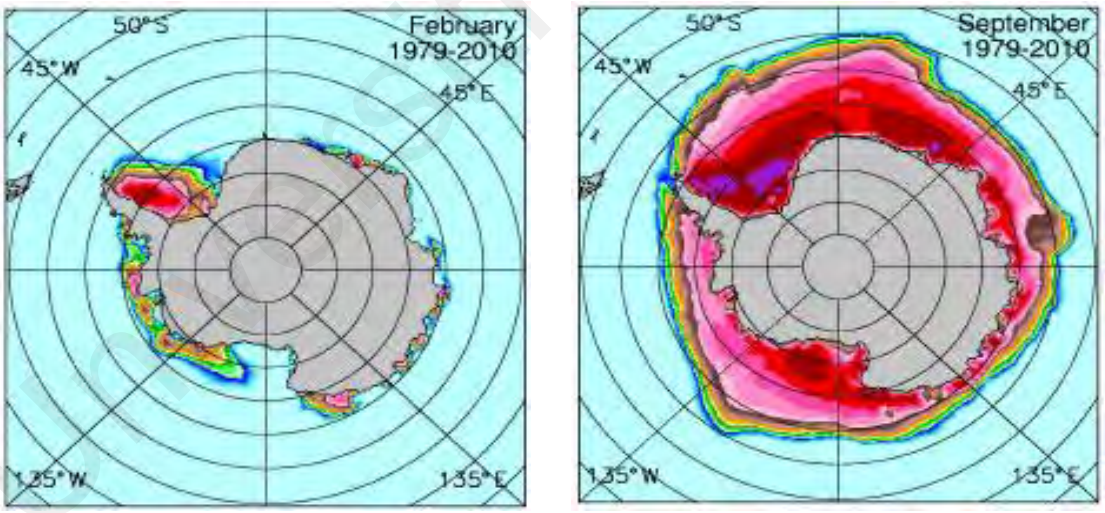

Figure 1.2: The Antarctic sea ice concentration during February (summer) and September (winter) from 1979 – 2010 (Caveleri and Parkinson, 2012)

1.3 Monsoon variability

The term "monsoon" was coined by ancient traders (Arab, Medieval European, and Greek explorers and sailors) from the Arabic word مَوْسِم)*mausim*(, which means season. It is used to illustrate the seasonally changing winds that persistently blow across the Indian

Ocean and the Arabian Sea during summer and winter (American Meteorological Society, 2012). In the most inhabited regions, the monsoon is regarded as a strong seasonal wind cycle with dry winters and extremely rainy summers. In the tropics, it is commonly identifiable when there is excessive or inadequate rain (Beaufort et al., 2010). However, as the term continues to develop, researchers have used various descriptions. The monsoon system is defined by seasonal reversals of wind direction, which migrate from the cold ocean towards the more temperate land, along with water vapor. During the monsoon, the wind is frequently accompanied by a great amount of moisture, resulting in excessive rain in some areas. The term monsoon is often used to describe seasonal reversals in atmospheric circulation and precipitation over the tropical and subtropical regions (Trenberth et al., 2000). Furthermore, the monsoon describes the seasonal variation in the tropospheric airflow and its weather implications, notably the extreme variability and unpredictability of rainfall.

The fundamental driving component of the monsoon phenomenon in the spring season; the heating up of the land by the sun causes a land-sea temperature differential. According to Lim et al. (2004) and Wang (2006), monsoons are created by the contrast in temperature between land and ocean induced by the heat released from the sun's radiation. Due to the land and ocean temperature differences, distinct pressure fluctuations (air moves from high-pressure zones to low-pressure areas) were formed at various surfaces. This phenomenon results in airflow from one area to another (Figure 1.3). The land-sea temperature differences will also cause changes in the pressure patterns and lower and upper wind circulations, altering precipitation patterns across the region (Sarthi et al., 2012). As widely known, monsoons are a major driver of weather and climate patterns around the world. It is also the predominant system of climatic variations in the tropics, with significant local, regional, and global consequences. Monsoons are a major weather pattern that affects over half of the world's population. Most of these people live in developing countries, where the monsoons can have a significant impact

on their economies and societies. Agriculture is still the most frequent form of land use in most of these places, and their culture and lifestyle have evolved around the monsoon cycle. The agricultural sector's reliance on monsoonal rains makes communities extremely sensitive to changes in monsoonal characteristics such as commencement and termination dates, total rainfall amounts, and rainfall intensities, especially in nations with weak infrastructure and significant urbanisation.

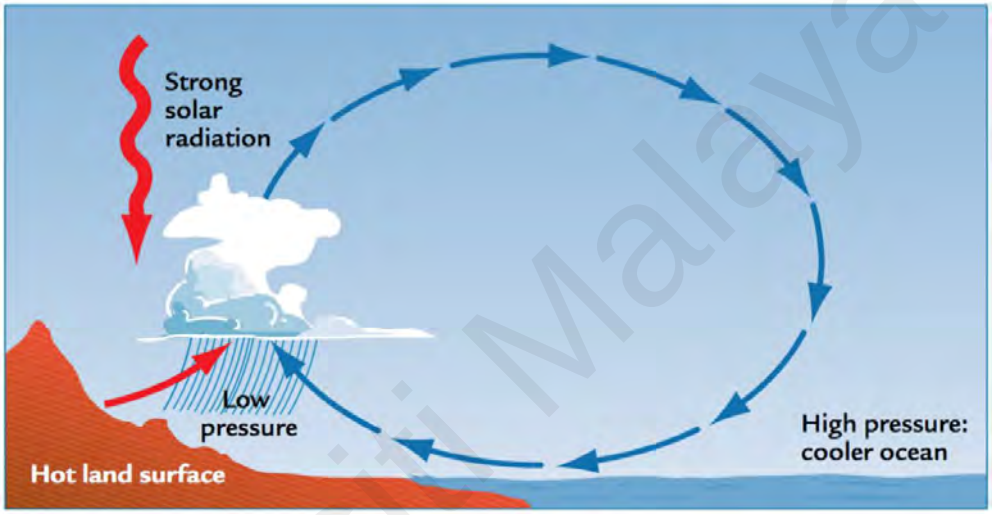

Figure 1.3: Illustration of the summer monsoon system (Ruddiman, 2008)

Monsoons can be predicted at several time scales, including seasonally, annually, and decadally (Webster and Yang, 1992; Goswami and Mohan, 2001). Variability on different time scales is commonly described by the main characteristics connected with particular monopoly modes or spatial patterns (Goswami and Mohan, 2001). Internal dynamics, differential heating between the continent and the ocean, teleconnections to climate variability in other regions, the Earth's Coriolis force, moisture transport, the meridional temperature gradient, and other factors all contribute to monsoon variability over many temporal periods (Webster, 1987; Krishnamurthy and Kinter, 2003). There are many types of monsoons. The summer and winter monsoons are the primary drivers of climate in most of India and Southeast Asia regions. The Indian summer monsoon or

southwest monsoon is a major part of the Asian monsoon, which is one of the world's largest monsoon systems. It is also recognised as the major monsoon subsystem in heat transport across the equatorial, making it one of the most dynamic ocean-atmosphere interactions on the planet (Nilsson-Kerr et al., 2019). The summer monsoon is linked to excessive or intense rainfall. Usually, the Indian monsoon rainfall variability has a deviation of roughly 10% from the average. This trend happens because of the Himalayan or Tibetan Plateau, which draws moist air upwards, where it condenses and falls as rain (Gadgil, 2003). When compared to large seasonal rainfall totals, even tiny percentage fluctuations can have a significant influence. The southwest monsoon typically occurs between April and September. This is when warm and moist air from the Indian Ocean flows to countries such as India, Sri Lanka, Bangladesh, and Myanmar. A detailed explanation of the Indian summer monsoon will be provided in Chapter 2. Despite more than a significant amount of research, determining interannual monsoon variability remains a challenge due to its complex and multi-scale variability. As a result, regional descriptions are inconsistent with one another or with the overall phenomenon. Despite these evident challenges, monsoon indexes have long been used to provide a quick and easy approach to characterizing the monsoon (Lau et al., 2004). The winter monsoon usually occurs from October to April, and it is somewhat linked with droughts. The flows of the dry winter monsoon originate from the northeast, where they start over Mongolia and northwest China. The winter monsoon is less intense than the summer monsoon because the Himalaya prevent the winds from carrying as much water vapour to the regions such as coast, southern India, and Sri Lanka. However, there are some places that experience rain during the winter monsoon, even if it's not as much as the summer monsoon. For example, the eastern Pacific coast of Southeast Asia has a dry winter, while the western part has a wet winter. Winter monsoons bring water vapour – rich air from the Southern Sea of China to Malaysia and Indonesia. There are other monsoon systems

in the world, including the Asian-Australian monsoon and the North American monsoon.

1.4 Coupled Model Intercomparison Project Phase 5 Model (CMIP5)

The CMIP5 models are experiments and extensions of the fourth phase of Coupled Model Intercomparison Project (CMIP) and were launched in 2008. This series of experiments was constructed and organized by the Working Group on Coupled Modelling (WGCM) under the World Climate Research Programme (WCRP) with input from the Analysis, Integration, and Modelling of the Earth System (IGBP's AIMES). It serves as an important platform for evaluating climate models and encouraging further development of climate model knowledge. The CMIP5 experimental activities are divided into three groups:

i. simulations of decadal hindcasts and predictions.
ii. long term simulations; and
iii. atmosphere only (prescribed sea surface temperature) simulations, which are particularly useful for computationally intensive models.

The simulation of decadal (10 to 30 years) and prediction categories is the near – term integration. The predictions include external forcing changes (e.g., GHG), anthropogenic aerosols, solar variability, volcanic eruptions, and the initial state of the ocean to perform decadal predictions (Meehl et al., 2009). The short-term integrations usually start with observed ocean and sea-ice conditions. Unlike the long-term experiments, the near-term prediction experiments are a new feature in the CMIP where the models will respond not just to climate forcing like rising concentrations of CO2 but also predict to a certain extent the outcome of climate change, including the unforced component of climate evolution (Taylor et al., 2012). The long term simulation categories

were divided into two main experiments, which are the atmospheric model intercomparison project protocol first described by Gates in 1992 and the climate system model experiment. The atmospheric model intercomparison project experiment specifies the observed sea surface temperature and sea ice for the past century. The integrations usually begin with multicentury preindustrial control (quasi equilibrium) integrations. The long term experiments in CMIP5 are built upon the successful CMIP3 experiments but include extra runs to offer a more thorough comprehension of the variability of climate change (Taylor et al., 2012). The two categories of computationally intensive atmospheric model experiments are historical studies spanning the period 1979 until 2008 and prediction studies spanning the period 2026 until 2035. The CMIP5 time slice option allows a wider range of modelling research groups to participate in and contribute to CMIP5 (Zhou et al., 2014).

The purpose of these experiments is to highlight some of the major scientific challenges raised by the IPCC Fourth Assessment Report (AR4), such as assessing the process, improving understanding of climate change, and providing estimates on future climate change scenarios. In particular, the objectives are to determine how accurate the models are in simulating recent events, forecasting future climate changes in the near-term (to roughly 2035) and long-term (to 2100 and beyond), fully appreciating some of the processes that generate discrepancies in model projections, such as cloud and carbon cycle feedbacks, and assessing why similarly forced models generate a variety of results.

The CMIP5 has gone on to become the most popular model suite among the CMIPs, as it involves over 50 climate system models and earth system models that were produced by over 20 modelling groups worldwide (Taylor et al., 2012). Despite the increasing number of models from various modelling groups, most models are similar

because they essentially describe and model the same system while incorporating the same biases 50 and parameterizations. Each model has its own unique set of characteristics and number of ensembles. These models include components for the atmosphere, ocean, land, and sea ice. The CMIP5 outputs include historical simulation, which is from years 1850 until 2005; climate projection for the near term for about till years 2035 and long term projection for years 2100 and beyond based on four Representative Concentration Pathways (RCPs). The RCPs are the four trajectories of greenhouse gas concentrations (not emissions) adopted by the IPCC in its Fifth Assessment Report (AR5). The four pathways are: RCP 8.5, RCP 6, RCP 4.5, and RCP 2.6 and were named based on the potential range of radiative forcing values in the year 2100. It should be noted that not all CMIP5 models have the complete set of RCP 2.6, RCP 4.5, RCP 6.0, and RCP 8.5 experiments. However, the common RCP scenarios used are RCP 4.5 and RCP 8.5 (Steven Soon-Kai Kong et al., 2015; Barredo et al., 2018). RCP 4.5 scenarios are named after a GHG concentration of +4.5 Wm^{-2} by 2100 and a global annual GHG emissions peak around 2040 at +4.5 Wm^{-2}, followed by a stabilization in GHG concentration. It is a moderate energy consumption scenario that considers the role of governments and international organizations in minimizing pollution and greenhouse gas emissions. The RCP 8.5 scenario, on the other hand, assumes the GHG concentration will continue to increase throughout the twenty-first century, reaching +8.5Wm^{-2} by the year 2100 (Moss et al., 2010). This scenario predicts high energy consumption due to rapid population growth and a slower pace of technological advancement (van Vuuren et al., 2011). There are many articles that go into great detail about the CMIP5 models, and one of them is Taylor et al. (2012).

1.5 Problem statement

In a rapidly warming world, it is essential to enhance knowledge of the mechanisms of the linkages between the high and low latitudes in order to comprehend the behaviour of the interaction between the atmosphere, ocean, and sea ice. The research on teleconnection between polar and tropical climatic variability is still in progress, particularly regarding the relationship between the Antarctic sea ice and the Indian summer monsoon rainfall. The limited amount of literature published on the topic supports this statement in either physical or dynamic mechanisms. The Arctic sea ice and the East Asian Monsoon are the topics of most studies, whether on processes or modelling (Bingyi et al., 2009: Wu et al., 2009; Guo et al., 2014). The teleconnection was adequately recognised and established in the prior study regarding statistical analysis (Prabu et al., 2009). However, none of the research looks into the connecting mechanism's physical or dynamical features. Similarly, no previous research has discussed the teleconnection between the Antarctic sea ice extent and the monsoon, particularly the Indian monsoon using climate models. This constraint might be due to the sluggish growth and other external causes (such as the greenhouse effect and internal forcing) of the Antarctic sea ice making it exceedingly difficult to detect using existing models. Furthermore, the sea ice simulations produced by the models contradict the observations. Another reason for the paucity of research on this topic could be due to the geography of the Antarctic, which is mainly surrounded by the ocean, making it too challenging to incorporate just one or two climate models. Lastly, there are no well established scientific or analytical procedures for analysing and identifying the potential factors that may cause the teleconnection.

1.6 Research questions

A preliminary literature review raises many critical questions about the teleconnection between the Antarctic sea ice and monsoon variability. These scientific questions are broadly classified into three components. Before delving deeper into this connection, the first component is examining the climatology of the sea ice extent in the Indian Ocean sector, Mascarene High, and Indian summer monsoon rainfall, both seasonal and monthly. The second component is determining whether there is a physical link between the sea ice extent in the Indian Ocean sector and Indian summer monsoon rainfall. As a result, the following key questions are addressed in the first and second component:

i. What is the climatology of sea ice extent in the Indian Ocean sector, Indian summer monsoon rainfall and Mascarene High, including annual, seasonal and monthly?
ii. Is there any significant relationship between the sea ice extent in the Indian Ocean sector and the Indian summer monsoon rainfall region?
iii. Are there any bridging or modulators linking the sea ice extent in the Indian Ocean sector and the rainfall over the Indian region?
iv. What happens to the subtropical high during high and low ice phase years?
v. How does the high subtropical variability affect the Indian summer monsoon rainfall variability?

The third component of the research question investigates the mechanisms involved in the linkages between the interannual variability of the sea ice extent in the Indian Ocean sector and the variability of Indian summer monsoon rainfall via atmospheric circulation features. Also, to assess how the CMIP5 models simulate

teleconnection patterns and mechanism. The following are the research questions for this section:

i. What is the possible route of the connection?
ii. How does the connection occur or by what mechanism, particularly in atmospheric circulations?
iii. Can the simulated data from the CMIP5 model provide comparable results to the reanalysis data?

1.7 Objectives of the study

The end goal of this study is to determine the relationship and possible mechanism between the sea ice extent in the Indian Ocean sector and Indian summer monsoon rainfall. To carry out this goal, the climatology of sea ice extent in the Indian Ocean sector, Indian summer monsoon rainfall, and Mascarene High need to develop. Subsequently, evaluating the statistical connection between the sea ice and Indian summer monsoon rainfall over different sub-regions for different composite months. This information will form the basis for further in-depth research to determine any physical or dynamic relationships involved.

The main objectives of this study are:

1. To develop a comprehensive climatology of the sea ice extent in the Indian Ocean sector and Indian summer monsoon rainfall.
2. To investigate the relationship between the sea ice extent in the Indian Ocean sector and Indian summer monsoon rainfall variability.

3. To investigate possible routes of the connection and modulating factors between the linkages of the sea ice extent in the Indian Ocean sector and Indian summer monsoon rainfall variability.
4. To propose a possible mechanism for how interannual variability of the sea ice extent in the Indian Ocean sector influences the variability of Indian summer monsoon rainfall.
5. To assess the efficacy of CMIP5 models in simulating patterns and mechanisms associated with the linkages of the sea ice extent in the Indian Ocean sector and Indian summer monsoon rainfall variability.

1.8 Scope and challenges of the study

The term "teleconnection" is frequently used in conjunction with "global." This phrase has an extensive definition. The study could include all possible interactions between the atmosphere, the ocean, or both. Nevertheless, the scope of this research effort is expanded to include all possible connections, but in this research, it focuses more on interactions through atmospheric aspects only. The area involved is the sea ice extent over the Antarctic region, especially in the Indian Ocean sector, some parts of the Indian Ocean (such as the Mascarene High), and the Indian continent. The region involved is shown and discussed in Chapter 3, which is in the section on the selection of the study area.

In this research study, there are a few difficulties faced. One of the challenges is scholars' lack of literature studies and research activity, particularly on the Antarctic sea ice teleconnection. As mentioned earlier, teleconnection with the Antarctic sea ice is relatively new and not fully explored. Furthermore, only a few researchers are knowledgeable in both fields of polar and tropic studies. Although the connection has been well-established in terms of statistics, the connection mechanism, whether physical

or dynamic, is extremely challenging. The teleconnection process is also non-linear; hence, the link cannot be found or established immediately. It can change or connect due to atmospheric or oceanic factors or both. Furthermore, the global model was unable to simulate the Antarctic sea ice, which necessitated the use of advanced technology (which Malaysia lacked) and coordination with other countries. The accomplishment of the global model would require more time and substantial capital. One of the other challenges was the relatively two-year Movement of Control Order (MCO) sanctioned by the government to curb the COVID-19 pandemic. Students were unable to enter the university premises, use laboratory facilities and perform analyses. This event slowed down or delayed the planned schedule.

1.9 Significance of the study

This research study is relevant due to the following reasons. Researchers can improve the forecasting of tropical weather and climate by understanding the physical or dynamic mechanisms of the process. In addition, scientists can anticipate or predict the long-term values and patterns of climate variability over a certain region, such as rainfall, floods, and drought. The recent availability of global satellite data and reanalysis data provides researchers with an opportunity to investigate this topic. These data discover potential components that may induce the teleconnection process between the polar and tropical regions, allowing researchers to regulate aspects that may cause extreme events. With clearer image accessibility, the physical process and dynamics involved are better understood. The developed indices can be used to quantify or measure the relationship. This study can also be used as a starting point for future scholars who are interested in exploring this topic further. This research could add to the existing collection of literature.

1.10 Thesis structures

This research study will be presented in the conventional thesis format, with the inclusion of two articles published in Institute for Scientific Information (ISI) cited journals. This thesis is organised into six sections. The following is a summary of the content of each chapter:

Chapter 1 is the ***Introduction*** section that consists of general views on teleconnection, including its definition and history, sea ice, and monsoon variability. This chapter also discusses the problem statements, research questions, objectives, scope, research challenges, and significance of the study.

Chapter 2 is the ***Historical review of the past studies*** section covers details about the variability of the Antarctic sea ice, the Indian summer monsoon, and the teleconnection of the Antarctic sea ice extent, including the atmospheric circulation variability and teleconnection indices of Indian summer monsoon rainfall. It also covers the teleconnection as simulated in the climate models.

Chapter 3 is the ***Data and Methodology*** section. This chapter discusses the sources of the dataset, including global and regional data, the selection of CMIP5 models, the study area, and methods used to investigate the amount of Antarctic sea ice, Indian monsoon rainfall, and teleconnection mechanisms. Last but not least are the equipment and software used to conduct the analysis.

Chapter 4 and **Chapter 5** are the ***Results and Discussion*** sections. Chapter 4, evaluating and examining the climatology of the Antarctic sea ice extent, particularly the sea ice extent over the Indian Ocean sector and Indian summer monsoon rainfall. This

chapter also examines the physical mechanism of teleconnection between the sea ice extent in the Indian Ocean sector and Indian summer monsoon rainfall. The content of this study was published in the Polar Science journal in an article titled "The linkage between Antarctic sea ice extent and Indian summer monsoon rainfall" (Azhar et al., 2020). Chapter 5, evaluating the possible mechanism linking the variability of the Antarctic sea ice extent in the Indian Ocean sector and Indian summer monsoon rainfall in terms of atmospheric circulation characteristics. Furthermore, evaluating the performance of CMIP5 models in simulating patterns and mechanisms The content of this study was published in the Climate Dynamics journal in an article titled "The mechanism linking the variability of the Antarctic sea ice extent in the Indian Ocean sector to Indian summer monsoon rainfall" (Azhar et al., 2022).

Chapter 6 is the ***Conclusion,*** highlights the overall finding, including summaries and major conclusions, limitations of the study, and future work.

Figure 1.4 depicts a summary of the thesis framework.

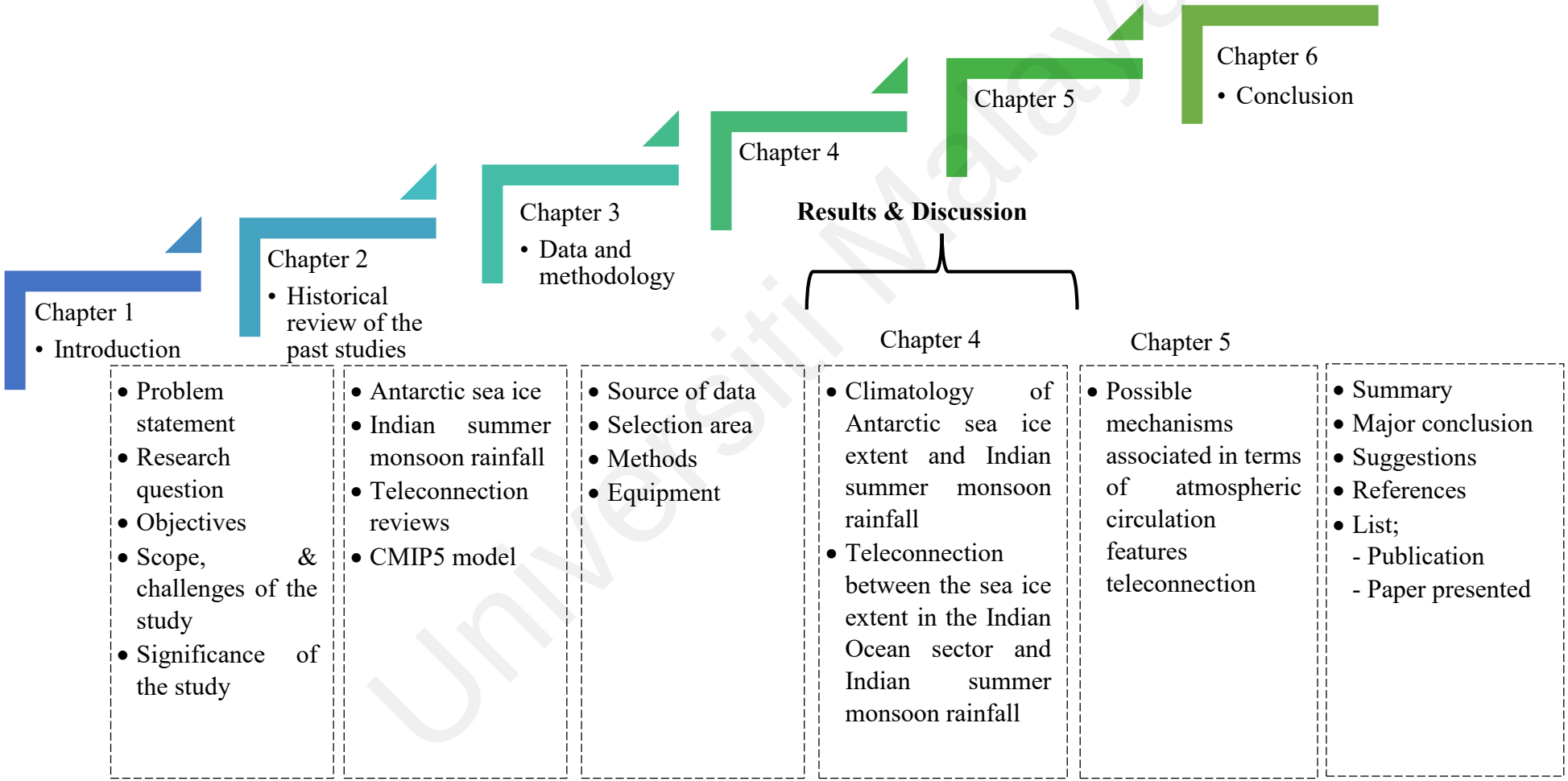

Figure 1.4: Structure of thesis flow

CHAPTER 2

HISTORICAL REVIEW OF THE PAST STUDIES

2.1 Introduction

This chapter contains several subsections. The first subsection examines the Antarctic sea ice variability in different sectors, how the sea ice is represented in climate models, and the variability of Indian summer monsoon rainfall. The following subsection will review the literature on the teleconnection between the Antarctic sea ice and climate pattern variabilities, as well as indices of sea surface temperature, precipitation, summer rainfall in China, and western South African rainfall. Furthermore, this chapter will also cover the representation of the teleconnection patterns of the Antarctic sea ice in climate models. Finally, the last subsection will summarize the prior research on Indian summer monsoon rainfall teleconnection, including with El Nino Southern Oscillation (ENSO), sea surface temperature, and the Australian monsoon.

2.2 Antarctic sea ice

The Antarctic sea ice has been increasing on average since 1979, and scientists have been studying the patterns and changes of the Antarctic sea ice in considerable detail since then (Cavalieri et al., 2003; Eayrs et al., 2019; Sun, 2021). According to the seasons and its regions, the Antarctic sea ice has various forms of variability and trends (Stammerjohn et al., 2008; Kimura and Wakatsuchi, 2011; Renwick et al., 2012; Hobbs et al., 2016). In most studies, researchers address the growth of the sea ice extent based on the seasonality of the specific regions (Parkinson and Cavalieri, 2012; Stammerjohn et al., 2012; Turner et al., 2015). In general, researchers have divided the sea ice in the Antarctic region into five sectors. There are the Ross Sea, Amundsen Sea, Bellingshusen

Sea, Weddell Sea, Indian Ocean, and Western Pacific Ocean. The different sectors of Antarctica have their own distinct features and natural variation, which are shaped by their geographic location (Figure 2.1). Therefore, some of the sectors show positive trends in sea ice, while others show negative trends at different timescales (Prabhu et al., 2010; Turner et al., 2015). In addition, the growth or retreat of the sea ice in each sector does not occur at the same rate and time. Typically, sea ice extent over the Indian Ocean sector produces more in September and retreats twice as much in November compared to the rest of the Antarctic regions. In comparison, the Weddle Sea had the highest retreat in October. Toward the end of the summer month, practically all of the sea ice in the Indian Ocean and Pacific sectors had gone; however, ice remained in the Amundsen-Bellingshusen Sea and Ross Sea, mainly the Weddell Sea, which has the most multi-year sea ice (Turner et al., 2017). The interconnections between the Antarctic sea ice variability and natural cycles are also complex due to the continent's physical geography, primarily surrounded by the ocean (Scott, 2009; Weeks, 2010).

From 1979 to 2013, the extent of Antarctic sea ice increased by an average of 1.5% per decade. This increase was primarily driven by the growth of sea ice in recent years. The rate of increase was slightly lower, at 1.0% per decade, for the shorter time period from 1979 to 2006 (Cavalieri and Parkinson, 2012; Turner et al., 2014; Turner et al., 2015). Over the 40-year period from 1979 to 2018, the Antarctic sea ice extent reached its maximum annual value of 12.8 million square kilometers in 2014. This was followed by a maximum value of 10.7 million square kilometers in 2017 (Parkinson, 2019). Multiple studies have linked the unprecedented melting of Antarctic sea ice in late 2016 to meteorological and oceanic conditions (Turner et al., 2017; Stuecker et al., 2017; Schlosser et al., 2018; Meehl et al., 2019; Wang et al., 2019). Despite this, the total Antarctic sea ice has shown a positive pattern in the yearly average sea ice extent over

the preceding 40 years, with each season bringing an increase, in which autumn having the highest and summer having the lowest (Parkinson, 2019). The yearly sea ice extent pattern was mostly characterized by an increase in ice in the Ross Sea sector and a decrease in ice in the Amundsen–Bellingshausen Sea sector (Figure 2.1). In addition to the Ross Sea sector, the other three regions (India Ocean sector, Weddell Sea and Western Pacific Ocean sector) have also seen an increase in yearly average sea ice extent. The Indian Ocean sector has seen the largest increase. The Ross Sea sector has been experiencing a sustained increase in sea ice extent in all seasons, while the Amundsen–Bellingshausen Sea sector has been declining steadily. The Western Pacific Ocean and Indian Ocean sectors have also seen an increase in sea ice extent in all months of the season. In contrast, sea ice extent in the Weddell Sea region increased during the summer and autumn months, but decreased during the winter and spring months (Turner et al., 2015). In different studies, similar results were stated by the authors, whereby four sectors had 40 year positive yearly patterns, except for the Amundsen Sea, which had a negative pattern (Parkinson, 2019).

Antarctic sea ice has been declining since 2014, according to recent research (Meehl et al., 2019; Eayrs et al., 2019; 2021), the lowest extent of sea ice was recorded in 2017 at 10.7 million square kilometers, which is the lowest extent in 40 years (1979 until 2018) of the satellite multichannel passive-microwave data. For 40 years, sea ice extent in the Ross Sea, Weddell Sea, Indian Ocean, and Western Pacific Ocean exhibited a positive trend. However, the Bellingshausen and Amundsen Seas exhibited a negative trend in sea ice extent over the same period (Parkinson et al., 2019). This was also stated in the study of Yadaz et al. (2022), where over the previous four decades, i.e., from 1979 to 2019, the annual sea ice extent in the Indian Ocean sector has seen a continuous increase, with the largest increase occurring in the austral summer. The primary drivers

or mechanisms of these decline trends are still in debate among the researchers, but it is widely acknowledged that the atmosphere plays a major role, as do seasonal time scales and regional scale processes (Eayrs et al., 2019; Wang et al., 2019). Some researchers also believe that the reason or mechanism for this declining trend is similar to the reason for the increasing and advancement trend of sea ice (Wang et al., 2019). Even though it is assumed to be linked with variation in large scale climate patterns and oceanic conditions, the explanation or reason behind the advanced in the amount of Antarctic sea ice remains unknown (Fan et al., 2014). There is no widespread agreement has been reached on the proposed mechanism for explaining this increasing trend (Blanchard-Wrigglesworth et al., 2021). Nonetheless, multiple explanations have been put forth to discuss the factors that are contributing to the increasing sea ice extent, and how atmospheric climate modes are involved.

There are several atmospheric climate modes that explained the regional variability of sea ice extent from year to year and from season to season. For example, the Antarctic Oscillation (AAO) is also known as the Southern Ocean Annual Mode (SAM). SAM, or AAO, is recognized as the dominant pattern of climate variability in the Southern Hemisphere outside of the tropics. It is characterized by a seesaw like pattern of atmospheric pressure, with high pressure at middle latitudes and low pressure at high latitudes (Kidson, 1988; Gong and Wang, 1999; Thompson and Wallace, 2000). SAM is in its positive (and negative) phase when MSLP decreases (and increases) at the Antarctic (and middle latitudes) and increases (and decreases) at the middle latitudes (and Antarctic) (Thompson and Wallace, 2000). SAM or AAO has a major impact on the variability of Antarctic sea ice extent (Pezza et al., 2008; 2012; Turner et al., 2013; Fogt and Wovrosh, 2015; Turner et al., 2015; Coggins and McDonald, 2015). The positive phase of the SAM index is associated with a decrease in sea ice extent in the Weddell Sea

and Antarctic Peninsula, and an increase in sea ice extent in the Ross and Amundsen Seas. This is consistent with the findings of Liu et al. (2004), who found that a positive SAM index is associated with more sea ice in the eastern Ross and Amundsen Seas, and less sea ice in the Bellingshausen and northern Weddell Seas. Kumar et al. (2021) investigated sea ice variability in the Weddell Sea sector of West Antarctica. They found that a positive SAM index is associated with an increase in sea ice extent in the austral summer, while a negative SAM index is associated with a decrease in sea ice extent in the winter.

Turner et al. (2015) also observed that the correlation pattern between sea ice extent and mean sea level pressure (MSLP) near middle latitude (the Antarctic) is similar to the SAM features. The Amundsen Sea Low (ASL) is a low pressure center located roughly 150°W of the western part of Antarctica, and it predominantly regulates atmospheric conditions over the Ross Sea sector and Antarctic Peninsula region. Turner et al. (2015) found that the ASL deepens when the southerly winds across the Ross Sea increase. This deepening of the ASL leads to an increase in sea ice extent. They also noted that a positive SAM index is associated with stronger cyclonic winds in the ASL region. This strengthening of the ASL leads to a dipole pattern of sea ice extent, with decreasing sea ice extent in the Bellingshausen Sea and increasing sea ice extent in the Ross Sea. The differences in air circulation patterns may not be the main reason for the variability in the Antarctic sea ice extent, both annually and seasonally. Yadav et al. (2022) recently found that sea ice extent particularly in the Indian Ocean sector shows a statistically significant relationship with both indicators ENSO and SAM over the summer and fall. Similarly, in the study of Ejaz et al. (2021), it was stated that SAM-ENSO teleconnections played a significant role in modifying interannual to decadal sea ice variability across the western Indian Ocean sector over the last two centuries. Furthermore, Crosta et al. (2021) also stated that the combination of El Nino and SAM events resulting in Indian Ocean

sector sea ice decreased as the Antarctic coast's sea ice grew thicker. Therefore, differences in air circulation patterns are one of the main causes of variability in Antarctic sea ice extent on an annual and seasonal basis.

The documented previous study acknowledges factors that drive the overall small positive trends in Antarctic sea ice, including the combinations of natural modes of effect of the atmosphere, ocean and cryosphere internal variability, the reaction to global warming, as well as the reaction to stratospheric ozone depletion (Blanchard-Wrigglesworth et al., 2021). Several research studies have presented various explanations and mechanisms for the continuous advancement of the Antarctic sea ice. For instance, the strengthening of westerly winds in the Southern Ocean because of ozone depletion results in the expansion of sea ice through equatorward Ekman ice transport (Thompson et al., 2002; Turner et al., 2009). Furthermore, variations in wind stress (Liu et al., 2004; Lefebvre and Goosse, 2008; Turner and Overland, 2009). Liu et al. (2004) discovered the growth of sea ice is due to the strong cyclonic circulation over the southeast Pacific and strong surface westerlies anomalies over the Ross-Amundsen Sea. The strong surface westerly anomalies encouraged Ekman to move northward. Apart from that, the increased of winds near the surface provide more surface mixing and upwelling of circumpolar deep water (Maksym et al., 2012; Holland and Kwok, 2012) also contribute to the expansion of sea ice. As discovered by Holland and Kwok (2012), the primary factor controlling ice patterns around the West Antarctica region is changes in wind driven ice advection, while others are controlled by wind-driven thermodynamic variation. Additionally, the melting of the Antarctic shelf is creating a layer of cold, fresh water on the surface of the ocean. This layer acts as a barrier, preventing the warmer, deeper waters from mixing with the surface waters (Martinson, 2012; Bintanja et al., 2013;2015). These activities may contribute to increased sea ice production, which might assist in describing the total

maximum value of the Antarctic sea ice extent trend in the autumn and early winter (Lieser et al., 2014; Turner et al., 2015). The advancement of the Antarctic sea is also influenced by random natural fluctuations (Polvani and Smith, 2013). Moreover, the expansion of sea ice is also due to the flow of tropically driven atmospheric circulation over West Antarctica (Meehl et al., 2016; Purich et al., 2016; Chung et al., 2020). A study by Purich et al. (2016) found that changes in the Interdecadal Pacific Oscillation (IPO) can lead to the strengthening of the Amundsen Sea Low (ASL), which can lead to increased sea ice levels in the Ross Sea. In a study by Chung et al. (2020), they found that changes in the Interdecadal Pacific Oscillation (IPO) and the Atlantic Multidecadal Variability (AMV) can contribute to the expansion of sea ice in the Pacific sector of Antarctica. However, the explanation for the overall increase in sea ice extent in Antarctica is still under debate, and our understanding of its variability is not as complete as in the Arctic (Shu et al., 2020). As a result, there is still much that we do not know about Antarctic climate variability beyond interannual time scales (Turner et al., 2009), and this is an area of active research, particularly in the field of numerical simulation and climate modelling.

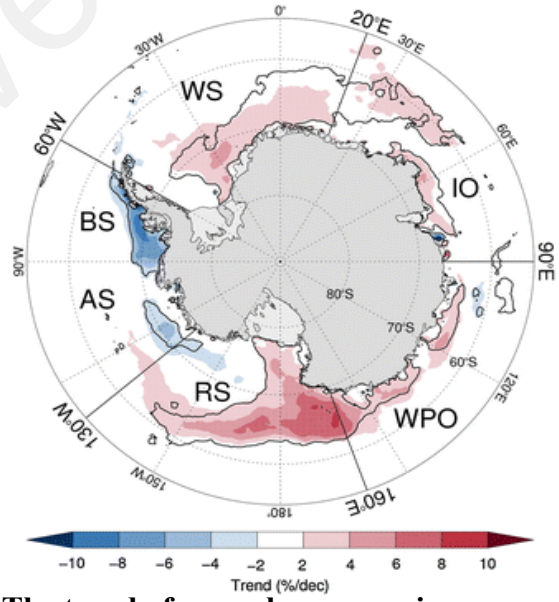

Figure 2.1: The trend of annual mean sea ice concentration for 1979 – 2013 for each sector (RS - Ross Sea; AS - Amundsen Sea; BS – Bellingshausen Sea; WS - Weddell Sea; IO - Indian Ocean; WPO - Western Pacific Ocean (Turner et al., 2016)

In prior studies, most researchers found that the Antarctic sea ice was scantily estimated in coupled climate models. Coupled climate models are a valuable tool for studying the relationship between sea ice and the environment, and they can be used to develop strategies for mitigating the effects of climate change. This platform provides a valuable opportunity for the research community to assess the accuracy of sea ice simulations in state of the art climate models. This information can be used to improve the accuracy of these models, which will lead to better predictions of future sea ice conditions (Shu et al., 2020). Most polar meteorologists believe that climate models feebly simulated the Antarctic sea ice. Almost every climate model produces complete contradictory results to the observation results (Hosking et al., 2013; Turner et al., 2013; Shu et al., 2015). Various interpretations have been proposed to explain why climate models consistently fail to reproduce the actual value of developing the Antarctic sea ice, including natural climate variability (Zunz et al., 2013), winds (Raphael, 2007; Lefebvre and Goosse, 2008; Holland and Kwok, 2012; Matear et al., 2015), the condition of the ocean (Zhang, 2007), and others (Turner et al., 2013; Ridley et al., 2018). The relationship between sea ice and climate change over an extensive range of time scales is also complicated. Additionally, each climate model includes its own unique set of physical and chemical processes factors that contribute to the simulation of sea ice. These factors may include wind, currents, and others. In conclusion, the models' inaccurate outputs are due to the physical differences between the models and the current thermodynamic state of sea ice (Roach et al., 2018).

According to Turner et al. (2013), most of the 18 climate models of CMIP5 employed in the study did not perform well and had a large spread in predicting the sea ice extent. The results of the sea ice extent patterns indicated negative trends in virtually all the models, which is the opposite of the trend in the observational data. They suspected

this might be caused by a number of factors, including failure to consider the condition of the actual trends in various ocean parameters, the complexity of the climate system and the lack of data on sea ice. However, the NORESMI-M model's simulation of sea ice extent is relatively realistic, especially when it comes to the annual cycle. The study by Uotila et al. (2014) found that the ACCESS1-0 and ACCESS1-3 models were more accurate in predicting the changes in Antarctic sea ice than most other climate models. This suggests that these models may be useful for understanding and predicting the future changes in Antarctic sea ice. The ACCESS model is generally considered to be one of the most realistic models of Antarctic sea ice. In addition, GFDL-CM3 models also show a comparable trend to the observation from 1980–2011, where the GFDL-CM3 model simulates an increase in Antarctic sea ice. While a study found that the IPSL-CM5A-LR and MPI-ESM-MR climate models were able to accurately simulate sea ice extent up until recently, but were unable to reproduce the recent increase in sea ice extent (Yang et al., 2016). The Mahlstein et al. (2013) found that natural variability alongside external forcing plays a significant role in the observed trends in Antarctic sea ice. The authors also cautioned that the CMIP5 models should not be interpreted too literally, as their ability to simulate the observed trend in Antarctic sea ice area is dependent on how well they represent the processes in the atmosphere and ocean that affect sea ice. Minor differences in the ocean or atmosphere are capable of producing inaccuracies in models of sea ice extent (Turner et al., 2013). The validity of previous studies' models of sea ice extent is uncertain due to artificial interventions, biases, and regional variations (Uotila et al., 2014). As previously stated, the study of climate models, specifically CMIP5 models, predict a decrease in Antarctic sea ice, but this is not supported by observations. The region's internal forcing and climate variability components must be taken into account to obtain better results. The causes of the gap between observed and modelled sea ice trends remain unexplained, although the weaknesses of some ocean and

atmosphere models that affect sea ice were identified (National Academies of Sciences, Engineering, and Medicine, 2017). Due to this ambiguity, the models have biases and uncertainties that make it difficult to judge future projections accurately.

Recently, researchers have used the sixth phase of the Coupled Model Intercomparison Project (CMIP6), a set of new climate models, to evaluate trends in Antarctic sea ice. Shu et al. (2020) evaluated the performance of the CMIP6 models in simulating sea ice extent. They found that the CMIP6 models performed similarly to the CMIP5 models, with both sets of models showing negative trends in seasonal and long term sea ice extent. Furthermore, they also found that 11% of the CMIP6 simulations showed an increase in sea ice extent from 1979 to 2005. The models are ACCESS-CM2, ACCESS-ESM1-5, BCC-CSM2-MR, BCC-ESM1, CAMS-CSM1-0, CNRM-ESM2-1, EC-Earth3-Veg, FGOALS-f3-L, GISS-E2-1-H, HadGEM3-GC31-MM, IPSL-CM6A-LR, MPI-ESM-1-2-HAM, MPI-ESM1-2-HR, MPI-ESM1-2-LR, MRI-ESM2-0, NESM3, and NorESM2-LM. However, these realization models are unable to reproduce the same spatial pattern as observed, which is consistent with the findings of CMIP5 (Shu et al., 2015). Roach et al. (2020) evaluated Antarctic sea ice in 40 CMIP6 models and found that many models were able to capture the main features of the seasonal cycle of the mean sea ice area. However, some models simulate historical mean conditions that are unrealistic in comparison to satellite observations, resulting in significant inter-model dispersion. In a recent study, Li et al. (2023) described that the majority of CMIP6 models exhibit reasonable variation and modest differences in sea ice extent and sea ice area under the scenario of SSP2-4.5 in comparison to Advanced Microwave Scanning Radiometer 2 (AMSR2). CMCC-CM4-SR5 model has the highest correlation coefficient and smallest root mean square deviation in both sea ice extent and sea ice area, with values of 0.99 and 0.98, respectively. However, the GFDL-CM4 and FGOALS-g3

models had the lowest mean bias and the most suitable interannual sea ice extent and sea ice area agreements with AMSR2. GFDL-CM4, FIO-ESM-2-0, and CESM2 models have quite high positive correlation coefficients with sea ice concentration observational data, reaching 0.60. From extensive sea ice cover evaluations, CESM2, CMCC-CM4-SR5, FGOALS-g3, FIO-ESM-2-0, and GFDL-CM4 show more realistic forecast performance.

2.3 The Indian summer monsoon variability

The southwest monsoon, often known as the Indian summer monsoon, is a component of the Asian monsoon system. It is recognized as the most significant phenomenon and powerful monsoon system in the northern hemisphere. It is also widely investigated compared to other global monsoon systems (Wang et al., 2012). The southwest monsoon is distinguished by a seasonal wind system that reverses direction throughout the year (Ramage, 1971). It is also caused by a difference in temperature between the land and the sea, as well as by the formation of a low-pressure area over the Indo-Gangetic plain and a high pressure area in the subtropical Indian Ocean (Krishnan et al., 2015). This phenomenon typically begins in June and ends in late September, though the process might start as early as May. The strong southwesterly winds in the lower atmosphere carry a large amount of moisture into India. This moisture is mostly released as rainfall over the Bay of Bengal and along India's Western Ghats (Slingo, 1999). The amount of rainfall received during this event is often around 80% of the region's yearly rainfall (Gadgil, 2003; Cane, 2010; Turner and Annamalai, 2012). The intensities of rainfall substantially impact economies, the environment, and social life (Clift and Plumb, 2008), such as through landslides and flash floods in certain regions.

The complexity of the Indian subcontinent is due to its topography, geography, and differing land use patterns. The subcontinent is surrounded by three bodies of water

on three sides: The Arabian Sea to the west, the Bay of Bengal to the east, and the Indian Ocean to the south. The Himalayas lie to the north (Figure 2.2). These factors have a major impact on the distribution of rainfall in India and its sub-regions. As a result, rainfall in the Indian summer monsoon varies significantly in temporal and spatial scales. In the period of summer monsoon event, India's west coast, northeast, and central areas received heavy to torrential rainfall (receiving more than 90% of their annual rainfall), which was influenced by orography. Heavy rainfall was also seen at about 20° N, which is identified as the core monsoon area since Indian summer monsoon rainfall is strongly linked to rainfall in this area (Sikka and Gadgil, 1980). Southern and north-western India, on the other hand, received 50 –70% of their yearly rainfall during this monsoon season. As a result, the monsoon rainfall variability distribution impacts agriculture productivity and stabilises India's economy. Rainfall in India at the time of the monsoon season, is associated with the development of convective systems and spreads over the subcontinent. Studies has shown that, beyond the Mascarene High and the Somali Jet, other factors, such as the surface heat low, the monsoon trough, the Tibetan anticyclone, and the tropical easterly jet stream, can also influence the intensity of the Indian summer monsoon (Krishnamurti and Bhalme, 1976). Additionally, some studies have found that the intensity of rainfall during the event is linked to small vortices that are associated with large-scale convective systems over the Arabian Sea (Rao, 1976; Mukherjee, 1980; Francis and Gadgil, 2006).

2.3.1 Mascarene High

The Mascarene High is one of the semi-permanent subtropical high pressure areas that can be found over the centre of the Indian Ocean. Its centre is theoretically positioned between 30° S and 60° E, near the Mascarene Islands in the centre of the Indian Ocean (Figure 2.2). The name "Mascarene" comes from the Mascarene Islands located near the

east of Madagascar. Typically, this high-pressure region starts to form in the middle of April and weakens at the beginning of September. The strong interannual variability of the region is hugely contributes to the variability of the sea surface temperature over the southern Indian Ocean (Behera et al., 2001). Previous studies have determined the Mascarene High's location. Manatsa et al. (2014) defined the strength of the Mascarene High as the maximum atmospheric pressure at sea level (MSLP) in the region between 25° S and 35° S and 40° E and 105° E. Ohishi et al. (2015) classified the Mascarene High as an area between 10° S – 50° S and 40° E – 120° E in the austral summer (November to January), while Morioka et al. (2015) described it as being between 30° S – 35° S and 80° E – 90° E. A recent research by Xulu et al. (2020) defined the Mascarene High based on monthly north – south and west – east MLSP. Vidya et al. (2020) identified the Mascarene High region between 20° S– 40° S and 45° E – 100° E. Table 2.1 lists the details of the position and definition of the Mascarene High.

Table 2.1: Location and definition of Mascarene High regions from previous studies

Researchers	Mascarene High location	Definition
Xue et al. (2004)	25° S – 35° S, 40° E - 90° E	MSLP climatology (Jun –July-August from 1970-1999)
Rai et al. (2008)	30° S - 36° S, 83° E - 88° E	Sea surface temperature (1982 – 2004)
Manatsa et al. (2012)	25° S - 35° S, 40° E - 105° E	The maximum isobaric ridge of the MSLP
Morioko et al. (2015)	30° S - 35° S, 80° E- 90° E	The maximum central pressure of sea level pressure (austral summer; 1982 – 2011)
Ohishi et al. (2015)	10° S – 50° S, 40° E – 102° E	The maximum sea level pressure (austral summer; 1979 – 2012)
Xulu et al. (2020)	25° S - 35° S, 40° E - 110° E	Monthly north–south and west–east MLSP
Vidya et al. (2020)	20° S – 40° S, 45° E – 100° E	MSLP climatology (boreal summer)

The variability of the Mascarene High is a major factor that contributes to the amount of rainfall that India receives during the summer monsoon season (Krishan et al., 2015; Rao et al., 2017). The region is recognised as the primary engine that drives the meridional monsoon circulation (Rao et al., 2017). The wind flows and MSLP locations of the Mascarene High and Somali Jet are illustrated in Figure 2.2. Winds blowing from the northeast originate from anticyclones in the Mascarene High region. As the north-easterly winds travel northward, crossing the equatorial, they convert into the south-westerly winds known as the Somali Jet. Mascarene High location and variability significantly impacted the Somali Jet intensity. The intense Mascarene High region will produce stronger south-westerly winds (Rao et al., 2017). The stronger Somali Jet transported a significant quantity of moisture across the Indian Ocean to the Indian subcontinent, leading to heavier rains across the country. Similar results were shown in the Krishan et al. (2015) study, where lessening of the Mascarene anticyclone across the subtropical Indian Ocean produced weakened monsoon circulation during 2015. This is illustrated by weakening circulation anomalies near southern Africa and east of Madagascar and low level easterly anomalies over the Arabian Sea and Indian region. Furthermore, the warm sea surface temperature and the sea level pressure anomalies over the east of Madagascar in the southern Indian Ocean demonstrated a weaker Mascarene High. These unusual features in 2015 point to the weak Mascarene High having a significant influence on large-scale monsoon flow and rains over India. While according to Vidya et al. (2020), the area of high atmospheric pressure in the southern hemisphere becomes stronger during the boreal summer, while a low atmospheric pressure area forms in the northern hemisphere because of the subcontinent's landmass is experiencing extreme heat from the sun. The difference in air pressure between the northern and southern hemispheres creates a strong wind that blows from the north to the south. This wind, known as the cross equatorial wind, helps to drive the monsoon flow over the

Arabian Sea. The Mascarene High anticyclonic circulation and the cross equatorial winds in the western Indian Ocean transport moisture from the southern Indian Ocean to South Asia. This creates an association between the Mascarene High and the Indian monsoon trough. However, during the Global Warming Hiatus period from 1998 until 2016, mean sea level pressure decreased, reducing the intensity of the Mascarene High. The pressure gradient between the Mascarene High and the Indian continent is reduced, which lessens the intensity of low level cross-equatorial winds in the western Indian Ocean (Vidya et al., 2020).

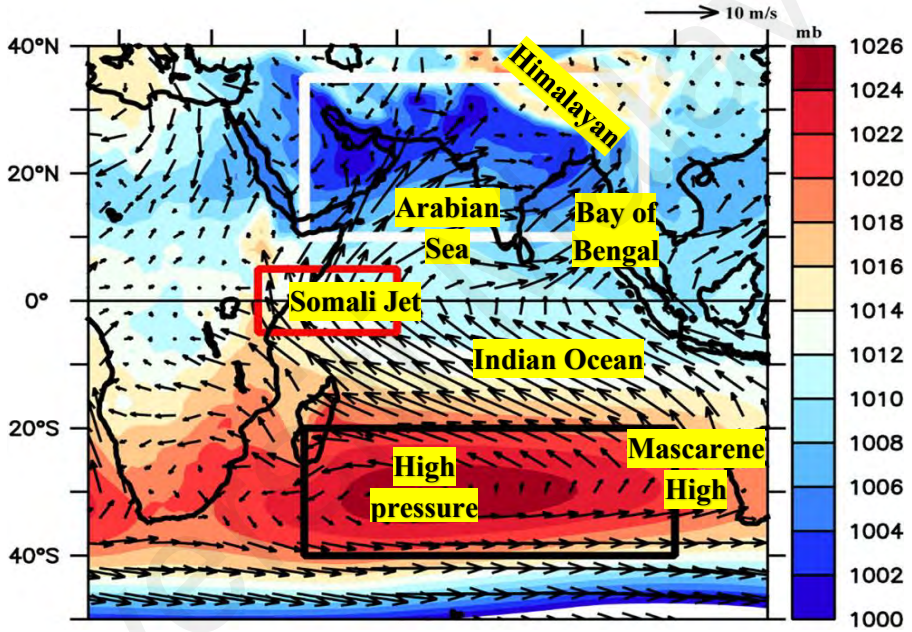

Figure 2.2: Wind vectors and sea level pressures (shaded colour) from 1998 -2016 over the Indian Ocean and monsoon region illustrating the Mascarene High and Somali Jet (Modified from Vidya et al., 2020)

However, to some extent, Mascarene High also play significant roles to interhemispheric circulation between the Indian Ocean in the south and the subcontinental landmass in the north (Vidya et al., 2020). Apart from that, the location and strength of the Mascarene High have also been documented as a powerhouse that generated weather and rainfall in East Asia, the southern African region, and the west of Australia (Washington et al., 2006; Miyasaka et al., 2010; Morioka et al., 2015; Rehman et al., 2019; Xulu et al., 2020). Xue et al. (2004) suggested that with the intensification of the

Mascarene High during boreal spring through summer, the rainfall over the Yangtze River valley to the Japan Islands tends to increase. Tao and Sun (2007) reported a significant positive correlation between the spring Mascarene High and Meiyu precipitation in the Changjiang-Huaihe basin. They noted that a stronger Mascarene High produces a stronger East Asian summer monsoon, and with a more southwestward position, the Western Pacific subtropical high tends to intensify, resulting in higher rainfall in the Changjiang-Huaihe basin and vice versa. Han et al. (2017) discovered that Mascarene High is significantly affecting the precipitation during the pre - rainy season in South China. A stronger index east of the Mascarene High contributes to more rainfall during the pre - rainy season in South China. They suggested that the extension and eastward movement of the Mascarene High strengthened the southerly winds, transporting a lot of water vapor towards the northern hemisphere and subsequently increasing South China's rainfall. Feng et al. (2013) found that summer rainfall variations across northwest Australia are connected to the intensity of the Mascarene High. They illustrated that a strong year of Mascarene High produced strong cyclonic vorticity in northwest Australia at the lower troposphere, thus transporting more moisture towards the region. In a Rehman et al. (2019) study found that the strength and position of the Indian Ocean subtropical high significantly impact the amount of precipitation that falls on Tasmania during austral autumn. The strong anomalies and eastern shift of the Indian Ocean subtropical high corresponded with a decreasing amount of rainfall over Tasmania and vice versa. Manatsa et al. (2013) revealed that the East Africa short rain variability is strongly linked to the position of Mascarene. The author showed that the southeast trade winds in the South Indian Ocean become stronger (or weaker) when the eastern ridge of the Mascarene high is displaced to the west (or east) of its usual location. The strengthening (or weakening) of the southeast trade winds, which are comparatively cool and dry, can lead to a cold (or warm) sea surface temperature anomaly in the South Indian

Ocean. Consequently, the decrease (or increase) in convection over the western equatorial South Indian Ocean leads to deficits (or excesses) in rainfall over East Africa. Similar results were found in the Nkurunziza et al. (2019) study. They discovered that the position of the Mascarene High was significantly correlated with the rainfall in Rwanda. In details, they stated that as the Mascarene High shifted eastward (and westward), the rainfall over Rwanda increased (and decreased) from its normal. In recent study (Xulu et al., 2020), authors reviewed and demonstrated the variability of Mascarene High has an influence on southern Africa weather and climate. They found that atmospheric blocking by the Mascarene High is linked to anomalous rainfall and temperature events over the African subcontinent. In other words, when the Mascarene High blocks the flow of air, it can cause unusual amounts of rain or snow to fall in some parts of Africa, while other parts may experience drought. Furthermore, Mascarene High is more likely to block the flow of moisture during El Nino years. This is because El Nino is a climate pattern that causes the sea surface temperature in the tropical Pacific Ocean to warm. This warming can lead to the formation of a stronger Mascarene High.

Furthermore, the factors that trigger the variability of Mascarene have been an interesting topic for researchers for many years. According to some previous studies, Mascarene High variability is responsible for several factors, including Antarctic oscillation, and sea surface temperature over the southern Indian Ocean (Behera et al., 2001; Xue et al., 2004). As Xue et al. (2004) stated that Mascarene High variability is controlled by the southern circumpolar low, and as the circumpolar low deepens, it will become intense. In comparison, Behera et al. (2001) show that the variability of the Mascarene High is affected by the sea surface temperature gradient between the northeast and southwest of the Indian Ocean, also known as the Indian Ocean subtropical dipole.

However, the solid reasons for the causes of Mascarene High remain hazy and unresolved. Researchers are continuously researching the topic.

2.3.2 The Somali Jet

The Somali Jet is a powerful south-westerly wind flow at the height of between 1 - 1.5 km from the surface with a speed of 25 ms^{-1}. It can be seen across eastern Africa in May and then travels through the northern Arabian Sea before arriving in India in June. The wind speed increases typically over a week (Halpern et al., 1999) during this event. During the summer monsoon season, the narrow core of this jet stream can reach speeds up to 50 ms^{-1} for several days. The existence of southerly low level flows crossing the equator across Kenya's east coast was discovered by Findlater (1971). East Africa's orography plays a significant role in structuring this flow. This low level jet is considered a crucial feature of the southwest monsoon because of its main function in transporting water vapour across the equatorial (Kumar et al., 1999; Kumar and Schluessel, 1998). It is also recognised as the most powerful low level jet on Earth during the boreal summer (Hoskins and Wang, 2006). It brings water vapour or moisture from the South Indian Ocean towards South Asia, connecting the Mascarene High with the Indian monsoon trough and completing the reverse Hadley cell's lower branch. The strong upwelling occurs near the Somali coast, and the cross-equatorial flow generates the seasonal Somali current (Krishnamurti and Bhalme, 1976; Love, 1985). Purwar et al. (2022) showed that the intensification and position of the low level jet stream has an influenced towards the Indian summer monsoon rainfall especially during September. The results suggested that intensity (height) of the monsoon low level Jet is positive (and negative) correlated with the Indian summer monsoon rainfall over the Western Ghats region and central India, except during the month of August. Alhubaishi et al. (2018) show that the strength of the Somali low level jet has an effect on the rainfall over Salalah, Oman. They found that

when the Somali low level jet reaches its maximum intensity in July and August, the rainfall accumulation in Salalah, Oman, also increases. Furthermore, they also stated that the intensification of Somalia's low level jet between years is influenced by ENSO and, subsequently, the amount of rainfall. In details, the maximum strength of the Somalia low level jet is weaker than average during the El Nino phase and higher than average during the La Nina phase. Similar results were found in the Halpern and Woiceshyn (2001) study. They illustrated the relationship of the Somali Jet in the Arabian Sea with the El Nino and La Nina episodes, where intensification of the monthly mean Somali jet was weaker during the El Nino episode compared with the La Nina. Thus, as the Somali Jet intensity is above or below normal, there is an excess or deficit of rainfall along the west coast of India. Apart from the ENSO event, the strength of the Somali Jet is also influenced by the variability of the Indian Ocean Dipole. The Jet moves northward and strengthens over northern and central India for the positive Indian Ocean dipole phase, bringing a large amount of moisture and rainfall. while the opposite is true for the negative Indian Ocean dipole phase (Jain et al., 2021). Vizy et al. (2020) illustrated that the low level cross equatorial flow along the East African coast weakens and reverses during the transition period (boreal spring and fall) and contributes to the increase and decrease of rainfall over East Africa. In contrast to the results stated by Camberlin et al. (2010) where the intensification of the Somali Jet is associated with decreasing of rainfall over East Africa particular northeastern Kenya. Chen et al. (2023) demonstrates a significant relationship between interannual variability in Somalia Jet intensity during boreal spring and the northwest-southeast migration of the South Asian High during the following summer. It has been discovered that when the previous spring Somali Jet is strong (and weaker), the summer South Asian High tends to shift northwestward (and southeastward). It is because of modifying of the sea surface temperature over tropical Indian Ocean and anomalous heating linked to the Indian summer monsoon rainfall. A different study by

Shi et al. (2017) shows a positive relationship between the strength of Somali Jet and South Asia High on an interdecadal timescale. The results illustrated that the weaker (stronger) Somali Jet strength corresponds to the weaker (and stronger) summertime South Asia High and retreats to the west (advances to the east). However, in recent study by Shi et al. (2021) discovered the intensities of summer Somali Jet and South Asia High is controlled by the phase of Atlantic Multidecadal Oscillation. Cold or warm phases of Atlantic Multidecadal Oscillation is associated with weakening or strengthening of Somali Jet and South Asia High.

2.3.3 Surface heat low

The surface heat low usually develops over northwest India and nearby Pakistan in the early of the pre monsoon month which is from May to September. The vertical structure of this low sea level pressure area is shallow, and it is constrained below 1.5 km, while above it, the high-pressure column stretches vertically. During the pre-monsoon months (April and May), the surface temperature linked with the heat low continuously develops (Rao, 1976). The desert zone over the Indian region is squarely under the heat low with the subtropical ridge aloft. The activity of dust storms over the heat low in May and June is a significant element in the radiative balance of the region. According to Bollasina et al. (2011), the surface heat low over northwestern India and Pakistan is affected by both local and remote forces. They discovered the deepening of the surface heat low from May to June and further deepening in July, which arises from remote forcing and leads to the development of convection in the monsoon over the Bay of Bengal and eastern India in June and July. They also suggested that the strengthening of the surface heat low in June is due to the associated upstream descent over Iran, Turkmenistan, and Afghanistan and related low-level northerlies over the Elburz, Zagros, and Hindu Kush mountains. Kakade and Kulkarni (2013) discovered the effect of surface

heat low temperature, or pressure on Indian summer monsoon rainfall depending on the phases of the effective strength index tendency. They concluded that May heat low pressure has an inversely significant relationship with Indian summer monsoon rainfall during the only negative phase of the effective strength index tendency. While February (and May) heat low temperatures have a significant relationship with Indian summer monsoon rainfall during the positive (and negative) phase of the effective strength index tendency.

2.3.4 Monsoon trough

The monsoon trough is a fundamental component of the Indian summer monsoon and was discovered by Blanford (1886). It is a lengthening of the low pressure zone stretching across the north of India's Indo-Gangetic plains. The extreme rainfall is limited to about 1–2 degrees south of the monsoon trough (Raghavan, 1973). The axis of the trough position is approximately from west-northwest to east-southeast, and it can reach up to 700 till 500 hPa (leans southward as it gets higher). Figure 2.3 illustrates an example of a classic monsoon trough. The position and strength of the monsoon trough have a significant impact on the distribution of rainfall in India. During the break monsoon, the western side of the trough has a higher possibility of extending north towards the foothills of the Himalayas. This is due to a westerly trough shifting eastward over the Northwest of India. Hence, the plains of central north India experienced less rainfall (Rao, 1976; Sikka and Narasimha, 1995). As the monsoon trough shifted to its normal position, the monsoon would be active, and rainfall would be evenly distributed across the Indian plains. In the Konduru and Mrudula (2021) study, it was reported that the offshore trough contributed 80% of rainfall across the south west of India, 68% over the south east of India, and 75% overall over south India in 2017. They discovered that during active offshore troughs, rain bands propagate eastward because of moisture flux convergence

and equivalent potential temperatures at different heights of the atmosphere. However, a recent study stated that ENSO and monsoon troughs, as well as associated variability in monsoon depression, are responsible for the spatial pattern of the Indian summer monsoon rainfall (Athira et al., 2022). According to the authors, the principal drivers of rainfall variability over central India were monsoon troughs and depression related variability. While variability in rainfall over south India was constantly influenced by the ENSO associated with monsoon troughs and depression related variability during the entirety of the period. In north India, the role of the variabilities of the monsoon trough and depression related factors is weaker, whereas the variability of rainfall in this region is dominated by ENSO.

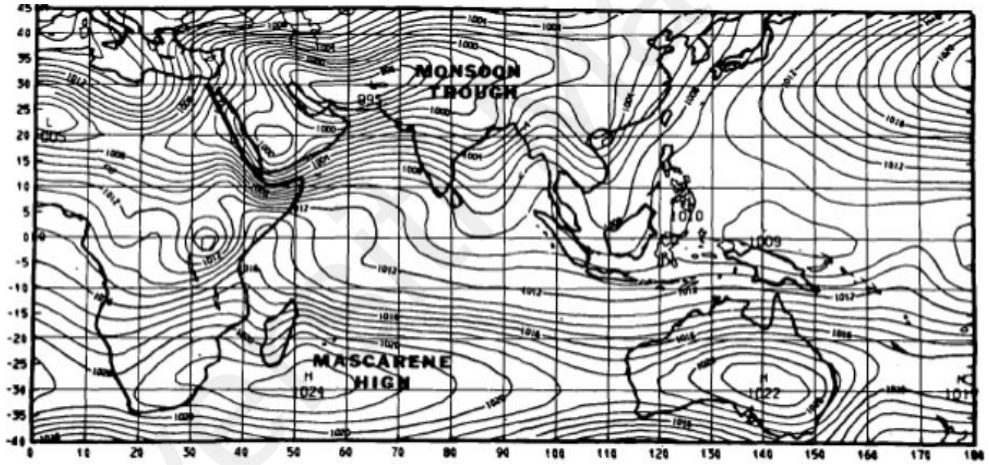

Figure 2.3: Example of the classic monsoon trough (Krishnamurti & Bhalme 1976)

2.3.5 The Tibetan High

The Tibetan High is another prominent feature linked to the monsoon onset, and it is known as a warm anticyclone wind in the upper troposphere. The existence of this Tibetan High is due to the development of a high-pressure zone over the Tibetan Plateau (Krishnamurti, 1973; Yanai and Wu, 2006; Liu et al., 2007). During the summer monsoon period, the Tibetan High reached its maximum intensity at a level of 150 – 200 hPa. Flohn (1968), Krishnamurti and Rodgers (1970), Krishnamurti (1971), and Krishnamurti et al. (1975) are among the pioneers who investigated the Tibetan High. The combination of

the Tibetan High and the monsoon trough at sea level will produce warm hydrostatic troposphere columns across northern India as well as the Himalayan foothills (Krishnamurti and Bhalme, 1976). Due to its higher altitude, the convection over the Tibetan Plateau is stronger than the Indian subcontinent. Fu and Fletcher (1985) discovered that the thermal contrast between the Tibetan Plateau and the equatorial oceans correlated to the interannual variability of the Indian monsoon rainfall. Ge et al. (2017) revealed that strong and weak Tibetan Plateau summer monsoons correspond to decreasing and increasing Indian summer monsoon rainfall. They illustrated that the stronger (and weaker) Tibetan Plateau summer monsoon is closely related to a cyclonic (and anticyclonic) anomaly near the surface over the western part of the Tibetan Plateau, increasing (and decreasing) the westerly flow along its southern flank, reducing (and enhancing) the meridional flow of warm and moist air from the Indian Ocean, and hence decreasing (and increasing) moisture supply over northern India and monsoonal rainfall. Singh et al. (2022) discovered that increasing surface pressure over the Tibetan Plateau is closely related to the increasing trends in rainfall over northwestern India and decreasing rainfall in the Indo-Gangetic Plains as well as in northeast India. The strengthening of the Tibetan Plateau surface pressure corresponds to the intensification of lower level easterlies over northwestern India and weakening middle tropospheric north westerlies across the east. This pattern of air circulation variability brings a lot of water vapour to northwest India and the Bay of Bengal. While weakening middle tropospheric north westerlies keep extratropical dry air out of India, increasing the rain generating process.

In general, the Tibetan Plateau acts as a significant heat engine that has direct implications for Asian monsoon variability, and several studies show the role of the Tibetan Plateau in forming and advancing the monsoon circulation (Liu et al., 2004;

Schneider and Bordoni, 2008; Wu et al., 2012; Tang et al., 2013; Chen et al., 2014). For example, positive precipitation anomalies over the middle and lower parts of the Yangtze and Huaihe Rivers, as well as decreasing rainfall over Southeast China, tend to correspond with an enhanced atmospheric heat source over the Tibetan Plateau (Zhao and Chen 2001; Duan et al. 2005; Wang et al. 2014). There are papers that examine the relationship between the Tibetan Plateau and rainfall over central Asia. Qi et al. (2015) found that the strong Tibetan Plateau summer monsoon corresponds to an abnormal convergence of southerly winds over Central Asia and an abnormal easterly wind over the south Xinjiang region, which contributes to more rainfall over this area. The influence of the Tibetan Plateau monsoon on weather and climate in Central Asia was later studied by several researchers by analyzing the relationship between the Tibetan Plateau monsoon and precipitation in the Tarim Basin. They discovered that mid-upper tropospheric temperature is crucial in coupling the Tibetan Plateau monsoon and the south Asian monsoon with summer rainfall over China's Tarim Basin (Zhao et al., 2016; and 2019). Zhang et al. (2022) investigated the association between the Tibetan Plateau and Central Asia's summer rainfall. The results of this study revealed a significant positive connection between the Tibetan Plateau monsoon index and Central Asian summer precipitation. In details, as the Tibetan Plateau monsoon strengthened, the upper troposphere of Central Asia underwent cold advection, leading to the formation of a cyclonic circulation anomaly across Central Asia in the mid-upper troposphere due to thermal wind. This resulted in a cyclonic circulation anomaly in water vapour transport at the lower troposphere.

2.3.6 The tropical easterly jet

The tropical easterly jet is an important feature of the Asian summer monsoon system, especially in the upper tropospheric region. It usually forms in June and will

remain until September (Krishnamurti and Bhalme, 1976). The jet core is observed between 70 and 200 hPa and is positioned at about 10° N, with a maximum speed of 40 ms^{-1} (Salunke et al.,2019). Along with other factors, the strength and position of this jet have a significant impact on the southwest monsoon rainfall intensity over India. The relationship between the variability of the tropical easterly jet and the Indian summer monsoon rainfall has been extensively studied by the researchers. It is proven by a substantial amount of literature (Tanaka, 1982; Madhu, 2014; Pattanaik and Satyan, 2000). Earlier studies have revealed that stronger (or weaker) tropical easterly jet correspond to an increase (or decrease) in the Indian summer monsoon rainfall. Also, the tropical easterly jet weakens and shifts southwards when the southwest monsoon retreats from the Indian subcontinent (Koteswaram, 1958; Ananthakrishnan and Ramakrishnan, 1965; Mokashi, 1974; Kanamitsu and Krishnamurti, 1978). However, there are studies investigating the decreasing trend in tropical easterly jet variability and its effect on monsoon rainfall. Sreekela et al. (2014) stated that the correlation of rainfall is found to be high with the speed of the tropical easterly jet over the decreasing trend of rainfall areas (Jammu and Kashmir, Arunachal Pradesh, the central Indian region, and the western coast of India). They also suggest that one of the key causes for the decreasing trend in tropical easterly jet as well as the observed geographical heterogeneity in summer rainfall is the reduced land-seat temperature difference in the pre-monsoon months. Rao et al. (2015) identified that the weakening of the relationship between the tropical easterly jet and the Indian summer monsoon rainfall is related to the decreasing trend rate of the tropical easterly jet that is caused by warming of the Indian Ocean.

Huang et al. (2021) revealed that the tropical easterly jet is strongly positively connected to the Indian summer monsoon rainfall except between 1994 untill 2003, where rainfall variability over the tropical eastern Indian Ocean plays an important role in

modifying this relationship. In detail, as the rainfall variability of the tropical eastern Indian Ocean strengthens, the Indian summer monsoon rainfall tends to weaken. The impact of tropical eastern Indian Ocean precipitation on tropical easterly jet variability has the potential to control and break this connection. Nicholson and Klotter (2019) show that the correlation coefficient between the Sahel rainfall and the tropical easterly jet is 0.72 over the period from 1948 to 2014. The authors stated that the factors that control the variability of the tropical easterly jet are the contrast of the sea surface temperature between the central equatorial Indian Ocean and the central equatorial Pacific, the contrast of the sea surface temperature between the southern subtropical Indian Ocean and the central equatorial, the latitudinal transition in the Southern Hemisphere between upper and westerly tropospheric easterlies, and the strength of the westerlies in the Southern Hemisphere. Apart from that, the tropical easterly jet can also impact rainfall through upper level differences (Nicholson and Grist 2003), easterly shear vertical (Rao et al. 2008), interaction with the easterly African wave activity (Grist et al. 2002), as well as the modification of the equatorial Rossby wave activity (Yang et al. 2018). Nithya et al. (2017) study the influence of ENSO on the tropical easterly jet and Asian summer monsoon region relationships. The tropical easterly jet exhibit different characteristics during El Nino and La Nina occurrences. During La Nina years, the tropical easterly jet intensifies and spreads horizontally and vertically, but it weakens and shrinks spatially during El Nino years. In La Nina events, Walker circulation across the summer monsoon region shows significant easterlies.

2.4 Antarctic sea ice teleconnection

Antarctic sea ice has been teleconnected with the tropics by the atmospheric circulation and climate variability indices. However, nowadays, researchers have shown an interest in utilizing climate models to investigate the connection between the Antarctic

sea ice and the tropics. Thus, this section will review previous studies on the Antarctic sea ice teleconnection.

2.4.1 Tropical atmospheric variability

A number of early papers have proven the interaction between the Antarctic sea ice and atmospheric circulation (Walsh, 1983; Wendler and Nagashima, 1987; James, 1988). According to Walsh (1983), the interaction occurred due to the strong fluctuation produced between the Antarctic sea ice and the atmosphere for observation and modelling. While based on James (1988), the physical profile of the Antarctic itself was one of the factors that drove the hemispheric planetary waves, which might influence the large scale feature of the middle latitude jet near New Zealand. Earlier investigations were primarily focused on sea ice and tropical variabilities, in particular, the ENSO (Simmonds and Budd, 1991; Simmonds and Wu, 1993; Godfred Spenning and Simmonds, 1996; Simmonds, 2003a; Parkinson, 2004; Simmonds et al., 2005; Pezza et al., 2008). The ENSO is a major natural tropical climate event that occurs over a period ranging from a year to a decade and is defined by changes in sea surface temperature, or MSLP, between the east and west of the tropical Pacific. This event has a significant impact on a variety of climate variables throughout the tropics and subtropics (Simmonds and Jacka, 1995). The impact of ENSO variability on the Antarctic climate has been explored in a number of research studies (White and Peterson, 1996; Yuan and Martinson, 2001; Turner, 2004; Turner et al., 2009; Schneider et al., 2012). All those previous studies indicate that the Ross, Bellingshausen, Weddell, and Southern Indian Ocean sectors were most affected by these phenomena. Yuan and Martinson (2000), in studying the effect of the ENSO variability, successfully reported a link between the surface air temperature in the Drake Passage and the central tropical Pacific. A study also identified the connection between the high latitude modes in the subpolar region and ENSO variabilities. For example,

White and Peterson (1996) discovered that ENSO influenced the Antarctic circumpolar wave. Antarctic circumpolar wave is a large-scale coupled ocean-atmospheric wave that propagated eastward movement across the Southern Ocean. This wave has an average speed of 6 - 8 cm/s and takes 8 – 10 years to circle the Southern Ocean (White and Peterson, 1998).

Extension from the ENSO linkage, Yuan and Martinson (2000; 2004) found the connection between tropic and interannual variability of sea ice which was dominated by a link of ENSO quasi-stationary wave named the Antarctic Dipole. Antarctic Dipole is a wave that consists of weaker expansion movement and a strong stationary mode. It is arising from ENSO where it elevated Rossby wave trains (Turner, 2004; Yuan, 2004; Yuan et al., 2018). It involves sea ice, surface air temperature, and sea surface temperature anomalies that are illustrated in the tropical Pacific and Atlantic Antarctic regions. In details, during the warm event, there was a warm temperature and less sea ice over the Pacific centre dipole and a cold temperature and more ice in the Atlantic centre dipole. Throughout previous studies, what can be summarized is that ENSO influences the Antarctic sea ice via the mechanisms of Rossby wave propagation caused by tropical convection (Mo and Higgins, 1998), change of the jet stream caused by tropical sea surface temperature change (Bals-Elsholz et al., 2001), and poleward affecting anomalous zonal and meridional circulation (Liu et al., 2002; Yuan, 2004).

Aside from ENSO, researchers have examined the relationship between the sea ice and the Indian Ocean dipole mode (Saji et al., 1999; Nuncio et al., 2015; Feng et al., 2019). Indian Ocean dipole mode is defined by the anomalous sea surface temperature difference between the western and eastern regions of the Indian Ocean. Positive and negative of Indian Ocean dipole corresponds to increase and decrease of the sea ice

anomalies over the Ross Sea sector. The signal from the wave train Indian Ocean dipole has aided in forming and retreat of the sea ice over the. The wave signal was generated by three pressure centre waves (low, high, low) propagating from the Indian Ocean to the Ross Sea. When the wave train moved northward and southward, the pressure centre wave brought cold and warm air to the polar seas, which caused weak positive and negative ice anomalies near 60° E and 90° E (Nuncio et al., 2015). In a different study, it was shown that Indian Ocean dipole has an influence on the variability of the sea ice anomalies in the Atlantic and Pacific Oceans, together with the Weddell and Ross Seas (Feng et al., 2019). However, because the fluctuating connection that exists between ENSO and Indian Ocean dipole is strong in the austral spring, it can be tough to determine which is responsible (ENSO or Indian Ocean dipole) for Antarctic sea ice variation, especially over west Antarctica. Nuncio and Yuan (2015) figured that the influence of Indian Ocean dipole on the Antarctic is insignificant in the absence of ENSO. When Indian Ocean dipole occurs in the absence of ENSO, it mostly impacts air circulation over the southern Indian Ocean and the western Ross Sea, with minimal impact in West Antarctica. When ENSO and Indian Ocean dipole occur together, the Rossby wave is likely to move farther toward the Antarctic Peninsula. While Feng et al. (2019) found that the sea ice anomalies in the eastern Ross Sea and the Pacific Ocean disappeared, the sea ice in the Atlantic Ocean reduced and drifted westward as the ENSO signal was removed from the Indian Ocean dipole. While the sea ice anomalies over the Weddell Sea remain almost unaffected. In a recent study by Kim et al. (2023), it was described that in the austral summer, ENSO and the Indian Ocean dipole contribute about 20% – 30% of the variations in total sea ice concentration over the West Antarctic. The study has identified two mechanisms for tropical variability affecting Antarctic sea ice. First, the Rossby wave train, which is connected with ENSO and Indian Ocean dipole, creates a high-pressure atmospheric circulation in the Amundsen-Bellingshausen Sea, resulting in the

accumulation and melting of sea ice along the Antarctic Peninsula or Weddell Sea and the Amundsen Sea, respectively, via atmospheric temperature advection. Second, the Amundsen-Bellingshausen Sea's high pressure air circulation anomalies transfer heat and water vapor from low latitudes into the Amundsen and Ross Seas, increasing downward energy flux and providing an ideal condition for sea ice melting.

Apart from Indian Ocean dipole, the variability of sea surface temperature in the tropical Indian Ocean is controlled by Indian Ocean Basin mode. The Indian Ocean Basin mode illustrated homogenous sea surface temperature variability over the tropical Indian Ocean at interannual time intervals (Saji et al., 1999). It also has a close connection with ENSO (Xie et al., 2016). A boreal wintertime El Nino event, in particular, is frequently an indicator of the positive phase of the Indian Ocean Basin mode in the following boreal spring (Wang et al., 2019). Based on Saji et al. (1999) and Yang et al. (2007), the Indian Ocean Basin mode is certainly induced by ENSO, while Wang et al. (2019) discovered that the boreal wintertime El Nino event may cause the positive phase of the Indian Ocean Basin mode in the following boreal spring. Meanwhile, Taschetto et al. (2011) discovered that after the ENSO forcing is eliminated, a part of the Indian Ocean Basin mode signal remains. Yu et al. (2022) revealed that the presence of an Indian Ocean Basin mode - Antarctic sea ice anomaly teleconnection is substantially stronger in autumn and austral spring than in winter and summer. Specifically, during the positive phase of the Indian Ocean Basin mode, the Bellingshausen and northern Weddell Seas have significant positive sea ice anomalies, whereas negative anomalies occur over the Amundsen Sea, the southern Atlantic Ocean, and coastal seas from Dronning Maud Land.

Antarctic sea ice variability within the Pacific sector, specifically in the eastern Ross, Amundsen, and Bellingshausen Seas, are particularly influenced by the primary

driving mechanism (Purich et al., 2016), the Interdecadal Pacific Oscillation (IPO). The IPO is defined based on sea surface temperature anomalies with a unique tripole pattern over the Pacific Ocean containing three large centres of action, which vary on a decadal timescale (Henley et al., 2015). The three main regions of high modal variability within the Pacific sea surface temperature pattern are the central west of the North Pacific, the eastern equatorial Pacific, and the central-west South Pacific (Henley et al., 2015). The negative phases of IPO have a more significant relationship to El Nino or La Nina variance (Parker et al., 2007). The connection between sea surface temperature anomalies inherent in the IPO and their relationship to ENSO varies depending on whether sea surface temperature is increasing or decreasing. When sea surface temperature increases in the tropical Pacific due to the IPO, there is no relation to ENSO (Power et al., 1999). The warm equator phase of the IPO is related to the warming of the sea surface temperature; this warming extends further west than it does when related to ENSO (Parker et al., 2007). However, when the sea surface temperature decreases in the topical Pacific due to the IPO, there is a slight relation to ENSO (Power et al., 1999). The IPO is not directly related to the ENSO variance, but it could potentially be a lagged ENSO signature (Parker et al., 2007). Another factor contributing to the increase in the average Antarctic sea ice extent is the intensification of the Amundsen Sea Low, mainly over the Antarctic Peninsula and Ross Sea (Meehl et al., 2016; Turner et al., 2016; Landrum et al., 2017; Raphael et al., 2018). The Amundsen Sea Low is defined as a low pressure centre at about 150^{o} W off the coast of West Antarctica. The area of the Amundsen Sea Low has the most variable MSLP of any location in the Southern hemisphere (Turner et al., 2014). Notably, the deepening of the Amundsen Sea Low is primarily connected to the IPO (Clem and Fogt, 2015; Meehl et al., 2016; Purich et al., 2016), and these changes in the Amundsen Sea Low affect the regional atmospheric circulation, which in turn modulates the local sea ice conditions. Regional Antarctic circulation changes can be traced back to

convective heating and precipitation anomalies correlated with the IPO in the equatorial eastern Pacific, as well as in the tropical Atlantic regions and South Pacific convergence zone (Meehl et al., 2016). In winter, the anomalous equatorial convection in the negative IPO phase generates a pair of upper tropospheric anticyclone circulation anomalies. These high-pressure cells in the upper troposphere alters the upper-level vorticity and divergence in the tropics and serve as a source for Rossby waves, which propagate poleward following a great circle trajectory. The teleconnection pattern ultimately appears as positive (high pressure) anomalies at low latitudes and negative (low pressure) anomalies at middle latitudes in the southern hemisphere due to larger zonally symmetric circulation anomalies (Karoly, 1989). These entire processes play a role in the climatological seasonal cycle, and understanding this cycle helps climate scientists observe what influence the Antarctic sea ice has on a global scale.

Another oscillation connected with the Antarctic sea ice is the Atlantic Multidecadal Oscillation (AMO). The AMO is also considered a leading model for global variability on decadal timescales (Li et al., 2014), particularly in the Atlantic sector. The AMO takes place over a much longer period than many other oscillations by occurring over 60 to 80 years (Wilby, 2017) in the North Atlantic Basin as a variability pattern in sea surface temperature (Henson, 2014; Wilby, 2017). The AMO contains two primary local maxima, one in the tropical Atlantic and the other in the south of Greenland (Li et al., 2014). Over half a degree of warming in West Antarctica was due to the AMO manifesting in the north Atlantic sea surface temperature as an upward trend since 1979 (Li et al., 2014). However, the complete spatial pattern of the West Antarctic warming cannot be fully clarified by the changes in the Atlantic sea surface temperature (Li et al., 2014). A study done by Li et al. (2014) indicated the sea ice cover and the surface air temperature in the Weddell Sea to be susceptible to AMO influence via an indirect change

in the tropical Atlantic circulation. The AMO also plays a key role in generating the thermohaline circulation, predominantly in the formation of the Antarctic bottom water (Li et al., 2014). The thermohaline circulation is the deep ocean circulation driven by water density (Hartmann, 1994). Therefore, the AMO is linked to thermohaline circulation changes since it is recognised as an ocean surface response. The Southern Ocean thermohaline circulation is speculated to interact with the AMO (Li et al., 2014).

Apart from the oscillation stated above, Madden – Julian oscillation (MJO) also has proven to have an influence on Antarctic sea ice extent. However, this teleconnection has not been extensively explored. The MJO is the most significant component of the tropical atmosphere's intraseasonal (30 – 90 day) variability. It is recognized as an indicator of weather and climate predictability, from sub seasonal to seasonal (Virtal et al., 2017). A study done by Lee et al. (2019), illustrated the anomalies of the sea ice extent shows significant melting and freezing as the development phases of MJO during the austral winter. This is because the circulation anomalies caused by the MJO reach high latitudes and lead to advection of meridional temperature anomalies, resulting in changes in sea ice extent over different sector. Hsu et al. (2021) found that the decadal variation of the MJO has contributed to the summer cooling trend in East Antarctica by about 20% - 40%. Both observational and experimental analyses of climate models illustrate consistent features, explaining that the decrease (and increase) of atmospheric convection in the Indian Ocean (and western Pacific) over the past two decades has produced a net cooling flow over East Antarctica via modification of the atmospheric circulation associated with poleward propagating Rossby wave trains. Lafleur et al. (2021) investigate the temporally delayed response of Antarctic sea ice concentration to tropical MJO forcing, with a particular emphasis on analyzing regional daily sea ice variability. The preliminary results show that sea ice anomalies vary regionally and time lag, with

the Bellingshausen and Amundsen and Ross Seas being the most impacted by intraseasonal effects. Yamazaki and Nakamura (2021) discovered that stratospheric quasi-biennial oscillation has an influence on tropical convection, causing the Rossby wave train to travel to southern high latitudes and, in turn, influencing austral winter Antarctic sea ice. During the easterly phase of quasi-biennial oscillation, sea ice concentrations over the Weddell Sea, Ross Sea, and approximately 90° E grew, while those in between retreated, generating a wave-3 pattern.

2.4.2 Climate variability indices

In addition to climate variabilities, the Antarctic sea ice has been closely related to the variability of meteorological parameters at different timescales, such as sea surface temperature, precipitation, summer rainfall in China, western South African rainfall and Indian summer monsoon rainfall (Yuan and Martinson, 2000; Xue et al., 2003; Dugam et al., 2004; Lijuan et al., 2006; Blamey et al., 2007; Rai et al., 2008; Prabhu et al., 2009; Liu et al., 2011; Liu et al., 2018; Prabhu et al., 2021; Zhou et al., 2021). In a study published by Bromwich et al. (1998) successfully found the loss of Antarctic sea ice can lead to significant changes in pressure, vertical circulation, and precipitation in the middle latitudes of the Northern Hemisphere (August-November). These changes are caused by a shift in the southern polar front jet, which merges with the subtropical jet in the upper troposphere. This shift results in a decrease of easterly winds at high latitudes. The loss of Antarctic sea ice is a contributing factor to the increased precipitation that falls in northern China in September, especially along the coast. In addition, studies have shown that Antarctic sea ice is closely linked to rainfall patterns in China during the boreal summer. This connection is evident in the fact that more rainfall falls in the north of the Yellow River region, while less rainfall falls in the south and northeast of the Zhujiang River region (Xue et al., 2003). The study found that as the amount of sea ice in Antarctica

is increasing, the East Asian summer monsoon will become stronger. This is because the expansion of sea ice will lead to a decrease in sea level pressure in East Asia and an increase in sea level pressure in the North Pacific. The resulting pressure difference will cause stronger winds to blow from the Pacific to East Asia, bringing with them more moisture and rainfall. The relationship can also be seen across different regions of Antarctica. For example, the increasing and declining of the sea ice in the eastern Ross Sea, the eastern Bellingshausen, and the Weddell Sea are connected to a higher and lesser southern China rainfall and the Yangtze River's lower streams, and less and higher rainfall in other locations. Also, the increasing sea ice in the eastern Ross Sea weakened the subtropical high of the western Pacific and the East Asian summer monsoon. The cross seasonal nature of this connection might be related to the impacts of sea surface temperature anomalies over the Indian Ocean and the eastern tropical Pacific Ocean (Liu et al., 2018). A study that was recently conducted found that changes in sea ice concentrations in the southern Indian and Pacific Ocean basins during the boreal summer are linked to changes in autumn rainfall in western China. The results show that the correlation coefficient between them is 0.51 at the 99% significance level. It is explained by the changes in the Lake Balkhash trough, the South Asian low-pressure system, the East Asian jet stream location, and the amount of water vapour transported (Zhou et al., 2021). Apart from that, there is also a study related to the rainfall variability in the South Africa. Blamey et al. (2007) study shows that the eastern of the Weddell Sea sector has a positive correlation with rainfall in the Western Cape during the winter months. The authors suggested that it may be because of the sifting of subtropical jets and middle latitude storm tracks, which changed the convergence and uplift over western South Africa.

In a different study, the sea surface temperature in the southeast Indian Ocean was identified to have a strong relationship with the variability of Antarctic sea ice, which has precursors towards the Australian summer monsoon, the Indian summer monsoon, and ENSO phenomena (Rai et al., 2008). In a different study, Rai et al. (2008) found that some parts of the Mascarene High are highly significantly associated with sea ice variability over a 6-season time period, with r equal to 0.36. The connection also has been seen over the western Indian Ocean where the sea ice concentration in the Indian Ocean, Ross Sea, and Antarctic Peninsula is the most affected by the change in sea surface temperature over the region (Liu et al., 2011). According to the authors, the teleconnection occurred due to the changes in the atmosphere at the tropospheric level. However, the explanation of the physical process is still unclear and needs further investigation.

Another meteorological parameter that has been connected to the Antarctic sea ice is Indian summer monsoon rainfall. Dugam et al. (2004) found that an increase in Antarctic sea ice extent during the previous winter was significantly correlated with a decrease in Indian summer monsoon rainfall across all of India, as well as two specific regions: west-central and north-west India. The results show that the correlation coefficients (r) are - 0.56, - 0.42, and - 0.46 for all of India, west central India, and north-west India. Deficient monsoon years lead to up to usual sea ice extent, whereas excess or normal monsoon years lead to less than normal sea ice extent. There was also a positive, coherent propagating pattern between the Antarctic sea ice extent in March and the summer monsoon rainfall in India, where interannual sea ice extent variability in the western Pacific Ocean sector displays favourable interactions with rainfall in all of India ($r = 0.52$), the centre north east ($r = 0.50$), and peninsular India ($r = 0.52$) (Prabu et al., 2009). While a decrease in sea ice in the Bellingshausen–Amundsen Sea sector during

the austral summer is linked to a decrease in Indian summer monsoon rainfall (Prabhu et al., 2010; Bajish et al., 2021). This was stated in the study of Prabhu et al. (2010), where the correlation coefficient between the austral summer sea ice extent of the Bellingshausen and Amundsen sea sectors of the previous year and all Indian summer monsoon rainfall is - 0.42. Bajish et al. (2021) also made similar statements. They found that the Bellingshausen and Amundsen sea sectors show the most significant relationship with the India summer monsoon rainfall for all seasons (autumn, $r = -0.5$; winter, $r = -0.44$; spring, $r = -0.34$; and summer, $r = -0.4$) without any time lag. This is caused by the presence of cyclonic (or anticyclonic) air flow in the Ross Sea and Bellingshausen–Amundsen Sea sector during periods of more (or less) sea ice leads to anomalously warm (or cold) sea air and sea surface temperatures, which in turn eases the anomalously low (or high) sea ice conditions in the Bellingshausen–Amundsen Sea sector. Furthermore, ENSO is also the possible bridge connecting the linkage (Bajish et a., 2021). A study published by Prabhu et al. (2021) found that there is a direct association between Indian summer monsoon rainfall and sea ice area over the Western Pacific Ocean, and an inverse association between Indian summer monsoon rainfall and sea ice area over the Bellingshausen and Amundsen Seas, where the highest significant correlation coefficient is in July with values of 0.44 and - 0.39, respectively. They believed the sea surface temperature variability over the equatorial Pacific modulated the large-scale atmospheric bridge connecting the Antarctic sea ice and Indian summer monsoon rainfall. The increase in sea ice area in the Bellingshausen and Amundsen Seas (Western Pacific Ocean), along with warm sea surface temperatures in the equatorial central Pacific (equatorial Western Pacific) and rising air currents over the region, can negatively (positively) impact the Indian summer monsoon rainfall.

Many studies have shown how the signal of atmospheric circulation over the polar region known as SAM or AAO can spread its influences across the northern hemisphere region. For example, the relationship between SAM or AAO and East Asia (Sun et al., 2009; Zheng et al., 2015; Wu et al., 2015; Dou et al., 2021) and precipitation over south-eastern South America (Silvestri and Vera, 2003), American Summer Monsoon (Jian-Qi, 2010) and Indian summer monsoon rainfall (Prabhu et al., 2016; Pal et al., 2017). The researchers proposed several physical mechanisms. One of the studies suggested that this is due to the anomalous meridional circulations along the central South Pacific where the Maritime Continent region serves as a bridge to connect the AAO and Yangtze River valley rainfall (Sun et al., 2009). Other than the Maritime continent, the Indian Ocean sea surface temperature also acts as an "ocean bridge" in modulating the rainfall over the Maritime continent, leading to wave energy propagation to the Yangtze River valley region (Dou et al., 2021). Some studies have found that SAM can influence tropical sea surface temperature variability (Jian-Qi, 2010; Fletcher and Kushner, 2011; Zheng et al., 2017; Pal et al., 2017). The negative (and positive) phase of SAM during February - March creates an abnormal meridional circulation over the central Pacific that lasts until the next boreal summer and propagates from subpolar to equatorial latitudes, warming (and cooling) the central equatorial Pacific region. As a result, the Indian subcontinent experiences weaker (and stronger) monsoon rainfall (Prabhu et al., 2016). While Pal et al. (2017) illustrated that high SAM index years cause a warm sea surface temperature at about 30^{o} S and lead to strengthened southerly flow over the south of India. Apart from that, Pohl et al. (2010) investigated the link between the AAO variability and the rainfall variability over South Africa under the influence of MJO and ENSO. The result illustrated that the AAO's opposing phase affects the quantity of daily rainfall in southern Africa, whereas the positive phase causes higher rainfall in central South Africa. This statistical association tends to be weak during El Nino years but very significant during La Nina

occurrences. While, AAO and MJO have a very low common variance. In a recent study by Gnanaseelan and Anila (2021), they found that SAM in the months of February and March has a significant effect on rainfall in Central India and the Western Ghats, whereas SAM in the month of May shows a strong positive association with June and July rainfall across India. They suggested that the connection of the February–March SAM to Indian summer monsoon rainfall is via the equatorial Pacific, while the May SAM connects via the subtropical (southern) and tropical Indian Oceans.

2.4.3 Climate model

Climate models are crucial tools for discovering how polar-tropical teleconnections work and how they might evolve in the future (Li et al., 2021). In advancing this knowledge, a few researchers used numerical and modelling experiments in studying and identifying the polar and tropic connections (Bromwich et al., 1998; Hines et al., 2002; Liu et al., 2002; Li et al., 2013; Guo et al., 2013). In a previous study by Bromwich et al. (1998), the authors used the National Center for Atmospheric Research (NCAR) Community Climate Model Version 2 (CCM2) to evaluate the impact of the Antarctic sea ice anomalies on the East Asian monsoon for 15 years. The numerical experiment results agree with an observational study where established monsoon parameters are correlated with the variability of Antarctic sea ice. Hines et al. (2002) discovered a similar result, where the NCAR CCM2 numerical simulation was able to produce similar teleconnection features during late boreal summer with the observation results from the same year. However, the models' compulsion is at high southern latitudes. Purich et al. (2019) investigated how changes in the tropical Indian and Pacific climates affected the amount of Antarctic sea ice in the springtime of 2016 using the ACCESS1.0 climate model, which is a fully coupled global climate model. The model illustrated that the decline of the sea ice was caused by a Rossby wave teleconnection from the tropical

Indian Ocean with less influence from the Pacific. Lee et al. (2021) used a linear baroclinic model (LBM) to study how the background flow influences the teleconnection between the tropical Indian Ocean and the Western Pacific to West Antarctica. However, most of the teleconnection studies involving the numerical simulation model were about the Arctic. For example, Guo et al. (2013) used computer atmosphere-ocean and atmosphere models to explore the process how the Arctic sea ice variability during spring affect the East Asian summer monsoon. The results of the study show that the way in which the mechanism works as observed is in line with the way it was simulated. As mentioned above, the sea ice over the Antarctic is not well represented in the CMIP5 climate model. This means that the model's ability to simulate teleconnections related to Antarctic sea ice is limited. The simulation results were in direct opposition to the observation data. Thus, further studies by the researchers are needed, especially using the coupled atmosphere - ocean model. Although the Antarctic sea ice extent plays an important role in the tropical climate system, the fundamental mechanism behind the connection between changes in Antarctic sea ice extent and Indian summer monsoon rainfall is still not well understood. This is due to a lack of teleconnection references and other factors, such as the nature of the relationship between the two systems, the ocean, and the atmosphere. These factors have limited researchers' ability to explore this topic using model simulations.

2.5 Indian summer monsoon rainfall teleconnection

The Indian summer monsoon has been observed to be teleconnected with various parameters. The tropical climate variability influences the large-scale movement of air and the rising of moist air over India via different teleconnections between the atmosphere and the ocean (Kumar et al., 1999; Asok et al., 2001; Chakraborty et al., 2018). El Nino have a major impact in determining the amount of rainfall that India receives during the

Indian summer monsoon season. ENSO causes significant changes in surface pressure, winds, and rainfall between the Pacific and Indian Oceans, which can have a major impact on India's climate. Several studies have proved in general, warm ENSO phase or El Nino events are frequently associated with the drought years in India, while the cold phase or La Nina event is associated with average wet years. This is because the Walker circulation, a band of strong winds that flows east-west across the tropical Pacific Ocean, shifts eastward or westward during El Niño and La Niña events (Walker et al., 1932; Sikka et al., 1980; Turner et al., 2005; Kumar et al., 2006; Roy, 2017).

The Indian summer monsoon is not solely connected to the Pacific Ocean, but there is also a link to the Atlantic Ocean. There is evidence that the Indian monsoon is inversely correlated with sea surface temperature in the subtropical Atlantic Ocean (Yadav, 2008; Wang et al., 2009; Rajeevan and Sridhar, 2008; Pottapinjara et al.,2016; Yadav et al., 2018; Sabeerali et al., 2019). Warm water in the tropical Atlantic Ocean can create a high-pressure system (anticyclonic circulation) over India and the western North Pacific Ocean, which can lead to decreased rainfall during the Indian summer monsoon (Kucharsk et al., 2007). The anomalous Atlantic sea surface temperatures in the Atlantic Ocean can also change the way the Asian jet stream blows, which can lead to an east-west pattern of rainfall in India (Yadav et al., 2018). Previous studies proposed that the tropical Atlantic also channels an interannual variability mode known as the Atlantic zonal mode or the Atlantic Nino, which is comparable to but weaker than ENSO (Zebiak 1993; Servain et al. 2000; Lubbecke et al. 2018). A warm (and cold) Atlantic Nino phase causes a low-level divergence (and convergence) across India, resulting in fewer (and stronger) summer monsoon rainfall in India (Kucharski et al., 2007; 2008; 2009). The monsoon depression trajectories are also affected by the Atlantic Nino. In reaction to a warm (and cold) Atlantic Nino event, the frequency of monsoon depressions originating

over the Bay of Bengal decreases (and increases), which can lead to a decrease (and increase) in rainfall across India (Pottapinjara et al., 2014). Although the number of studies on the Atlantic Niño's effect on the Indian monsoon is still relatively low, it is gaining traction among scientists (Kucharski et al., 2016; Barimalala et al., 2013; Pottapinjara et al., 2014; 2016;2020; Yadav et al., 2018; Sabeerali et al., 2019).

The North Atlantic Oscillation (NAO), an extratropical oscillation in the North Atlantic Ocean, also has an important influence on summer rainfall in India. The relationship is stronger for rainfall in smaller regions of India (Kakade and Dugam, 2006). All studies have found that NAO has an inverse relationship with Indian summer monsoon rainfall in the same and subsequent years (Dugam et al., 1997; Kakade dan Dugam, 2000, 2006; Bhatla et al., 2016). The connection was enhanced when the spring NAO index was categorised according to Quasi-Biennial Oscillation phases (Bhatla et al., 2016). Moreover, strong negative (and positive) NAO produces tropospheric temperature anomalies in Eurasia and results in the decrease (and increase) of the Indian monsoon rainfall (Goswami et al., 2006; 2008).

Some scientists believe that the Indian Ocean dipole also has a significant impact on the Indian summer monsoon (Ashok et al., 2001; Anil et al., 2016; Cherchi et al., 2021; Prajeesh et al., 2021). In particular, the positive (and negative) Indian Ocean dipole phase has been linked with an increase (and decrease) in monsoon rainfall over the Indian region (Prajeesh et al., 2021). During a positive Indian Ocean dipole phase, the warm water in the western Indian Ocean causes winds to blow towards the east. This brings more moisture from the southeastern Indian Ocean to the Bay of Bengal, which leads to increased rainfall in the region (Annamalai et al., 2010; Cherchi et al., 2021). The effect of negative Indian Ocean dipole on Indian summer monsoon rainfall was due to a change

in the location of the convective system (Ajayamohan et al., 2008). However, the Indian Ocean dipole and ENSO have a simultaneous influence on Indian summer monsoon rainfall (Pokhrel et al., 2012). The positive Indian Ocean dipole considerably lessens the negative effect of ENSO when these events occur in the same phase. As a result, an Indian Ocean dipole event's presence can help alleviate the rainfall deficit due to ENSO over western India and the western monsoon trough (Ashok et al., 2004; Ashok and Saji, 2007).

Early studies show a connection between the Indian summer monsoon and Australian summer monsoon (Gregory, 1991). It is due to the strong convection over the Indian monsoon region that migrates southeast to Australia and creates a robust Australian monsoon (Meehl, 1997). Interestingly, the Australian monsoon has no effect on the next Indian summer monsoon (Hung et al., 2004). Furthermore, low temperatures over Australia have also been linked with the Indian monsoon. It has been discovered that enhancing the evaporation rates over the eastern tropical Indian Ocean will lead to increased rainfall in western India (Lee and Koh, 2012). Additionally, several authors indicate that the recent trend toward drier conditions in northern China during the summer is, at least in part, the result of a synchronized drying trend over India during the summer (Greatbatch et al., 2013).

The Indian summer monsoon has also been intensely connected with the sea ice over the different sectors of the Arctic region (Prabhu et al., 2011; 2017; Chatterjee et al., 2021). Prabhu et al. (2012) found that there is a negative relationship between the amount of sea ice in the Kara and Barents Seas in the preceding autumn and the amount of rainfall in India during the following summer monsoon season. Specifically, extreme negative anomalies of sea ice in October could be an indication of a drought in the following year.

In a different study, Prabhu et al. (2017) showed that changes in the Greenland Sea ice area can affect Indian monsoon rainfall indirectly, through atmospheric disturbances caused by warm sea surface temperatures in the equatorial central Pacific. An extreme negative of sea ice in the Greenland Sea ice during the fall of the year caused a pattern of atmospheric circulation similar to the negative phase of the Arctic Oscillation. This pattern features a high-pressure system at the North Pole and a low-pressure system at mid-latitudes. This pattern persisted until the following winter. The following summer, a disturbance in the atmosphere caused an anomalous meridional wave train over the equatorial central Pacific. This wave pattern featured an ascending branch from the surface to the troposphere. Once the central Pacific Ocean warms up in the spring and gets even warmer in the summer, it causes an anomalous zonal-wave circulation to form over the Indian subcontinent. This pattern features sinking air that weakens the monsoon circulation, which is responsible for bringing rain to India. As a result, there is less rainfall. A recent study by Chatterjee et al. (2021) suggested that there may be a connection between the sea ice in the Arctic and the rainfall in India during the late summer monsoon season. The loss of sea ice in the Kara Sea has changed the jet stream variability and the anomalous meridional circulation over northwestern Europe. This caused a Rossby wave train to form, which has led to warm air and sea surface temperatures in the northwestern Arabian Sea. The increased convection in the central Indian region can be seen from the anomalous upward vertical velocity. In another study by Sundaram et al. (2022), they revealed the teleconnection between the Indian summer monsoon rainfall and Arctic sea ice in the month of September. The results documented that a stronger (and weaker) Indian summer monsoon year corresponds to the increase (and decrease) of Arctic sea ice, primarily over the Chukchi and Beaufort Seas. Specifically, a stronger (or weaker) Indian summer monsoon can lead to a positive (or negative) NAO, which in turn can weaken (or strengthen) the Beaufort Sea High. This

can then cause more (or less) sea ice to form over the Chukchi-Beaufort Sea region.

2.6 Conclusion

After reviewing previous research, it is clear that there is no convincing evidence to explain the connection between Antarctic sea ice and Indian summer monsoon rainfall. There is currently a lack of literature on Antarctic sea ice and the tropics, particularly when it comes to physical or dynamical causes. The literature on the connections between Antarctica's sea ice and the Asian monsoon, notably over the Indian subcontinent, is still sparse. Most previous studies have examined the relationship between Arctic sea ice, the East Asian monsoon, and rainfall over China, particularly the mechanisms involved, using either observational or modelling techniques (Zhao et al., 2004; Wu et al., 2009a; 2009b; Guo et al., 2014; Lin et al., 2018; He et al., 2018; Shen et al., 2019; Han et al., 2021; Zhou et al., 2021; Zhang et al., 2021). For example, Wu et al. (2009a) revealed that the spring negative sea ice concentration anomalies in the Greenland Sea and the western Arctic Ocean created the summer wave train over Eurasia at 500 hPa height anomalies. The summer wave train is a major reason for the increasing the summer rainfall in northern and northeastern China, and central China between the Yangtze River and the Yellow River, and the regions along the Yangtze River, while also decreasing the summer rainfall in south and southeast China. A study by Shen et al. (2019) suggests that sea ice anomalies over the Barents and Kara Seas could influence the atmospheric circulation and precipitation in eastern China during August. The analysis revealed that the negative sea ice area anomalies over the Barents and Kara Seas cause divergence anomalies in the polar region and convergence anomalies in the Caspian Sea at upper levels. The anomalous divergent and convergent flows produce an eastward propagated Rossby wave train towards East Asia. Energy growth in East Asia developed teleconnections between the Pacific and Japan, which were favourable for the dipole rainfall anomaly pattern over

eastern China. A study that has recently been conducted by Han et al. (2021) found that early spring sea ice loss in the Barents Sea can influence midsummer rainfall patterns in northeastern China, using observational data and atmospheric modelling experiments. The findings indicated that an increase in sea ice area in the Barents Sea is followed by positive rainfall anomalies in the north of the northeast of China and by negative anomalies in the south. This is due to the surface air temperature anomalies and vertical stability over the Barents Sea changing due to turbulent heat flux. Furthermore, the anomalous circulation that developed over Europe and the Mediterranean Sea produced the Rossby wave, which propagated eastward from the Silk Road toward East Asia. Zhang et al. (2021) found that a decrease in sea ice concentration in the Barents Sea before winter can lead to positive geopotential height anomalies over the polar region. This weakens the polar vortex and westerly winds, resulting in an indirect cyclonic anomaly over West Siberia. These anomalous atmospheric circulation patterns led to a zonal dipole pattern of snow water equivalent anomalies in the mid-high latitudes of Eurasia before winter, with less snow water equivalent over Eastern Europe and more snow water equivalent over West Siberia. This will likely result in more precipitation over northeast China. Although a lot of research has been conducted on the teleconnection between sea ice and the tropics, the underlying physical processes are still not fully understood. More research is needed, especially in the southern hemisphere (Liu et al., 2011). Furthermore, it is important to understand how anthropogenic forgings ill affect and alter teleconnection signals in the future. Climate models are a vital tool for comprehending the mechanisms of tropical-polar teleconnections and their projected changes (Li et al., 2021). Despite their capabilities, the models have limitations and uncertainties, which prevent accurate projections of the future. This study also evaluated the performance of selected CMIP5 models in simulating the observed teleconnection pattern between Antarctic sea ice extent and the Indian summer monsoon.

CHAPTER 3

DATA AND METHODOLOGY

3.1 Introduction

This chapter provides the sources and descriptions of the datasets includes reanalysis and observation data, the selection of study area, description of selected CMIP5 models includes the historical and future projection, as well as the methods used to analyze the data in this study. Tools used for the analysis also will be discussed in this chapter.

3.2 Sources of the dataset (reanalysis and observation data)

3.2.1 Reanalysis data

Reanalysis is a process of combining historical observations with numerical weather prediction (NWP) models to create a consistent gridded dataset of climate data. This dataset can be used to monitor climate change, study past climate variability, and improve NWP models. As technology and processing capacity have advanced, reanalysis datasets have become an extensively used resource for the study of atmospheric and oceanic processes and predictability. This is due to the fact that reanalysis data provides the most complete picture of previous weather and climate that is currently accessible. Reanalysis datasets are used in areas other than meteorology, such as renewable energy, agriculture, policy - making and business, telecommunication, and even bird migration (Dee et al., 2011). The benefits of using the global reanalysis dataset are that the data is not influenced by method modifications because of the way reanalysis datasets are generated. They are basically generated based on fixed, modern versions of numerical climate models integrated with observation data (Bromwich et al., 2011). Aside from that,

the calculated variables are compatible with physical principles and observations. This is because a forecast model is utilized as the unifying context in which disparate observations from various sources can be absorbed and matched (Dee et al., 2011).

Reanalysis data can be categorized into multiple types that are provided by various organizations across the globe. It depends on the data sources used, the methods employed, and the spatial and temporal resolutions. Some of the most commonly used reanalysis datasets include the ERA-Interim, NCEP-NCAR (first generation), NOAA, and ERA5, the newest reanalysis data. The quality of each generation of the data was improved by using more advanced methods of combining observations with model predictions. However, it is worth noting that each reanalysis dataset has its own constraints, such as limited periods of time and climate variables. Therefore, the ERA-Interim, and NOAA reanalysis fields are used in this study to evaluate the relationship and mechanism and also as a standard of comparison for the model simulations. In the following section, a brief description of ERA-Interim and NOAA is presented.

3.2.1.1 ERA-Interim

The ERA-Interim is a global dataset of atmospheric data that is created by the European Centre for Medium-Range Weather Forecasts (ECMWF) by combining observations from radiosondes, ground stations, and satellites with forecast models. It is a project of continuity for the 40 year ECMWF Reanalysis (ERA-40) (Simmons et al., 2007). The ERA-Interim dataset covers the period from 1979 to the present. Data prior to 1979 is not available because satellite sounder data, which is used in the data assimilation process, was not available before then. The goal of this project is to address the challenges that were encountered in the previous version of the ERA reanalysis, such as simulating the hydrological cycle, accurately representing the stratospheric circulation,

and ensuring the consistency of reanalyzed geophysical fields over time (Dee et al., 2011). They also aim to enhance several technical problems in reanalysis, for instance, the collection of data, quality control, error remediation, and performance monitoring. In this project, they use a spectral approach to represent the basic dynamical fields and a reduced Gaussian grid with a resolution of 79 km, which is approximately uniform across the entire globe (Dee et al., 2011). ERA-Interim performs four analyses every day, at 00:00, 06:00, 12:00, and 18:00 UTC. The gridded data product is available from 0.125 degrees of spatial resolution until 3.0 degrees of spatial resolution (0.125° × 0.125 °, 0.5 ° × 0.5 °, 0.75 ° × 0.75 °, 1 ° × 1 °, 1.5 ° × 1.5 °, 2 ° × 2 °, 2.5 ° × 2.5 °, and 3 ° × 3 °) with 37 vertical heights describing the weather, ocean waves, and land surface conditions. The data covers hourly, daily, and monthly information from 1979 until August 2018. The details of the documentation of this reanalysis product were described by Dee et al. (2011). In this study, various monthly mean meteorological parameters used, such as the mean sea level pressure (MSLP), three different levels of geopotential height (250hPa, 500hPa, and 700hPa), 11 different levels of zonal and meridional component winds, and also vertical velocity or omega (1000, 925, 850, 800, 700, 600, 500, 400, 300, 200, and 100hPa). The data used is from the last 35 years, from January 1979 to December 2013, with a 0.75 degrees of spatial resolution (0.75º x 0.75º). The specific parameters used in this study are listed in Table 3.1. ERA-Interim is considered to be the most accurate of the various climate datasets, according to several studies, including those by Bromwich et al. (2011), Bracegirdle and Marshall (2012), and Simmons et al. (2014). It is worth noting that the ERA5 data integration method has significant improvements over ERA-Interim, with temporal resolutions and higher spatial. The research project was started before ERA5 was available, and the COVID-19 lockdown further delayed it.

3.2.1.2 National Oceanic and Atmospheric Administration Earth System Research Laboratory (NOAA-ESRL)

The Earth System Research Laboratory (ESRL) is a part of the National Oceanic and Atmospheric Administration (NOAA) research. The NOAA has been collecting and disseminating climate and weather data quite long time. The data available from 1850 until present. This system supports and operates datasets in various fields such as physical, biological, environmental, and chemical. The physical includes weather, atmosphere and climate. The ESRL is responsible for monitoring and investigating the atmospheric, physical, and chemical processes of the Earth's systems and producing informative products. They also responsible in improving the critical forecasting tools and weather for the private and public sectors ranging from hourly prediction, air quality and drought forecasts, to international science assessments that contain policy-relevant findings. The data provided a critical, long-term history of the Earth system required for evaluating global patterns. The monthly mean interpolated dataset of emitted outgoing long radiation (OLR) is available online at https://iridl.ldeo.columbia.edu/SOURCES/.NOAA/.NCEP/.CPC/.GLOBAL/.monthly/.olr/index.html?Set-Language=en. The gaps were filled with temporal and spatial interpolation. Details of the interpolation techniques has documented by Liebmann et al. (1996). The monthly data covers the period from June 1974 to December 2022 with a spatial resolution of approximately 2. 5º × 2. 5º latitude-longitude grids. In this study, the data spans a period of 35 years, from January 1979 to December 2013. This dataset was utilised to investigate the occurrences of convective activity near India during different phases of sea ice extent.

3.2.2 Observations data

Observation data is data that can be collected in various ways, such as from stations, satellite sensors, buoy and shipping records, and others. The advantage of using satellite data is that they provide extensive spatial coverage, especially where gauges can be installed. Moreover, satellite and radar technologies are free from the harsh conditions required to survey large swaths of land and ocean. The common observation datasets used in studying meteorology variability include sea ice, rainfall, sea surface temperature, and others such as GPCP, NSIDC, and HadS1TT. In this study, the GPCP, NSIDC, HadS1TT, and IITM observation data are used to evaluate the relationship and mechanism between the variables, as well as to provide a standard of comparison for the model simulations. In the following section, a brief description of GPCP, IITM, NSIDC, and HadS1TT is presented.

3.2.2.1 Global Precipitation Climatology Project (GPCP)

The Global Precipitation Climatology Project (GPCP) dataset is widely and frequently used among researchers regarding precipitation (Su and Neelin, 2003; John et al., 2009; Trenberth, 2011; Allan et al., 2013; Loeb et al., 2014). It is part of the Global Energy and Water Cycle Exchanges (GEWEX) activity under the World Climate Research Program (WCRP). The first version of the GPCP monthly dataset was released in 1997, covering the period from 1987 until December 1995 (Huffman et al., 1997). In August 2012, the GPCP product released its second version, known as GPCP v2.2. It uses improved emission and dispersion algorithms, GPCC precipitation gauge analysis, and DMSP F17 SSMIS input. The data is available until 2012 only, and the production of GPCP v2.2 datasets has ended. The current version of GPCP is v2.3 was improved by updating the procedures for cross-calibrating data from various satellite sensors and by updating the analysis of ground-based rain gauges (Adler et al., 2018). The GPCP v2.3

monthly product provides a reliable and uniform global precipitation analysis based on the integration of multiple satellite data sets over land and ocean, as well as a gauge analysis over land. The data is a combination of microwave and infrared, satellites, and rain gauge observations. The GPCP data is available for the period from January 1971 to the present. In this study, the latter version of GPCP v2.3 will be used to broaden the spatial scope and investigate the rainfall distribution pattern over the Indian subcontinent during different phases of the sea ice extent. The monthly global precipitation data with a spatial resolution of 2.5° x 2.5° latitude-longitude grids covers form period January 1979 to December 2013. This GPCP dataset is available via https://psl.noaa.gov/data/gridded/data.gpcp.html..

3.2.2.2 Indian Institute of Tropical Meteorology (IITM)

The Indian Institute of Tropical Meteorology (IITM) is a research institute under the Ministry of Earth Sciences of India. This research institute focused on producing scientific information, specifically in the fields of meteorology and atmospheric science, that can be used in a variety of industries such as economics, agriculture, water resources, communication, health, transportation, and others. It is also known as a national centre with special reference to monsoon meteorology research and Indian monsoon air-sea interaction. They are also responsible for weather forecasts, observation of the climatological, and earthquake predictions in India. The IITM has obtained various time series datasets, such as rainfall, surface temperature, OLR and others, for various periods over the Indian regions. Other than that, they also provided the Monsoon Intraseasonal Oscillation Index data using extended empirical orthogonal function analysis that is available from 1998 until 2019. The meteorological data sets above are available and can be archived at https://www.tropmet.res.in/DataArchival-51-Page. This study used monthly, seasonal, and yearly rainfall data from a homogeneous region of India and the

entire country. The data is available from January 1874 through December 2016. The rainfall distribution of India's regions and homogenous regions, or sub regions, has been calculated using 306 stations that are located over the specific area of the subdivisions. The northwest, northeast, central northeast, west central, and peninsular are among the locations included in the homogeneous region and sub regions. Figure 3.1 depicts the positions of the sub-regions. The time series rainfall dataset is available online at https://tropmet.res.in/static_pages.php?page_id=53. The time period that is covered in this study is from January 1979 until December 2013. This dataset was used to examine the climatology of Indian summer monsoon rainfall and also investigate the connection between sea ice extent phases in the Indian Ocean sector and rainfall.

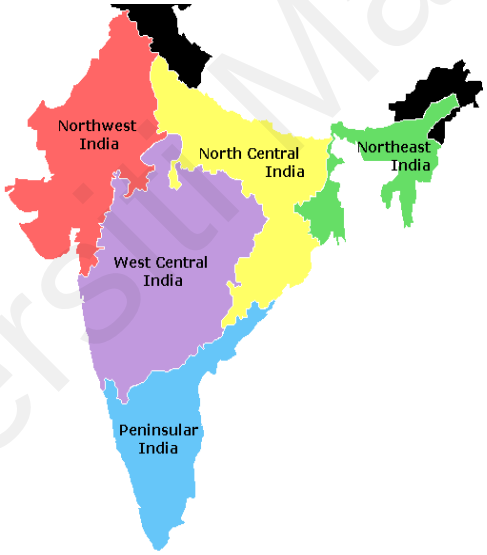

Figure 3.1: Map showing different sub regions of India. Image modified from http://www.monsoondata.org/hist/region.html

3.2.2.3 National Snow and Ice Data Centre (NSIDC)

The National Snow and Ice Data Centre (NSIDC) is a research institution that collaborates with the Cooperative Institute for Research in Environmental Sciences at the University of Colorado Boulder. They are also cooperating with and funded by the National Oceanic and Atmospheric Administration (NOAA) and the National Science

Foundation. The NSIDC is responsible for managing and providing access to scientific data; developing data access tools and providing assistance to data users; delivering the mission of public education; conducting scientific research and educating the public about the cryosphere. The primary subjects of research studies and data are climate interaction, snow, ice, glaciers, and frozen ground. The NSIDC provides observation data and information on a variety of topics, including sea ice, ice sheets, snow, frozen ground, glaciers, freshwater ice, and other cryosphere-related topics. The data provided by NSIDC is derived from various satellite imagery collected and processed by the National Aeronautics and Space Administration Goddard Space Flight Center. The Scanning Multichannel Microwave Radiometer (SMMR), Special Sensor Microwave Imager (SSM/I), Special Sensor Microwave Imager/Sounder (SSMIS), Snow Experiment (SnowEX), Visible Infrared Imaging Radiometer Suite (VIIRS), and others were among the satellites used. The list of sensors used is available at https://www.earthdata.nasa.gov/eosdis/daacs/nsidc. The monthly Antarctic sea ice extent used in this study was derived from the Scanning Multichannel Microwave Radiometer and Special Sensor Microwave Imager of satellite passive-microwave. It was available at ftp://sidads.colorado.edu/DATASETS/NOAA/G02135/. The period of the data is updated, and the users will receive the updated data by registered email. The data on sea ice extent includes the entire Antarctic continent and five of its sectors: the Weddell Sea, the Indian Ocean, the Western Pacific, the Ross Sea, the Bellingshausen Sea, and the Amundsen Sea. The data for each sector is available as a time series, showing the extent of sea ice per unit km2 in that sector over time. In this study, the data covered January 1979 until December 2013, which is 35 years. The monthly sea ice extent is the area of the ocean where at least 15% of the surface is covered by ice. This dataset is used to develop the climatology as well as the variability in Antarctic sea ice extent. Additionally, it is used to evaluate the connection between sea ice extent in the Indian Ocean sector and

Indian summer monsoon rainfall over the sub region of India in various composite months. Apart from that, it is also used to develop the sea in the Indian Ocean sector index and identify the phases of the sea ice extent.

3.2.2.4 Hadley Centre Global Sea Ice and Sea Surface Temperature

The Met Office Hadley Centre Global Sea Ice and Sea Surface Temperature (HadISST) is substituted by the Global Sea Ice and Sea Surface Temperature (GISST). It provides long term observational data on the concentration of sea ice and the temperature of the sea surface from January 1871 to the present (Rayner et al., 2003). The data set includes monthly average values of various parameters across the globe, with a gridded spatial resolution of 1.0º × 1.0º latitude - longitude. HadISST produces the most adequate and longest-set gridded sea ice data for both the Arctic and Antarctic. The spatially complete, continuous, and long-term gridded sea ice data set is merged from many data sources. The merging of the data comes from several activities, including expeditions and other activities; historical ice charts from shipping, digitized sea ice charts, NCEP operational ice analyses; and passive microwave satellite retrievals. Furthermore, the dataset is updated regularly. In this study, the data covers the period from January 1979 until December 2013, and it is available online at https://www.metoffice.gov.uk/hadobs/hadisst/data/ download.html. The sea ice extent in the Indian Ocean sector, from 20° E to 90° E, was calculated when the area of sea ice covered at least 15% of the ocean surface. The following table lists the variables used in the analysis, along with their descriptions, symbols, and notation:

Table 3.1: Notation and description for each variable in the study

Variables	Unit	Notation	Data
Sea ice extent in the Indian Ocean sector	km	time - series	text
		1.0 x 1.0	netCDF
MSLP	hPa	0.75 x 0.75	netCDF
Geopotential height (250, 500, 700hPa)	m	0.75 x 0.75	netCDF
Zonal wind at 11 level pressure, u: (1000, 925, 850, 800, 700, 600, 500, 400, 300, 200,100hPa)	ms^{-1}	0.75 x 0.75	netCDF
Meridional wind at 11 level pressure, v: (1000, 925, 850, 800, 700, 600, 500, 400, 300, 200,100hPa)	ms^{-1}	0.75 x 0.75	netCDF
Vertical velocity @Omega at 11 level pressure, ω: (1000, 925, 850, 800, 700, 600, 500, 400, 300, 200,100hPa)	Pas^{-1}	0.75 x 0.75	netCDF
Rainfall of Indian sub-regions	mm	time-series	text
Precipitation (Global)	m	2.5 x 2.5	netCDF
Outgoing Long Radiation, OLR	Wm^{-2}	2.5 x 2.5	netCDF

3.3 CMIP5 models

3.3.1 Models descriptions

A group of selected climate models from the CMIP5 project were used as the main model data for this research study. Six CMIP5 models were chosen from the 56 available CMIP5 models to assess the models' ability to reproduce the climate pattern found in the reanalysis data. The models ACCESS, GFDL-CM2.1, IPSL-CM54-LR, MPI-ESM-MR, and NorESM1-M were chosen because they could simulate Antarctic sea ice well. These models were evaluated by comparing them to reanalysis results (Collins et al., 2008; Bi et al., 2013; Turner et al., 2013; Rashid et al., 2013; Uotila et al., 2014; Yang et al., 2016). The historical simulation output of the model has ensembles with different hybrid vertical

coordinate systems with a horizontal resolution of approximately 2.5º x 1.9º, whereas the sea ice output is gridded with a horizontal resolution of 0.5º x 0.5º. For models with multiple ensembles, an unweighted average of all the ensembles was calculated first and then employed to represent the model. The monthly historical simulation output of various parameters is accessible from January 1850 to December 2005. To compare and ensure consistency with the reanalysis data, seven years 2006 to 2013 of simulation data from the RCP4.5 experiment were used. There are various reasons why RCP 4.5 was utilized in this study. The RCP 4.5 experiment is a climate change scenario that aims to limit global warming to 2 °C above pre-industrial levels. This is done by reducing greenhouse gas emissions through the use of a variety of technologies and strategies, such as renewable energy, energy efficiency, and carbon capture and storage. The RCP 4.5 experiment is considered to be a realistic that is achievable with current technology (Moss et al., 2010; Thomson et al., 2011). However, it will require significant investment in renewable energy, energy efficiency, and carbon capture and storage. The worst impacts of climate change can be avoided by implementing the RCP 4.5 experiment or a similar scenario. In addition, RCP 4.5 is a reference scenario that does not take into account any climate policies. It based on data from the past that has been updated and adjusted to reflect changes in climate up to the year 2000 (Lamarque et al., 2010). Table 3.2 lists the names of all the models used in this study, along with the institutions that developed them whereas Table 3.3 provides more detailed information about each model, such as its resolution. The CMIP5 models variables were downloaded from the Program for Climate Model Diagnosis and Intercomparison (PCMDI) website (http://cmip-pcmdi.llnl.gov/cmip5/). Sea ice extent in the Indian Ocean sector was calculated when the percentage of sea ice in the concentartion was greater than or equal to 15%. The CMIP5 model output will be compared to the ERA-Interim reanalysis datasets to evaluate how well the CMIP5 models can recapture the relationship pattern between sea ice and

monsoon. However, before the availability of ERA5, ERA-Interim was considered the most reliable reanalysis dataset (Simmons et al., 2014).

Table 3.2: Namelist of CMIP5 models used in this study, with the institutions/modelling centres and the countries of origin

Model	Country	Institution/Modelling centre
NorE1SM1-M	Norway	Norwegian Climate Centre (NCR)
MPI-ESM-MR	Germany	MPI-M
GFDL-CM2p1	USA	Geophysical Fluid Dynamics Laboratory (GFDL)
IPSL – CM5A-LR	France	Institute Pierre – Simon Laplace (IPSL)
ACCESS 1.0 & ACCESS 1.3	Australia	Commonwealth Scientific and Industrial Research Organization (CSIRO), Bureau of Meteorology (BOM)

Table 3.3: Resolutions, parameters and ensemble numbers of CMIP5 models used in this study

Model	**Parameter**	**Resolution (sea ice/atmosphere)**	**Ensemble members**
NorE1SM1-M	Sea ice concentration; Geopotential height, Zonal wind, Meridional wind, Vertical velocity, Ongoing longwave	0.5 x 0.5/ 2.5 x 1.9	3
MPI-ESM-MR			3
GFDL-CM2p1			10
IPSL – CM5A-LR		0.5 x 0.5 / 3.75 x 1.9	6
ACCESS 1.0 & ACCESS 1.3		0.5 x 0.5 / 1.25 x 1.875	3

3.4 Selection of the study area

The Indian Ocean sector of the Antarctic sea ice extent was chosen for various reasons. The main reason is that the sea ice extent in the Indian Ocean sector is the only sector that has a significant correlation with the Indian summer monsoon rainfall. The full explanation of this correlation will be presented in Chapter 4. This is why the extent of Antarctic sea ice across the Indian Ocean region is used to investigate teleconnections. Aside from that, the Indian Ocean sector was selected as the study's primary focus because of its geographical proximity to the Mascarene High and India. The Indian Ocean sector of Antarctica experiences a significant expansion of sea ice in all seasons, compared to other Antarctic sectors (Purich et al., 2018; Yadav et al., 2022). In addition to the significant expansion of sea ice in all seasons, the Indian Ocean sector of Antarctica also experiences the second highest rate of rising sea ice extent every year, after the Ross Sea sector (Turner et al., 2015). The sea ice dynamics in the Indian Ocean sector, such as surface cooling and freshening (Purich et al., 2018), are important to global climate and weather (Smith et al., 2008; Deb et al., 2017). However, this sector has been less researched than other sectors, such as the Ross, Weddle, and Bell sectors (Comiso et al., 2011; Murphy et al., 2014). Finally, most previous research on Antarctic sea ice has focused on all sectors (Rai et al., 2008; Prabhu et al., 2009). However, the physical mechanisms that cause sea ice to form and change from year to year are not well understood, particularly in the Indian Ocean sector. This is evident from the limited number of articles on this topic. The study area is depicted in Figure 3.2, which is a rectangular box with a blue line. The Indian Ocean sea ice extent is centred between 20^{o} E and 90^{o} E. Although the regions 35° S – 47° S and 65° E – 90° E were chosen to serve as a proxy for the Mascarene High system, they do not reflect the system as a whole.

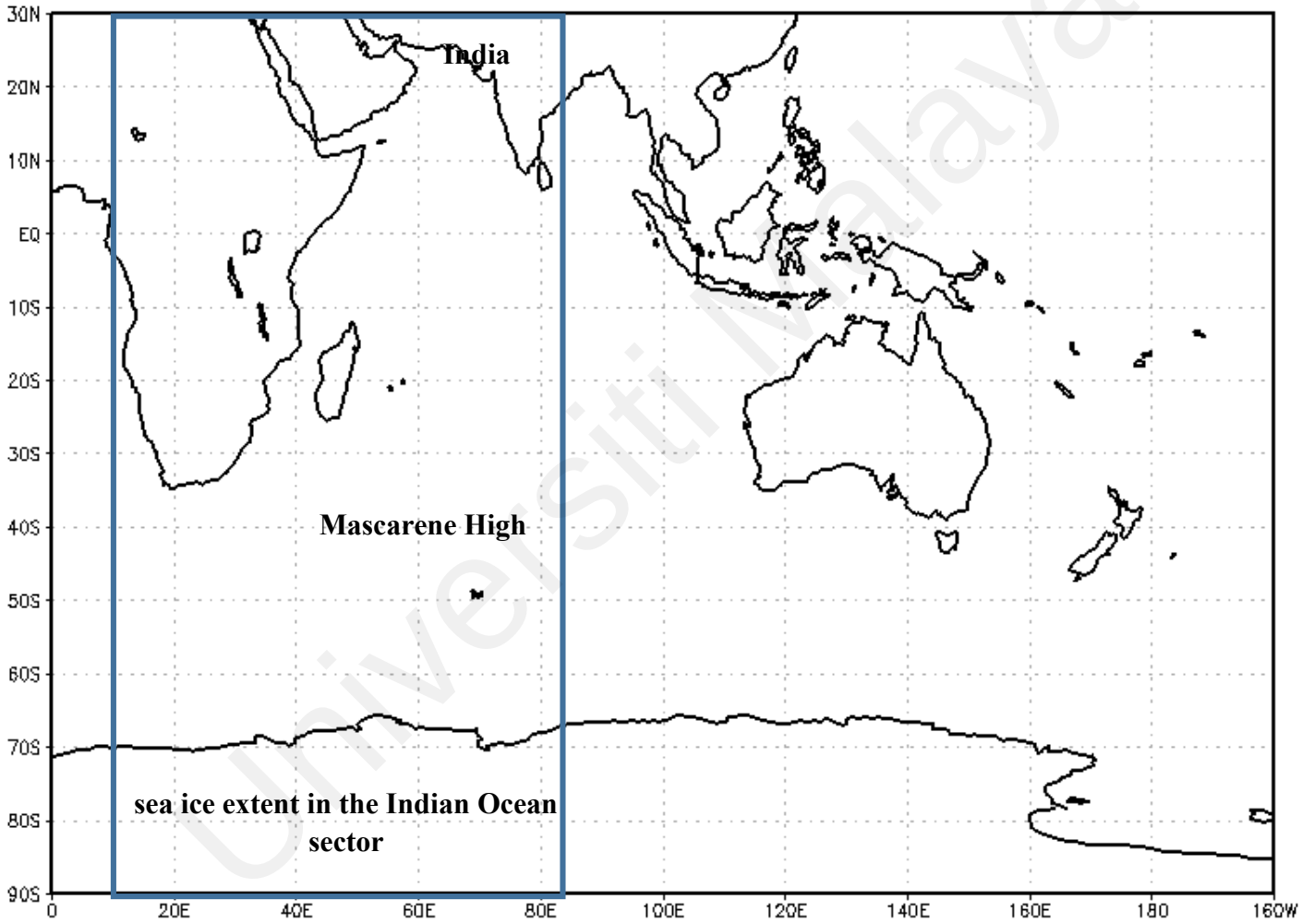

Figure 3.2: Selected area of study

3.5 Method adapted in the study

This research study used a variety of analytical techniques, including temporal and spatial correlation, partial correlation, spatial regression, composite analysis, and empirical orthogonal function (EOF) analysis. Apart from that, wave activity flux was also performed in this study. The purpose of the temporal and spatial correlation analysis is to assess the teleconnections between sea ice extent in the Indian Ocean sector and Indian summer monsoon rainfall. The partial correlation was employed to determine the influence of atmospheric circulation on the relationship. Furthermore, the composite analysis is used to evaluate and identify the characteristics as well as mechanisms that are involved in different phases of the sea ice years. The EOF analysis was conducted to investigate the variability of sea ice in the Indian Ocean sector and precipitation over the Indian region. The spatial regression and wave activity flux were used to determine the potential pathways of wave propagation that are associated with the relationship. The Student t-test was used to assess the statistical significance of the results. The following sections provide more detail on each analytical approach.

3.5.1 Climatology

Climatology is the study of climate, which is the average weather conditions in a place over a long period of time. It is commonly known as the study of climate, yet it may have other synonym definitions. It describes the average weather patterns over time, often over time periods of 20 - 30 years. Climatology is generally used in atmospheric sciences and can be evaluated for a diverse range of time periods, including hourly, daily, monthly, seasonally, annually, or decadal (Harman and Winkler, 1991). For example, a monthly climatology will obtain average values for each month, whereas a daily climatology will obtain average values for each day over a given time period. It helps in giving a complete picture of the characteristic variables of interest. It also helps in providing a

comprehensive view of the parameters' characteristics. They can be illustrated using time series, the seasonal cycle, or as a spatial variation. The climatology of the given variables can be expressed in terms of average, total average, anomalies, and standardized or normalized anomalies (World Meteorological Organization, 2017). Details about anomalies and standardized anomalies will be elaborated in the next topic. In this study, the climatology of the sea ice extent in the Indian Ocean sector's climatology is examined over a 35 year period, covering long term monthly mean and composite months. The months involved are the spring months of March, April, and May (MAM), the summer months of June, July, and August (JJA), the fall months of September, October, and November (SON), and the winter months of December, January, and February (DJF). Similarly, the climatology of rainfall in India and its sub regions was examined over a period of 35 years, covering the monthly mean and the period during the Indian summer monsoon. The study area includes five sub regions: The Northwest, Central North, Northeast, West Central, and Peninsular. Furthermore, the climatology of the Mascarene High was also examined over a period of 35 years, covering the monthly mean of the mean sea level pressure.

3.5.2 Statistical and spatial correlation analysis

Correlation analysis is a statistical technique for measuring the magnitude at which two or more parameters are linearly connected. The numerical value that measures the strength and direction of the relationship between two variables of time series data is known as the correlation coefficient (r). In meteorology, especially in teleconnection studies, Pearson correlation is the most common tool used by researchers at the outset of their analysis to quantify the relationship between two variables. The Pearson r correlation calculated using the following formula (Tattar et al., 2016; Prium, 2018):

$$r_{xy} = \frac{n\sum x_i y_i - \sum x_i \sum y_i}{\sqrt{n\sum x_i^2 - (\sum x_i)^2}\sqrt{n\sum y_i^2 - (\sum y_i)^2}} \quad \ldots\ldots\ldots\ldots\ldots\ldots (1)$$

where:

r_{xy} = Pearson r correlation coefficient between x and y

n = number of observations or samples

x_i = variable of x for ith observation

y_i = variable of y for ith observation

A positive relationship is shown by a linear correlation coefficient greater than zero, whereas a negative relationship is indicated by a value smaller than zero. Specifically, the Pearson correlation coefficient is always between -1 and 1, in order words $-1 \leq r_{xy} \geq 1$. A $r_{xy} = -1$ indicates a perfect negative linear relationship between two variables, while a r_{xy}= 1indicates a perfect positive linear relationship. The correlation coefficient was classified into three groups: weak (0.0 to ±0.3), moderate (±0.3 to ±0.7), and strong (±0.7 to ±1.0) (Ratner, 2009; Tattar et al., 2016; Prium, 2018). A comprehensive statistical analysis of the correlation between sea ice and rainfall was conducted (Prabhu et al., 2009). However, studies have shown that correlation coefficient values in teleconnections involving Antarctic sea ice rarely exceed 0.5 (Dugam et al., 2004; Rai et al., 2006, 2008; Prabhu et al., 2010; Bajish et al., 2021). Even though the correlation coefficient value is small and not strong, it is still important because it provides an initial idea about the probability of the relationship. This information can then be used to conduct further analysis and research to determine the mechanism or process involved. This study investigated the statistical connection between sea ice extent in the Indian Ocean sector during various composite months and Indian summer monsoon rainfall across different sub regions over a 35 year period (Figure 3.3). This analysis aims

to investigate which composite month of sea ice extent in the Indian Ocean sector has a significant relationship with the Indian summer monsoon rainfall. It is also used to determine the best location for the Temporal Mascarene High area Furthermore, it is used to identify which sea ice concentration EOF mode is statistically associated with the Indian summer monsoon rainfall EOF mode, and it is evaluated by the principal component of each EOF mode. More details can be found in the EOF analysis topic.

The spatial correlation analysis has many applications in meteorology or climate practice and research. It is a geographical assessment that attempts to understand climate or weather features. These correlations are critical for understanding both short and long-term climate patterns. Most significant spatial correlations are recorded as teleconnection patterns, which are simultaneous correlations in large scale atmospheric parameter fluctuations different spatial locations on the planet. However, the spatial correlation analysis is straightforward. For example, geopotential height a meteorological field that shows the height of an imaginary surface in the atmosphere where the air pressure is constant. Geopotential height, ϕ, is a measure of the height of the atmosphere at a given location. It is a function of longitude and latitude, and is defined at M grid points. The height at the ith grid point is represented by ϕ_i. Geopotential height can also change over time, and its average value for each month is available for several winters. The interest in climate variability The study of climate variability involves looking at the differences between monthly mean heights and their average values for each month. The differences are denoted by $\phi'_{i,k}$, which represents the height departure at the ith grid point in the kth month. Therefore, the relationship between the height departures at two grid points, i and j, is denoted by H_{ij}, and is defined as follows (Nigam et al., 2015):

$$H_{i,j}=\frac{\sum_{k=1}^{N}\phi'_{i,k}\phi'_{j,k}}{\left(\sum_{k=1}^{N}\phi'^{2}_{i,k}\right)^{1/2}\left(\sum_{k=1}^{N}\phi'^{2}_{j,k}\right)^{1/2}} \quad \ldots\ldots\ldots\ldots\ldots\ldots (2)$$

Similarly, the spatial correlation analysis was classified into three groups: weak (0.0 to ±0.3), moderate (±0.3 to ±0.7), and strong (±0.7 to ±1.0) (Ratner, 2009; Tattar et al., 2016; Prium, 2018). Furthermore, the knowledge of the correlation matrix, ***H,*** can be used to create the teleconnectivity map that detects the base points that related to varying teleconnection patterns. To construct the correlation map in GrADS, ***'tcorr()'*** functions were used. This functions only need a time-series variable, a spatial variable, as well as time-constraints. In this study, the spatial correlation analysis was performed to get better visualization the association between sea ice extent in the Indian Ocean sector and Indian summer monsoon rainfall. It is also used to identify the Temporal Mascarene High region, which will be explained in detail in Chapter 4. Additionally, the spatial correlation analysis of anomalies in zonal wind between ERA-Interim reanalysis and CMIP5 models was performed to assess the CMIP5 model's capacity to capture the teleconnection pattern during different phases of sea ice extent.

		Indian summer monsoon rainfall at different sub-region					
		All India (AI)	Northwest (NW)	Central Northeast (CN)	Northeast (NE)	West Central (WC)	Peninsular (Pen)
Composite months of sea ice extent in the Indian Ocean sector	January-February-March (JFM)						
	February-March-April (FMA)						
	March-April-May (MAM)						
	April-May-June (AMJ)						
	May-June-July (MJJ)						
	June-July-August (JJA)						

Figure 3.3: Example table in examining the correlation between the sea ice extent in the Indian Ocean sector at different composite months with the Indian summer monsoon rainfall over different sub regions for 35 years

3.5.3 Partial correlation analysis

Partial correlation analysis is closely related with correlation analysis. It is an expression of expression of analyses that applied to questions of prediction and relationship. It is having one continuous independent variable (the x-value) and one continuous dependent variable. However, partial correlation analysis investigating the linear relationship between two variables after one or more independent factors have been eliminated (Tattar et al., 2016; Prium, 2018). The correlation coefficient between two variables can be misleading if there is a third variable that is correlated with both of them. Controlling for the covariance, which is done by computing the partial correlation coefficient, can help to avoid misrepresenting information. Note the subscription symbol for a partial correlation coefficient is $\boldsymbol{r_{xyz}}$, which indicates that the correlation coefficient is for X and Y controlling Z. The formula for partial correlation is (Tattar et al., 2016; Prium, 2018):

$$r_{xyz} = \frac{r_{xy} - r_{yz}r_{xz}}{\sqrt{(1 - r^2{}_{yz})(1 - r^2{}_{xz})}} \quad \text{..... (3)}$$

where:

r_{xy} = correlation coefficient of variable x and y

r_{yz} = correlation coefficient of variable y and z

r_{xz} = correlation coefficient of variable x and z

Similarly as both correlation above, partial correlation bounded by −1 and 1; that is $-1 \leq r_{xy} \geq 1$. A $r_{xy} = -1$ indicates a perfect negative linear relationship between two variables, while a r_{xy}= 1indicates a perfect positive linear relationship. The correlation coefficient was classified into three groups: weak (0.0 to ±0.3), moderate (±0.3 to ±0.7),

and strong (±0.7 to ±1.0) (Ratner, 2009; Tattar et al., 2016; Prium, 2018). In this study, the partial correlation analysis was used to investigates the impact or influence of atmospheric climatic variabilities such as SAM or AAO, ENSO, and Indian Ocean dipole on the teleconnection between the sea ice in the Indian Ocean sector and Indian summer monsoon rainfall.

3.5.4 Spatial regression analysis

Spatial regression is a numerical technique that is widely utilised in physical geography to investigate causal relationships between variables. It also can be defined as a statistical method that measures the strength and direction of spatial relationships between a dependent variable and independent variables, while taking into account the location of each observation (Faiz et al., 2016). It is enables the modelling, examination, and exploration of spatial relationships and can assist in explaining the causes underlying observed spatial patterns. In terms of mathematical, the spatial regression is similar as linear regression. The least squares regression of Y and X is often expressed as linear equation (Brown, 2012):

$$Y = slope * X + intercept \quad \text{..... (4)}$$

where X is independent variable, Y is dependent variable. The calculation is simplified if not involving the time average. If x and y are the anomalies from the X and Y time averages:

$$x = X_{ave}$$

$$y = Y_{ave}$$

then the regression equation becomes:

$$y = coefficient * x$$

where

$$coefficient = (sum\ of\ x * y\ over\ time)/(sum\ of\ x * x\ over\ time)$$

This coefficient is the output from the ***tregr*** function. Similarly, as correlation analysis, to construct the spatial regression map in GrADS, ***'tregr ()'*** functions were used. This functions only need a time-series variable, a spatial variable, as well as time-constraints. Example of the calculation available at http://cola.gmu.edu/grads/gadoc/gradfunctregr.html.

3.5.5 Composite analysis

The composite analysis is a sampling tool. It is frequently used to determine some of the fundamental structural elements of a meteorological or climatological occurrence that are difficult to detect on their own or phenomena that happen over time (for example, the weather or climate over a specific geographic region). In particular, it is acknowledged as a simple and reliable tool for identifying conditions observed during specific climate states (Boschat et al., 2016). Composites are effective in climate research for examining the comprehensive and wide-ranging effects of teleconnections. It involves selected time periods that usually correspond to a pattern, event, or something else, whether directly or indirectly. The selected time period does not need to be continuous and can be separated. It may also involve collecting a large number of cases of a particular meteorological phenomenon and standardizing the cases in some way. The cases are then composited as a collection, possibly with different types of stratification based on one or more covariates suspected of having an effect on the pattern. The composite analysis then normally requires computing the composite mean as well as possibly other statistical measures such as standard deviation and statistical significance (Boschat et al., 2016).

The outcomes of the analysis will provide meaningful information about how the components used in the composite stratification affect that meteorological phenomenon (Tan et al., 2007).

In this study, the composite analysis of the parameters (MSLP, geopotential height, wind, wave activity flux, vertical velocity, rainfall, and OLR) was performed based on the highest and significant values of the correlation coefficient as well as EOF modes between the sea ice and monsoon rainfall. The composite analysis was conducted for both high ice phase (HIP) years and low sea ice phase (LIP) years. The HIP and LIP years of the sea ice extent in the Indian Ocean sector were identified and classified according to the standardized anomalies or normalization value of the sea ice extent in the Indian Ocean sector (sea ice extent in the Indian Ocean sector index) as well as normalization of the principal component of the sea ice extent during AMJ; that is more than or less than 1 standard deviation from the mean. Standardized anomalies, also known as normalized anomalies, are computed by dividing anomalies by the climatological standard deviation. They commonly provide more information about the magnitude of the anomalies because dispersion influences have been removed. However, it is not necessary for a dataset to be expressed in terms of standardized anomalies. Note that the normalisation value is dimensionless. The formula for calculating the normalisation value is as follows (World Meteorological Organization, 1989; Brown, 2012; Hai, 2013):

$$Z_n = \frac{x_{n,m} - \bar{x}_m}{\sigma_m} \qquad \text{..... (3)}$$

where:

Z_n = the normalization value variables of interest at n years,

$x_{n,m}$ = value of the interested variables for the composite months (m) in years (n),

$\bar{x}_m$ = long term average of the variables for the composite months (m) from 1979 – 2013, 35 years' period,

σ_m = long term standard deviation of variables for the composite months (m) from January 1979 until December 2013, 35 years' period

Anomalies known as deviation from mean, are generated by subtracting climatological values from observed data. In other words, the anomalies for each climate parameter calculated by extracting the composite monthly mean value with the climatology of the composite month mean value for each year;

$$X_n = x_{n,m} - \bar{x}_m \quad \text{..... (4)}$$

where:

X_n = the anomalies value of interest at n years

Similarly, a composite of monsoon rainfall was also computed based on the positive and negative values of the Temporal Mascarene High (TMH) index. The details of the TMH index, including its definition and its location, will be explained in the next chapter (Chapter 4). Indexes such as the Temporal Mascarene High (TMH) index and the Indian summer monsoon rainfall index were also calculated based on Equation 3 and categories based on greater and lower than one standard deviation (≥ 1 and ≤ -1). Furthermore, the composite anomaly difference between HIP and LIP years is also generated in this study. A composite vertical profile structure was also performed in this study to examine the circulation of air in the atmosphere from the lowest levels to the upper troposphere. The composite map is generated using GrADs.

3.5.6 Wave activity flux

The wave-activity flux is a powerful tool for visualizing the propagation of a packet of stationary or migratory quasi-geostrophic wave disturbances, and can be used to infer where the packet is emitted and absorbed. It could also help with routine climate diagnoses in an operational center. Wave activity flux can be determined by various method such as Plumb wave activity flux (Plumb et al., 1985) and T-N wave activity flux (Takaya and Nakamura, 2001). However, the meridional component of the T-N wave activity flux is stronger than that of the Plumb wave activity flux, which can better describe the Rossby long-wave disturbances in the westerly zone with larger amplitude in the non - uniform zonal airflow (Tang et al., 2022). In this study the wave activity flux was computed using the method Takaya and Nakamura (TN 2001) adopted to understand better the dynamics behind the atmospheric processes linked with the sea ice extent in the Indian Ocean sector area. The wave activity flux reveals the various wave propagation paths and the source regions and propagation features of wave anomalies. The geopotential height anomalies and mean winds are used as input factors. In the zonally asymmetric basic condition, the wave activity flux (Takaya and Nakamura, 2001) is estimated to describe the three-dimensional propagation of stationary waves. The horizontal Takaya and Nakamura (2001) wave-activity flux formula is as follows:

$$\boldsymbol{W} = \frac{p\cos\varphi}{2|U|}\begin{pmatrix} \frac{U}{a^2\cos^2\varphi}\left[\left(\frac{\partial\psi'}{\partial\lambda}\right)^2 - \psi'\frac{\partial^2\psi'}{\partial\lambda^2}\right] + \frac{V}{a^2\cos\varphi}\left[\frac{\partial\psi'}{\partial\lambda}\frac{\partial\psi'}{\partial\varphi} - \psi'\frac{\partial^2\psi'}{\partial\lambda\partial\varphi}\right] \\ \frac{U}{a^2\cos\varphi}\left[\frac{\partial\psi'}{\partial\lambda}\frac{\partial\psi'}{\partial\varphi} - \psi'\frac{\partial^2\psi'}{\partial\lambda\partial\varphi}\right] + \frac{V}{a^2}\left[\left(\frac{\partial\psi'}{\partial\varphi}\right)^2 - \psi'\frac{\partial^2\psi'}{\partial\varphi^2}\right] \\ \frac{f_o^2}{N^2}\left\{\frac{U}{a\cos\varphi}\left[\frac{\partial\psi'}{\partial\lambda}\frac{\partial\psi'}{\partial z} - \psi'\frac{\partial^2\psi'}{\partial\lambda\partial z}\right] + \frac{V}{a}\left[\frac{\partial\psi'}{\partial\varphi}\frac{\partial\psi'}{\partial z} - \psi'\frac{\partial^2\psi'}{\partial\varphi\lambda\partial z}\right]\right\} \end{pmatrix}$$

……. *(5)*

where

a = earth radius, 6400000

(φ, λ) = are latitude and longitude

ψ' = perturbation geostrophic stream function, $(g/f * za;\ 2 * 7.24/100000 * sinlat, g = 9.8$; f is the Coriolis parameter)

$(\frac{\partial\psi'}{\partial\lambda}\frac{\partial\psi'}{\partial\varphi})$ = perturbation geostrophic velocity

(U, V) = the geostrophic basic-flow velocity

R_a = gas constant of dry air

f_o = $2 * 7.24/100000 * sin\ (43 * 3.14/180)$

p = $pressure/1000\ hPa$

$N2$ = buoyancy frequency squared $\left(\frac{R_a p^{\kappa}}{H}\right)\left(\frac{\partial\theta}{\partial z}\right)$ where θ denotes potential temperature, H is a constant scale height, Ra is the gas constant of dry air, and k is defined as a normalised by the specific heat of air for constant pressure.

$\boldsymbol{W}$ denotes the wave activity's sources (positive divergence) and sinks (negative divergence). These wave "sources" or "sinks" help determine the dynamics underlying a variety of atmospheric phenomena involving the wave-mean flow interaction (Rai et al., 2015). The modified script based on the GrADS was used to calculate the wave activity flux (http://www.atmos.rcast.utokyo.ac.jp/nishii/programs/index.html).

3.5.7 Empirical Orthogonal Function (EOF) analysis

Empirical orthogonal function (EOF) analysis, a major technique for explaining climate variability, has been widely adopted by meteorologists. EOF analysis is a powerful tool for identifying and tracking spatial patterns of climate variability over time. It has been introduced in atmospheric science since early 50's for a discussion of relevant

problems in multivariate data analysis in meteorology (Craddock, 1973). EOF analysis is a beneficial pattern recognition tool. It reduces space-time data set to spatial patterns known as EOFs or modes of EOF, which describe the majority of the variance in the data, and temporal patterns known as Principal Components (PCs). In particular, EOF is a decomposes a signal or data set into a set of orthogonal basis functions, which are derived from the data itself. The EOF method is similar to principal component analysis (PCA), but it also looks for spatial patterns in addition to temporal projections. Physical principles are not used in EOF analysis. The EOF analysis identifies the spatial patterns of variability in a data set, and the temporal evolution of those patterns. These pattern of variability can then be used to understand the distribution and association of the data. The most significant modes are those that account for the highest percentage of the original variation. These modes are represented by orthogonal spatial patterns (eigenvectors) and time series (principal components). The representation of fields of climate variables in terms of their eigenvectors and eigenvalues has been observed to be formulated in a number of forms. EOFs are typically found by computing the eigenvalues and eigenvectors of a field's spatially weighted anomaly covariance matrix. The most common spatial weights used in EOF analysis are the square root of the cosine of latitude. The derived eigenvalues estimate the percentage of variance accounted for by each mode. Instead, in some cases, the field is divided into mathematical (independent) orthogonal modes, which can be interpreted as atmospheric and oceanographic ('structural') modes. Atmospheric and oceanographic processes are typically 'red,' indicating that the majority of the variance (power) is concentrated in the first few modes. By projecting the derived eigenvectors onto the spatially weighted anomalies, the time series of each mode or principal components are calculated. As a result, the magnitude of each mode during the recording period will be calculated. The EOF patterns and the principal components do not affect each other (Hannachi, 2004;2007).

In this study, EOF analysis was carried out to identify the most significant modes of sea ice extent in the Indian Ocean sector and Indian summer monsoon rainfall variations. The spatial functions are used to examine the variability of the sea ice in the Indian Ocean sector and precipitation over the Indian region. While the temporal function was used to determine the most significant relationship between the sea ice extent in the Indian Ocean sector and Indian precipitation. The EOF analysis was analyzed and determined by using the climate data operating system (CDO) command line tools under the Ubuntu interface. Below is an example command line used to determine the EOF's modes, total variance, and principal component. Other example is available online at https://geoclimatologyblog.wordpress.com/2017/06/17/performing-eofs-analysis-with-cdo/

****

cdo -f nc import_binary rlut.test.ctl rlut.test.nc # convert ctl file to nc file
cdo sellonlatbox,50,100,-10,35 rlut.test.nc rlut.Ind.nc # set India domain
cdo eoftime,5 rlut.Ind.nc eval.rlut.nc eof.rlut.nc # 5 EOF mode and 5 PCs
cdo eofcoeff eof.rlut.nc rlut.Ind.nc obase.rlut.nc # PC in obasexxx.nc file
cdo -div eval.rlut.nc -timsum eval.rlut.nc explvar.rlut.nc#total variance of EOF
cdo -s -r settaxis,1979-01-01,00:00:00,3year eof.rlut.nc eof.rlut.adjust.nc
cdo -s -r settaxis,1979-01-01,00:00:00,3year explvar.rlut.nc explvar.rlut.adjust.nc

****

3.5.8 Statistical significance of test and the student's t-test

Hypothesis testing is a statistical method used to determine whether the data provides enough evidence to support a hypothesis or to cast doubt on it. Hypothesis testing can be divided into two types: parametric and non-parametric tests. Parametric tests assume that the data follows a normal distribution, while non-parametric tests do not make any assumptions about the distribution of the data. The p-value is a parametric test that is commonly used to determine the level of significance of an analysis. The statistical

significance of the results was assessed using the Student's t-test, as recommended by the World Meteorological Organization, WMO Climatology Practices (2011). The statistical significance test is given by:

$$t = r\sqrt{\frac{n-2}{1-r^2}} \qquad \text{..... (6)}$$

where:

r = correlation or average of parameters for HIP or LIP years

n = number of observations and samples

The t is compared to the student's t tabular value with n-2 degrees of freedom, that are statistically significant at a 95% or 99% confidence level. GrADs and R Studio were used to calculate the p-value, which was considered significant if it was less than 0.05 or less than 0.1 (< 0.05 or < 0.1), respectively. For composite figures, the statistical significance is denoted with dashed lines.

3.6 Software and Equipment used in analysing the data

There is several software used in study to analysing the data. There are Grid Analysis and Display System (GrADS), climate data operator (CDO), R Studio, and Microsoft Office includes Words and Excel.

GrADS: The Grid Analysis and Display System (GrADS) is a powerful desktop tool for earth science data analysis, with features for accessing, manipulating, and visualizing data (Berman et al., 2001). It can handle two types of data: gridded data and station data. Gridded data is data that is organized on a regular grid, such as temperature

data at different points on a map. Station data is data that is collected from individual weather stations, such as temperature, pressure, and humidity. GrADS supports a variety of data file formats, including binary, Network Common Data Form (NetCDF), gridded binary (GRIB), Binary Universal Form for the representation of meteorological data (BUFR), and Hierarchical Data Format (HDF). This makes it a versatile tool for working with a wide variety of earth science data. It is a versatile tool that and one of the most widely used software packages in the operational research and meteorological communities around the world. GrADS is a free and open-source software that can be downloaded from the GrADS website. This system uses a 5-dimensional data environment, which is composed of the four conventional dimensions of longitude, latitude, vertical level, and time. The fifth dimension is optional and is typically used for ensembles. It is a system to analyze and visualize various computations of all the global gridded data. Data can be visualized using a variety of graphical techniques, including smoothed contours, wind vectors, shaded contours, streamlines, scatter plots, line and bar graphs, and others. The user can customize each aspect of the graphic output, even if the GrADS provides intuitive geophysical defaults. GrADS comes with a scripting language that enables advanced analysis and visualization applications. Furthermore, GrADS can be run in batch mode, which allows users to run long-term, overnight batch jobs with the help of the scripting language. Details about this software are available at cola.gmu.edu/grads/, including the command line and other information. In this study, the latest version of GrADS 2.2.1 was used, and it is used for gridded data (NetCDF). The high-performance terminal is needed to read and analyze raw data amounting to more than 5 TB.

CDO: The climate data operator (CDO) software is a collection of command-line tools that can be used to manipulate and analyze climate and numerical weather prediction

data. It is also known as a collective of many operators for standardizing the computation of forecast model data and climate. It is able to handle various types of data, including netCDF-3, netCDF-4, GRIB1, GRIB2, and other formats. CDO also has the ability to analyse non-climate science gridded data. CDO offers over 600 operators, including file operations and file information, comparison and selection, metadata modification, operations with numbers, statistical investigation, interpolation, and regression, transformations of vectors and spectral data, I/O format, and climate indices. Furthermore, CDO requires very small memory and able to process a very large file. This operator can be used under three interfaces, which are Linux (e.g., Ubuntu), MacOS, and Windows. In this study, CDO was used under Ubuntu. Ubuntu is a Linux-based operating system, and it is freely available for use and open source. Aside from being a free operating system, it is recognized as a solid interface with a command line, more secure, regularly updated, and etc. The CDO command line used in this study is to combine CMIP5 model ensemble data time, CMIP5 model ensemble average, modify CMIP5 model metadata, convert data from binary format to NetCDF and calculate and analyze EOF analysis.

R Studio: R Studio is an R-based integrated development environment. It is a statistical computing and graphics programming language. The primary goal is to develop freely available and open-source software for technical communication, data science, and scientific research. In this study, R Studio was used to analysing the data includes matrix correlation analysis, linear regression, partial correlation. It is also used to determine the significant test of the correlation analysis. Other than that, it used to plot the figures such as boxplot. Packages used in this study are `readxl, ggpubr, corrplot,Hmisc, ppcor, dplyr, tidyr, ggplot2.`

Other than scientific software, basic programmes such as Microsoft Office includes Excel and Words were used in this study to sorting the time series data and perform simple plotting, calculation, and documentation. The calculation is involving the time series data such as average, standard deviation, anomalies, standard anomalies for 35 years from 1979 until 2013. All the analysis and simulation of data were processed mainly using the existing computer cluster in the National Antarctic Research Centre (NARC), Institut Pengurusan & Pemantauan Penyelidikan (IPPP), University Malaya. The high-performance computer cluster (HPC) can handle the analysis of gridded climatological data sets (ERA-Interim/ NOAA/NSIDC/CMIP5 data), which are very large (amounting to more than 5TB of raw data).

Table 3.5: Description of analysis tools used in this research study

No.	Software	Symbols	Type of data	Description
1.	Grid Analysis and Display System	GrADS	NetCDF	1. Analysing gridded data 2. Plotting the spatial figures
2.	R language	R Studio	time series	1. Analysing the data, i.e., matrix correlation analysis, linear regression, partial correlation and determine the significant test. 2. Plotting the figures, i.e., boxplot
3.	Linux e.g in Ubuntu		NetCDF	1. Running the cdo operating system
4.	Climate Data operate	CDO	NetCDF	1. Merge time of the ensemble data 2. Average the ensemble data 3. Convert data from the binary to netcdf 4. Calculating and analysing EOF

CHAPTER 4

THE LINKAGE BETWEEN ANTARCTIC SEA ICE EXTENT IN THE INDIAN OCEAN SECTOR WITH THE INDIAN SUMMER MONSOON RAINFALL

4.1 Introduction

This chapter focuses on exploring the relationship between the Antarctic sea ice extent in the Indian Ocean sector and Indian summer monsoon rainfall through the variability of Mascarene High for the period 1979 – 2013. The climatology of the sea ice extent in the Indian Ocean sector, Indian monsoon's rainfall, and Mascarenes High were examined in Section 4.2. Section 4.3 assesses the statistical and spatial relationship between the sea ice extent in the Indian Ocean sector and Indian summer monsoon rainfall, Section 4.4 examines the impact of the sea ice extent in the Indian Ocean sector on Mascarene High, and Section 4.5 discusses the Mascarene High's role in Indian summer monsoon rainfall.

4.2 Climatology of the sea ice extent in the Indian Ocean sector, Indian summer monsoon rainfall and Mascarene High

The climatology of the sea ice extent in the Indian Ocean sector, Indian rainfall, and Mascarenes High was examined annually, seasonally, and monthly.

4.2.1 The sea ice extent in the Indian Ocean sector: Monthly and seasonally

Long term monthly and seasonal climatologies of the sea ice extent for the total Antarctic and Indian Ocean sectors were developed from January 1979 to December

2013. The study can provide a general overview of the sea ice extent's characteristics and behavior

over the past 35 years.

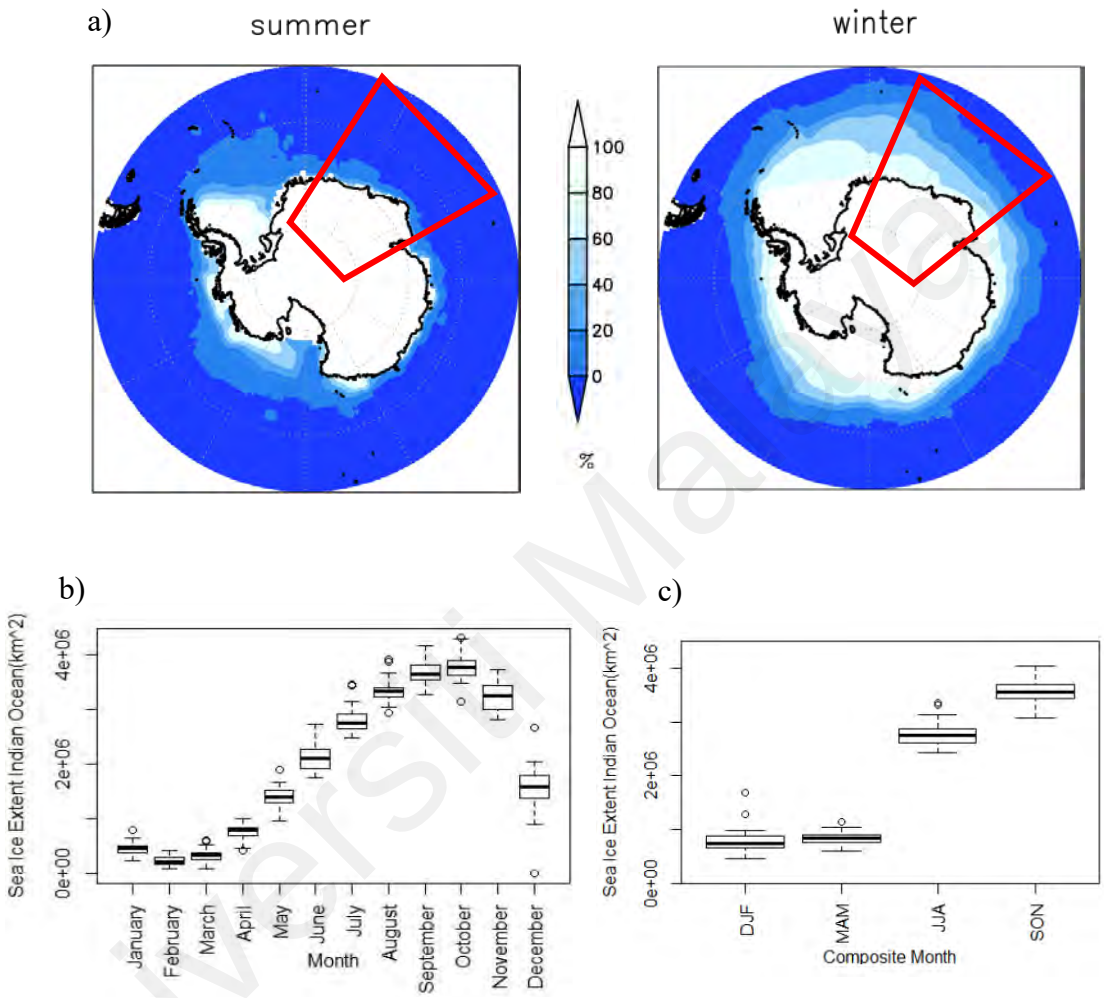

Figure 4.1: a) Spatial pattern of total Antarctic sea ice concentration during summer and winter for years 1979 – 2013. The red box shows the Indian Ocean sector b) Boxplot of the long-term monthly average c) Seasonal climatology of sea ice extent in the Indian Ocean sector (in km^2) from 1979 – 2013 (March-April-May (MAM), June-July-August (JJA), September-August-November (SON), December-January-February (DJF)). The median value is denoted by (thick black) lines and outliers by circles

Since 1979, the seasonal total Antarctic sea ice extent has averaged 18.7 x 10^6 km^2 during winter and 3.5 x 10^6 km^2 during summer (Figure 4.1). On the other hand, the monthly mean sea ice extent in the Indian Ocean sector reaches its lowest point in

February (0.23 x 10^6 km^2), following the summer season, and its highest point in October (3.79 x 10^6 km^2), following the winter season, whereas in April the sea ice begins to grow or form. This is illustrated by the boxplot in Figure 4.1b. The median value is represented by the thick black line, and outliers are represented by the circles. The upper and lower whisker lines of each boxplot represent the maximum and minimum sea ice extent values, respectively. Over the last decades, the sea ice extent in the Indian Ocean sector has demostrated a steady increase of yearly with $0.5 \pm 12.6 \times 10^4$ km^2 $year^{-1}$. Yadav et al. (2022) and Simmonds (2015) concur with this finding, both noting that the sea ice extent in the Antarctic in this sector had demonstrated a significant upward trend in most months during the 34-year period from 1979 to 2013. Seasonally, September-August-November (SON) recorded the highest and largest expansion of sea ice extent in the Indian Ocean sector for 35 years with $0.6 \pm 20 \times 10^4$ km^2 $year^{-1}$, whereas the least amount of sea ice occurred in DJF with $0.8 \pm 18.1 \times 10^4$ km^2 $year^{-1}$. This is illustrated by Figure 4.1c.

4.2.2 The climatology of Indian monsoon rainfall

Figure 4.2 depicts the mean annual variability of Indian rainfall in different sub-regions from 1979 to 2013. The highest rainfall was recorded in June, July, August, and September, corresponding to the southwest monsoon season, better known as the Indian summer monsoon rainfall. The average amount of rainfall received by the India region during this summer monsoon is approximately 2070 mm $year^{-1}$. While the least amount of rainfall was noticed from November until April with 230.69 mm $year^{-1}$. This period of time corresponds to the northeast monsoon, which occurred from October until December (404.43 mm $year^{-1}$). The amount of rainfall received by each sub region varies during the season (Figure 4.3). In comparison to other sub regions, the northeastern Indian region has the highest mean annual rainfall or receives an excessive amount of rain with 3386 mm $year^{-1}$. This is followed by the north-central, west central, and peninsula with values

of 2246.3 mm year^{-1}, 3334.1 mm year^{-1}, and 1661.9 mm year^{-1} respectively. Northwest India experiences the lowest mean annual rainfall and receives less rainfall during monsoon events with 1211 mm year^{-1}. According to Parthasarathy et al. (1993), the summer monsoon event brought more than 80% of the region's annual rainfall to the central and northeastern regions. On the other hand, south and northwest India receive only between 50 and 75% of their annual rainfall during the monsoon season. This is because rainfall during the Indian summer monsoon varies intraseasonally and inconsistent across the entire Indian subcontinent. Furthermore, during this event, an inter-tropical convergence zone forms over this region, which is responsible for large-scale rainfall (Rajeevan et al., 2012).

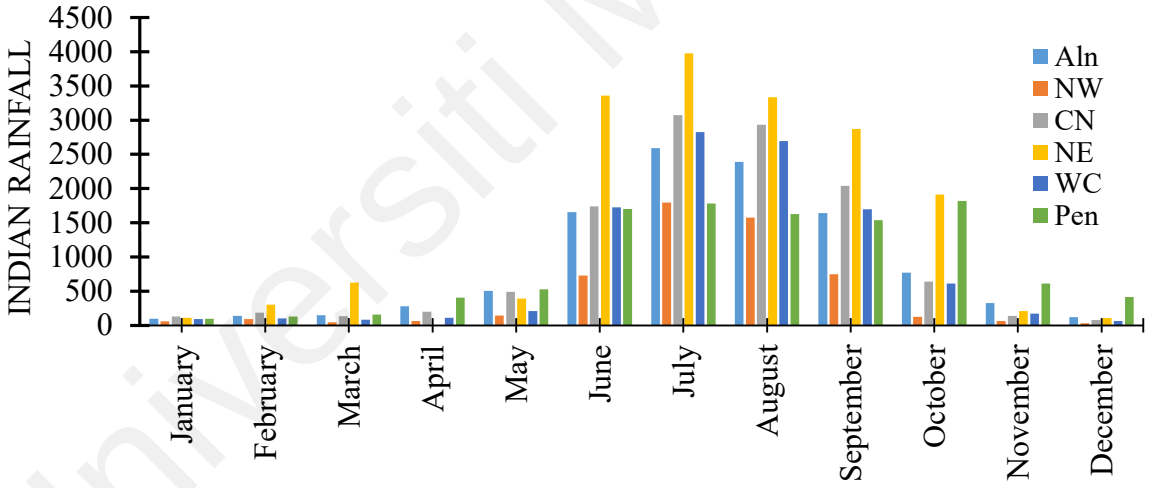

Figure 4.2: Long term monthly variability of the Indian rainfall (in mm) over India and its sub-regions from 1979 - 2013. (Al: All India, NW: Northwest, CN: Central north, NE: Northeast, WC: West central, Pen: Peninsular)

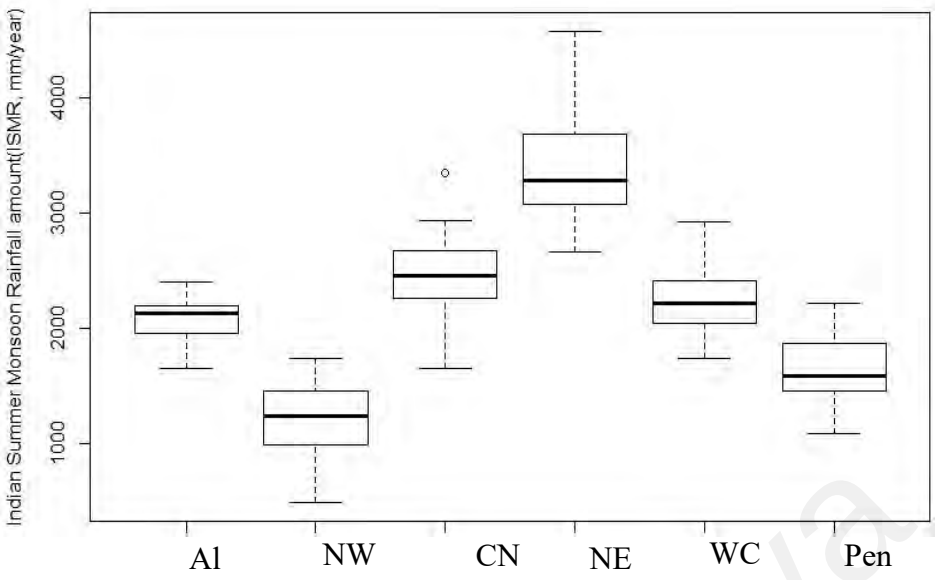

Figure 4.3: Amount of rainfall during Indian summer monsoon rainfall over the Indian region and its sub-region from 1979 – 2013. (Al: All India, NW: Northwest, CN: Central north, NE: Northeast, WC: West central, Pen: Peninsular)

4.2.3 The climatology of Mascarene High

The monthly mean sea level pressure (MSLP) of the Mascarene High is shown in Figure 4.4 for the period 1979-2013. The climatology of the MSLP is illustrated from January to December. According to the figure, the MSLP over the Mascarene High regions began to develop in May. It intensifies in July and August, with a maximum value of 1025 hPa at the centre at about 50° E – 80° E; 25° S – 35° S. The intensification of the Mascarene High lasts only until August, and the MSLP value continues to fall until February of the following year. As its intensity decreases, Mascarene High moves farther east from its centre.

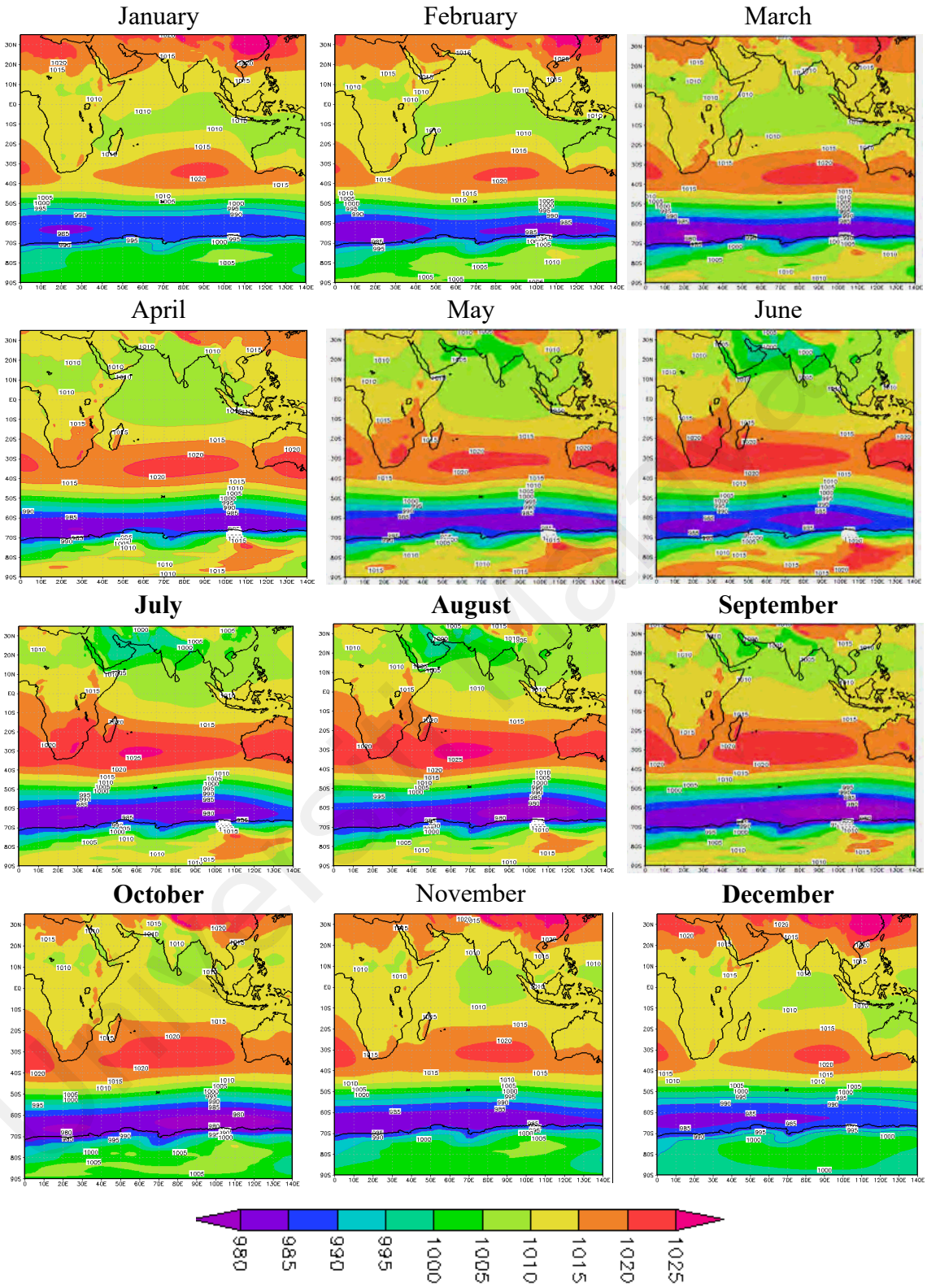

Figure 4.4: Climatology of monthly MSLP for 35 years (1979 -2013)

4.3 Linkages between the sea ice extent in the Indian Ocean sector and Indian summer monsoon rainfall

The correlation of the two time series between the Indian summer monsoon rainfall index and the sea ice extent in the Indian Ocean sector index was measured for 35 years between 1979 and 2013 in order to study the effects of sea ice extent in the Indian Ocean sector on Indian summer monsoon rainfall. It is important to note that sea ice extent was analyzed for all sectors at the beginning of the study to determine if there is any relationship between sea ice extent and rainfall. However, all sectors except the Indian Ocean sector showed an insignificant relationship with monsoon rainfall. Table 4.1 displays the correlation coefficient between sea ice extent in the Indian Ocean sector index and Indian summer monsoon rainfall in the Indian sub region for various composite months. The findings demonstrate that, in comparison to other months and sub regions, the AMJ sea ice extent in the Indian Ocean sector has the highest positive correlation with the rainfall produced by the Indian summer monsoon over Peninsular India, with a statistically significant correlation value of 0.44 ($p > 0.05$). While the sea ice extent in the Indian Ocean sector composite months FMA and MAM has a negative correlation with the Indian summer monsoon rainfall across the central north and northeastern parts of India. Furthermore, Figures 4.5 and 4.6 clearly show the positive association between the AMJ sea ice extent in the Indian Ocean sector and Indian summer monsoon rainfall over Peninsular India. The scatter plot illustrated that the two variables had a positive linear relationship and the points on the scatterplot nearly have the appearance of a straight line. Therefore, this statistical relationship indicates that the sea ice extent in the Indian Ocean sector has a significant influence on the variability of Indian summer monsoon rainfall. It should be noted that although the correlation is only moderate and not strong, this significant value does suggest that there is a possibility of teleconnection between these two variables. Hence, the analysis continues with an in-depth investigation to determine

the mechanism involved.

Table 4.1: Correlation coefficient between sea ice extent in the Indian Ocean sector during different composite months January-February-March (JFM), February-March- April (FMA), March-April-May (MAM), April-May-June (AMJ), May-June- July (MJJ), June-July-August (JJA) and Indian summer monsoon rainfall at different sub-regions of India (All India (Al), Northwest (NW), Central north (CN), Northeast (NE), West central (WC), Peninsular (Pen) India) from 1979 to 2013

		Indian summer monsoon rainfall at different sub-regions					
		Al	NW	CN	NE	WC	Pen
Composite month of sea ice extent in Indian Ocean sector	JFM	0.02	-0.02	0.23	0.05	-0.09	0.38*
	FMA	-0.2	0.05	-0.39*	-0.17	-0.15	-0.21
	MAM	0	0.1	0.02	-0.34*	0.17	0.07
	AMJ	0.08	0.13	0	-0.03	0.04	0.44*
	MJJ	0.08	0.13	-0.03	-0.11	0.11	0.31
	JJA	0.05	0.11	-0.06	-0.13	0.14	0.21

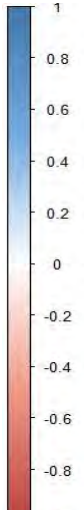

(* and red circles is statistically significant at $p < 0.05$)

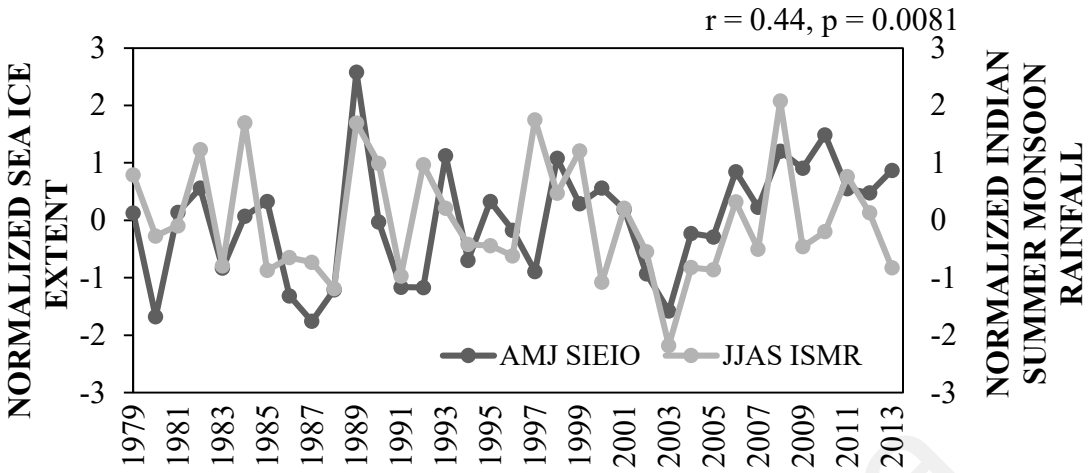

Figure 4.5: Correlation coefficient (r) between normalized time series of the AMJ sea ice extent in the Indian Ocean sector (black) and Indian summer monsoon rainfall (grey) over the Peninsular India region from 1979 to 2013, statistically significant at p < 0.05

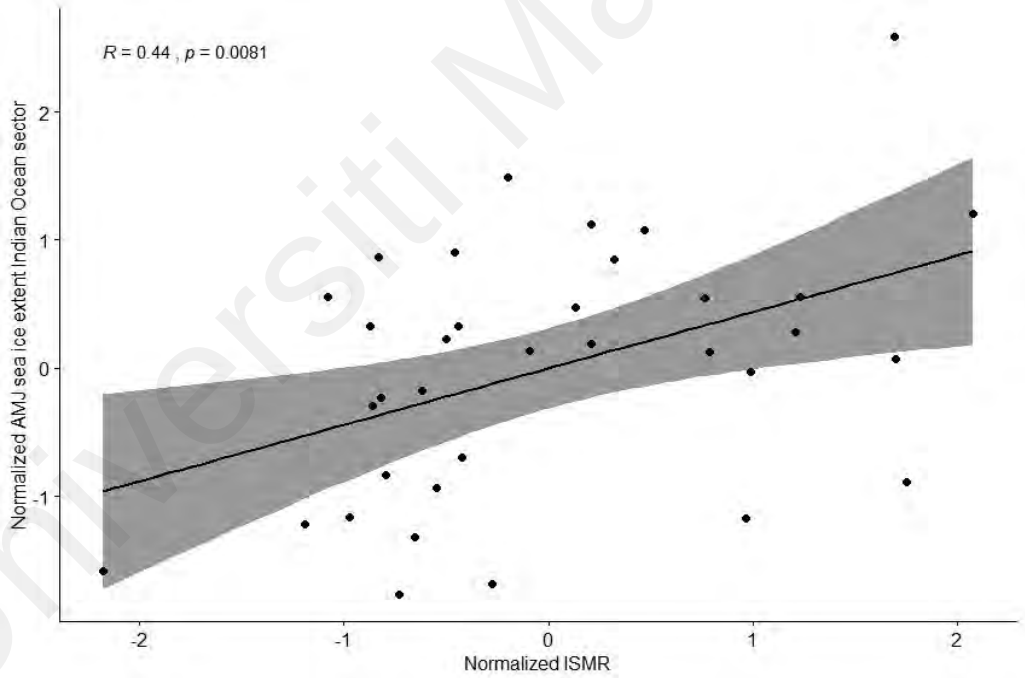

Figure 4.6: Scatterplot between the normalized AMJ sea ice extent in the Indian Ocean sector and Indian summer monsoon rainfall over the Peninsular India region from 1979 – 2013, statistically significant at p < 0.05

Additionally, to gain a better understanding and visualization of the relationship between AMJ sea ice extent in the Indian Ocean sector and Indian summer monsoon rainfall from 1979 to 2013, the spatial correlation between the two variables was further investigated. (Figure 4.7). The results of the analysis showed a significant positive

correlation coefficient over the Peninsular India region, as indicated by the shaded areas. This is consistent with the findings of previous statistical correlation analyses. As mention in Chapter 2, rainfall on the Indian subcontinent is impacted by difficulties related to the physical features, the natural and human-made aspects, and different land use patterns of the region. Specifically, The Indian subcontinent from the west, east, and south is bounded on three sides by the Arabian Sea, the Bay of Bengal, and the Indian Ocean, respectively. In contrast, the Himalayas are located in the northern part of India. All of these factors influence the climate of India and its sub regions significantly. As a result, rainfall in India during the summer monsoon varies considerably temporally and spatially. The peninsular region of India receives more precipitation during the summer monsoon than northern and central India because it is on the windward side of the Western Ghats mountain range. The rain-shadow areas of northern and central India, on the other hand, receive less precipitation (< 500 mm) because they are located on the leeward side of the mountains, where the air is already dry (Kumar et al., 1995; Fukushima et al., 2019). Francis and Gadgil (2006) showed that the west coast of Peninsular India experiences more rainfall during the southwest monsoon season than other parts of the region. Overall, as the sea ice extent in the Indian Ocean sector increases, the Indian summer monsoon rainfall tends to increase.

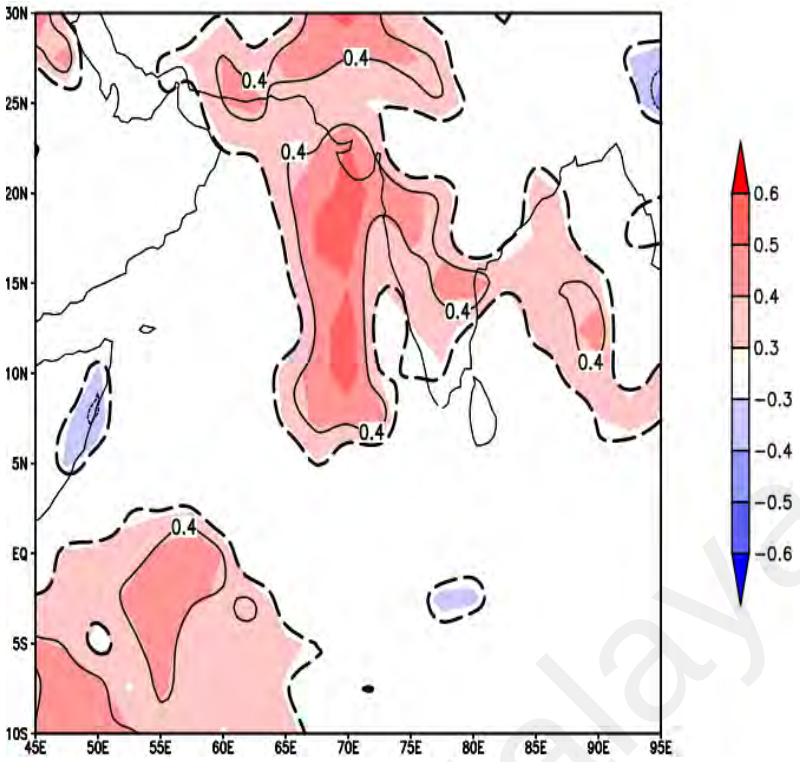

Figure 4.7: Spatial correlation between the AMJ sea ice extent in the Indian Ocean sector and Indian summer monsoon rainfall over India region from 1979 - 2013. The dashed lines are statistically significant at $p < 0.05$

The variability of Antarctic sea ice is well known to be affected by the variation of the SAM, ENSO, and the southern Indian Ocean Dipole (Raphael et al., 2011). In a previous study, Turner et al. (2015) discovered that SAM plays an important essential role in the variability of the sea ice extent in the Indian Ocean sector. The features of the correlation between the sea ice extent in the Indian Ocean sector and MSLP had the same characteristics as the SAM features. This suggests that SAM plays a significant role in sea ice extent variability, particularly over the Indian Ocean sector. As a result, a partial correlation was carried out between the AMJ sea ice extent in the Indian Ocean sector, Indian summer monsoon rainfall, and the atmospheric variability of SAM, ENSO, and southern Indian Ocean Dipole over a period of 35 years (Table 4.2). The results show the partial correlation coefficient remains significant at 0.40 ($p < 0.05$) after controlling for SAM variability (Marshall 2003) or removing the influence of SAM. In other words, SAM did not have any influence in this relationship. Similar findings were noted for the

ENSO and the southern Indian Ocean Dipole; both have a negligible impact on the variability of the sea ice extent in the Indian Ocean sector and Indian summer monsoon rainfall.

Table 4.2: Partial correlation coefficient between sea ice extent in the Indian Ocean sector, Indian summer monsoon rainfall and atmospheric variability

	Sea ice extent in the Indian Ocean sector and Indian summer monsoon rainfall	
Atmospheric variability	Partial correlation coefficient (removed influence of)	p-value
SAM	0.400	0.029*
ENSO	0.434	0.010*
SIOD	0.457	0.007*

(* is statistically significant at $p < 0.05$; SIOD: southern Indian Ocean Dipole)

4.4 Composite analysis: Influence of the sea ice extent in the Indian Ocean sector on the Mascarenes High

The previous section and previous studies (Prabhu et al. 2006; 2009) show a statistical relationship between the sea ice extent in the Indian Ocean sector and Indian summer monsoon rainfall. In investigating the sea ice extent influence in the Indian Ocean sector on Indian summer monsoon rainfall, the correlations between the sea ice extent in the Indian Ocean sector and MSLP from 1979 to 2013 were analysed. The maximum coefficient value for the correlation between the AMJ sea ice extent in the Indian Ocean sector and the MJJ MSLP was found over the southern Indian Ocean between 30^{o} S and 50^{o} S. (Figure 4.8). On the other hand, negative correlations were observed over the Antarctic continent and in some parts of Southeast Asia. The composite of the sea ice extent in the Indian Ocean sector in different phase years was classified as HIP and LIP in order to get more insight into the variability of sea ice extent in the Indian Ocean sector. As mentioned in the methodology section, years were categorised based on

the sea ice extent in the Indian Ocean sector index greater than one or less than the negative one standard deviation. Therefore, the years classified as HIP years are 1989, 1993, 1998, 2008, 2009, and 2010, while 1980, 1986, 1987, 1988, 1991, 1992, and 2003 are LIP years. Figure 4.9 depicts the HIP and LIP years in greater detail.

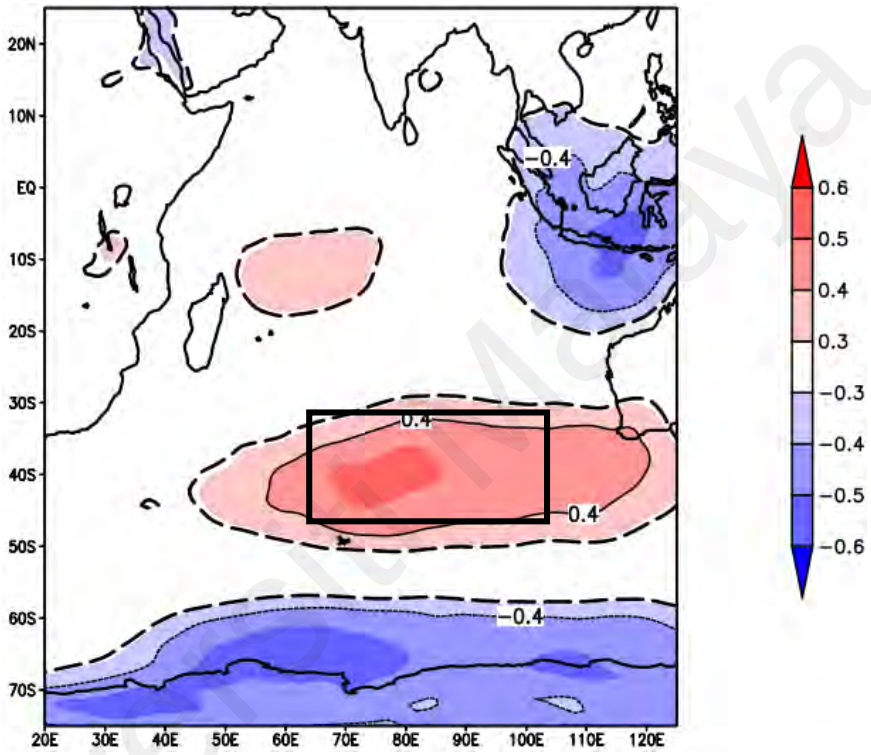

Figure 4.8: Spatial correlation between AMJ sea ice extent in the Indian Ocean sector and MJJ MSLP (in hPa) from 1979 - 2013. The dashed lines are statistically significant at p < 0.05. The black box is defined as Temporal Mascarene high (TMH) area

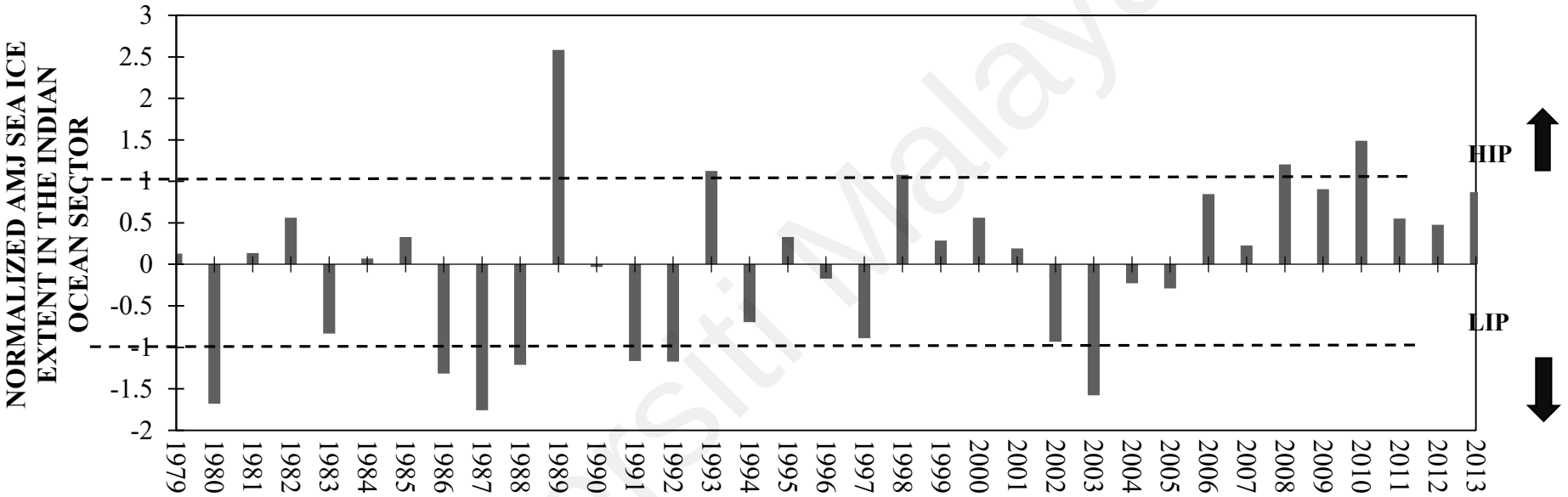

Figure 4.9: Normalized value of sea ice extent in the Indian Ocean sector (sea ice extent in the Indian Ocean sector index) during AMJ from 1979 – 2013. The dashed lines are the threshold above +1 and below -1 standard deviation

The composite analysis of MSLP, 500 hPa geopotential height, and wind vector at 850 hPa anomalies were further analysed during the HIP and LIP years to investigate the physical mechanisms of the sea ice extent in the Indian Ocean sector influence on the variability of Mascarene High.

During the HIP years, the features of the composite MSLP anomaly demonstrated a positive anomaly value between 30° S and 58° S. In comparison, a negative anomaly value existed near the Antarctic continent at 66° S (Figure 4.10a). The maximum positive anomaly was about 2 hPa. It covered the eastern and southern Indian Ocean at about 100° E and 35° S. This positive value implies that the MSLP has intensified over the southern Indian Ocean, including some of the Mascarenes High regions. However, this inclusive region does not reflect the whole Mascarenes High system. Furthermore, this positive anomaly value strongly suggests that the Mascarenes High region is more intense than in normal years, and its location is more eastwards during this phase, consistent with findings by Manatsa et al. (2014). They discovered that when the location of the Mascarene High was shifted east of its normal position, the convection over the western equator of the southern Indian Ocean increased. Furthermore, the intensification of the Mascarene High is modulated by the development of the circumpolar lows in the high latitudes of the Antarctic region due to the AAO signal (Xue et al., 2004). Another possible explanation for the positive association between the sea ice extent in the Indian Ocean sector and Mascarene High is the modification in circulation variabilities that occur at the upper and lower levels during the phases of sea ice extent in the Indian Ocean sector. According to Parise et al. (2015), as sea ice increases, the polar jet is strengthened and shifted poleward at the upper level, while the subtropical jet is weakening and expanding northward. Meanwhile, lower-level data show a seesaw feature between the high and middle latitudes, with a decrease in MSLP over the high latitudes and an increase

in MSLP over the middle latitudes. This finding is consistent with Smith et al. (2017) and Bader et al. (2013). They discovered the southern hemisphere middle latitude tropospheric jet shifted poleward to the enhanced Antarctic sea ice extent, which altered equatorward in response to less sea ice. A similar pattern appeared at 500 hPa geopotential height, implying a barotropic feature during the HIP years (Figure 4.10b). The positive anomaly was noticed over the southern Indian Ocean, where the prominent ridge lengthened eastward, whereas the negative anomaly was detected over the Antarctic continent. Furthermore, the contour line features were also nearest to each other, indicating a tightened gradient during this phase.

The wind anomaly at 850 hPa significantly changes as the MSLP anomaly over the southern Indian Ocean strengthens, forming a powerful anticyclonic anomaly at 30°–50° S (Figure 4.10c). As it crossed the equator, the northern branch of this strong anticyclonic wind anomaly generated a stronger westerly wind or Somali Jet. According to Shi et al. (2016), the intensification of the Somali Jet carries a massive amount of water vapour towards the Western Ghats, causing an increase in heavy rainfall across western India. This is compatible with Li et al. (2014) study, the anticyclonic anomalies over the Mascarene High region strengthened the southwesterly wind near the Somali coast or the Somali Jet and therefore enhanced the Indian summer monsoon rainfall. A similar conclusion was made by Xue et al. (2004) and Rao et al. (2017), they demonstrated that as the Mascarene High intensifies, so does the Somali Jet and the Indian summer monsoon rainfall. Furthermore, the strong westerly wind and outflow winds over the high latitudes at about 70^{o} S, particularly from the Indian Ocean sector, play an important role in sea ice expansion (Jena et al., 2018) during the HIP years. This is also due to increased Ekman drift in the ocean, allowing strong westerly winds to move sea ice to the north (Stammerjohn et al., 2008).

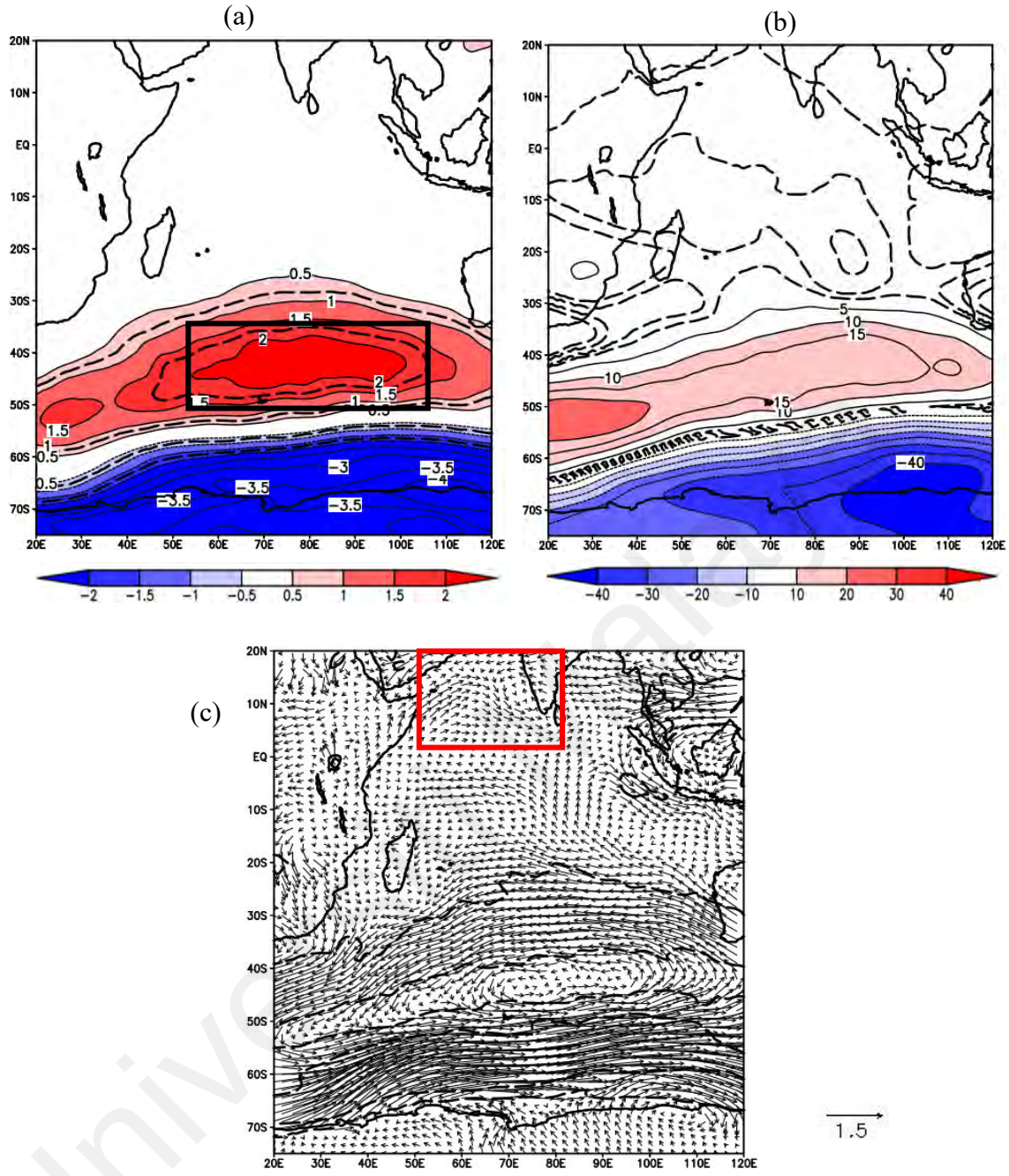

Figure 4.10: Composite anomalies of MJJ a) MSLP (in hPa), b) geopotential height at 500 hPa (in m) c) wind vector at 850hPa (in ms^{-1}) during HIP years. The black box denotes the maximum positive MSLP anomaly, the red box is the area that corresponds to the Somali Jet. The dashed lines are statistically significant at p < 0.05

In contrast to the HIP years, a negative anomaly of MSLP was observed over the south Indian Ocean sector while a positive anomaly appeared at the south of the latitude circle, 60° S, including the Antarctic continent (Figure 4.11a). The maximum negative

anomaly value dropped below - 2hPa over the south Indian Ocean, centring on the latitude of 56° S, extending towards Madagascar's coast. This feature implies the weakening of the Mascarenes High during the LIP years and also that the position of the Mascarenes High was more westwards than its normal position. At 500 hPa geopotential height (Figure 4.11b), the decreased value occurred over the western part of the southern Indian Ocean near the coast of Madagascar. The maximum value of the negative anomaly dropped to 20 m from the normal reading. This pattern is similar to the MSLP composite anomaly, where a significantly positive anomaly was noticed over the Antarctic region. Both patterns correspond to a weakened Mascarenes High region during the LIP phase years. The weakening of the Mascarene High area is associated with the development of an intense cyclonic wind anomaly at 850 hPa over the western part of the southern Indian Ocean, close to the coast of Madagascar (Figure 4.11c). A strong wind anomaly towards the Antarctic continent corresponded to the retreat of ice during this phase. Also, contrary to the HIP years, the strong easterly wind anomaly was seen between 3° N – 10° N.

The composite analysis of all the above parameters (Figures 4.10 and 4.11) revealed that the variability of sea ice extent in the Indian Ocean sector influences the Mascarene High variability. It is possible to conclude that the sea ice extent in the Indian Ocean sector is related to the high variability of Mascarene, with Mascarene High strengthening during the HIP years and weakening during the LIP years. This phenomenon, in turn, affects the intensity of Somali Jets. Furthermore, the Mascarene High shifted westward and eastward from its normal position during the HIP and LIP years.

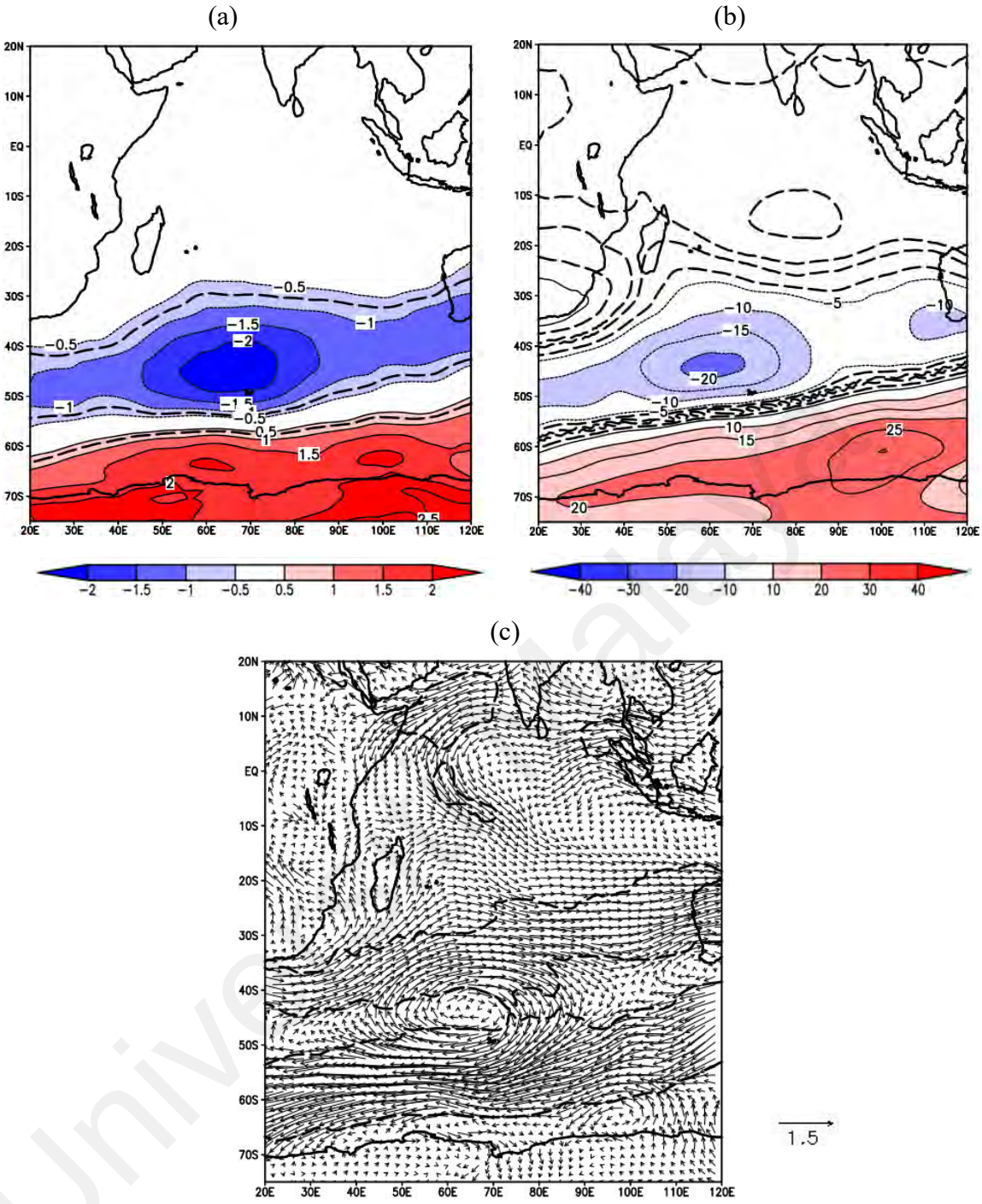

Figure 4.11: Composite anomalies of MJJ a) MSLP (in hPa), b) geopotential height (in m) at 500 hPa c) wind vector at 850hPa (in ms^{-1}) during LIP years. The dashed lines are statistically significant at $p < 0.05$

4.5 Role of the Mascarene High towards Indian summer monsoon rainfall

The Mascarene High variability is essential in defining the strength of Indian summer monsoon rainfall (Wu et al., 2012; Ahasan et al. 2014) by the influence of the intensity of the Somali Jet. The intensification of the Mascarene High strengthens the

Indian monsoon westerlies and Somali Jet (Xue et al., 2004; Li and Li, 2014), which transport a large amount of moisture to the Indian subcontinent. The Temporal Mascarene High (TMH) index was developed to explore Mascarene High's influence on monsoon rainfall. The normalisation of MSLP determines the TMH index during MJJ over the TMH region. For this purpose, the TMH is defined as the correlation coefficient highest value with the sea ice extent in the Indian Ocean sector, as shown in Figure 4.8. The latitude and longitude of the region are 35° – 47° S and 65° – 90° E, respectively. The correlation coefficient between the time series of the AMJ sea ice extent in the Indian Ocean sector index and the TMH index for 35 years was 0.53, statistically significant at $p < 0.05$ (Figure 4.12). Therefore, from the value, it can be concluded that the chosen TMH region is the best area to investigate the relationship between sea ice extent in the Indian Ocean sector and Mascarene High. Even so, as previously stated, this TMH region does not encompass the entire Mascarene High system.

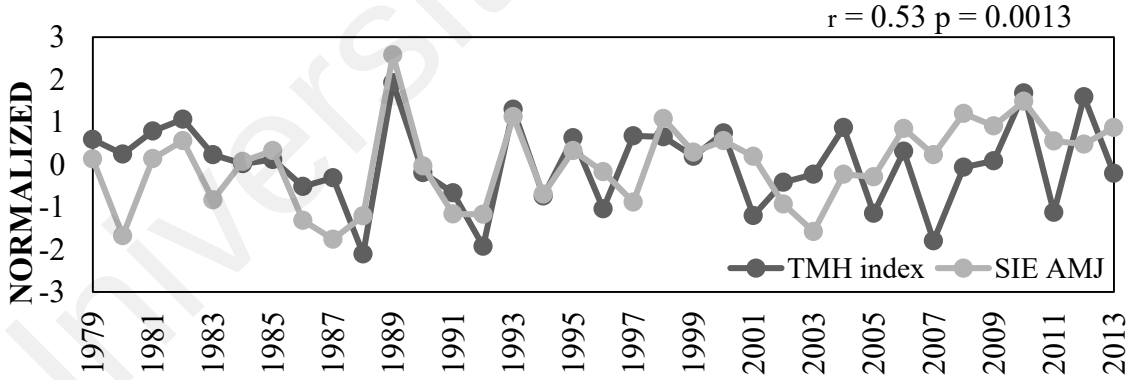

Figure 4.12: Correlation coefficient between the time series of normalized AMJ sea ice extent in the Indian Ocean sector (grey) and the Temporal Mascarene High (TMH) index (black), statistically significant at $p < 0.05$

For many decades, researchers have investigated the relationship between the Mascarene High and Indian summer monsoon rainfall (Krishnamurti and Bhalme 1976). However, the mechanism is still poorly understood. Here, the influence of the TMH on the Indian summer monsoon rainfall was investigated further by utilising the composite anomalies of the velocity potential at the lower level (850 hPa) and upper (200hPa)

troposphere. The purpose of this analysis was to describe the convergence and divergence anomaly features over the Indian region during the strengthening and weakening phases of the Mascarene High. TMH indexes are categorised based on one standard deviation value: greater than one is positive TMH, while less than 1 is negative TMH. As a result, the TMHI+ years were 1982, 1989, 1993, 2010, and 2012, while the TMHI- years were 1988, 1992, 1996, 2001, 2005, 2007, and 2011. Figures 4.13 and 4.15 show the composite anomaly of velocity potential and divergence wind for TMHI+ and TMHI- at 850 hPa and 200 hPa, respectively. During the TMHI+ years or strengthening of TMH, there is a strong convergence anomaly zone at 850 hPa, especially over the region of the western Peninsular Indian and Arabian Sea (Figure 4.13a) and a strong divergence anomaly over in the same area at 200 hPa (Figure 4.13b). This implies a strong vertical upward flow of air, which contributes to the formation of clouds and produces heavy rainfall over the region (Dike et al., 2014). Compatible features are seen in rainfall composite anomalies, where positive anomalies are found along the Indian Peninsula's west coast, the Bay of Bengal, and a narrow region of the eastern coast of the Indian Peninsular. In comparison, a negative anomaly is seen over the eastern part of India (Figure 4.14). Consistent with Saeed et al. (2011) and Sinhaa et al. (2013), both mentioned the Indian Peninsula's west coast region received an excessive amount of rainfall, while the eastern central of India received less rainfall during the Indian summer monsoon rainfall period. As previously stated, this is because of the orographic impacts on the precipitation and the other regions are mostly influenced by the northeast monsoon.

The TMHI- years or period of TMH weakening exhibit the opposite characteristics (Figure 4.15). Strong divergence and convergence anomalies are seen at 850 hPa and 200 hPa, covering almost the entire Indian region (Figure 4.15a and 4.15b). The strong divergence surface and upper-level convergence anomalies are centred over India's north

and central regions, respectively, resulting in clear skies and pleasant weather. Besides, during the weakening years, the composite rainfall shows a negative anomaly over the west coast of Peninsular India, central India, and the Bay of Bengal, implying less rainfall than normal (Figure 4.16).

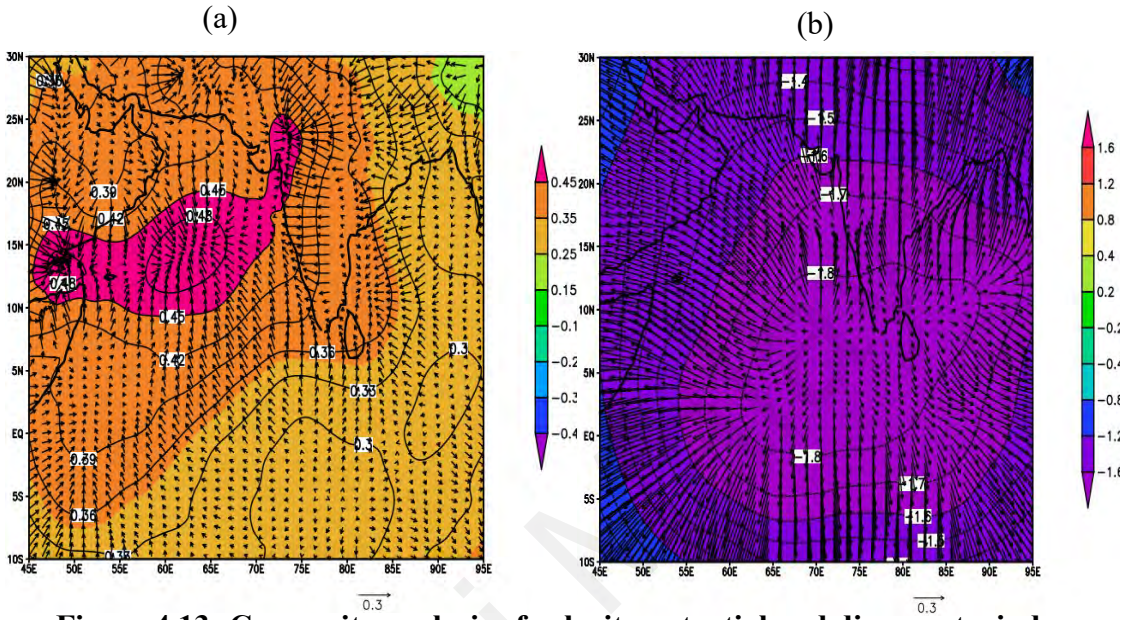

Figure 4.13: Composite analysis of velocity potential and divergent wind anomalies for the positive TMHI (TMHI+) years during JJAS at (a) 850hPa (in 10^6 m^2/s) and (b) 200hPa (in 10^6 m^2/s)

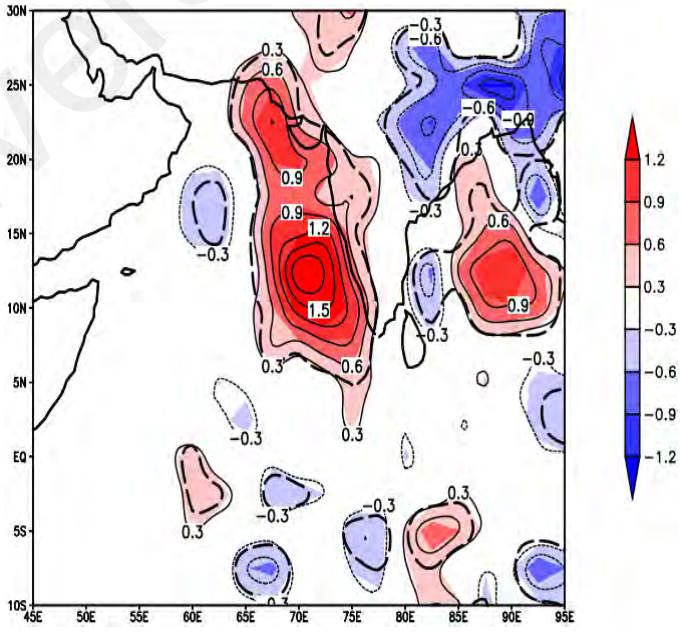

Figure 4.14: Composite analysis of GPCP rainfall anomaly (in mm/year) during Indian summer monsoon rainfall for the positive TMHI (TMHI+) years. The dashed lines are statistically significant at $p < 0.05$

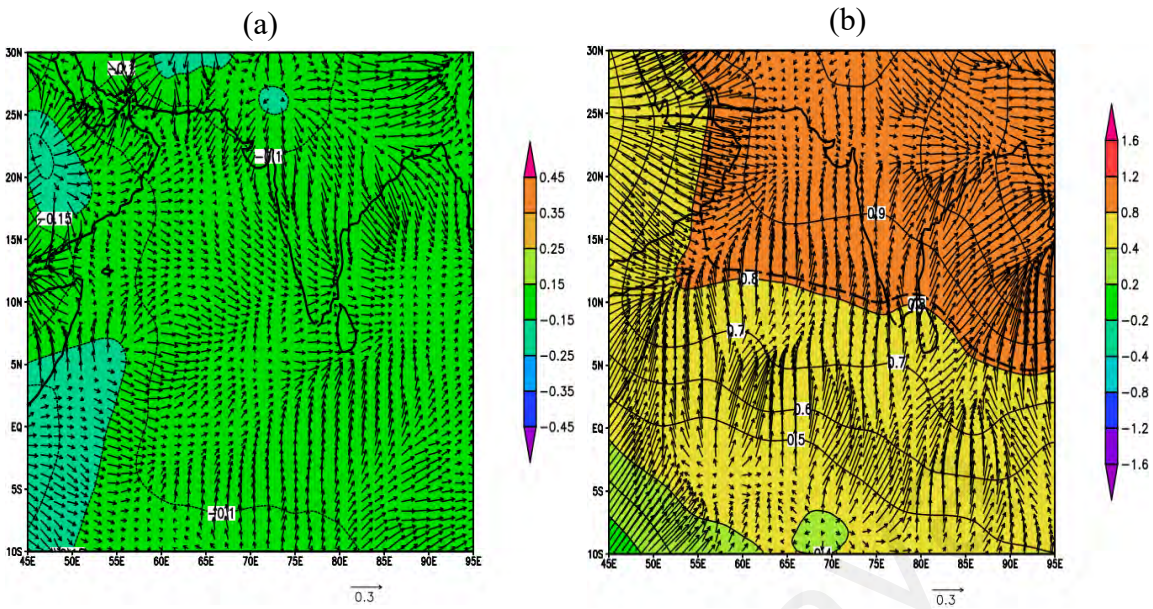

Figure 4.15: Composite analysis of velocity potential and divergent wind anomalies for the negative TMHI (TMHI-) years during summer at (a) 850hPa (in 10^6 m^2/s) and (b) 200hPa (in 10^6 m^2/s)

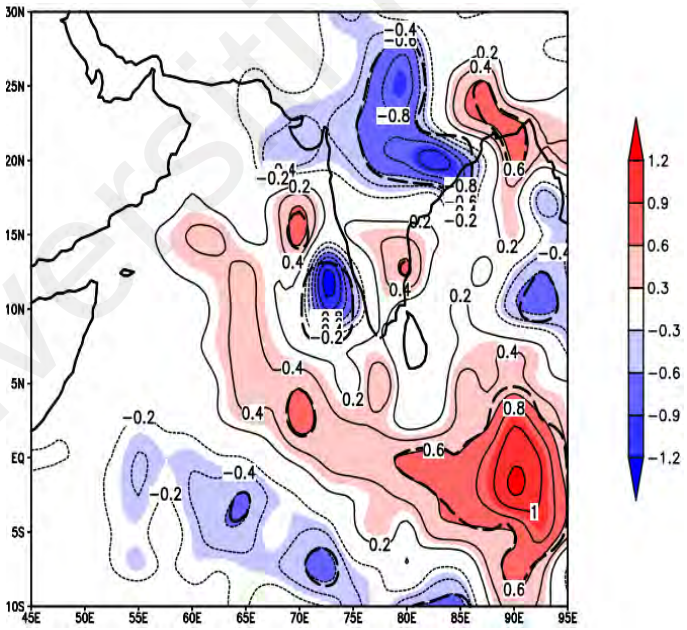

Figure 4.16: Composite analysis of GPCP rainfall anomaly (in mm/year) during Indian summer monsoon for the negative TMHI (TMHI-)year. The dashed lines are statistically significant at $p < 0.05$

4.6 Conclusion

In summary, there is a relationship between sea ice extent in the Indian Ocean sector during AMJ with the Indian summer monsoon rainfall, especially over Peninsular India from 1979 – 2013, for both statistical and spatial correlation analysis. Furthermore, the composite and phase analysis demonstrated that Mascarene High is a bridge that links the AMJ sea ice extent in the Indian Ocean sector and the Indian summer monsoon rainfall. The results illustrated the increased sea ice extent in the Indian Ocean sector (HIP years) strengthened the Mascarene High and southerly winds, resulting in more rainfalls along with the west Peninsular India during the Indian summer monsoon rainfall period. Opposite features for the decreased sea ice extent in the Indian Ocean sector (LIP years), weakened Mascarene High and the southerly winds or Somali Jet and caused dry weather in central India and the surrounding area.

CHAPTER 5

MECHANISMS ASSOCIATED WITH TELECONNECTION BETWEEN THE SEA ICE EXTENT IN THE INDIAN OCEAN SECTOR AND THE INDIAN SUMMER MONSOON RAIFALL

5.1 Introduction

Several studies have reported the teleconnection between Antarctic sea ice and Indian summer monsoon rainfall (Dugam et al., 2004; Prabhu et al., 2009; Azhar et al., 2020; Prabhu et al., 2021; Bajish et al., 2021). The statistical relationship has been recognized and well-established in previous studies, as mentioned previously. This includes the study by Azhar et al. (2020). Nonetheless, the mechanisms that explain the connection have not yet been fully explored. For example, how does the sea ice extent signal variability in the Indian Ocean sector affect the Indian summer monsoon rainfall variability? Is there any involvement in wave propagation? All these questions are not explained in Chapter 4. Therefore, this chapter will illustrate the response of answering those arising questions by identifying the possible routes and propagation of any wave signal. In addition, how the CMIP5 model simulates these teleconnection patterns will also be discussed.

5.2 Possible mechanisms of interaction: How does the sea ice extent in the Indian Ocean sector affect Indian summer monsoon rainfall?

Based on the findings of the previous chapter, sea ice extent in the Indian Ocean during AMJ is the most significantly positively associated with Indian summer monsoon rainfall. An EOF analysis was conducted on datasets of AMJ sea ice extent and JJAS precipitation from 1979 to 2013 to get a more in-depth understanding of the connection.

The results of the analysis of these two variables are shown in Figure 5.1. Figures 5.1a – 5.1c show the spatial patterns of the first three leading EOF modes of AMJ sea ice extent over the last 35 years. The first EOF mode (EOF1) accounts for over 40.47% of the total variance in sea ice extent. The spatial distribution of EOF1 shows negative sea ice extent anomalies across the entire Indian Ocean sector. The second EOF mode (EOF2) mode accounts for 17.03% of the total variance and shows a spatial pattern of positive sea ice extent anomalies over the western Indian Ocean and negative sea ice extent anomalies over the eastern Indian Ocean. The third EOF mode (EOF3) accounts for 8.40% of the total variance and is illustrated by a spatial pattern of a positive sea ice extent anomaly in the center of the sector and negative sea ice extent anomalies to the east and west. In other words, sea ice extent is more pronounced in the center and northwest of the region, while it is less pronounced in the west and east towards the coast. On the same note, EOFs explained 27.01%, 12.66%, and 10.44%, respectively, of the total variance in precipitation during the JJAS monsoon season. This is shown in Figures 5.1d-5.1f. Positive anomalies of precipitation were observed in the spatial pattern of EOF1 in the northern part of Peninsular India, up to the Bengal Bay and the western part of the Indian Ocean. On the other hand, negative anomalies of precipitation were observed over the southwest of Peninsular India, the eastern of Indian Ocean, and the north of India. In the meantime, the EOF2 spatial pattern reveals the most prominent characteristics of positive anomalies of precipitation observed over the Indian subcontinent, the Arabian Sea, and the Bay of Bengal. Contrasting with the EOF2 mode, the EOF3 spatial pattern reveals negative precipitation anomalies over the Indian subcontinent and Bay of Bengal, while positive precipitation anomalies are observed over the Indian Ocean.

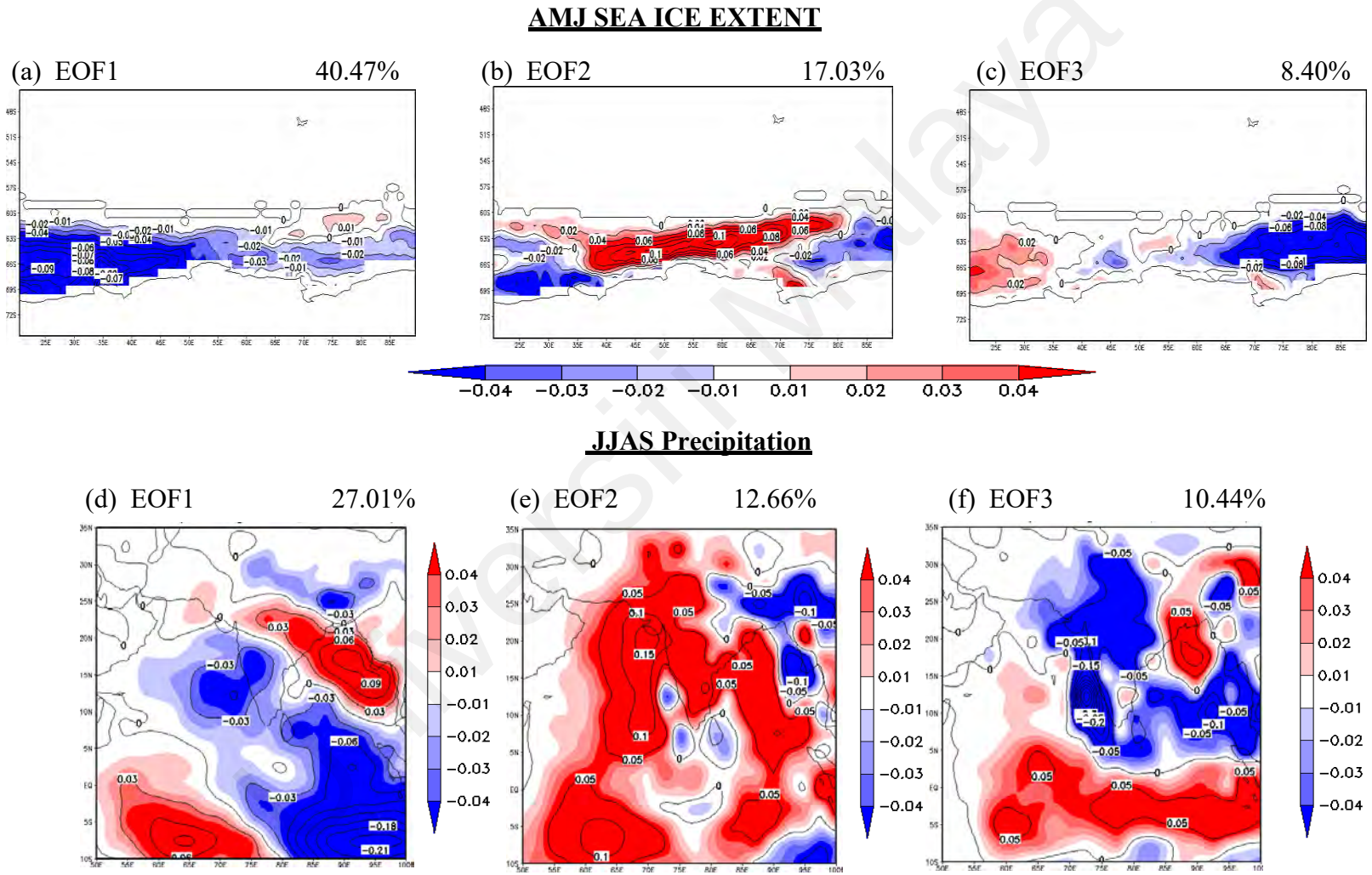

Figure 5.1: The spatial pattern of three leading EOF modes of sea ice extent (a) – c)) (in %) in AMJ and precipitation (d) – f)) (in mm/year) in JJAS

The investigation was furthered by examining the correlation between the PCs of the EOF modes of Antarctic sea ice extent in the austral summer and precipitation in the Indian summer monsoon season. Table 5.1 provides an overview of the findings. The results demonstrate that the first principal component (PC1) and third principal component (PC3) of sea ice extent in AMJ are statistically significant with the second principal component (PC2) of precipitation. The table reveals an inverse association between PC1 of sea ice extent in AMJ and PC2 of precipitation, with a statistically significant correlation coefficient of $r = 0.49$ ($p < 0.05$) (as shown in Figure 5.2a). While, positive association between the PC3 of sea ice extent in AMJ with the PC2 of precipitation, with a statistically significant correlation coefficient of $r = 0.4$ ($p < 0.05$) (as shown in Figure 5.2b). Thus, both correlation coefficient values show that the variability of precipitation during the summer monsoon is significantly impacted by AMJ sea ice extent in the Indian Ocean sector.

Table 5.1: Summary of the correlation coefficient between the PC's time series of AMJ sea ice extent in the Indian Ocean sector and PC's time series of JJAS precipitation from 1979 to 2013

		Precipitation		
		P1.precip	**P2.precip**	**P3.precip**
sea ice extent in the Indian Ocean sector	**P1.sea ice extent**	-0.17	-0.49*	-0.12
	P2.sea ice extent	-0.18	-0.28	-0.09
	P3.sea ice extent	0.22	0.40*	-0.01

* and red circles statistically significant at $p < 0.05$

In actuality, the two patterns actually resemble one another in some ways; EOF1 exhibits negative anomalies of sea ice extent across the Indian Ocean sector, whereas EOF3 depicts positive anomalies of sea ice extent. However, in EOF3, especially close to the western and eastern boundaries, there is a mixed signal of negative and positive anomalies of sea ice extent. This implies that the Indian Ocean sector will be

predominantly characterized by negative or positive anomalies of sea ice extent when the time series of EOF is positive for EOF1 or EOF3. These two EOFs also exhibit distinct temporal patterns (as shown in Figures 5.2a and 5.2b). The time series of EOF1 shows a decreasing trend (as shown in Figure 5.2a), whereas the time series of EOF3 show no trend (as shown in Figure 5.2b). This implies that although these two patterns could be produced by distinct mechanisms, but they both lead to similar changes in sea ice extent. The decreasing trend in the time series of EOF1 suggests that anomalies of sea ice extent are increasing in the Indian Ocean sector. As a result, PC1 and PC3 of the sea ice extent in AMJ are chosen to determine the HIP and LIP years for a more in-depth examination of this association. The HIP and LIP years are classified according to the absolute and normalized values of PC1 and PC3 of sea ice extent in the Indian Ocean sector during AMJ, which are greater than or equal to 1 or less than or equal to -1 (≥ 1or ≤ -1). Table 5.2 contains a list of HIP and LIP years for each principal component of sea ice extent in AMJ. The existence of positive or negative anomalies of sea ice extent in the spatial patterns for EOF1 and EOF3 was determined according to HIP or LIP years.

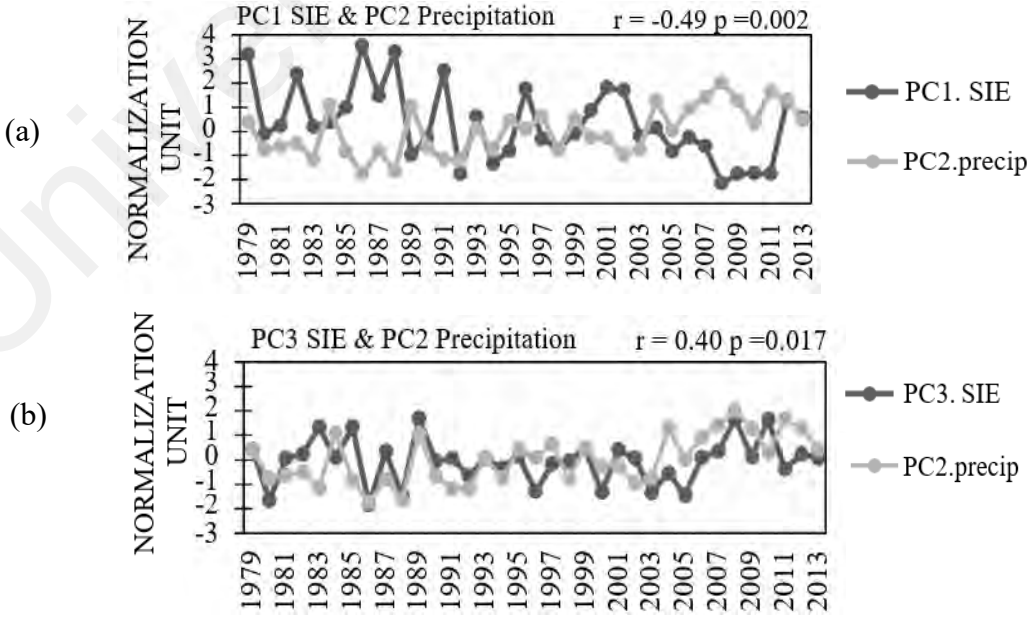

Figure 5.2: The correlation coefficient between the a) PC1 b) PC3 time series of AMJ sea ice extent in the Indian Ocean sector (black) with the PC2 time series of precipitation over the Indian region (grey) from 1979 -2013, statistically significant at p < 0. 05

Table 5.2: Summary of HIP and LIP years corresponding to PC1 and PC3 time series of AMJ sea ice extent in the Indian Ocean sector

PC's time series of AMJ sea ice extent in the Indian Ocean sector	HIP years	LIP years
PC1	1989, 1992, 1994, 2008, 2009, 2010,2011 **(7)**	1979, 1982, 1986, 1987, 1988,1991, 1996, 2001, 2002,2012 **(10)**
PC3	1983, 1985, 1989, 2008, 2009, 2010 **(6)**	1980, 1986, 1988, 1996,2000,2003, 2005 **(7)**

() is the numbers of years

The contour of geopotential height and wave activity flux at 250 hPa were analyzed during May, June, and July (MJJ) to identify every possible wave energy transmission. Figure 5.3 depicts the spatial regression of geopotential height at 250 hPa level for 35 years superposed with the difference between the wave activity flux composites that corresponds to the time series of PC1 (Figure 5.3a) and PC3 (Figure 5.3b) for the sea ice extent in the Indian Ocean sector during AMJ. Over the Indian Ocean, the geopotential height anomaly's contour at 250 hPa exhibit a tripolar pattern for both principal component modes. Figure 5.3a shows that anomalies are positive over the polar region, negative over the middle latitudes, and positive over the tropics from approximately 20° S to 10° S. Two paths are visible for the composite difference of wave activity flux as it travels south from the tropics to the polar region. One source is located in South Australia, and the other is located in the western Indian Ocean, near 30º S. Both wave trains travelled to the middle latitudes at 50º S, and then continuously travelled to the polar region. Additionally, it appears that the wave train diverges into the vicinity of the Mascarene high, altering the low level circulation there and promoting low level convergence (Ogwang et al., 2015; Jin et al., 2017) in the LIP years of the PC1 time series of EOF1. In contrast to Figure 5.3a, Figure 5.3b shows the contrary characteristics of the

geopotential height anomaly. A negative anomaly is present in the Southern Ocean's Indian Ocean sector, whereas approximately between 50° S to 30° S, a positive anomaly is present extending from the middle to the tropics and approximately between 30° S to 10° S over the tropics, a negative anomaly is present. The difference in the composite of wave activity flux anomalies showed a northward-moving wave train with two distinct routes that originated in the polar region and propagated towards the middle latitudes and the tropics. Begins its journey from the Indian Ocean sector, one is moving toward the middle latitude throughout the center of the Indian Ocean at approximately 35° S, especially over the Mascarene High region, and then it keep moving its journey toward the tropics at approximately 15° S. Furthermore, the wave train appears to converge into the Mascarene High region and increases low-level divergence during the HIP years of the PC3 time series of EOF3. It's worth noting that the anomalies of the geopotential height patterns for both EOFs presented are similar but in opposing phases. As previously stated, the reason for this is that EOF1 or EOF3 positive phases are marked by negative or positive anomalies of the sea ice. In short, positive sea ice anomalies (HIP years) in both EOFs will produce similar wave propagation. Stronger easterlies emerge from the Mascarene High, bringing powerful cross - equatorial flows and strong south westerlies over the India region. Consequently, rainfall increases in the Indian region when sea ice anomalies in the Indian Ocean sector are positive. As a result, when sea ice anomalies in the Indian Ocean sector are positive, rainfall increases in the Indian region. This feature was previously discussed in Chapter 4 (section 4.4), and Sun et al. (2009) agreed on it. It was found that the enhancement of the upper level meridional teleconnection wave train is strongly associated with the variability of the Mascarene High and the wind circulation at lower levels. These circulation patterns between the upper and lower levels provides clear evidence of the variability of sea ice extent affects the Mascarene High, which in turn influences rainfall over the Indian region. It is important to note that there are no data

in the areas from 0 ~ 10° S latitude since the calculation of wave activity flux includes the Coriolis parameter in the denominator of the formula. The values at the equator are masked due to the low Coriolis effect and may not represent realistic levels of wave activity flux. In addition, the anomalous geopotential height of 250 hPa is followed by an alteration in the polar front and subtropical jet.

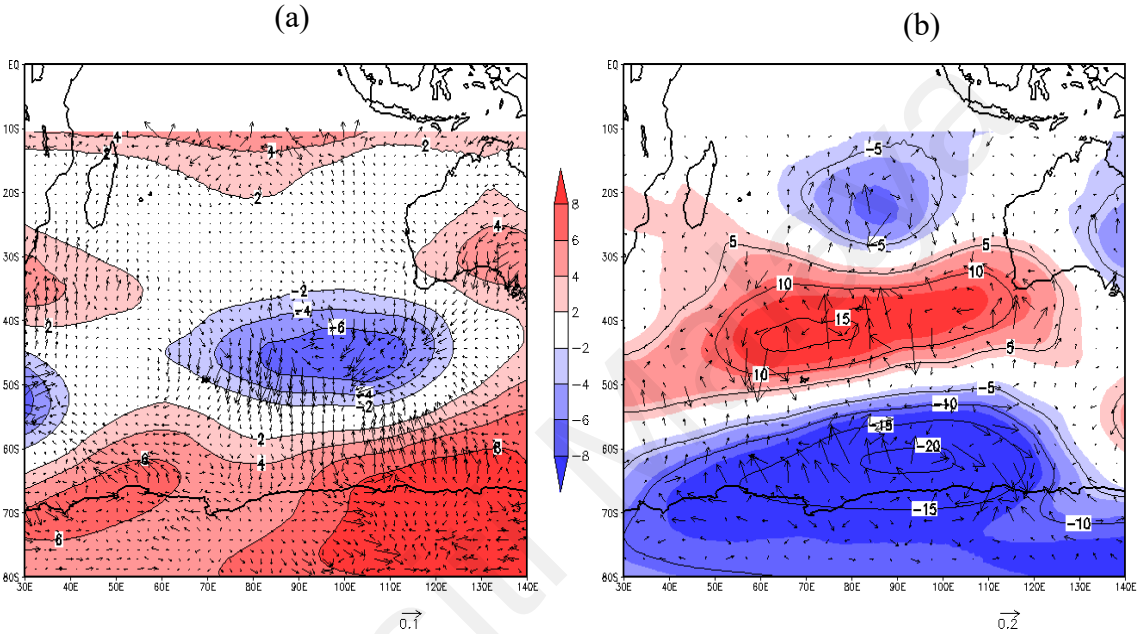

Figure 5.3: The regressed anomalous contour of geopotential height (shaded and contour, in m)for 35 years superimposed with the composite difference of wave - activity flux (in m^2s^{-2}) for high and low phases of EOF1/EOF3 corresponding to a) PC1 b) PC3 time series of AMJ sea ice extent in the Indian Ocean sector during MJJ at 250 hPa

Figure 5.4 displays the vertical profiles of difference in the composite of zonal wind average for PC1 (Figure 5.4a) and PC3 (Figure 5.4b) time series of the sea ice extent in the Indian Ocean sector during AMJ. Since EOF1 and EOF3 both represent opposite phases of sea ice anomalies in the Indian Ocean sector (more and less), the composites created from them also represent these opposite phases. The aforementioned explanations are comparable to those in Figure 5.3. Simmonds and Budd (1991) investigated how variations in the amount of open water in the polar ice packs would affect the Southern Hemisphere Circulation using General Circulation Models (GCMs). Experiments with

different amounts (50% and 100%) of open water in the pack ice showed that the winds in the region between 40° S and 60° S were anomalously easterly, while the winds further south were anomalously westerly. Furthermore, the same features existed for 80% of the open water, but an anomalously easterly band did not reach the surface. The difference in the composite of zonal wind shown in Figure 5.4 exhibits barotropic nature, and its characteristics and structure are similar to those reported by Simmonds and Budd (1991). Figure 5.4a illustrates that the zonal wind average has its maximum negative anomalies at 58° S and its maximum positive anomalies at 38° S. These anomalies occur at an altitude of about 400 hPa and 250 hPa. The polar front jet is weaker during the LIP years of the PC1 time series of EOF1 as evidenced by the difference of -2 ms^{-1} in the maximum anomalies of the HIP and LIP years. On the other hand, the subtropical jet showed only a slight difference in the value of maximum anomalies in both phases, suggesting that it was minimally affected as contrasted with the polar front jet. Figure 5.4b depicts the opposing features of zonal wind averages, with the maximum positive anomalies located at about 56° S and negative anomalies located at 36° S, respectively, at levels of roughly 450 hPa and 150 hPa. The maximum anomalies of the PC3 time series of EOF3 show a difference of 4 ms^{-1}, demonstrating that in the HIP years saw an increase in the strength of the polar front jet. Similar to EOF1, the subtropical jet also has little effect during both phases.

(a)

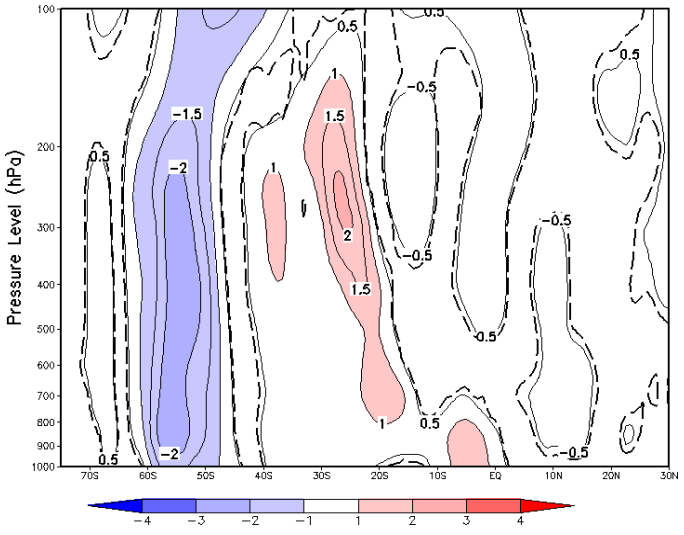

(b)

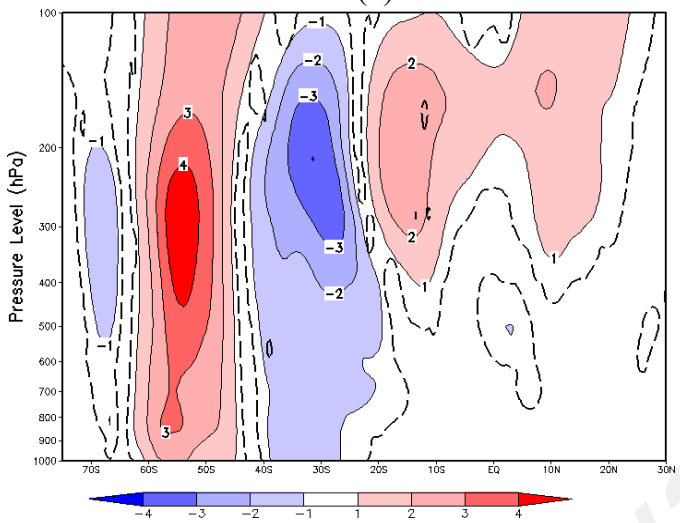

Figure 5.4: The vertical profile of composite difference of zonal wind average for high and low phases of EOF1/EOF3 (in ms^{-1}, averaged over 55° E– 85° E) corresponding to a) PC1 b) PC3 time series of AMJ sea ice extent in the Indian Ocean sector. The dashed lines are statistically significant at $p < 0.05$

As stated by Carvalho et al. (2005), the variability of the jet stream, which affects the characteristics of the atmospheric circulation, is strongly associated with the anomalies of zonal wind variability at the upper troposphere. Additionally, the simultaneous change in the strength and position of the polar front jet and subtropical jet provides a crucial sign of the teleconnection between at circulation systems at high and low latitudes (Luo et al., 2015). Figure 5.5 depicts the difference in the composite of the zonal wind anomalies overlapping with the composite difference of the wind anomalies during MJJ at 250 hPa for the time series of PC1 (Figure 5.5a) and PC3 (Figure 5.5b) of the sea ice extent in the Indian Ocean sector during AMJ. Figures 5.5a and 5.5b demonstrate a quadrupole pattern distribution in anomalies of the zonal wind at 250 hPa from high to low latitudes for both principal components of EOF modes. The anomalies of zonal wind in Figure 5.4a depict positive anomalies over the small portions of the eastern and western Indian Ocean sector, negative anomalies over the high latitudes from approximately 65° S to 55° S, positive anomalies from approximately 45° S to 25° S over the middle latitudes, and negative anomalies from approximately 20° S to 10° S over the

low latitudes. The distributions of the pattern are linked with the strong cyclone and anticyclone anomalies of winds at approximately 60° S and 20° S, respectively. The strong cyclone and anticyclone anomalies of winds suggest strong upper level divergence and lower level convergence during the LIP years of the PC1 time series of EOF1(Cheng et al., 2019; Zhao et al., 2021). The opposing characteristics of anomalies of the zonal wind anomalies are shown in Figure 5.4b along with the anomalies of the wind. The anomalies of zonal wind illustrate negative anomalies over the Indian Ocean sector region, positive anomalies from approximately 70° S to 55° S over the high latitudes, negative anomalies from approximately 50° S to 25° S over the middle latitudes, and positive anomalies from approximately 20° S to equatorial over the low latitude. The distributions of the pattern are linked with the strong anticyclone anomalies of winds at a latitude of 50° S over the southwestern Indian Ocean, indicating a stronger upper level divergence, which would result in more subsidence and more significant lower level convergence. Furthermore, the pattern distributions are also linked with strong cyclone anomalies of winds at a latitude of 70° S over the Indian Ocean sector region and at a latitude of 20° S over the central Indian Ocean. The strong cyclone anomalies of the winds suggest strong upper convergence and lower divergence anomalies during the HIP years of the PC3 time series of EOF3(Cheng et al., 2019; Zhao et al., 2021). From the finding above, it is obviously shown that the weather patterns of middle latitude are influenced by HIP and LIP years, as inferred by EOF1 and EOF3. This influence is exerted by altering the jet stream variability, which is caused by several factors such as an increase in the disparity in temperature between the poles and the middle latitudes, an increase in the strength of the westerly winds, etc. Furthermore, the shifting of the westerly jet to the poles during the austral summer is also linked to both emissions of greenhouse gases and substances that harm the ozone layer (Cohen et al., 2014; Screen et al., 2018; Blackport and Screen, 2020). Therefore, the change in anomalies of zonal wind during HIP and LIP years of

the sea ice extent in the Indian Ocean sector suggests a meridional upper and lower level teleconnection between the polar region and summer monsoon rainfall. In accordance with Hoskins and Ambrizzi (1993) findings, infer that zonal winds at the upper level is capable serve as characteristic of teleconnection, enabling a more in-depth comprehension of propagation features from the middle to the low latitude.

Furthermore, the variation in jets are closely related with the Ferrel cell variability and Hadley cell position (Sun et al., 2009; He et al., 2011; Shi et al., 2016; Manzel et al., 2019). The tropical and subtropical climates, together with the global circulation of the atmosphere between the high and middle latitudes, are significantly influenced by the Ferrel and Hadley cells (Li and Wang, 2003; Nguyen et al., 2013; Hu et al., 2018; Rudeva et al., 2019). Hudson et al. (2001) proposed that changes in atmospheric pressure at sea level are confirmed by change in vertical air motion. The positive anomalies of the sea level pressure are induced by the intensification and southward expansion of the high pressure belt in subtropics. When the pressure is reduced, the ascending branch of the Ferrel cell experiences a greater upward motion of air. The following section goes into more detail about the atmospheric circulation in relation to the Polar cell, Ferrel cell and local Hadley cell variability.

(a)

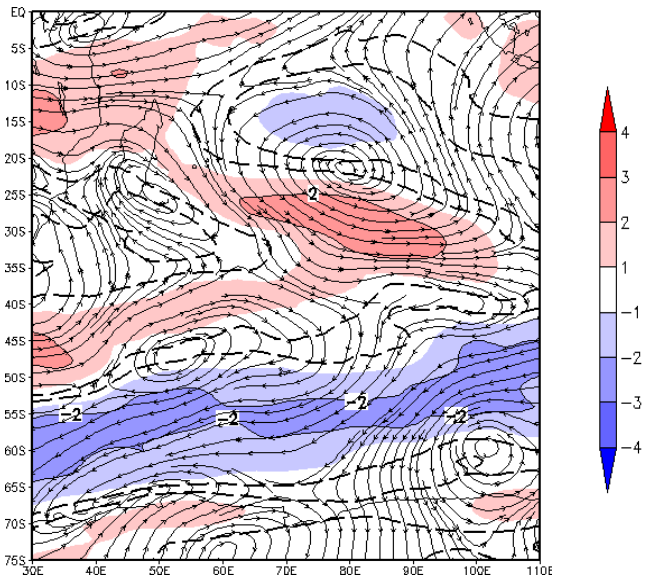

(b)

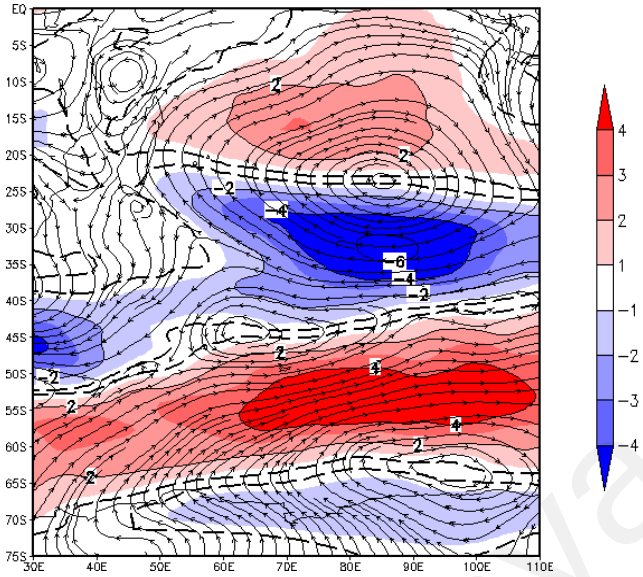

Figure 5.5: The composite difference of zonal (shaded) wind (streamlines) anomalies at 250 hPa (in ms^{-1}) for high and low phases of EOF1/EOF3 and corresponding to a) PC1 b) PC3 time series of AMJ sea ice extent in the Indian Ocean sector. The dashed lines are statistically significant at $p < 0.05$

5.3 Variation in meridional circulation: Polar Cell, Ferrel Cell and Hadley Cell

The changes in meridional circulation have a major influence on climate change (Hu and Fu, 2007). It also makes up the majority of the linkages between the polar and tropical regions (Liu et al., 2002). Nevertheless, the mechanism is not well understood, particularly in terms of how sea ice extent variability associate to the tropical disturbances. The difference of composite meridional circulation is averaged over the Indian Ocean longitudinal belt (55º E to 85º E) from 1000 to 200 hPa corresponds to the PC1 (Fig. 5.6a) and PC3 (Fig. 5.6b) time series of the sea ice extent in the Indian Ocean sector during AMJ shown in Figure 5.6. The red areas on the map represent upwards airflows, while the blue areas represent downward airflows. These airflows are indicated by the positive and negative anomalies of vertical velocities, respectively. The Polar cell in Fig. 5.6a illustrates lesser activity during the LIP years of the PC1 time series of EOF1. This is evident in the weaker upward motion anomalies from 80° S to 70° S during these years. The Ferrel cell has its downward branch at approximately 30° S and its upward

branch at approximately 60° S, respectively, and they illustrate weaker downward and upward of airflows. Regarding the Hadley cell, the primary ascending branch is approximately 10º N and the principal descending branch is approximately 10° S to 15° S. They also illustrate weaker upward and downward of airflows. The spatial regression features of anomalies in the geopotential height at 250 hPa in Figure 5.3a fits with this finding. The positive anomalies of geopotential height from 60° S to 90° S are signs that the Polar cell is not as active as usual, which is causing less sinking air subsidence in the polar region. The same goes for the negative anomalies of geopotential height from 55º S to 40º S a sign that the Ferrel and Hadley cells are not as active as usual and refer to the weaker descend branch of these two cells. Additionally, the features shown in Figure 5.5a also show similar justification. The strong anticyclonic circulation over the high latitudes during the LIP years refers to the less sinking of air at the surface, which would lead to a weakened Polar cell. Hence, all the features during the LIP years of the PC1 time series of EOF1 illustrates weaker of Polar, Ferrel, and Hadley cells. Furthermore, a decrease in the strength of the Hadley cell and upward motion branch signified decreased convection activity in the region between 10° N and 15° N latitude, which in turn led to reduced precipitation in the region during those phase years. Figure 5.6b, on the other hand, depicts the opposite features. During HIP years of the PC3 time series of EOF3, the Polar cell in Fig. 5.6b illustrate more activity with strong upward motion of airflows branch at about 80º S to 70º S. The Ferrel cell had strong upward and downward motion of airflows branch at about 30º S and 60º S, whereas the Hadley cell illustrate strong upward motion branch at about 10º N and the downward motion branch at about 10º S to 15º S. The strong upward and downward motion of the airflow indicates stronger of the three cells during these phase. Likewise, Figures 5.3b and 5.5b both provide support for the features. The negative value of geopotential anomalies between 60° S and 80° S is a sign of intense air sinking in the polar region. This is due to the stronger descending branch of the Polar

cell. The increased outward movement of polar air out of the plateau during the HIP years may also be seen as evidence of this at the surface. Meanwhile, the positive value of geopotential anomalies between 30° S to 40° S refers to the strong descending branch of the Ferrel and Hadley cells. Kim et al. (2015) found that a stronger Ferrel cell creates a dipole pattern of a difference in mean sea level between high and middle latitudes. The features described above are also discussed in the preceding chapter (Chapter 4, Figure 4.10a). In addition, a strong cyclonic circulation identified at 70o S depicted in Figure 5.5b also displays more sinking of air at the surface, which leads to a stronger Polar cell. Hence, all the features during the HIP years of the PC3 time series of EOF3 illustrates strengthen of Polar, Ferrel, and Hadley cells. Furthermore, increase in the strength of the Hadley cell and upward motion branch signified increase convection activity in the region between 10° N and 15° N latitude, which contribute to more precipitation over the latitudes of the Indian region (Dima et al., 2003).

As a result, the features mentioned above show that Polar, Ferrel, and Hadley cells are strengthening (weakening) during the HIP (LIP) year. Furthermore, Figure 5.6 clearly depicts the transmission of the meridional wave train from the polar regions to the tropics, as well as the alteration in the downward and upward motion of airflow during the HIP and LIP years. In summary, although EOF1 and EOF3 seem to be different types of sea ice variability in the Indian Ocean sector, the analysis of composites for HIP and LIP years suggests that both modes exhibit comparable outcomes in geopotential height, wave activity flux, zonal winds, and meridional circulation.

(a)

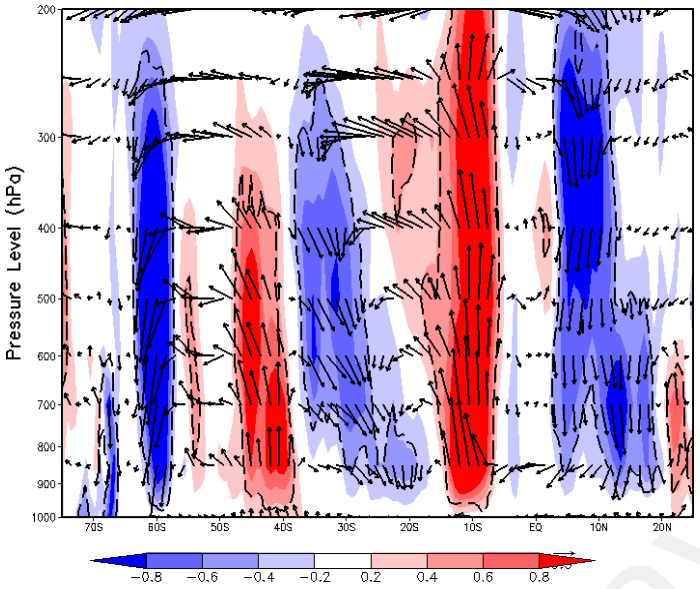

(b)

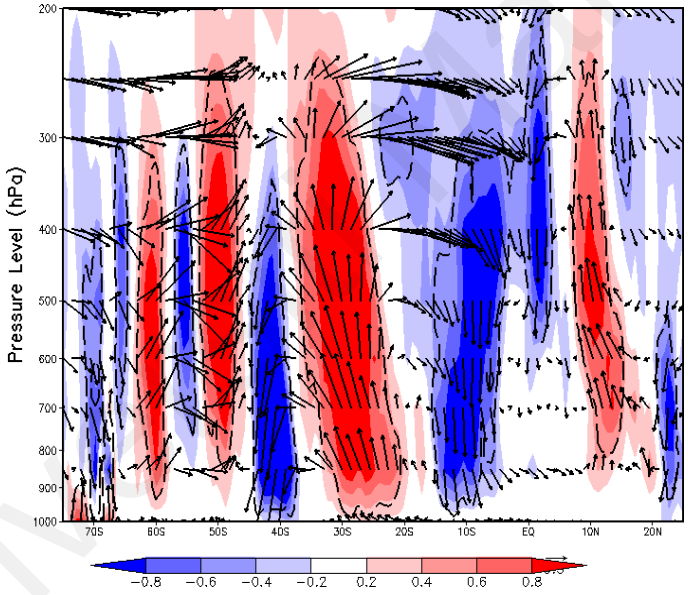

Figure 5.6: The composites difference of meridional circulation averaged over the Indian Ocean longitudinal belt of 55° E – 85° E, for high and low phases of EOF1/EOF3 corresponding to a) PC1 b) PC3 time series of AMJ sea ice extent in the Indian Ocean sector. The shaded plot is the vertical velocity anomaly (in Pa/s, scaled by -0.01) and superimposed by the vectors of meridional component wind(in ms^{-1}) and vertical velocity anomalies. The dashed lines are statistically significant at $p < 0.05$

The features of the difference in composite OLR anomalies shown in Figure 5.7 are consistent with the latitude of ascending air in the Hadley cell circulation. Figure 5.7a depicts positive anomalies of OLR throughout India, the Arabian Sea, and the western Indian Ocean, whereas negative anomalies of OLR are also observed in the north India region, during the LIP years of the PC1 time series of EOF1. Figure 5.7b depicts negative anomalies of OLR throughout the Indian region, the Arabian Sea, and the Bengal Sea, whereas positive anomalies of OLR are also observed across the north India, western Indian Ocean, northeast India, and eastern India, during the HIP years of the PC3 time series of EOF3. The positive and negative anomalies of OLR indicate weak and strong convection activity over the regions, which contributes less and more to the formation of clouds as well as precipitation.

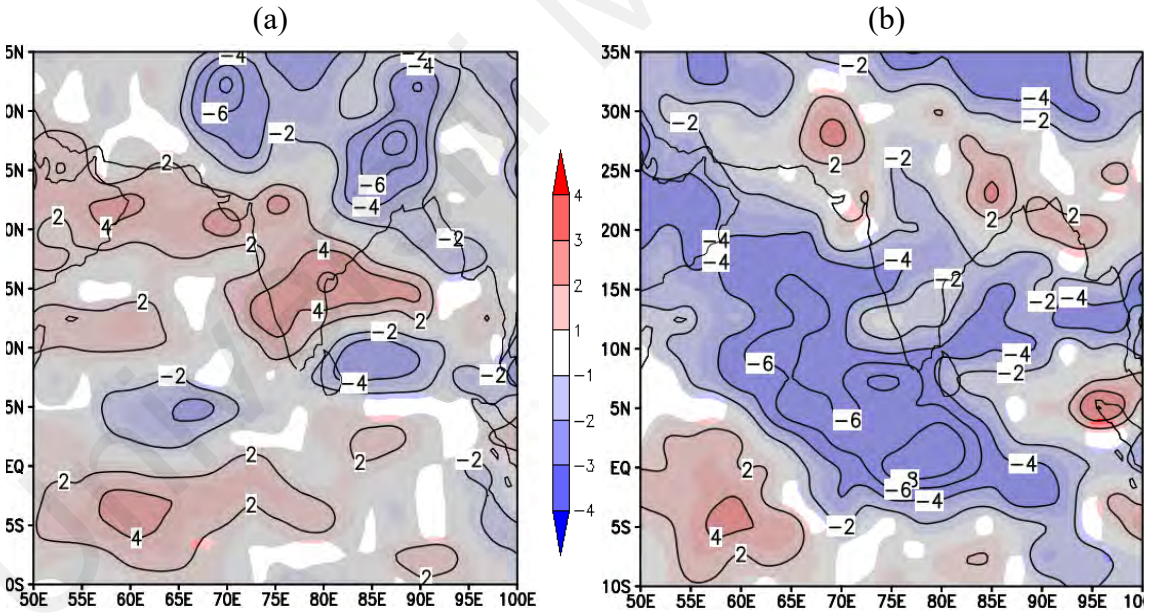

Figure 5.7: The composites difference of OLR anomalies (in W/m$^{2)}$ for high and low phases of EOF1/EOF3 corresponding to a) PC1 b) PC3 time series of AMJ sea ice extent in the Indian Ocean sector during Indian summer monsoon rainfall. The shaded are in grey is statistically significant at $p < 0.05$

This is further supported by the spatial distribution of the difference in composite precipitation anomalies shown in Figure 5.8, corresponding to the PC1 (Figure 5.8a) and PC3 (Figure 5.8b) time series of sea ice extent in the Indian Ocean sector during AMJ.

The negative anomalies of the precipitation shown in Figure 5.8a are noted throughout the east of the Arabian Sea, certain portions of the Bengal Sea, and the Indian region during the LIP years of the PC1 time series. Figure 5.8b shows features that are diametrically opposed. The positive anomalies of precipitation were recorded across the Indian Peninsula, the eastern Arabian Sea that is close to India, and it lengthened to the western and northern parts of India during the HIP years of the PC3 time series. In the previous chapter, it was revealed that the Arabian Sea and the western Peninsular India were found to have significant anomalies of divergence at an altitude of 200 hPa and anomalies of convergence at an altitude of 850 hPa (Chapter 4, Figures 4.13 and 4.15). Nevertheless, since precipitation is regulated by additional elements, for example, topography, it is possible that the distribution of the precipitation position will not exactly match OLR.

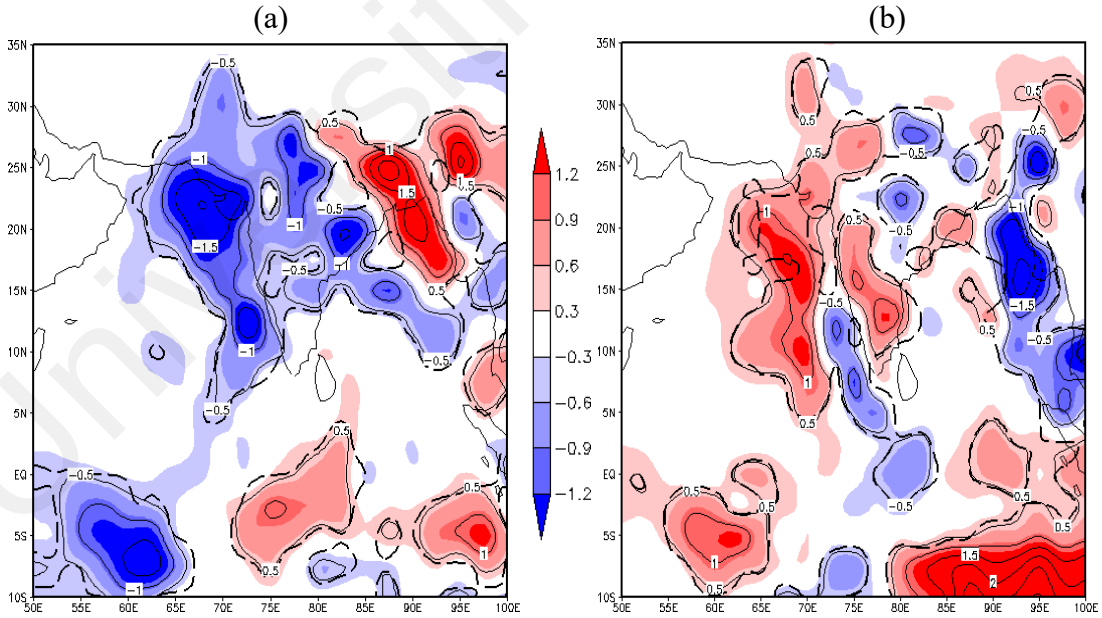

Figure 5.8: The composite difference of precipitation anomalies (in mm/year) for high and low phases of EOF1/EOF3 corresponding to a) PC1 b) PC3 time series of AMJ sea ice extent in the Indian Ocean sector during Indian summer monsoon rainfall. The dashed lines are statistically significant at $p < 0.05$

The analysis above suggests that the connection between sea ice extent in the Indian Ocean sector and Indian summer monsoon rainfall is caused by meridional wave trains throughout the higher and lower tropospheres of the Indian Ocean. These meridional wave trains alter the jet stream variability, which can change the circulation of the wind at both lower and higher levels. This can have a significant impact on the strength of the three cells: the Polar cell, the Ferrel cell, and the Hadley cell. Furthermore, affecting the convective activity over the Indian region, which in turn impacted the Indian summer monsoon's rainfall variability. The meridional circulation and anomalous meridional zonal wave train pattern described above represent the propagation of signals from the high latitudes (polar region) to the low latitudes (tropical region), or the other way around. Additionally, the increasing of the Antarctic sea ice extent trends affected the global circulation of the atmosphere and the way that surface temperature changes differ across different regions (Comiso et al., 2017; Simmonds et al., 2021). This has subsequently had an impact on the Hadley cell's strength and location (Hudson et al., 2001), as well as the distribution of surface winds and the vertical structure of the atmosphere (Simmonds et al., 2021). Despite this, the effects of the increasing pattern in Antarctic sea ice extent are not uniform across sectors. The reason for this is that sea ice in each sector is distinctive and has its own natural variability, which is impacted by its geography and topography (Weeks, 2010).

5.4 CIMP5 models simulation

These following subsection assesses the CMIP5 model's bias in resimulating the teleconnection’s spatial features between the sea ice extent and the Indian summer monsoon rainfall by comparing it to reanalysis observations. Similarly, the years with sea ice extent values that were greater than or less than 1 standard deviation above or below the mean for each model were categorized as HIP (LIP) years. It is noteworthy that the

majority of the CMIP5 models over the period 1979 to 2013 predicted decreases in Antarctic sea ice extent, whereas the observations showed the opposite pattern of behaviour. Despite the fact that past studies found an increase in sea ice extent in autumn for all sectors, including the sector of the Indian Ocean, the exception was the Bellingshausen and Amundsen Seas (Shu et al., 2012,2015). Additionally, the Antarctic sea ice extent seasonal pattern can only be reproduced nearly well by a small number of models (Turner et al. 2013; Shu et al., 2015). The ability of the CMIP5 models to reproduce the teleconnection pattern was assessed by examining the zonal wind anomalies' spatial correlation between the CMIP5 models and the ERA-Interim reanalysis for the HIP and LIP years (Figure 5.9 and Figure 5.10). Each model's correlation coefficient is positively associated with the ERA-Interim reanalysis, as indicated by the red shaded area. The opposite is true for the blue shaded area. Additionally, to more precisely describe how the teleconnection pattern's amplitude is represented by the CMIP5 models and the ERA-Interim, the average anomaly correlation coefficient is calculated within the study area of interest (Figures 5.11a and 5.11b). The average anomaly correlation coefficient for all models was statistically significant at $p < 0.05$. The models ACCESS 1.3, IPSL-CM5A-LR, MPI-ESM-MR, and NorESM1-M all exhibit a positive correlation in HIP years ranging from 0.50 to 0.62 (Figure 5.11a). The IPSL-CM5ALR model has the strongest positive correlation of 0.62 in LIP years, subsequently, the MPI-ESM-MR and NorESM1-M models have the second and third strongest positive correlations, respectively (Figure 5.11b). On the other hand, some models show a negative correlation. The models ACCESS 1.3, IPSL-CM5A-LR, MPI-ESM-MR, and NorESM1-M exhibit comparable patterns in anomalies of zonal wind during HIP years, as evidenced by their moderate to high values of correlation coefficients. However, in LIP years only the IPSL-CM5A-LR model shows a comparable pattern in anomalies of zonal wind.

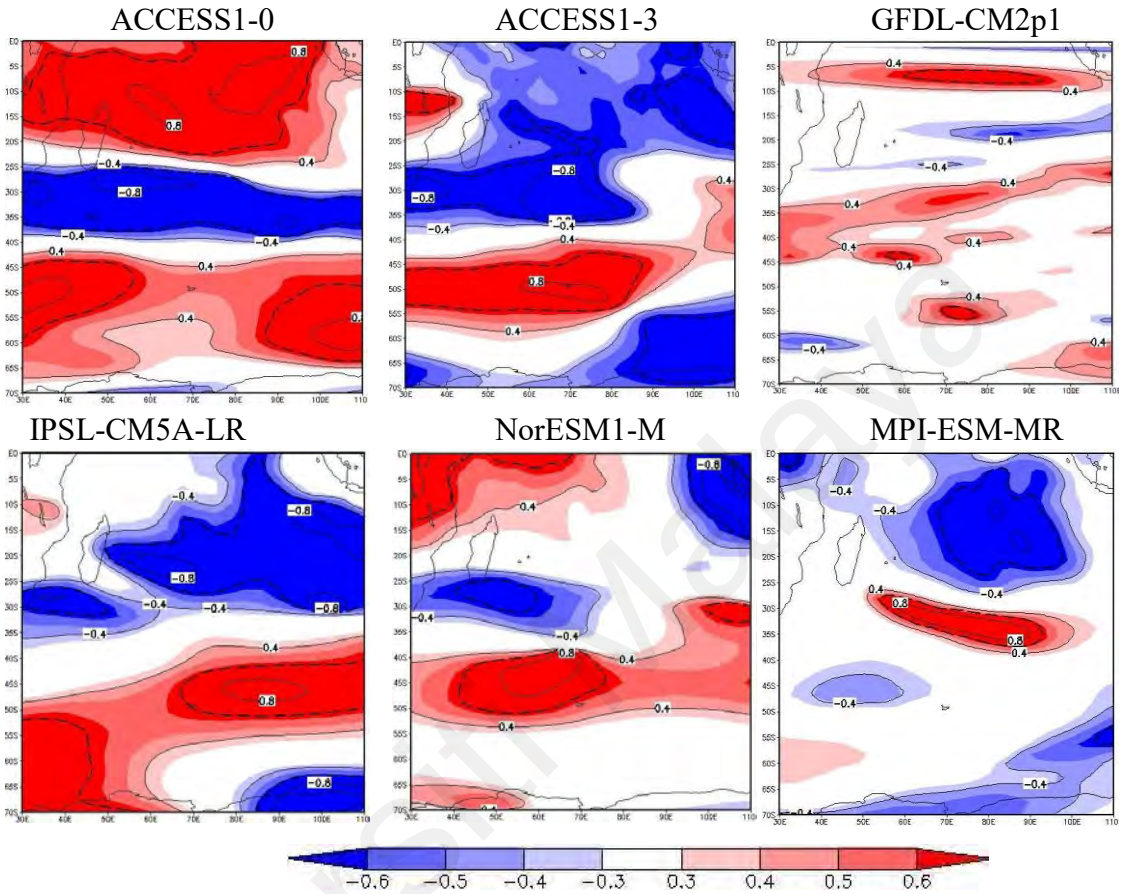

Figure 5.9: The correlation of zonal wind between the ERA- Interim reanalysis and CMIP5 models during MJJ for HIP years at level 250 hPa. The dashed lines are statistically significant at p < 0.05

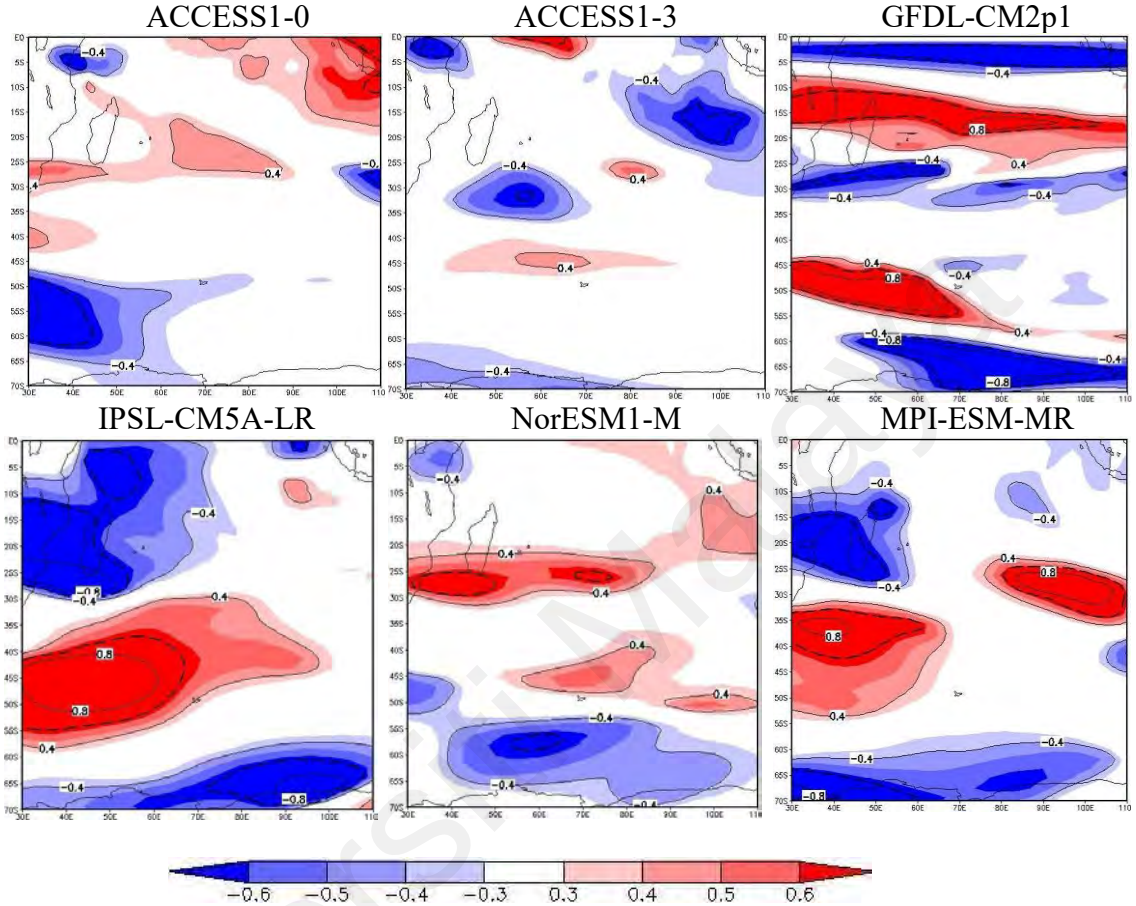

Figure 5.10: The correlation of zonal wind between the ERA- Interim reanalysis and CMIP5 models during MJJ for LIP years at level 250 hPa. The dashed are statistically significant at p < 0.05

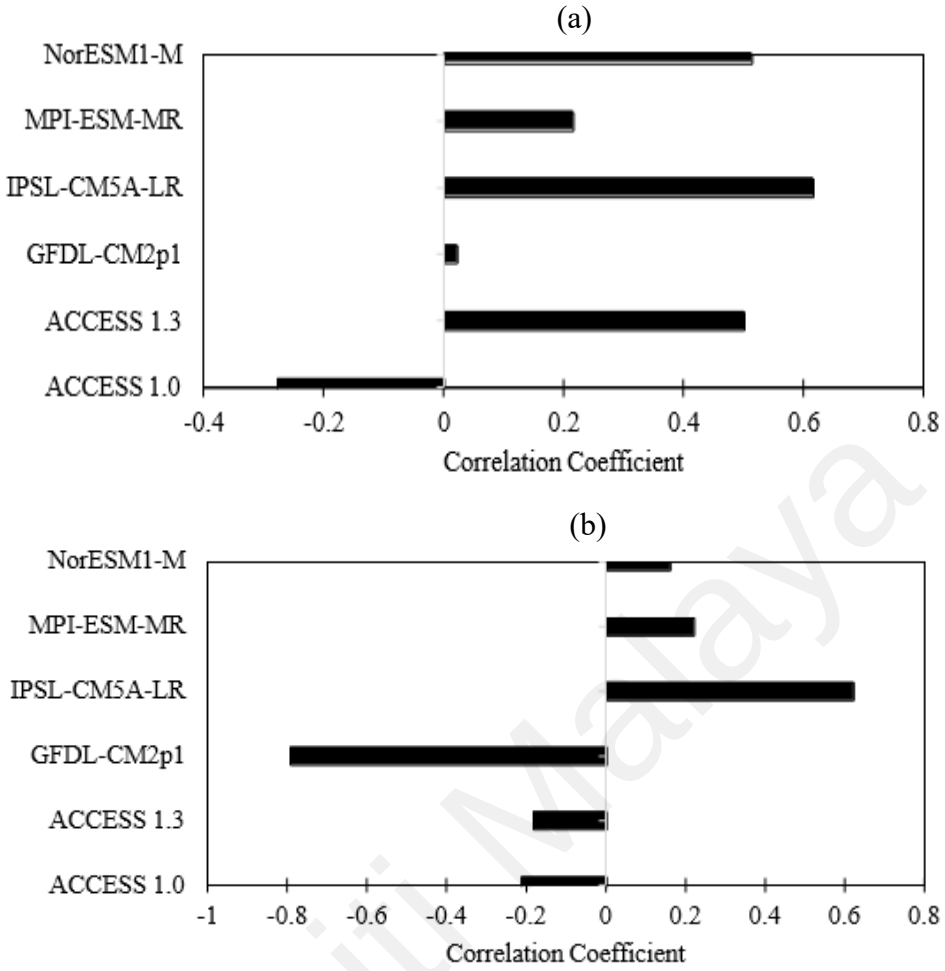

Figure 5.11: The correlation coefficient of zonal wind anomalies between the ERA-Interim and CMIP5 models during MJJ for a) the HIP and b) the LIP years from the study area (lon: 55° E - 85 ° E, lat: 30 °S - 60 ° S) at 250 hPa

The analysis presented in the earlier sections suggests that during the HIP and LIP years, there were variations in the anomalous atmospheric circulation across the Indian Ocean and convective activity across the Indian region. Hence, a comparable evaluation was done to determine whether the chosen CMIP5 models were capable of capturing the teleconnection between the sea ice extent and rainfall during the Indian summer monsoon. The correlation analysis found that the NorESM1-M model's AMJ sea ice extent shows the most significantly correlated with the PC2 time series of Indian summer monsoon rainfall from 1979 to 2012, with a correlation coefficient of 0.32, which is statistically significant level at $p < 0.1$. However, the IPSL-CM5A-LR model's sea ice extent shows

a diametrically opposed association with the PC2 time series of rainfall during the Indian summer monsoon, with a correlation coefficient of -0.30, which is statistically significant level at $p < 0.1$ level. The other four models that are ACCESS 1.0, ACCESS 1.3, GFDL - CM2.1, and MPI-ESM-MR demonstrate a negligible connection with Indian summer monsoon rainfall throughout the entire of the composite months. Table 5.3 presented summarized of the correlation coefficients between sea ice extent and precipitation from the CMIP5 models and HadISST. Similar results are shown for the 33 year spatial correlation distribution between the sea ice extent of CMIP5 models and precipitation data (Figure 5.11), where NORESMI-M models demonstrate a positive correlation along Peninsular India's west coast. On the contrary, the IPSL-CM5A-LR models reveal a negative connection across the Indian subcontinent. As a result, the two models NORESMI-M and IPSL-CM5A-LR that demonstrate a substantial association with the Indian summer monsoon rainfall will be used for future investigations.

Table 5.3: Summary of correlation coefficient of selected CMIP5 models and HadISST dataset.

Sea ice extent in the Indian Ocean sector (AMJ) and PC2 of Precipitation (GPCP) during Indian summer monsoon rainfall		
CMIP5 models (1979 - 2012):	**correlation coefficient (r)**	**p value**
NorESM1-M	0.32	0.069**
IPSL – CM54-LR	- 0.30	0.089**
HadISST datasets (1979 – 2013):		
PC1	-0.49	0.0028*
PC3	0.40	0.0173*

p value statistically at *p < 0.05 and **p < 0.1

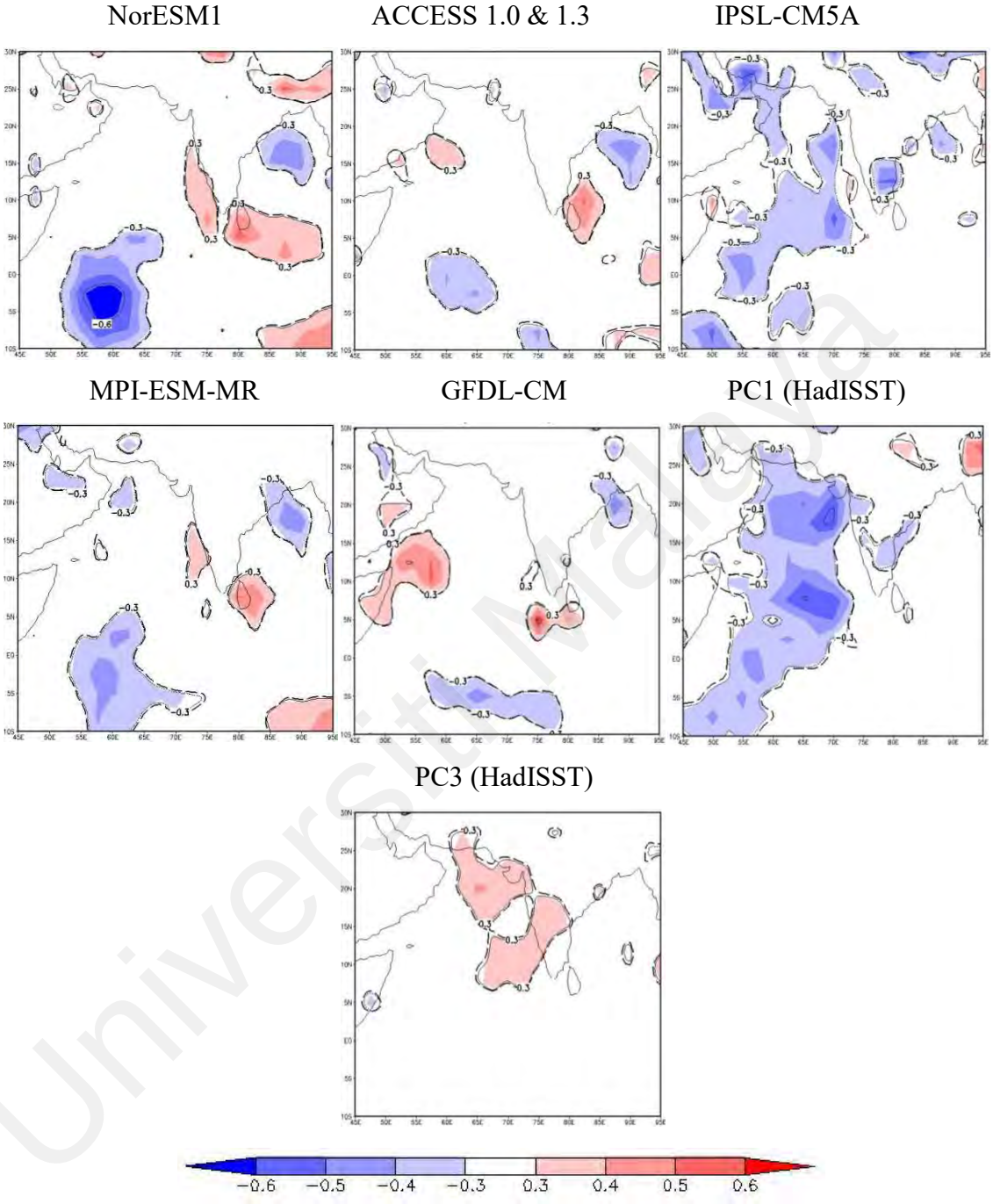

Figure 5.12: The spatial correlation between the sea ice (CMIP5 models and HadISST dataset) with Indian summer monsoon rainfall. The dashed lines are statistically significant at $p < 0.05$

Figure 5.13 depicts a parameter similar to that in Figure 5.2 for the two climate models, NORESMI-M and IPSL-CM5A-LR. However, The NORESMI-M model outperforms the IPSL-CM5A-LR model and generates a features that is somewhat comparable to the reanalysis result (ERA-Interim). The NORESMI-M model depicts the geopotential height dipole features in a shaded area throughout the Indian Ocean. The positive geopotential height anomaly in this model is located further west and significantly lower than the reanalysis result. Furthermore, there are no distinct trends in the wave activity flux difference across the polar and middle latitudes. The results record the wave activity flux equatorward movement at approximately 25o S over the western Indian Ocean close to the island of Madagascar. Despite this, along the longitudes at approximately 10°S, the NORESMI-M model depicts a strong wave activity flux flow toward the equator. As for the IPSL-CM5A-LR model, the Indian Ocean does not exhibit a geopotential height dipole features.

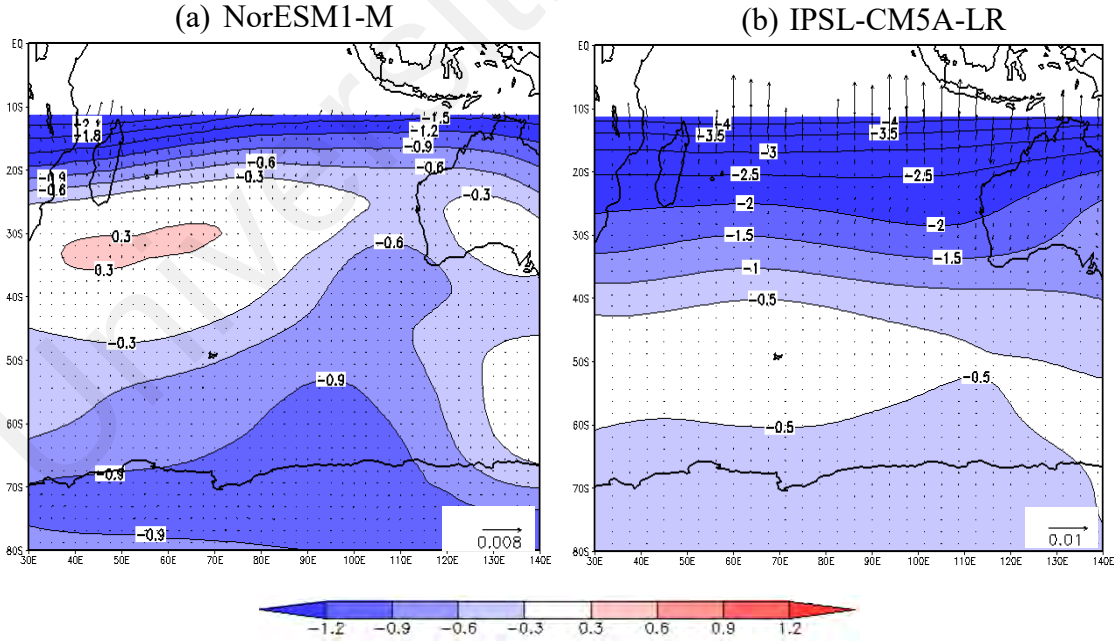

Figure 5.13: The regressed anomalous contour of geopotential height anomalies (shaded, in m) for 35 years superimposed with the composite difference of HIP and LIP years of wave activity flux (vector, in m^2s^{-2}) during MJJ at 250 hPa for the a) NorESM1-M and b) IPSL–CM5A-LR models

The upper and lower troposphere wind variability is a key factor in the teleconnection between the sea ice extent in the Indian Ocean sector and Indian summer monsoon rainfall, as revealed by reanalysis results. Figure 5.14 display the vertical profile of the difference in composite zonal wind average for the NorESM1-M and IPSL-CM5A-LR models. At pressure levels ranging from 200 to 400 hPa, both of the models were capable of simulating the polar and subtropical jets features. In comparison to reanalysis results, the IPSL-CM5A-LR model produces features in Figure 5.4b that are almost identical, particularly polar and subtropical jets. The NorESM1-M model, on the other hand, exhibits the opposite features. The disparity between the anomaly values for the two models, however, is comparatively small, indicating that the polar and subtropical jets are not significantly affected in either phase.

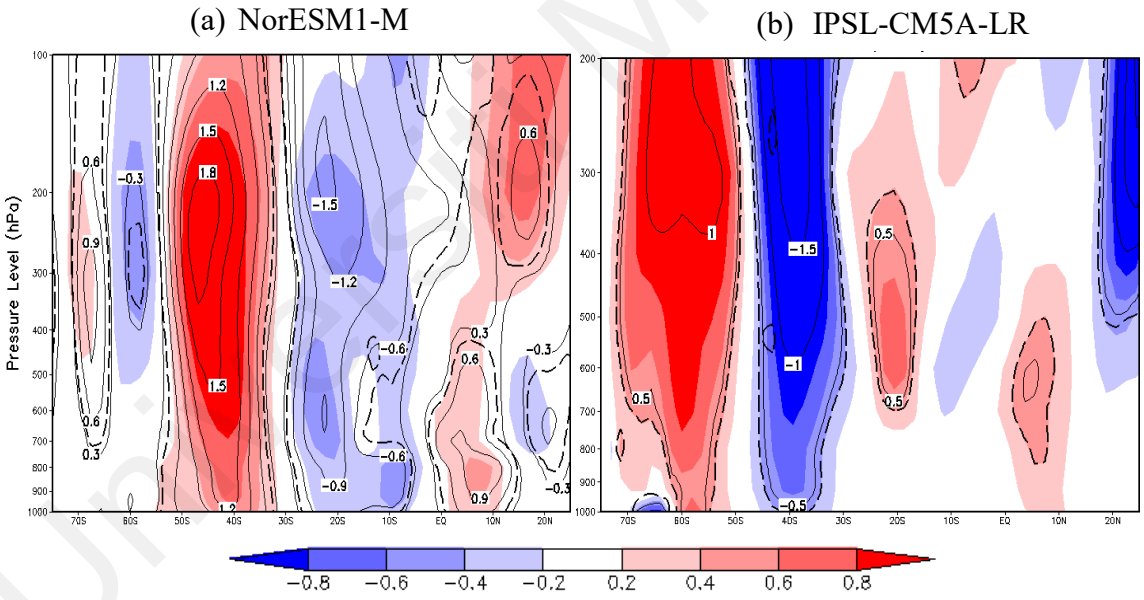

Figure 5.14: The vertical profile of composite difference of HIP and LIP years of zonal wind average (in ms^{-1}, average over 55° E – 85° E) a) NorESM1-M and b) IPSL–CM5A-LR models. The dashed lines are statistically significant at $p < 0.05$

Figure 5.15 depicts the spatial distribution of the zonal wind anomalies composite difference overlapping with the wind anomalies composite difference in the two climate models at 250 hPa. The two models were both able to capture the essential features of the wind pattern throughout the Indian Ocean. The zonal and wind circulation features

generated by the IPSL-CM5A-LR model are remarkably comparable to those of the reanalysis findings (Figure 5.5b). Nonetheless, the features of the anomalies zonal wind are located further south, and the anticyclone circulation is only visible between approximately 75° S to 55° S in the western Indian Ocean. Conversely, the features exhibit by the NorESM1-M model is contrary to the reanalysis.

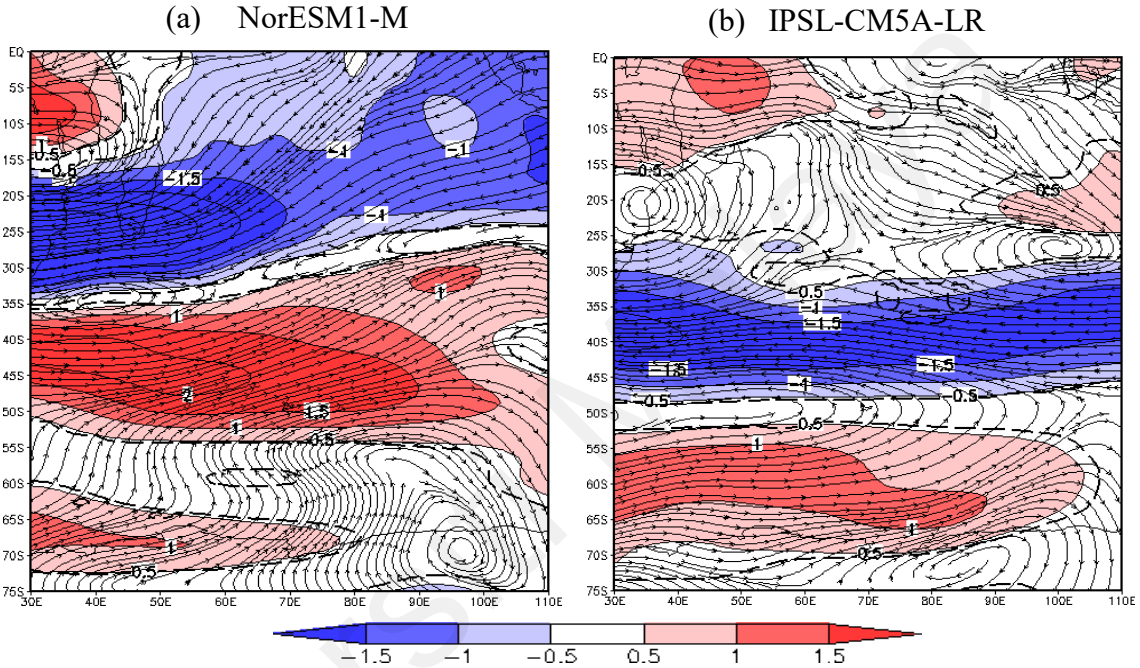

Figure 5.15: The composite difference of HIP and LIP years of zonal wind anomaly (shaded) superimposed with wind anomaly (streamlines) at 250 hPa (in ms^{-1}) for a) NorESM1-M and b) IPSL–CM5A-LR models. The dashed lines are statistically significant at p < 0.05

Figure 5.16 depicts the difference in the composite of meridional circulation that is simulated by the two climate models. The results of both models, particularly the IPSL-CM5A-LR model, exhibit undiscernible features when compared to the reanalysis results. While, the NorESM1-M model exhibits comparable features with Figure 5.6b at approximately 10° N in the two phases. During the HIP years, the upward anomalous movement of air was only noticeable at latitudes between approximately 10° S and 10° N. This demonstrates the increase in convective activity over the region. In contrast to

the reanalysis results, the downward anomalous movement of air is observed during these phase years at approximately 30°S. However, similar patterns to those seen in the reanalysis may be observed during the LIP years, with the upward anomalous movement of air at approximately 70° S and the downward anomalous movement of air at approximately 15° N. In summary, the NorESM1-M model shows that the presence of upward movement of air at approximately 10° N during HIP years is indicative of enhanced convective activity, while the presence of downward movement of air at about 10° N during LIP years is indicative of depressed convective activity.

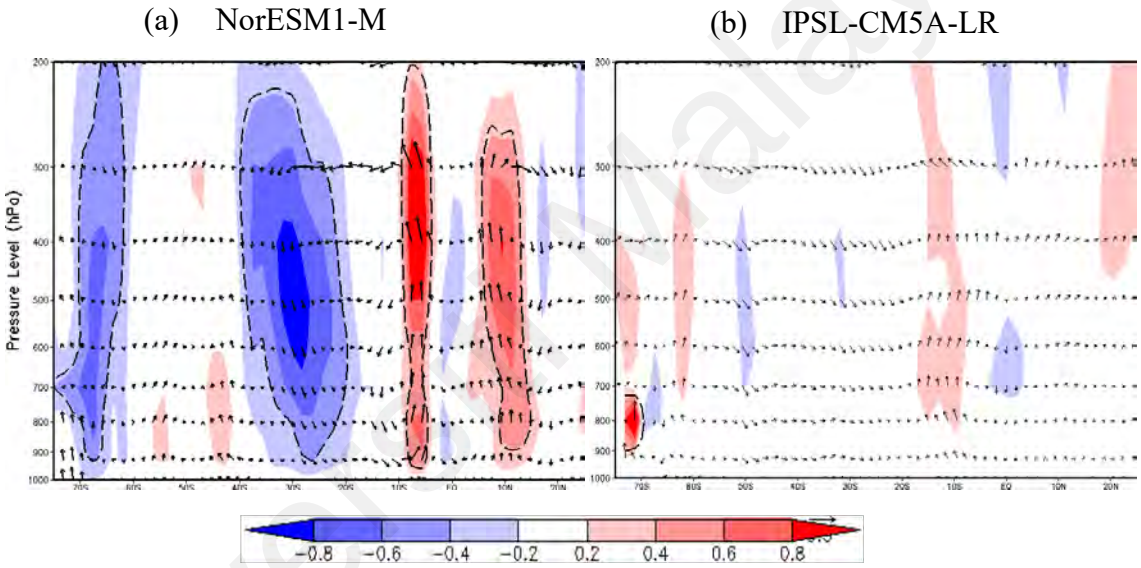

Figure 5.16: The composites difference of HIP and LIP years of anomalous meridional circulation averaged over the Indian Ocean longitudinal belt of 55º E –85º E for the NorESM1-M and IPSL–CM5A-LR models. The shaded plot is the vertical velocity (in Pa/s, scaled by -0.01) and superimposed by the vectors of meridional component wind (in ms^{-1}) and vertical velocity anomalies. The dashed lines are statistically significant at $p < 0.05$

The spatial distribution of the difference between the composite anomalies of OLR generated by the two climate models is depicted in Figure 5.17. The NorESM1-M model's OLR anomaly features are somewhat similar to the reanalysis, particularly in LIP years (Figure 5.7b). Despite the insignificant difference in the shady region's position (Figure 5.17a). Positive anomalies of OLR are observed over southern India and some

regions of northeastern India, whereas negative anomalies of OLR are observed over northwestern India, central India, and the Arabian Sea. The IPSL-CM5A-LR model produces results that are the opposite of the reanalysis in both phases. The model shows positive anomalies of OLR across the entire India region and the surrounding seas, namely the Arabian Sea and Bay of Bengal (Figure 5.17b).

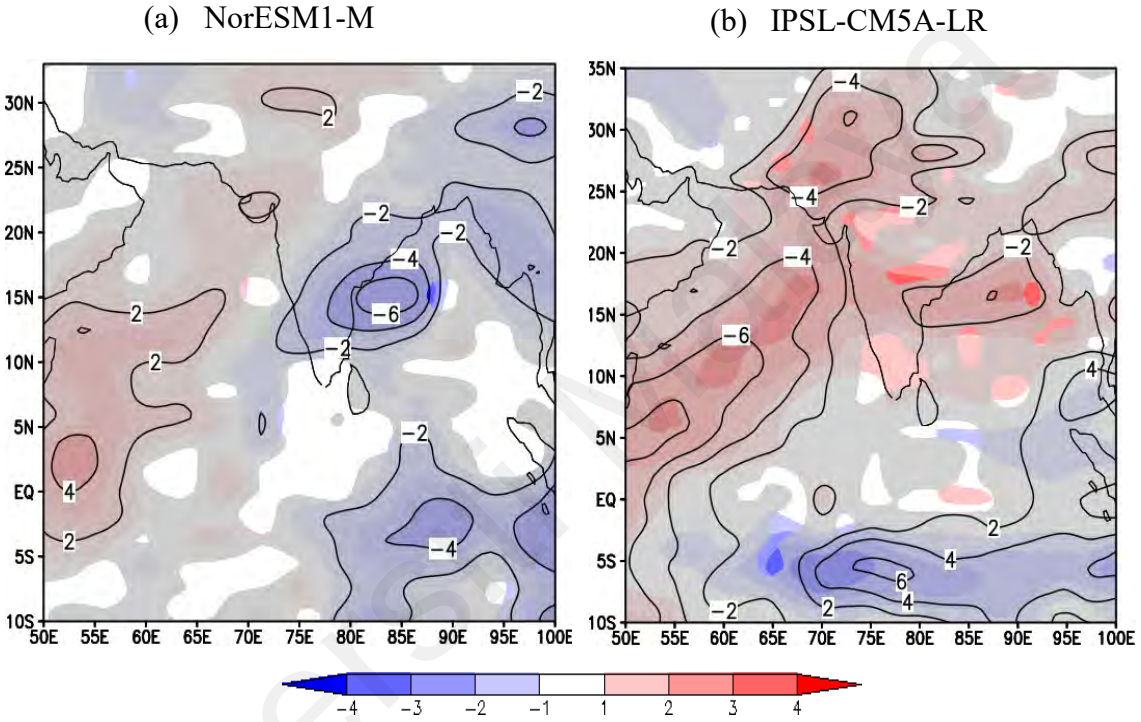

Figure 5.17: The composite difference of HIP and LIP years of OLR anomaly (in W/m^2) for the a) NorESM1-M & b) IPSL–CM5A-LR models during Indian summer monsoon rainfall. The shaded area in grey statistically significant at p < 0.05

Overall, both models have the capability of demonstrating particular features. The IPSL-CM5A-LR model, as an example, can produce features that are nearly equal to the reanalysis results in the HIP and LIP years. There is the polar jet, subtropical jet, zonal winds, and wind circulation anomalies. The NorESM1-M model, on the other hand, was successful in capturing features such as meridional circulation, convective activity, and OLR, particularly in the LIP years. In addition, the features produced from the reanalysis and numerical model are only applicable to the years 1979 through 2013. Therefore, the

teleconnection features may vary and change slightly if the duration is prolonged. In a study published by Simmonds et al. (2021), the Antarctic sea ice extent increased annually until 2014, followed by a dramatic fall until 2017. However, the sea ice extent increased back to a level that was very close to the long term average value in 2020. According to their findings, the primary causes influencing baroclinicity alteration over the polar regions are substantial modifications in the spatial arrangement of sea level pressures, the change in wind direction with height, and the resistance of the atmosphere to vertical motion. However, as noted earlier, Antarctica's different sectors could undergo distinct alterations owing to their individual geophysical characteristics. The authors, for instance, noted strong baroclinic zone in all seasons over the near the Antarctic continent, to the north, especially over the Indian Ocean sector and southern of Australia and New Zealand. The pattern of teleconnections may have been different if the circulation and trends of the sea ice taken into consideration for the time period, but it is impossible to say for certain. Additionally, the biases in the models can be addressed by taking into account a variety of factors, for example complex interplay between internal variability, dynamics, and thermodynamics. Therefore, it is essential to comprehend the capacity of these models to simulate the behaviour of measurable aspects of sea ice and the mechanisms that govern them (Bracegirdle et al., 2019).

5.4 Conclusion

According to the correlation analysis, the PC1 and PC3 of AMJ sea ice extent in the Indian Ocean sector have a significantly associated with PC2 of Indian summer monsoon rainfall. A wave train with anomalous meridional structure in the lower and upper troposphere along the Indian Ocean travelled from the polar regions to the middle latitudes and the tropics. During the HIP years, the polar front jet is strengthened while the subtropical jet has a small relative impact during both phases. Furthermore, it shows

wind anomalies with extreme anticyclonic and cyclonic intensities over the central and southern of Indian Ocean. at 250 hPa, indicating greater surface convergence and divergence. The meridional propagating wave trains resulted in the intensifying of the three major atmospheric circulation cells that is Polar cell, Ferrel cell, and Hadley cell. The enhanced Hadley cell leads to more vigorous convective activity over India, particularly in western Peninsular India. This increased convective activity results in higher Indian summer monsoon rainfall. In contrast to the current conditions, the LIP years were characterized by opposite features. The NorESM1-M and IPSL-CM5A-LR models, in contrast, were successful in simulating some features of atmospheric circulation that the reanalysis was able to capture. The features of atmospheric circulation that successful captured by the NorESM1-M model particularly during the LIP years are meridional circulation, convective activity, and OLR. The meridional circulation cell was located a little bit further north in the NorESM1-M model than in the reanalysis. Simultaneously, the IPSL-CM5A-LR model regenerate comparable anomalous features of the polar jet, subtropical jet, zonal wind, and wind circulation during the two phases of sea ice. The discrepancy between the simulated and observed results could be due to the models' inadequate representation of variability in natural climate (Stroeve et al., 2014).

CHAPTER 6

SUMMARY AND CONCLUSION

6.1 Introduction

This chapter contains an overall summary of chapters 4 and 5, including the main conclusions of the research study, and future work for this study.

6.2 Overall summary

The long term monthly average of the sea ice extent in the Indian Ocean sector for 35 years shows that the maximum amount of sea ice extent produced is in October (3.79×10^6 km^2) while the minimum amount is in February (0.23×10^6 km^2). The highest seasonal month in the sea ice extent in the Indian Ocean sector for 35 years was during SON ($0.6 \pm 20 \times 10^4$ km^2 year^{-1}), and the lowest composite month was in DJF ($0.8 \pm 18.1 \times 10^4$ km^2 year^{-1}). Furthermore, the northeastern region of India receives the highest mean annual rainfall of 3386 mm year^{-1} during the summer monsoon rainfall season, whereas the northwestern region of India receives the lowest mean annual rainfall of 1211 mm year^{-1}.

The correlation analysis revealed that AMJ sea ice extent in the Indian Ocean sector was statistically significantly positively correlated with the Indian summer monsoon rainfall over Peninsular India for 35 years, with a value of $r = 0.44$, $p < 0.05$. In agreement with the spatial correlation analysis, a significant positive correlation was seen over the western Peninsular India region. Furthermore, the partial correlation result of sea ice extent in the Indian Ocean sector, Indian summer monsoon rainfall, and atmospheric circulation variability (SAM, ENSO, and the southern Indian Ocean dipole)

demonstrates that SAM, ENSO, and the southern Indian Ocean dipole have no effect on this relationship.

The MSLP composite anomaly revealed a strengthening of the Mascarene High region and a shift in the Mascarene High's centre eastward from its climatology position during the HIP years. The composite anomaly of 500 hPa geopotential height displayed similar characteristics. Furthermore, at 850 hPa in the lower troposphere, a very strong anticyclonic anomaly was observed over the Mascarene High region during this phase. While the LIP years show a weakening of the Mascarene High region, the position of the centre is more westward, and there is also a strong cyclonic anomaly seen over the Mascarene High region.

The TMH domain was defined by the highest positive correlation between AMJ sea ice extent in the Indian Ocean sector and the MJJ MSLP (35º– 47º S, 65º – 90º E). The correlation coefficient between the AMJ sea ice extent in the Indian Ocean sector index and the TMH index for 35 years is 0.53, with a statistically significant $p < 0.05$. The TMHI+ years revealed a strong convergence (and divergence) anomaly at 850 hPa (200 hPa) over western Peninsular India and the Arabian Sea. Therefore, those regions experienced more rainfall. The TMHI- years showed a strong divergence (and convergence) anomaly at 850 hPa (200 hPa) covering almost the entire Indian region, resulting in clear skies and dry weather.

In conclusion, the Mascarene High intensifies during the HIP years, and strong anticyclone winds appear over the region. Thus, increased southerly winds caused more clouds and rainfall along the west coast of Peninsular India during the Indian summer monsoon rainfall event. During the LIP years, the Mascarene High weakens and the

opposite features emerge, in which air descends from the troposphere to the surface, resulting in dry weather in central India and the surrounding areas. Figure 6.1 depicts a schematic diagram of the proposed mechanism.

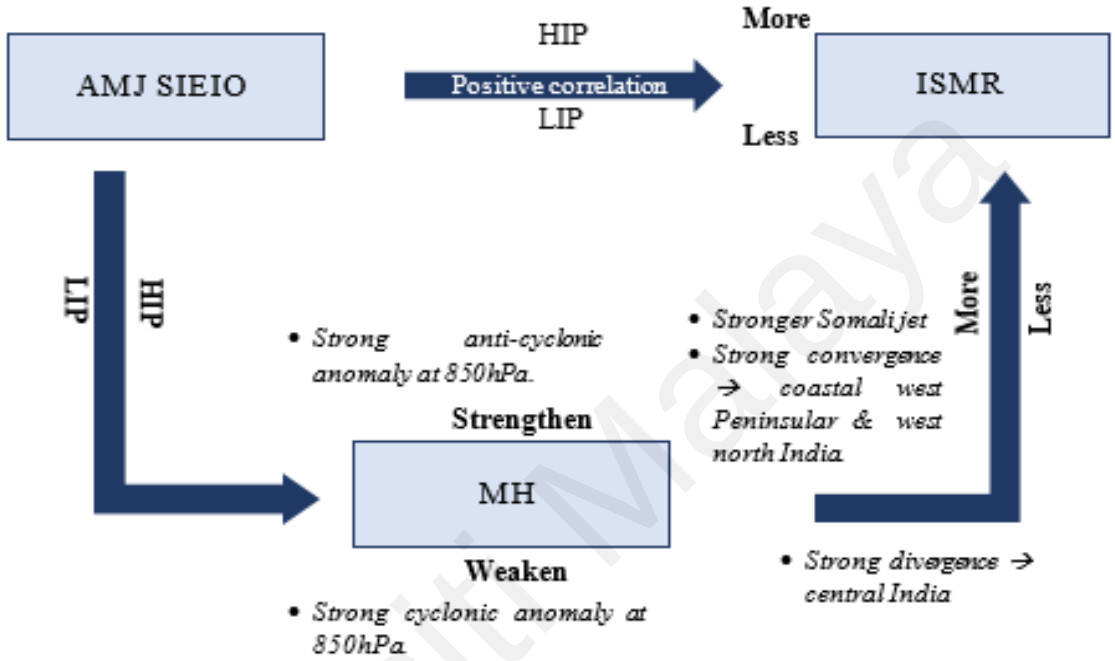

Figure 6.1: Schematic diagram of the proposed teleconnection

The EOF analysis shows that EOF1 modes of sea ice extent during AMJ for 35years explains 40.47% of the total variance. While, the EOF3 modes of sea ice extent during AMJ for 35 years explains 8.40% of the total variance. Similarly, the EOF2 modes of precipitation during JJAS is 12.66% of the total variance. The correlation analysis between PCs of the EOF modes of AMJ sea ice extent and JJAS precipitation show that the PC1 and PC3 of sea ice extent in the Indian Ocean sector during AMJ are significantly correlated with the PC2 of Indian summer monsoon rainfall with a value r = - 0.49 and r = 0.40 (both $p < 0.05$). Furthermore, EOF1 time series (PC1) depict a negative trend,

while EOF3 time series (PC3) do not shows any trend. The negative trend seen in the EOF1 time series indicates an increase in sea ice anomalies in the Indian Ocean sector.

Based on the reanalysis results, an anomalous meridional wave train appears at the lower and upper tropospheres along the Indian Ocean for both principal component modes, propagating from the polar region towards the middle latitudes and the tropics. The zonal wind anomalies show that the polar front jet strengthened during the HIP years. In contrast, the subtropical jet shows little difference between the two phases. During the HIP years, an intense anticyclonic and cyclonic wind anomaly was observed over the southern and central Indian oceans at upper level, 250 hPa. These features imply more substantial surface convergence and divergence during the HIP years.

Furthermore, composite anomalies of the meridional circulation and vertical velocity during HIP phase years illustrate meridionally propagating wave trains, leading to the strengthening of the Polar, Ferrel, and Hadley cells. As a result of the enhanced Hadley cell, the more vigorous convective activity over the India region, particularly in western India, hence increases Indian summer monsoon rainfall. The opposite features were observed for the LIP years, with a weaker polar front jet. Weak divergence and convergence anomalies at the upper level are associated with weak convergence and divergence at the lower level and weakening of the Polar, Ferrel, and Hadley cells. Consequently, low convective activity and decreased cloud formation, as well as precipitation, occurred over the India region. The proposed mechanism of teleconnection during HIP years is summarized in Figure 6.2.

An evaluation of the correlation coefficient of zonal wind anomalies between the ERA-Interim and CMIP5 models reveals that more than half of the selected models

exhibit a significant positive correlation during the HIP years. Furthermore, NorESM1-M and IPSL–CM5A-LR could capture certain atmospheric circulation features similar to the reanalysis. For example, the NorESM1-M model captured the teleconnection features in meridional circulation, convective activity, and OLR, especially during the LIP years. However, the location of the meridional circulation cell is shifted slightly more northward than in the reanalysis results. At the same time, the IPSL-CM5A-LR model reproduced similar features of polar jet, subtropical jet, zonal wind, and wind circulation anomalies with the reanalysis in both sea ice phases. The disparity in results between simulations and observations could be attributed to a poor representation of natural climate variability (Stroeve et al., 2014). In summary, NorESM1-M and IPSL–CM5A-LR could be used to examine how the linkages between sea ice variability and the Indian summer monsoon might change in the future.

In summary, the meridional wave train's propagation along the Indian Ocean connects the variability of the sea ice extent in the Indian Ocean sector of the Southern Ocean to the variability of Indian summer monsoon rainfall. The major keys to the teleconnection mechanisms are the jets' variabilities and wind circulation at upper and lower troposphere.

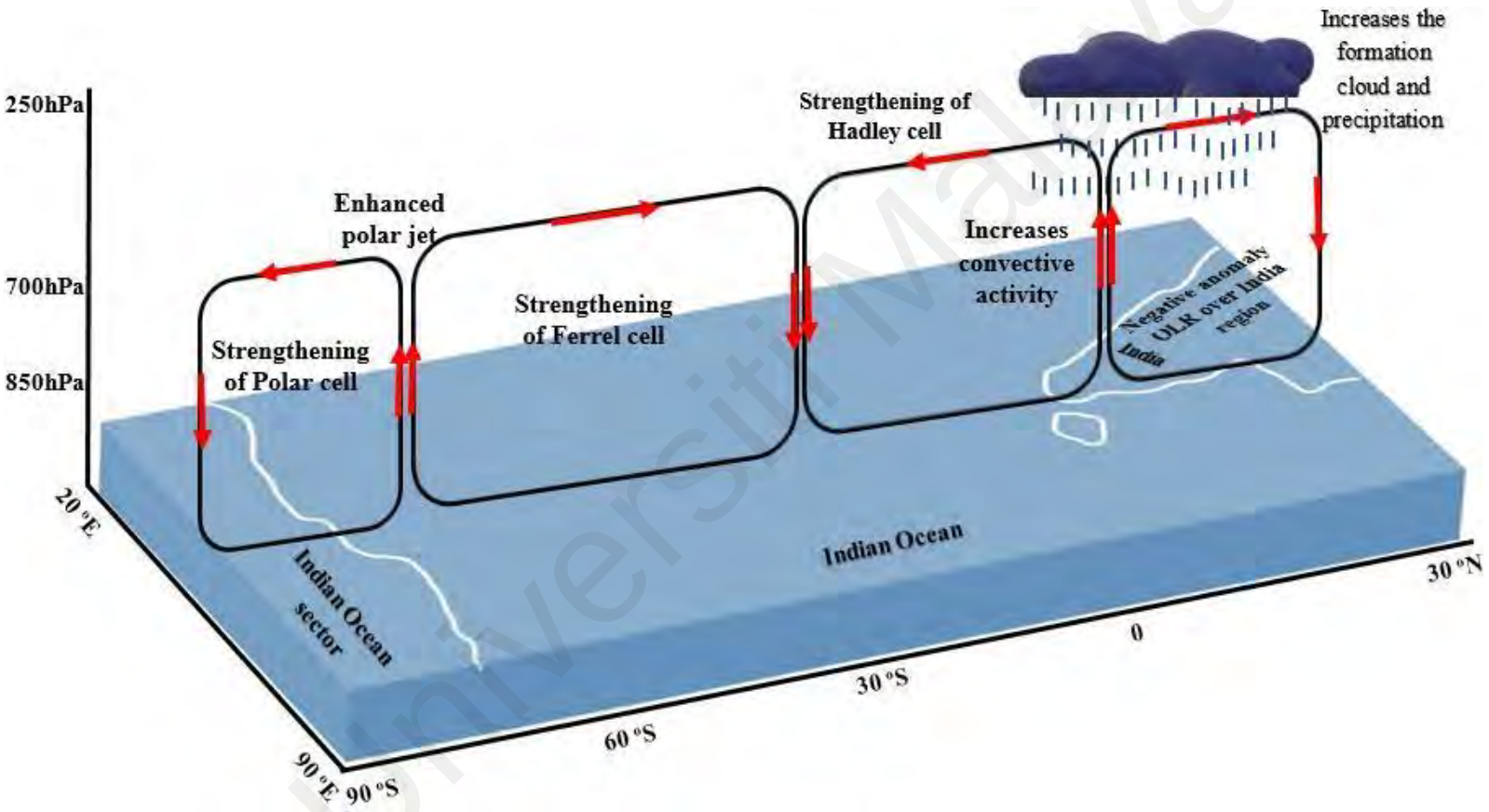

Figure 6.2: Schematic diagram of the mechanism of teleconnection during a HIP year

6.3 Major conclusions

The long term monthly average of the sea ice extent in the Indian Ocean sector for 35 years shows that the maximum amount of sea ice extent produced is in October while the minimum amount is in February. The maximum seasonal month in the sea ice extent 35 years was during SON, and the lowest was in DJF. Furthermore, the northeastern region of India receives the highest mean annual rainfall during the summer monsoon season, whereas the northwestern region of India receives the lowest mean annual rainfall.

Over a period of 35 years, there was a significant positive correlation between the sea ice extent in the Indian Ocean sector during AMJ and the Indian summer monsoon rainfall over the Peninsular region of India. The correlation coefficient was 0.44, which is statistically significant at the 0.05 level. In addition, the partial correlation study revealed that SAM, ENSO, and southern Indian Ocean dipole have no effect on this association. In agreement with the spatial correlation analysis, a significant positive correlation was also noticed over the western Peninsular India region.

During the HIP years, the MSLP and 500 hPa geopotential height composite anomalies demonstrated a strengthening of the Mascarene High region, associated with a very significant anticyclonic anomaly across the Mascarene High region at 850 hPa. The LIP years demonstrate a weakening of the Mascarene High centre, as well as a stronger cyclonic anomaly over the Mascarene High region.

The TMHI+ years indicated an anomalies of substantial convergence (and divergence) across western Peninsular India and the Arabian Sea at 850 hPa (200 hPa). As a result, those areas receive more rain. The TMHI-years revealed an anomalies of

major divergence (and convergence) at levels 850 hPa (200 hPa) that covered practically the whole Indian region, resulting in bright skies and dry weather.

A correlation analysis of the AMJ PC1 and PC3 time series of sea ice extent in the Indian Ocean sector with the PC2 of Indian summer monsoon rainfall reveals a significant association.

During the HIP years, the polar front jet strengthened, while the subtropical jet showed little change. Additionally, strong anticyclonic and cyclonic winds were observed at 250 hPa over the southern and central Indian Oceans, suggesting stronger surface convergence and divergence. These features led to the development of meridionally propagating wave trains, which in turn strengthened the Polar, Ferrel, and Hadley cells. The enhanced Hadley cell caused stronger convective activity over India, especially in western India, which led to higher Indian summer monsoon rainfall during the HIP years.

During the LIP years, the polar front jet weakened, and the upper and lower level divergence and convergence also weakened. This weakened the Polar, Ferrel, and Hadley cells, which in turn led to less convective activity, cloud formation, and precipitation in the Indian region.

The features that are able reproduce by NorESM1-M model particularly during the LIP years are meridional circulation, convective activity, and OLR. The IPSL-CM5A-LR model is able to produce identical features of the polar jet, subtropical jet, zonal wind, and wind circulation in both the high and low sea ice phases.

6.4 Limitation of the study and recommendations for future research

There are several significant limitations to this study. First, the time range of this research study is confined to 1979 to 2013. Extending this time period may result in somewhat different characteristics. Second, the selected area of the research study. As mentioned, sea ice in each sector has different characteristics, so selecting sea ice in other sectors might produce different results. It is important to note that the teleconnection pattern produced by CMIP5 models in this study was only used to compare the relationship between the pattern and the reanalysis of the data. However, for forecasting or prediction, more advanced models are needed that take into account other factors.

Researchers are increasingly interested in the teleconnections that link Antarctic sea ice to other parts of the globe. These teleconnections are not limited to the tropics of the Northern Hemisphere, but can extend all the way to the Northern Polar Cap. The dynamic interactions between the atmosphere and ocean components must be taken into account to determine the causes or gain more knowledge about the underlying mechanism. Previous research on teleconnections has primarily focused on the role of the tropics in driving the dynamics of climate change in Antarctica. In addition, it is acknowledged that the results of the model simulation analysis are still unsatisfactory. As previously mentioned, many external and internal factors must be taken into account in order to achieve optimal results. Improved global models and experimental methods can be used to address critical issues regarding the dynamics of tropical-polar teleconnection mechanisms. Quantifying the impacts of teleconnections is essential to understanding how these relationships will evolve in a warming climate.

REFERENCES

Adler, R. F., Sapiano, M. R. P., Huffman, G. J., Zhang, J., Gu, G., Bolvin, D. T., Chiu, L. S., Schneider, U., Becker, A. C., Nelkin, E., Xie, P., Ferraro, R., & Shin, D. B. (2018). The Global Precipitation Climatology Project (GPCP) Monthly Analysis (New Version 2.3) and a Review of 2017 Global Precipitation. *Atmosphere, 9*(4), 138. https://doi.org/10.3390/atmos9040138

Ahasan, M. N., Chowdhury, M. A. M., & Quadir, D. A. (2014).The summer monsoon weather systems and its relationship with rainfall over South Asia. *Open Journal Atmospheric Climate Change*,1(2), 2374 – 3808.

Ajayamohan, R., Rao, S. A., & Yamagata, T. (2008). Influence of Indian ocean dipole on poleward propagation of boreal summer intraseasonal oscillations. *Journal Climate*, 21, 5437–5454.

AlHubaishi, A. (2018). The *effect of Somali low level jet on the southwest monsoon rainfall variability in Salalah*, Oman. Iowa State University. https://lib.dr.iastate.edu/cgi/viewcontent.cgi?article=1036&context=mteor_sthesis

Allan, R. P., Liu, C., Zahn, M., Lavers, D. A., Koukouvagias, E., & Bodas-Salcedo, A. (2013). Physically Consistent Responses of the Global Atmospheric Hydrological Cycle in Models and Observations. *Surveys in Geophysics*, 35, 533–552.

American Meteorological Society (2018). Monsoon. Glossary of Meteorology. Retrieved from http://glossary.ametsoc.org/wiki/Monsoon

Annamalai, H. (2010). Moist dynamical linkage between the equatorial Indian Ocean and the South Asian monsoon trough. *J. Atmosph. Sci.,* 67, 589–610.

Antarctic Sea Ice Variability in the Southern Ocean-Climate System. (2017). In *National Academies Press eBooks*. https://doi.org/10.17226/24696

Antarctica Sea Ice, NASA Earth Observatory. (2015). Retrieved from http://earthobservatory.nasa.gov/Features/SeaIce/page4.php.

Ashok, K., & Saji, N. H. (2007). On the impacts of ENSO and Indian Ocean dipole events on sub-regional Indian summer monsoon rainfall. *Nat Hazards*, *42*(2), 273–285.

Ashok, K., Guan, Z. Y., Saji, N. H., & Yamagata, T. (2004). Individual and combined influences of ENSO and the Indian Ocean Dipole on the Indian summer monsoon. *J Clim*, 17, 3141–3155.

Ashok, K., Guan, Z., & Yamagata, T. (2001). Impact of the Indian Ocean dipole on the relationship between the Indian monsoon rainfall and ENSO. *Geophys. Res. Lett.*, 28, 4499–4502.

Athira, K., Roxy, M. K., Dasgupta, P., Saranya, J. S., Singh, V. K., & Attada, R. (2022). Regional and Temporal Variability of Indian Summer Monsoon Rainfall in relation to El Niño Southern Oscillation. *Research Square* (Research Square). https://doi.org/10.21203/rs.3.rs-1825980/v1

Azhar, S. S., Chenoli, S. N., Samah, A. A & Kim, S., J. (2020). The linkage between Antarctic sea ice extent and Indian summer monsoon rainfall. *Polar Science*, *25* (100537), 1- 10.

Bader, J., Flügge, M., Kvamstø, N. G., Mesquita, M. D. S., & Voigt, A. (2013). Atmospheric winter response to a projected future Antarctic sea – ice reduction: A dynamical analysis. *Climate Dynamics*, *40*(11-12),2707 – 2718.

Bajish, C. C., Jena, B., Anilkumar, N. (2021). Is the Indian monsoon rainfall linked to the Southern Ocean sea ice conditions?. *Weather and Climate Extremes*, *34* (100377),1- 8.

Bals-Elsholz, T. M., Atallah, E. H., Bosart, L. F., Wasula, T. A., Cempa, M. J., & Lupo, A. R. (2001). The Wintertime Southern Hemisphere Split Jet: Structure,

Variability, and Evolution. *Journal of Climate, 14*(21), 4191–4215. https://doi.org/10.1175/1520-0442(2001)014

Barimalala, R., Bracco, A., Kucharski, F., McCreary, J. P., & Crise, A. (2013). Arabian Sea ecosystem responses to the South Tropical Atlantic teleconnection. *Journal of Marine Systems*, *117–118*, 14–30. https://doi.org/10.1016/j.jmarsys.2013.03.002.

Beaufort, L., Van Der Kaars, S., Bassinot, F., & Moron, V. (2010). Past dynamics of the Australian monsoon: precession, phase and links to the global monsoon concept. *Climate of the Past*, *6*(5), 695–706. https://doi.org/10.5194/cp-6-695-2010.

Behera, S. C., Krishnan, R., & Yamagata, T. (1999). Unusual ocean-atmosphere conditions in the tropical Indian Ocean during 1994. *Geophysical Research Letters*, *26*(19), 3001–3004. https://doi.org/10.1029/1999gl010434.

Berdon, N. (2013). The Impact of Teleconnection on Pressure, Temperature and Precipitation in Serbia. *International Journal of Remote Sensing Applications*, *3*(4), 185. https://doi.org/10.14355/ijrsa.2013.0304.03

Bhatla, R., Singh, A. K., Mandal, B. N., Ghosh, S., Pandey, S., & Sarkar, A. (2016). Influence of North Atlantic Oscillation on Indian Summer Monsoon Rainfall in Relation to Quasi-Binneal Oscillation. *Pure and Applied Geophysics*, *173*(8), 2959–2970. https://doi.org/10.1007/s00024-016-1306-z

Bi, D., Dix, M., Marsland, S. J., O'Farrell, S., Rashid, H. A., Uotila, P., Hirst, A. C., …, Puri, K. (2013). The ACCESS Coupled Model: Description, Control Climate and Preliminary Validation. *Australian Meteorological and Oceanographic Journal*, 63, 41–64.

Bingyi, W., Renhe, Z., & Wang, B. (2009). On the Association between Spring Arctic Sea Ice Concentration and Chinese Summer Rainfall: A Further Study. *Advances in Atmospheric Sciences, 26* (4), 666–678.

Bintanja, R., Wanders, N., & Katsman, C. A. (2015). The effect of increased fresh water from Antarctic ice shelves on future trends in Antarctic sea ice. *Annals of Glaciology*, *56*(69), 120–126. https://doi.org/10.3189/2015aog69a001

Bintanja, R., Wanders, N., Drijfhout, S., Wouters, B., & Katsman, C. A. (2013). Important role for ocean warming and increased ice-shelf melt in Antarctic sea-ice expansion. *Nature Geoscience*, *6*(5), 376–379. https://doi.org/10.1038/ngeo1767

Bjerknes, J. (1969). Atmospheric Teleconnections from the Equatorial Pacific. *Monthly Weather Review*, *97*(3), 163–172. https://doi.org/10.1175/1520-0493(1969)097

Blackport, R., & Screen, J. A. (2020). Insignificant effect of Arctic amplification on the amplitude of midlatitude atmospheric waves. *Science Advances*, *6*(8). https://doi.org/10.1126/sciadv.aay2880

Blamey, R. W., & Reason, C. J. C. (2007). Relationships between Antarctic sea-ice and South African winter rainfall. *Climate Research*, *33*, 183–193. https://doi.org/10.3354/cr033183

Blanchard-Wrigglesworth, E., Roach, L. A., Donohoe, A., & Ding, Q. (2021). Impact of Winds and Southern Ocean SSTs on Antarctic Sea Ice Trends and Variability. *Journal of Climate, 34*(3), 949–965. https://doi.org/10.1175/jcli-d-20-0386.1

Blandford, H., F. (1886). Rainfall of India. Monsoon Monograph. India Meteorological Department, 3, 658.

Bollasina, M., & Nigam, S. (2011). The summertime "heat" low over Pakistan/northwestern India: evolution and origin. *Climate Dynamics, 37*(5–6), 957–970. https://doi.org/10.1007/s00382-010-0879-y

Boschat, G., Simmonds, I., Purich, A., Cowan, T., & Pezza, A. B. (2016). On the use of composite analyses to form physical hypotheses: An example from heat wave – SST associations. *Scientific Reports*, 6(1). https://doi.org/10.1038/srep29599

Bracegirdle, T. J., & Li, Z. (2012). The Reliability of Antarctic Tropospheric Pressure and Temperature in the Latest Global Reanalyses. *Journal of Climate, 25*(20), 7138–7146. https://doi.org/10.1175/jcli-d-11-00685.1

Bromwich, D. H., Chen, B., & Hines, K. M. (1998). Global atmospheric impacts induced by year-round open water adjacent to Antarctica. *Journal of Geophysical Research*, *103*(D10), 11173–11189. https://doi.org/10.1029/98jd00624

Bromwich, D. H., Nicolas, J., & Monaghan, A. J. (2011). An Assessment of Precipitation Changes over Antarctica and the Southern Ocean since 1989 in Contemporary Global Reanalyses*. Journal of Climate, 24(16), 4189–4209. https://doi.org/10.1175/2011jcli4074.1

Brown, G. (2012). Module: Introduction to Statistics for Climatology - UCAR COMET.

Camberlin, P., Fontaine, B., Louvet, S., Oettli, P., & Valimba, P. (2010). Climate Adjustments over Africa Accompanying the Indian Monsoon Onset. *Journal of Climate, 23*(8), 2047–2064. https://doi.org/10.1175/2009jcli3302.1

Cane, M. A. (2010). Climate: A moist model monsoon. *Nature, 463*(7278), 163– 164.

Carvalho, L. M. V., Jones, C. I., & Ambrizzi, T. (2005). Opposite Phases of the Antarctic Oscillation and Relationships with Intraseasonal to Interannual Activity in the Tropics during the Austral Summer. *Journal of Climate*, *18*(5), 702–718. https://doi.org/10.1175/jcli-3284.1

Cavalieri, D. J., Parkinson, C. L., & Vinnikov, K. Y. (2003). 30-Year satellite record reveals contrasting Arctic and Antarctic decadal sea ice variability. *Geophysical Research Letters*, *30*(18). https://doi.org/10.1029/2003gl018031

Chakraborty, A. (2018). Preceding winter La Niña reduces Indian summer monsoon rainfall. *Environmental Research Letters*, *13*(5), 054030. https://doi.org/10.1088/1748-9326/aabdd5

Chatterjee, S., Ravichandran, M., Murukesh, N., Raj, R. P., & Johannessen, O. M. (2021c). A possible relation between Arctic sea ice and late season Indian Summer Monsoon Rainfall extremes. *Npj Climate and Atmospheric Science*, *4*(1). https://doi.org/10.1038/s41612-021-00191-w

Chen, C., Guan, Z., Jiao, M., & Hu, P. (2019). Anomalous Circulation Patterns in Association with Summertime Regional Daily Precipitation Extremes over Northeast China. *Advances in Meteorology*, *2019*, 1–9. https://doi.org/10.1155/2019/5085897

Chen, G., Liu, Z. A., & Kutzbach, J. E. (2014). Reexamining the barrier effect of the Tibetan Plateau on the South Asian summer monsoon. *Climate of the Past, 10*(3), 1269–1275. https://doi.org/10.5194/cp-10-1269-2014

Chen, S., Shi, W., Wang, Z., Xiao, Z., Chen, W., Wu, R., Xing, W., & Duan, W. (2023). Impact of interannual variation of the spring Somali Jet intensity on the northwest–southeast movement of the South Asian High in the following summer. *Climate Dynamics, 60*(5–6), 1583–1598. https://doi.org/10.1007/s00382-022-06399-7

Cherchi, A., Terry, P., Ratna, S. B., …, & Behera, S. (2021). Indian ocean dipole influence on Indian summer monsoon and ENSO: A review. Indian Summer Monsoon Variability El-Nino Teleconnections and Beyond (Chapter 8, 157–182). Retrieved from https://www.sciencedirect.com/science/article/abs/pii/B9780128224021000119

Chowdary, J. S., Parekh, A., & Gnanaseelan, C. (2021). *Indian Summer Monsoon Variability: El Niño-Teleconnections and Beyond*. Elsevier.

Chung, E., Kim, S., Timmermann, A., Ha, K., Lee, S. Y., Stuecker, M. F., Rodgers, K. B., Lee, S., & Huang, L. (2022). Antarctic sea-ice expansion and Southern Ocean cooling linked to tropical variability. *Nature Climate Change, 12*(5), 461–468. https://doi.org/10.1038/s41558-022-01339-z

Clift, P. D., & Plumb, R. A. (2008). *The Asian Monsoon: Causes, History and Effects*. Retrieved from https://assets.cambridge.org/97805218/47995/frontmatter/9780521847995_frontmatter.pdf.

Coggins, J., & McDonald, A. (2015). The influence of the Amundsen Sea Low on the winds in the Ross Sea and surroundings: Insights from a synoptic climatology. J*ournal of Geophysical Research: Atmospheres, 120*(6), 2167–2189. https://doi.org/10.1002/2014jd022830

Cohen, J., Screen, J. A., Furtado, J. C., Barlow, M., Whittleston, D., Coumou, D., Francis, J. A., Dethloff, K., Entekhabi, D., Overland, J. E., & Jones, J. A. (2014). Recent Arctic amplification and extreme mid-latitude weather. *Nature Geoscience*, *7*(9), 627–637. https://doi.org/10.1038/ngeo2234

Collins, M., Knutti, R., Arblaster, J., Dufresne, J.-L., Fichefet, T., Friedlingstein, P., Gao, …, & Wehner, M. (2013). *Long-term Climate Change: Projections, Commitments and Irreversibility. In: Climate Change 2013: The Physical Science Basis*. Contribution of Working Group I to the Fifth Assessment Report of the Intergovernmental Panel on Climate Change. Retrieved from https://www.ipcc.ch/site/assets/uploads/2018/02/WG1AR5_Chapter12_FINAL.pdf.

Collins, W. J., Bellouin, N., Doutriaux-Boucher, M., Gedney, N., Hinton, T., Jones, C. D., …, & Woodward, S. (2008). Evaluation of the HadGEM2 model. Retrieved from http://www.metoffice.gov.uk/publications/HCTN/index.html.

Comiso, J. C., Kwok, R., Martin, S., & Gordon, A. L. (2011). Variability and trends in sea ice extent and ice production in the Ross Sea. *Journal of Geophysical Research*, *116*(C4). https://doi.org/10.1029/2010jc006391

Crosta, X., Etourneau, J., Orme, L., Dalaiden, Q., Campagne, P., Swingedouw, D., Goosse, H., Massé, G., Miettinen, A., McKay, R. M., Dunbar, R. B., Escutia, C., & Ikehara, M. (2021). Multi-decadal trends in Antarctic sea-ice extent driven by ENSO–SAM over the last 2,000 years. *Nature Geoscience, 14*(3), 156–160. https://doi.org/10.1038/s41561-021-00697-1

Dawson, J., Hoke, W., Lamers, M., Liggett, D., Ljubicic, G., Mills, B. M., Stewart, E., & Thoman, R. (2017). Navigating Weather, Water, Ice and Climate Information for Safe Polar Mobilities. *World Meteorological Organization*. Retrieved from https://epic.awi.de/id/eprint/46211/.

Deb, P., Dash, M., Dey, S. P., & Pandey, P. C. (2017). Non-annular response of sea ice cover in the Indian sector of the Antarctic during extreme SAM events. *International Journal of Climatology, 37*(2), 648–656. https://doi.org/10.1002/joc.4730

Dee, D. P., Uppala, S. M., Simmons, A. J., Berrisford, P., Poli, P., Kobayashi, S., Andrae, U., Balmaseda, M. A., Balsamo, G., Bauer, P., Bechtold, P., Beljaars, A. C. M., Van De Berg, L., Bidlot, J., Bormann, N., Delsol, C., Dragani, R., Fuentes, M., Geer, A. J., . . . Vitart, F. (2011). The ERA-Interim reanalysis: configuration and performance of the data assimilation system. Quarterly Journal of the Royal Meteorological Society, 137(656), 553–597. https://doi.org/10.1002/qj.828

Deser, C., Walsh, J., & Timlin, M. S. (2000). Arctic Sea Ice Variability in the Context of Recent Atmospheric Circulation Trends. *Journal of Climate*, *13*(3), 617–633. https://doi.org/10.1175/1520-0442(2000)013.

Dieckmann, G., & Hellmer, H. (2010). The Importance of Sea Ice: An Overview. In *Wiley-Blackwell eBooks* (pp. 1–22). https://doi.org/10.1002/9781444317145.ch1.

Dike, V. N., Shimizu, M. H., Diallo, M. A., Lin, Z., Nwofor, O. K., & Chineke, T. C. (2015). Modelling present and future African climate using CMIP5 scenarios in

HadGEM2-ES. *International Journal of Climatology*, *35*(8), 1784–1799. https://doi.org/10.1002/joc.4084

Dima, I. M., & Wallace, J. L. (2003). On the Seasonality of the Hadley Cell. *Journal of the Atmospheric Sciences*, *60*(12), 1522–1527. https://doi.org/10.1175/1520-0469(2003)060.

Dugam, S. S. (2008). Role of North Atlantic oscillation and Southern oscillation in deficient and excess monsoon years. *Indian Journal of Science and Technology*, *1*(5), 1–6. https://doi.org/10.17485/ijst/2008/v1i5.7

Dugam, S. S., & Kakade, S. B. (2004). Antarctica sea-ice and monsoon variability. *Indian Journal of Radio & Space Physics*, 33, 306 - 309.

Dugam, S. S., Kakade, S. B., & Verma, R. K. (1997). Interannual and long-term variability in the northern Atlantic oscillation and Indian summer monsoon rainfall. *Theor. Appl. Climatol*., 58, 21–29.

Eayrs, C., Holland, D. M., Francis, D., Wagner, T. J. W., Kumar, R., & Li, X. (2019). Understanding the Seasonal Cycle of Antarctic Sea Ice Extent in the Context of Longer-Term Variability. *Reviews of Geophysics*, *57*(3), 1037–1064. https://doi.org/10.1029/2018rg000631

Ejaz, T., Rahaman, W., Laluraj, C. M., Mahalinganathan, K., & Thamban, M. (2021). Sea Ice Variability and Trends in the Western Indian Ocean Sector of Antarctica During the Past Two Centuries and Its Response to Climatic Modes. *Front. Earth Sci, 126*(23). https://doi.org/10.1029/2020jd033943

Fan, T., Deser, C., & Schneider, D. J. (2014). Recent Antarctic sea ice trends in the context of Southern Ocean surface climate variations since 1950. *Geophysical Research Letters*, *41*(7), 2419–2426. https://doi.org/10.1002/2014gl059239

Feldstein, S. B., & Franzke, C. (2017). Atmospheric Teleconnection Patterns. In *Cambridge University Press eBooks* (pp. 54–104). https://doi.org/10.1017/9781316339251.004

Feng, J., Li, J., & Xu, H. (2013). Increased summer rainfall in northwest Australia linked to southern Indian Ocean climate variability. *Journal of Geophysical Research: Atmospheres, 118*(2), 467–480. https://doi.org/10.1029/2012jd018323

Feng, J., Zhang, Y., Cheng, Q., Liang, X. S., & Jiang, T. (2019). Analysis of summer Antarctic sea ice anomalies associated with the spring Indian Ocean dipole. *Global and Planetary Change*, 181, 102982. https://doi.org/10.1016/j.gloplacha.2019.102982

Findlater, J. (1971). Mean Monthly Air Flow at Low Levels over the Western Indian Ocean. Geoph. Memoirs No. 115 London Published by Her Majesty's Office

Fletcher, C. D., & Kushner, P. J. (2011). The Role of Linear Interference in the Annular Mode Response to Tropical SST Forcing. *Journal of Climate*, *24*(3), 778–794. https://doi.org/10.1175/2010jcli3735.1

Flohn, H. (1968). *Contributions to a meteorology of the Tibetan highlands*. http://ci.nii.ac.jp/ncid/BB07816232

Fogt, R. L., & Wovrosh, A. J. (2015). The Relative Influence of Tropical Sea Surface Temperatures and Radiative Forcing on the Amundsen Sea Low. *Journal of Climate, 28*(21), 8540–8555. https://doi.org/10.1175/jcli-d-15-0091.1

Francis, P. A., & Gadgil, S. (2006). Intense rainfall events over the west coast of India. *Meteorology and Atmospheric Physics*, *94*(1–4), 27–42. https://doi.org/10.1007/s00703-005-0167-2

Fu, C., & Fletcher, J. O. (1985). The Relationship between Tibet-Tropical Ocean Thermal Contrast and Interannual Variability of Indian Monsoon Rainfall. *Journal of Climate and Applied Meteorology, 24*(8), 841–847. https://doi.org/10.1175/1520-0450(1985)024

Fukushima, A., Kanamori, H., & Matsumoto, J. (2019). Regionality of long-term trends and interannual variation of seasonal precipitation over India. *Progress in Earth and Planetary Science*, *6*(1). https://doi.org/10.1186/s40645-019-0255-4

Gadgil, S. (2003). The Indian Monsoon and Its Variability. *Annual Review of Earth and Planetary Sciences*, *31*(1), 429–467. https://doi.org/10.1146/annurev.earth.31.100901.141251

Gadgil, S. (2006). The Indian Monsoon, GDP and agriculture. *Economic Political Weekly, 41* (47),4887–4895.

Ge, F., Sielmann, F., Zhu, X., Fraedrich, K., Zhi, X., Peng, T., & Wang, L. (2017). The link between Tibetan Plateau monsoon and Indian summer precipitation: a linear diagnostic perspective. *Climate Dynamics, 49*(11–12), 4201–4215. https://doi.org/10.1007/s00382-017-3585-1

Glantz, M., Katz, R. H., & Nicholls, N. (2009). *Teleconnections Linking Worldwide Climate Anomalies*. Retrieved from https://research.monash.edu/en/publications/teleconnections-linking-worldwide-climate-anomalies.

Gnanaseelan, C., & Anila, S. (2021). *Southern annular mode teleconnections to Indian summer monsoon*. In Elsevier eBooks (pp. 335–352). https://doi.org/10.1016/b978-0-12-822402-1.00026-0

Godfred-Spenning, C. R., & Simmonds, I. (1996). AN ANALYSIS OF ANTARCTIC SEA-ICE AND EXTRATROPICAL CYCLONE ASSOCIATIONS. *International Journal of Climatology*, *16*(12), 1315–1332. https://doi.org/10.1002/(sici)1097-0088(199612)16:12

Goswami, B. N., & Mohan, R. S. A. (2001). Intraseasonal Oscillations and Interannual Variability of the Indian Summer Monsoon. *Journal of Climate*, *14*(6), 1180–1198. https://doi.org/10.1175/1520-0442(2001)014.

Greatbatch, R. J., Sun, X., & Yang, X. (2013). Impact of variability in the Indian summer monsoon on the East Asian summer monsoon. *Atmospheric Science Letters, 14*(1), 14–19. https://doi.org/10.1002/asl2.408

Gregory, S. G. (2007). Interrelationships between Indian and northern Australian summer monsoon rainfall values. *International Journal of Climatology*, *11*(1), 55–62. https://doi.org/10.1002/joc.3370110104.

Guo, D., Gao, Y., Bethke, I., Gong, D., Johannessen, O. M., & Wang, H. (2014). Mechanism on how the spring Arctic sea ice impacts the East Asian summer monsoon. *Theoretical and Applied Climatology*, *115*(1–2), 107–119. https://doi.org/10.1007/s00704-013-0872-6.

Hai, O. S. (2013). *Essential of Meteorology and Climatology*. National Antarctic Research Center University of Malaya.

Hall, A., & Visbeck, M. (2002). Synchronous Variability in the Southern Hemisphere Atmosphere, Sea Ice, and Ocean Resulting from the Annular Mode*. *Journal of Climate*, *15*(21), 3043–3057. https://doi.org/10.1175/1520-0442(2002)015.

Halpern, D., & Woiceshyn, P. M. (1999). Onset of the Somali Jet in the Arabian Sea during June 1997. *Journal of Geophysical Research*, *104*(C8), 18041–18046. https://doi.org/10.1029/1999jc900141

Halpern, D., & Woiceshyn, P. M. (2001). Somali Jet in the Arabian Sea, El Niño, and India Rainfall. *Journal of Climate, 14*(3), 434–441. https://doi.org/10.1175/1520-0442(2001)014

Han, T., Zhang, M., Zhu, J., Zhou, B., & Li, S. (2021). Impact of early spring sea ice in Barents Sea on midsummer rainfall distribution at Northeast China. *Climate Dynamics*, *57*(3–4), 1023–1037. https://doi.org/10.1007/s00382-021-05754-4

Han, X., Wei, F., & Chen, X. (2017). Influence of the Anomalous Patterns of the Mascarene and Australian Highs on Precipitation during the Prerainy Season in

South China. *Advances in Meteorology*, *2017*, 1–12. https://doi.org/10.1155/2017/6408029

Hannachi, A. (2004). *A primer for EOF analysis of climate data*. University of Reading.

Hannachi, A., Jolliffe, I. T., & Stephenson, D. (2007). Empirical orthogonal functions and related techniques in atmospheric science: A review. *Int. J. Climatol*, 27, 1119–1152.

Harman, J. R., & Winkler, J. A. (1991). Synoptic Climatology: Themes, Applications, and Prospects. *Physical Geography*, *12*(3), 220–230. https://doi.org/10.1080/02723646.1991.10642429

He, J., Lin, H., & Wu, Z. (2011). Another look at influences of the Madden-Julian Oscillation on the wintertime East Asian weather. *Journal of Geophysical Research*, *116*(D3). https://doi.org/10.1029/2010jd014787

He, S., Gao, Y., Furevik, T., Wang, H., & Li, F. (2018). Teleconnection between sea ice in the Barents Sea in June and the Silk Road, Pacific–Japan and East Asian rainfall patterns in August. *Advances in Atmospheric Sciences*, *35*(1), 52–64. https://doi.org/10.1007/s00376-017-7029-y

Henley, B. J., Gergis, J., Karoly, D. J., Power, S. B., Kennedy, J. F., & Folland, C. K. (2015). A Tripole Index for the Interdecadal Pacific Oscillation. *Climate Dynamics, 45*(11–12), 3077–3090. https://doi.org/10.1007/s00382-015-2525-1

Hines, K. M. (2002). A pole to pole west Pacific atmospheric teleconnection during August. *Journal of Geophysical Research*, *107*(D18). https://doi.org/10.1029/2001jd001335

Hobbs, W., Massom, R. A., Stammerjohn, S., Reid, P., Williams, G. B., & Meier, W. N. (2016). A review of recent changes in Southern Ocean sea ice, their drivers and forcings. *Global and Planetary Change*, *143*, 228–250. https://doi.org/10.1016/j.gloplacha.2016.06.008

Holland, P. R. (2014). The seasonality of Antarctic sea ice trends. *Geophysical Research Letters*, *41*(12), 4230–4237. https://doi.org/10.1002/2014gl060172

Holland, P. R., & Kwok, R. (2012). Wind-driven trends in Antarctic sea-ice drift. *Nature Geoscience*, *5*(12), 872–875. https://doi.org/10.1038/ngeo1627.

Holmes, C. R., Holland, P. V., & Bracegirdle, T. J. (2019). Compensating Biases and a Noteworthy Success in the CMIP5 Representation of Antarctic Sea Ice Processes. *Geophysical Research Letters*, *46*(8), 4299–4307. https://doi.org/10.1029/2018gl081796.

Hosking, J. S., Orr, A., Li, Z., Turner, J. A., & Phillips, T. (2013). The Influence of the Amundsen–Bellingshausen Seas Low on the Climate of West Antarctica and Its Representation in Coupled Climate Model Simulations. *Journal of Climate, 26*(17), 6633–6648. https://doi.org/10.1175/jcli-d-12-00813.1

Hoskins, B. J., & Ambrizzi, T. (1993). Rossby Wave Propagation on a Realistic Longitudinally Varying Flow. *Journal of the Atmospheric Sciences*, *50*(12), 1661–1671. https://doi.org/10.1175/1520-0469(1993)050

Hoskins, B. J., & Wang, B. (2006). *Large-scale atmospheric dynamics*. In Springer eBooks. https://doi.org/10.1007/3-540-37722-0_9

Hsu, P., Fu, Z. F., Murakami, H., Lee, J., Yoo, C., Rosati, A., Chang, C., & Liu, Y. (2021). East Antarctic cooling induced by decadal changes in Madden-Julian oscillation during austral summer. *Science Advances, 7*(26). https://doi.org/10.1126/sciadv.abf9903

Hu, Y., & Fu, Q. (2007). Observed poleward expansion of the Hadley circulation since 1979. *Atmospheric Chemistry and Physics*, *7*(19), 5229–5236. https://doi.org/10.5194/acp-7-5229-2007.

Hu, Y., Huang, H., & Zhou, C. (2018). Widening and weakening of the Hadley circulation under global warming. *Science Bulletin*, *63*(10), 640–644. https://doi.org/10.1016/j.scib.2018.04.020

Huang, S., Wang, B., Wen, Z., & Chen, Z. (2021). Enhanced Tropical Eastern Indian Ocean Rainfall Breaks down the Tropical Easterly Jet-Indian Rainfall Relationship. *Journal of Climate,* 1–44. https://doi.org/10.1175/jcli-d-20-0631.1

Hudson, D. A., & Hewitson, B. (2001). The atmospheric response to a reduction in summer Antarctic sea-ice extent. *Climate Research*, *16*, 79–99. https://doi.org/10.3354/cr016079

Huffman, G. J., Adler, R. F., Arkin, P. A., Chang, A. E., Ferraro, R., Gruber, A., Janowiak, J. J., McNab, A. A., Rudolf, B., & Schneider, U. (1997). The Global Precipitation Climatology Project (GPCP) Combined Precipitation Dataset. *Bulletin of the American Meteorological Society, 78*(1), 5–20. https://doi.org/10.1175/1520-0477(1997)078

Hung, C. W., Liu, X., & Yanai, M. (2004). Symmetry and Asymmetry of the Asian and Australian Summer Monsoons. *Journal of Climate*, *17*(12), 2413–2426. https://doi.org/10.1175/1520-0442(2004)017

Hunke, E., Lipscomb, W. N., & Turner, A. K. (2010). Sea-ice models for climate study: retrospective and new directions. *Journal of Glaciology*, *56*(200), 1162–1172. https://doi.org/10.3189/002214311796406095

Intergovernmental Panel on Climate Change, (2014). Climate Change 2014: Synthesis Report. Contribution of Working Groups I, II and III to the Fifth Assessment Report of the Intergovernmental Panel on Climate Change.

Jain, S., Mishra, S. K., Anand, A., Salunke, P., & Fasullo, J. T. (2021). Historical and projected low-frequency variability in the Somali Jet and Indian Summer Monsoon. *Climate Dynamics, 56*(3–4), 749–765. https://doi.org/10.1007/s00382-020-05492-z

James, I. N. (1988). On the forcing of planetary-scale Rossby waves by Antarctica. *Quarterly Journal of the Royal Meteorological Society*, *114*(481), 619–637. https://doi.org/10.1256/smsqj.48104

Jena, B., Kumar, A., Ravinchandran, M., Kren, S. (2018). Mechanism of sea ice expansion in the Indian Ocean sector of Antarctic: Insights from satellite observation and model reanalysis. PLoS ONE, 3(10), 1 - 16.

Jian-Qi, S. (2010). Possible Impact of the Boreal Spring Antarctic Oscillation on the North American Summer Monsoon. *Atmospheric and Oceanic Science Letters*, *3*(4), 232–236. https://doi.org/10.1080/16742834.2010.11446870

Jin, D., Guan, Z., Huo, L., & Wang, X. (2017). Possible impacts of spring sea surface temperature anomalies over South Indian Ocean on summer rainfall in Guangdong-Guangxi region of China. *Climate Dynamics*, *49*(9–10), 3075–3090. https://doi.org/10.1007/s00382-016-3494-8.

John, V. O., Allan, R. P., & Soden, B. J. (2009). How robust are observed and simulated precipitation responses to tropical ocean warming? *Geophysical Research Letters*, *36*(14). https://doi.org/10.1029/2009gl038276.

Joseph, P., Liebmann, B., & Hendon, H. (1991). Interannual variability of the Australian summer monsoon onset – possible influence of Indian-summer monsoon and El-Nino. *Journal Climate,* 4,529–538.

Kakade, S. B., & Dugam, S. S. (2000). The simultaneous effect of NAO and SO on the monsoon activity over India. *Geophysical Research Letters*, *27*(21), 3501–3504. https://doi.org/10.1029/1999gl011201

Kakade, S. B., & Dugam, S. S. (2006). Spatial monsoon variability with respect to NAO and SO. *Journal of Earth System Science*, *115*(5), 601–606. https://doi.org/10.1007/bf02702912

Kakade, S. B., & Kulkarni, A. (2013). Prediction of Indian summer monsoon rainfall using surface temperature and sea-level pressure cluster parameters. *Current Science, 105*(7), 964– 970.

Kanamitsu, M., Krishnamurti, T. N., & Depradine, C. (1972). On Scale Interactions in the Tropics During Northern Summer. *Journal of the Atmospheric Sciences*, *29*(4), 698–706. https://doi.org/10.1175/1520-0469(1972)029

Karahalil, M., Ozsoy, B., Başar, E., & Satir, T. (2021). The evaluation of the Polar Code by the survey conducted with those who have sailed in polar regions, and suggestions for further improvement. *Marine Policy*, *128*, 104502. https://doi.org/10.1016/j.marpol.2021.104502

Kim, J., Kang, D., Lee, M., Jin, E. K., Kug, J., & Lee, W. S. (2023). Remote Influences of ENSO and IOD on the Interannual Variability of the West Antarctic Sea Ice. Journal of Geophysical Research: *Atmospheres, 128*(10). https://doi.org/10.1029/2022jd038313

Kim, Y., Kim, M., Lau, W. K. M., Kim, K., & Cho, C. (2015). Possible mechanism of abrupt jump in winter surface air temperature in the late 1980s over the Northern Hemisphere. *J. Geophys. Res. Atmos*, *120*(24), 12474–12485. https://doi.org/10.1002/2015jd023864

Kimura, N., & Wakatsuchi, M. (2011). Large-scale processes governing the seasonal variability of the Antarctic sea ice. *Tellus A*, *63*(4), 828. https://doi.org/10.1111/j.1600-0870.2011.00526.x

Konduru, R. T., & Mrudula, G. (2021). Effect of offshore troughs on the South India erratic summer monsoon rainfall in June 2017. *Dynamics of Atmospheres and Oceans*, 93, 101187. https://doi.org/10.1016/j.dynatmoce.2020.101187

Koteswaram, P. (1958). The Easterly Jet Stream in the Tropics. Tellus B: *Chemical and Physical Meteorology, 10*(1), 43–57. https://doi.org/10.3402/tellusa.v10i1.9220

Krishnamurthy, V., & Goswami, B. N. (2000). Indian Monsoon–ENSO Relationship on Interdecadal Timescale. *Journal of Climate*, *13*(3), 579–595. https://doi.org/10.1175/1520-0442(2000)013

Krishnamurthy, V., & KinterIII, J. L. (2003). The Indian Monsoon and its Relation to Global Climate Variability. In *Springer eBooks* (pp. 186–236). https://doi.org/10.1007/978-3-662-05285-3_10

Krishnamurti, T. N., & Bhalme, H. N. (1976). Oscillations of a Monsoon System. Part I. Observational Aspects. *Journal of the Atmospheric Sciences*, *33*(10), 1937–1954. https://doi.org/10.1175/1520-0469(1976)033

Krishnamurti, T. N., Daggupaty, S., Fein, J. S., Kanamitsu, M., & Lee, J. D. (1973). Tibetan High and Upper Tropospheric Tropical Circulations during Northern Summer. *Bulletin of the American Meteorological Society, 54*(12), 1234–1250. https://doi.org/10.1175/1520-0477-54.12.1234

Krishnamurti, T. N., Stefanova, L., & Misra, V. (2013). Tropical Meteorology. In *Springer atmospheric sciences*. Springer Nature (Netherlands). https://doi.org/10.1007/978-1-4614-7409-8

Krishnamurti, T., N., & Rodgers, E., B. (1970). *200 mb wind field, June, July, August 1971*. Dept. of Meteorology, Florida State University, 114

Krishnan, R., & Sugi, M. (2003). Pacific decadal oscillation and variability of the Indian summer monsoon rainfall. *Climate Dynamics*, *21*(3–4), 233–242. https://doi.org/10.1007/s00382-003-0330-8

Krishnan, R., Sabin, T. P., Vellore, R., Mujumdar, M., Sanjay, J., Goswami, B. N., Hourdin, F., Dufresne, J., & Terray, P. (2016). Deciphering the desiccation trend of the South Asian monsoon hydroclimate in a warming world. *Climate Dynamics, 47*(3–4), 1007–1027. https://doi.org/10.1007/s00382-015-2886-5

Krishnan, R., Singh, B. B., Vellore, R., … & Rajeevan, M. (2020). A short perspective on the Mascarene High and the abnormal Indian Monsoon during 2015. *The Transporters - Physics: Ocean, Atmosphere*. The Indian Ocean Bubble, 17 – 19.

Kucharski, F., Bracco, A., Yoo, J. C., Tompkins, A. M., Feudale, L., Ruti, P., & Dell'Aquila, A. (2009). A Gill-Matsuno-type mechanism explains the tropical Atlantic influence on African and Indian monsoon rainfall. *Quarterly Journal of the Royal Meteorological Society*, *135*(640), 569–579. https://doi.org/10.1002/qj.406

Kucharski, F., Bracco, A., Yoo, J., & Molteni, F. (2007). Low-Frequency Variability of the Indian Monsoon–ENSO Relationship and the Tropical Atlantic: The "Weakening" of the 1980s and 1990s. *Journal of Climate*, *20*(16), 4255–4266. https://doi.org/10.1175/jcli4254.1

Kucharski, F., Bracco, A., Yoo, J., & Molteni, F. (2008). Atlantic forced component of the Indian monsoon interannual variability. *Geophysical Research Letters*, *35*(4). https://doi.org/10.1029/2007gl033037.

Kucharski, F., Parvin, A., Rodríguez-Fonseca, B., Farneti, R., Martín-Rey, M., Polo, I., Mohino, E., Losada, T., & Mechoso, C. R. (2016). The Teleconnection of the Tropical Atlantic to Indo-Pacific Sea Surface Temperatures on Inter-Annual to Centennial Time Scales: A Review of Recent Findings. *Atmosphere*, *7*(2), 29. https://doi.org/10.3390/atmos7020029

Kumar, A., Yadav, J., & Mohan, R. (2021). Seasonal sea-ice variability and its trend in the Weddell Sea sector of West Antarctica. *Environmental Research Letters*. https://doi.org/10.1088/1748-9326/abdc88

Kumar, K. S., Rajagopalan, B., & Cane, M. A. (1999). On the Weakening Relationship Between the Indian Monsoon and ENSO. *Science*, *284*(5423), 2156–2159. https://doi.org/10.1126/science.284.5423.2156

Kumar, K. S., Soman, M. K., & Kumar, K. S. (1995). Seasonal forecasting of Indian summer monsoon rainfall: A review. *Weather*, *50*(12), 449–467. https://doi.org/10.1002/j.1477-8696.1995.tb06071.x

Kumar, M., & Schlüssel, P. (1998). Air-Sea Interaction over the Indian Ocean During the Two Contrasting Monsoon Years 1987 and 1988 Studied with Satellite Data. *Theoretical and Applied Climatology,* *60*(1–4), 219–231. https://doi.org/10.1007/s007040050045

Landrum, L., Holland, M. M., Raphael, M. N., & Polvani, L. M. (2017). Stratospheric Ozone Depletion: An Unlikely Driver of the Regional Trends in Antarctic Sea Ice in Austral Fall in the Late Twentieth Century. *Geophysical Research Letters*, *44*(21). https://doi.org/10.1002/2017gl075618

Lau, K. M., Lau, N. C., & Yang, S. (2004). Current topics on interannual variability of the Asian monsoon. The global monsoon system: Research and forecast, World Meteorological Organization, Hangzhou, China, 440-454.

Lau, K. Y., Kim, K. W., & Yang, S. (2000). Dynamical and Boundary Forcing Characteristics of Regional Components of the Asian Summer Monsoon. *Journal of Climate*, *13*(14), 2461–2482. https://doi.org/10.1175/1520-0442(2000)013

Leathers, D. J., Yarnal, B., & Palecki, M. A. (1991). The Pacific/North American Teleconnection Pattern and United States Climate. Part I: Regional Temperature and Precipitation Associations. *Journal of Climate*, *4*(5), 517–528. https://doi.org/10.1175/1520-0442(1991)004

Lee, H., & Jin, E. K. (2021). Seasonality and Dynamics of Atmospheric Teleconnection from the Tropical Indian Ocean and the Western Pacific to West Antarctica. *Atmosphere*, *12*(7), 849. https://doi.org/10.3390/atmos12070849

Lee, H., & Lee, J. (2019). Impact of the Madden-Julian oscillation on Antarctic sea ice and its dynamical mechanism. *Scientific Reports, 9*(1). https://doi.org/10.1038/s41598-019-47150-3

Lee, S. Y., & Koh, T.Y. (2012). Teleconnection between Australian winter temperature and Indian summer monsoon rainfall. Atmos. Chem. Phys., 1, 669–681.

Lefebvre, W., & Goosse, H. (2008). An analysis of the atmospheric processes driving the large-scale winter sea ice variability in the Southern Ocean. *Journal of Geophysical Research*, *113*(C2). https://doi.org/10.1029/2006jc004032

Li, C., & Li, S. (2014). Interannual Seesaw between the Somali and the Australian Cross-Equatorial Flows and its Connection to the East Asian Summer Monsoon. *Journal of Climate*, *27*(11), 3966–3981. https://doi.org/10.1175/jcli-d-13-00288.1

Li, J., & Wang, J. (2003). A modified zonal index and its physical sense. *Geophysical Research Letters*, *30*(12). https://doi.org/10.1029/2003gl017441

Li, S., Zhang, Y., Chen, C., Zhang, Y., Xu, D., & Hu, S. (2023). Assessment of Antarctic Sea Ice Cover in CMIP6 Prediction with Comparison to AMSR2 during 2015–2021. *Remote Sensing, 15*(8), 2048. https://doi.org/10.3390/rs15082048

Li, X., Cai, W., Meehl, G. A., Chen, D., Yuan, X., Raphael, M. N., Holland, D. M., Ding, Q., Fogt, R. L., Markle, B. R., Wang, G., Bromwich, D. H., Turner, J. A., Xie, S., Steig, E. J., Gille, S. T., Xiao, C., Wu, B., Lazzara, M. A., . . . Song, C. (2021). Tropical teleconnection impacts on Antarctic climate changes. *Nat Rev Earth Environ*, *2*(10), 680–698. https://doi.org/10.1038/s43017-021-00204-5

Liebmann, B. (1996). Description of a complete (interpolated) outgoing longwave radiation dataset. *Bulletin of the American Meteorological Society, 77*(6), 1275–1277. https://ci.nii.ac.jp/naid/10010122825/

Lieser, J. L., Massom, R. A., Fraser, A. D., Haward, M. G., Heil, P., Lannuzel, D., Meiners, K., Melbourne-Thomas, J., Press, A. J., and Williams, G. D. (2014). Position analysis: Antarctic sea ice and climate change 2014, Report, Antarctic Climate and Ecosystems Cooperative Research Centre, Hobart, Tasmania, Australia.

Lim, J.T., & Samah, A.A. (2004). Weather and climate of Malaysia. University of Malaya Press, Malaysia.

Lin, Z., & Li, F. (2018). Impact of interannual variations of spring sea ice in the Barents Sea on East Asian rainfall in June. *Atmospheric and Oceanic Science Letters*, *11*(3), 275–281. https://doi.org/10.1080/16742834.2018.1454249

Liu, J., Curry, J. A., & Martinson, D. G. (2004). Interpretation of recent Antarctic sea ice variability. *Geophysical Research Letters*, *31*(2). https://doi.org/10.1029/2003gl018732

Liu, J., Martinson, D. G., Yuan, X., & Rind, D. (2002). Evaluating Antarctic sea ice variability and its teleconnections in global climate models. *International Journal of Climatology*, *22*(8), 885–900. https://doi.org/10.1002/joc.770

Liu, J., Yuan, X., Rind, D., & Martinson, D. G. (2002). Mechanism study of the ENSO and southern high latitude climate teleconnections. *Geophysical Research Letters*, *29*(14), 24–4. https://doi.org/10.1029/2002gl015143

Liu, N., & Li, S. (2018). Connection of Antarctic sea ice variability with China summer rainfall on the interannual timescale. AGU Fall Meeting Abstract. Retrieved from https://ui.adsabs.harvard.edu/abs/2018AGUFM.A11N2456L/abstract

Liu, N., Zhang, Z., Chen, H., & Lin, L. (2011). Western Indian Ocean SST signal and anomalous Antarctic sea-ice concentration variation. *Acta Oceanologica Sinica*, *30*(2), 9–13. https://doi.org/10.1007/s13131-011-0100-0

Liu, Z., & Alexander, M. (2007). Atmospheric bridge, oceanic tunnel, and global climatic teleconnections. *Reviews of Geophysics, 45* (2005RG000172), 1 - 34.

Liu, Z., Colin, C., Trentesaux, A., Blamart, D., Bassinot, F., Siani, G., & Sicre, M. (2004). Erosional history of the eastern Tibetan Plateau since 190 kyr ago: clay mineralogical and geochemical investigations from the southwestern South China Sea. *Marine Geology, 209*(1–4), 1–18. https://doi.org/10.1016/j.margeo.2004.06.004

Loeb, N. G., Rutan, D. A., Kato, S., & Wang, W. (2014). Observing Interannual Variations in Hadley Circulation Atmospheric Diabatic Heating and Circulation Strength. *Journal of Climate*, *27*(11), 4139–4158. https://doi.org/10.1175/jcli-d-13-00656.1

Love, G. (1985). Cross-Equatorial Influence of Winter Hemisphere Subtropical Cold Surges. *Monthly Weather Review, 113*(9), 1487–1498. https://doi.org/10.1175/1520-0493(1985)113

Lübbecke, J. F., Rodríguez-Fonseca, B., Richter, I., Martín-Rey, M., Losada, T., Polo, I., & Keenlyside, N. (2018). Equatorial Atlantic variability—Modes, mechanisms, and global teleconnections. *Wiley Interdisciplinary Reviews: Climate Change*, *9*(4). https://doi.org/10.1002/wcc.527

Luo, X., & Zhang, Y. (2015). The Linkage between Upper-Level Jet Streams over East Asia and East Asian Winter Monsoon Variability. *Journal of Climate*, *28*(22), 9013–9028. https://doi.org/10.1175/jcli-d-15-0160.1

Madhu, V. (2014). Variation of Zonal Winds in the Upper Troposphere and Lower Stratosphere in Association with Deficient and Excess Indian Summer Monsoon Scenario. *Atmos. Climate Sci, 04*(04), 685–695. https://doi.org/10.4236/acs.2014.44062

Mahlstein, I., Gent, P. R., & Solomon, S. (2013). Historical Antarctic mean sea ice area, sea ice trends, and winds in CMIP5 simulations. *Journal of Geophysical Research: Atmospheres*, *118*(11), 5105–5110. https://doi.org/10.1002/jgrd.50443.

Maksym, T., Stammerjohn, S., Ackley, S. F., & Massom, R. A. (2012). Antarctic Sea Ice—A Polar Opposite? *Oceanography*, *25*(3), 140–151. https://doi.org/10.5670/oceanog.2012.88

Manatsa, D., Morioka, Y., Behera, S. K., Matarira, C. H., & Yamagata, T. (2014). Impact of Mascarene High variability on the East African 'short rains.' *Climate Dynamics*, *42*(5–6), 1259–1274. https://doi.org/10.1007/s00382-013-1848-z

Marshall, G. J. (2003). Trends in the Southern Annular Mode from Observations and Reanalyses. *Journal of Climate,* 16, 4134 – 4143. https://doi.org/10.1175/1520-0442(2003)016<4134:TITSAM>2.0.CO;2

Marshall, J. C., Scott, J. R., Armour, K. C., Campin, J., Kelley, M., & Romanou, A. (2015). The ocean's role in the transient response of climate to abrupt greenhouse gas forcing. *Climate Dynamics*, *44*(7–8), 2287–2299. https://doi.org/10.1007/s00382-014-2308-0

Martinson, D. G. (2012). Antarctic circumpolar current's role in the Antarctic ice system: An overview. *Palaeogeography, Palaeoclimatology, Palaeoecology*, *335–336*, 71–74. https://doi.org/10.1016/j.palaeo.2011.04.007

Massom, R.A., Stammerjohn, S.E. (2010). Antarctic sea ice change and variability – Physical and ecological implication. Polar Science 4: 149 – 186. DOI: 10.1016/j.polar.2010.05.001.

Meehl, G. (1987). The annual cycle and interannual variability in the tropical Pacific and Indian-ocean regions, Mon. Weather Rev. 115: 27–50.

Meehl, G. (1997). The south Asian monsoon and the tropospheric biennialoscillation, J. Climate 10; 1921–1943.

Meehl, G. A. et al. (2019). Sustained ocean changes contributed to sudden Antarctic sea ice retreat in late 2016. Nat. Communications 10 (14).

Meehl, G. A., Arblaster, J. M., Bitz, C. M., Chung, C. B., & Teng, H. (2016). Antarctic sea-ice expansion between 2000 and 2014 driven by tropical Pacific decadal climate variability. *Nature Geoscience, 9*(8), 590–595. https://doi.org/10.1038/ngeo2751

Menzel, M.E., Waugh, D., Grise, K. (2019). Disconnect between Hadley cell and subtropical jet variability and response to increased CO2. Geophys Res Lett 46(12):7045–7053.

Misra, V. (2020). *Teleconnections. Regionalizing Global Climate Variations: A Study of the Southeastern US Regional Climate*. Elsevier.

Miyasaka, T., & Nakamura, H. (2010). Structure and Mechanisms of the Southern Hemisphere Summertime Subtropical Anticyclones. *Journal of Climate, 23*(8), 2115–2130. https://doi.org/10.1175/2009jcli3008.1

Mo, K. C., & Higgins, R. (1998). The Pacific–South American Modes and Tropical Convection during the Southern Hemisphere Winter. *Monthly Weather Review, 126*(6), 1581–1596. https://doi.org/10.1175/1520-0493(1998)126

Mock, C. J. (2014). Paleoclimate Modeling of Paleo-ENSO☆. In *Elsevier eBooks*. https://doi.org/10.1016/b978-0-12-409548-9.09410-0

Morioka, Y., Takaya, K., Behera, S.K., Masumoto, Y. (2015). Local SST Impacts on the Summertime Mascarene High Variability. Journal of Climate 28:678 – 694. DOI: 10.1175/JCLI-D-14-00133.1.

Murphy, E.J., Clarke, A., Abram, N.J., Turner, J. (2014). Variability of sea-ice in the northern Weddell Sea during the 20th century. Journal of Geophysical Research: Oceans 119: 4549–4572. DOI:10.1002/ 2013JC009511.

Nan, S., Li, J., Yuan, X., Zhao, P. (2009). Boreal spring Southern Hemisphere Annular Mode, Indian Ocean sea surface temperature, and East Asian summer monsoon. Journal of Geophysical Research 114 (D02103): 1- 13. DOI:10.1029/2008JD010045

Nguyen, H. T., Evans, A., Lucas, C., Smith, I. T., & Timbal, B. (2013). The Hadley Circulation in Reanalyses: Climatology, Variability, and Change. *Journal of Climate*, *26*(10), 3357–3376. https://doi.org/10.1175/jcli-d-12-00224.1

Nicholson, S. E., & Klotter, D. (2021). The Tropical Easterly Jet over Africa, its representation in six reanalysis products, and its association with Sahel rainfall. *International Journal of Climatology, 41*(1), 328–347. https://doi.org/10.1002/joc.6623

Nigam, S., & Baxter, S. (2015). *Teleconnections*. Encyclopedia of Atmospheric Sciences, 2nd edition, 3, 90–109

Nilsson-Kerr, K., Anand, P., Sexton, P. M., Leng, M. J., Misra, S. P., Clemens, S. C., & Hammond, S. J. (2019). Role of Asian summer monsoon subsystems in the inter-hemispheric progression of deglaciation. *Nature Geoscience*, *12*(4), 290–295. https://doi.org/10.1038/s41561-019-0319-5

Nithya, K., Manoj, M. G., & Mohankumar, K. (2017). Effect of El Niño/La Niña on tropical easterly jet stream during Asian summer monsoon season. *International Journal of Climatology, 37*(15), 4994–5004. https://doi.org/10.1002/joc.5137

Nkurunziza, I. F., Guirong, T., Ngarukiyimana, J. P., & Sindikubwabo, C. (2019). Influence of the Mascarene High on October-December Rainfall and their associated atmospheric circulation anomalies over Rwanda. *Journal of Environmental & Agricultural Sciences*, 20, 1-20.

Nuncio, M., & Yuan, X. (2015). The Influence of the Indian Ocean Dipole on Antarctic Sea Ice*. *Journal of Climate*, *28*(7), 2682–2690. https://doi.org/10.1175/jcli-d-14-00390.1

Ogallo, L., Janowiak, J. J., & Halpert, M. S. (1988). Teleconnection between Seasonal Rainfall over East Africa and Global Sea Surface Temperature Anomalies.

Journal of the Meteorological Society of Japan, *66*(6), 807–822. https://doi.org/10.2151/jmsj1965.66.6_807

Ogwang, B. A., Ongoma, V., Xing, L., & Ogou, F. K. (2015). Influence of Mascarene High and Indian Ocean Dipole on East African Extreme Weather Events. *Geographica Pannonica*, *19* (2),64 -72. https://doi.org/10.5937/geopan1502064o

Ohishi, S., Sugimoto, S., & Hanawa, K. (2015). Zonal movement of the Mascarene High in austral summer. *Climate Dynamics*, *45*(7–8), 1739–1745. https://doi.org/10.1007/s00382-014-2427-7

Oza, S. R., Rajak, D. R., Dash, M. K., Bahuguna, I. M., & Kumar, R. (2017). Advances in Antarctic Sea Ice Studies in India. *Proceedings of the Indian National Science Academy, 83* (2), 427-435. DOI: 10.16943/ptinsa/2017/4894.

Pal, J., Chaudhuri, S., Roychowdhury, A., & Basu, D. (2017). An investigation of the influence of the southern annular mode on Indian summer monsoon rainfall. *Meteorological Applications*, *24*(2), 172–179. https://doi.org/10.1002/met.1614.

Parise, C. K., Pezzi, L. P., Hodges, K. I., & Justino, F. (2015). The Influence of Sea Ice Dynamics on the Climate Sensitivity and Memory to Increased Antarctic Sea Ice. *Journal of Climate*, *28*(24), 9642–9668. https://doi.org/10.1175/jcli-d-14-00748.1

Parkinson, C. L. (2004). Southern Ocean sea ice and its wider linkages: insights revealed from models and observations. *Antarctic Science*, *16*(4), 387–400. https://doi.org/10.1017/s0954102004002214

Parkinson, C. L. (2019). A 40-y record reveals gradual Antarctic sea ice increases followed by decreases at rates far exceeding the rates seen in the Arctic. *Proceedings of the National Academy of Sciences*, *116*(29), 14414–14423. https://doi.org/10.1073/pnas.1906556116

Parkinson, C. L. (2019). A 40-y record reveals gradual Antarctic sea ice increases followed by decreases at rates far exceeding the rates seen in the Arctic. *Proceedings of the National Academy of Sciences, 116*(29), 14414–14423. https://doi.org/10.1073/pnas.1906556116

Parkinson, C. L., & Cavalieri, D. J. (2012). Antarctic sea ice variability and trends, 1979–2010. *The Cryosphere*, *6*(4), 871–880. https://doi.org/10.5194/tc-6-871-2012

Parthasarathy, B., Kumar, K. S., & Munot, A. A. (1993). Homogeneous Indian Monsoon rainfall: Variability and prediction. *Journal of Earth System Science*, *102*(1), 121–155. https://doi.org/10.1007/bf02839187

Pattanaik, D. R., & Rajeevan, M. (2010). Variability of extreme rainfall events over India during southwest monsoon season. *Meteorological Applications, 17*(1), 88–104. https://doi.org/10.1002/met.164

Pattanaik, D. R., & Satyan, V. (2000). Fluctuations of Tropical Easterly Jet during contrasting monsoons over India: A GCM study. *Meteorology and Atmospheric Physics, 75*(1–2), 51–60. https://doi.org/10.1007/s007030070015

Pellichero, V., Sallée, J., Chapman, C., & Downes, S. M. (2018). The Southern Ocean meridional overturning in the sea-ice sector is driven by freshwater fluxes. *Nature Communications*, *9*(1). https://doi.org/10.1038/s41467-018-04101-2

Perovich, D. K., Light, B., Eicken, H., Jones, K., Runciman, K., & Nghiem, S. V. (2007). Increasing solar heating of the Arctic Ocean and adjacent seas, 1979–2005: Attribution and role in the ice-albedo feedback. *Geophysical Research Letters*, *34*(19). https://doi.org/10.1029/2007gl031480

Pezza, A. B., Durrant, T. H., Simmonds, I., & Smith, I. F. C. (2008). Southern Hemisphere Synoptic Behavior in Extreme Phases of SAM, ENSO, Sea Ice Extent, and Southern Australia Rainfall. *Journal of Climate*, *21*(21), 5566–5584. https://doi.org/10.1175/2008jcli2128.1

Pezza, A. B., Rashid, H., & Simmonds, I. (2012). Climate links and recent extremes in antarctic sea ice, high-latitude cyclones, Southern Annular Mode and ENSO. *Climate Dynamics*, *38*(1–2), 57–73. https://doi.org/10.1007/s00382-011-1044-y

Pohl, B., Fauchereau, N., Reason, C. J. C., & Rouault, M. (2010). Relationships between the Antarctic Oscillation, the Madden–Julian Oscillation, and ENSO, and Consequences for Rainfall Analysis. *Journal of Climate, 23*(2), 238–254. https://doi.org/10.1175/2009jcli2443.1

Pokhrel, S., Chaudhari, H. S., Saha, S., Dhakate, A., Yadav, R., Salunke, K., Mahapatra, S. S., & Rao, S. A. (2012). ENSO, IOD and Indian Summer Monsoon in NCEP climate forecast system. *Climate Dynamics*, *39*(9–10), 2143–2165. https://doi.org/10.1007/s00382-012-1349-5

Pottapinjara, V. (2020). *A study on links between the tropical Atlantic and Indian summer monsoon on interannual timescales* (Doctoral thesis, University of Hyderabad). Retrieved from https://www.researchgate.net/publication/343097538_A_study_on_links_between_the_tropical_Atlantic_and_Indian_summer_monsoon_on_interannual_timescales

Pottapinjara, V., Girishkumar, M. S., Murtugudde, R., Ashok, K., & Ravichandran, M. (2019). On the Relation between the Boreal Spring Position of the Atlantic Intertropical Convergence Zone and Atlantic Zonal Mode. *Journal of Climate, 32*(15), 4767–4781. https://doi.org/10.1175/jcli-d-18-0614.1

Pottapinjara, V., Girishkumar, M. S., Ravichandran, M., & Murtugudde, R. (2014). Influence of the Atlantic zonal mode on monsoon depressions in the Bay of Bengal during boreal summer. *Journal of Geophysical Research Atmospheres, 119*(11), 6456–6469. https://doi.org/10.1002/2014jd021494

Pottapinjara, V., Girishkumar, M. S., Sivareddy, S., Ravichandran, M., & Murtugudde, R. (2016). Relation between the upper ocean heat content in the equatorial Atlantic during boreal spring and the Indian monsoon rainfall during June-September. *International Journal of Climatology*, *36*(6), 2469–2480. https://doi.org/10.1002/joc.4506.

Prabhu, A., Kripalani, R. H., Preethi, B., & Pandithurai, G. (2016). Potential role of the February–March Southern Annular Mode on the Indian summer monsoon rainfall: a new perspective. *Climate Dynamics*, *47*(3–4), 1161–1179. https://doi.org/10.1007/s00382-015-2894-5

Prabhu, A., Mahajan, P. N., & Khaladkar, R. M. (2012). Association of the Indian summer monsoon rainfall variability with the geophysical parameters over the Arctic region. *International Journal of Climatology*, *32*(13), 2042–2050. https://doi.org/10.1002/joc.2418

Prabhu, A., Mahajan, P. N., Khaladkar, R. M., & Chipade, M. D. (2010). Role of Antarctic circumpolar wave in modulating the extremes of Indian summer monsoon rainfall. *Geophysical Research Letters*, *37*(14), n/a. https://doi.org/10.1029/2010gl043760

Prabhu, A., Mahajan, P. V., Khaladkar, R. M., & Bawiskar, S. M. (2009). Connection between Antarctic sea-ice extent and Indian summer monsoon rainfall. *International Journal of Remote Sensing*, *30*(13), 3485–3494. https://doi.org/10.1080/01431160802562248

Prabhu, A., Mandke, S. K., Kripalani, R. H., & Pandithurai, G. (2021). Association between Antarctic Sea ice, Pacific SST and the Indian summer monsoon: An observational study. *Polar Science*, *30*, 100746. https://doi.org/10.1016/j.polar.2021.100746

Prabhu, A., Oh, J., Kim, I., Kripalani, R. H., & Pandithurai, G. (2018). SMMR-SSM/I derived Greenland Sea ice variability: links with Indian and Korean Monsoons.

Climate Dynamics, *50*(3–4), 1023–1043. https://doi.org/10.1007/s00382-017-3659-0

Prajeesh, A. G., Swapna, P., Krishnan, R., Ayantika, D. C., Sandeep, N., Manmeet, S., Aditi, M., & Sandip, I. (2021). The Indian summer monsoon and Indian Ocean Dipole connection in the IITM Earth System Model (IITM-ESM). *Climate Dynamics*, *58*(5–6), 1877–1897. https://doi.org/10.1007/s00382-021-05999-z.

Pruim, R. (2018). Foundations and Applications of Statistics. American Mathematical Society.

Purich, A., & England, M. H. (2019). Tropical Teleconnections to Antarctic Sea Ice During Austral Spring 2016 in Coupled Pacemaker Experiments. *Geophysical Research Letters, 46*(12), 6848–6858. https://doi.org/10.1029/2019gl082671

Purich, A., England, M. H., Cai, W., Chikamoto, Y., Timmermann, A., Fyfe, J. C., Frankcombe, L. M., Meehl, G. A., & Arblaster, J. M. (2016). Tropical Pacific SST Drivers of Recent Antarctic Sea Ice Trends. *Journal of Climate, 29*(24), 8931–8948. https://doi.org/10.1175/jcli-d-16-0440.1

Putnam, A. E., & Broecker, W. S. (2017). Human-induced changes in the distribution of rainfall. *Science Advances*, *3*(5). https://doi.org/10.1126/sciadv.1600871

Puwar, S., Rakesh, V., Banker, A., & Mohapatra, G. N. (2022). Relationship between the position and intensity of Low-Level Jet stream and Indian summer monsoon rainfall. *Theoretical and Applied Climatology* (under review by a journal)

Qi, Y., Feng, S., Huang, J., Ran, J., and Long, Z. (2015). Influence of Plateau Summer Monsoon on Summer Precipitation in the Arid and Semi-arid Regions of the central and East Asia. *Plateau Meteorology, 34* (6), 1566–1574. doi:10.7522/j.issn.1000-0534.2014.00088

R: A Language and Environment for Statistical Computing : Reference Index. (2010).

Raghavan, K. (1973). Break-Monsoon Over India. *Monthly Weather Review, 101*(1), 33–43. https://doi.org/10.1175/1520-0493(1973)101

Rai, A., Saha, S., Pokhrel, S., K, S., & Halder, S. (2015). Influence of preonset systems and its relationship with rainfall over South Asia. *Open Journal Atmospheric Climate Change, 1*(2), 2374 – 3808.

Rai, S., & Pandey, A. C. (2006). Antarctica sea ice variability in recent years and its relationship with Indian Ocean SST. *Journal Indian Geophysical Union*, 10,219–229.

Rai, S., Khare, N., Pandey, A. K., Banerjee, K., & Sada, H. (2008). Antarctica sea ice variability and southeast Indian Ocean SST: Possible relationship. *Indian Journal of Marine Science*. http://nopr.niscair.res.in/bitstream/123456789/485/1/IJMS%2037%281%29%20%282008%29%2035-39.pdf

Rajeevan, M., Unnikrishnan, C. K., Bhate, J., Kumar, K. S., & Sreekala, P. P. (2012). Northeast monsoon over India: variability and prediction. *Meteorological Applications*, *19*(2), 226–236. https://doi.org/10.1002/met.1322

Ramage, C. S. (1971). *Monsoon Meteorology*.

Rao, P. C., Thorat, V. S., & Raval, S. A. (2017). Intra – Seasonal Variability of Cross Equatorial Flow, Mascarene High and Circumpolar Lows: Monsoon Season 2015. *Vayu Mandal, 43* (2), 106– 119.

Rao, Y. P. (1976). Southwest Monsoon.

Raphael, M. N., Hobbs, W., & Wainer, I. (2011). The effect of Antarctic sea ice on the Southern Hemisphere atmosphere during the southern summer. *Climate Dynamics*, *36*(7–8), 1403–1417. https://doi.org/10.1007/s00382-010-0892-1

Raphael, M. N., Holland, M. M., Landrum, L., & Hobbs, W. (2019). Links between the Amundsen Sea Low and sea ice in the Ross Sea: seasonal and interannual

relationships. *Climate Dynamics*, *52*(3–4), 2333–2349. https://doi.org/10.1007/s00382-018-4258-4

Rashid, H., Hirst, A., & Dix, M. (2013). Atmospheric circulation features in the ACCESS model simulations for CMIP5: historical simulation and future projections. *Australian Meteorological and Oceanographic Journal*, *63*(1), 145–160. https://doi.org/10.22499/2.6301.009

Ratner, B. (2009). The correlation coefficient: Its values range between +1/−1, or do they? *Journal of Targeting, Measurement and Analysis for Marketing, 17(*2), 139–142. https://doi.org/10.1057/jt.2009.5

Rayner, N. A. (2003). Global analyses of sea surface temperature, sea ice, and night marine air temperature since the late nineteenth century. *Journal of Geophysical Research*, *108*(D14). https://doi.org/10.1029/2002jd002670

Rehman, S., Khan, K., & Simmonds, I. (2019). Links between Tasmanian precipitation variability and the Indian Ocean subtropical high. *Theoretical and Applied Climatology*, *138*(3–4), 1255–1267. https://doi.org/10.1007/s00704-019-02891-z

Renwick, J. A., Kohout, A. L., & Dean, S. M. (2012). Atmospheric Forcing of Antarctic Sea Ice on Intraseasonal Time Scales. *Journal of Climate*, *25*(17), 5962–5975. https://doi.org/10.1175/jcli-d-11-00423.1

Ridley, J., Blockley, E., Keen, A. B., Rae, J. G. L., West, A. R., & Schröder, D. (2017). The sea ice model component of HadGEM3-GC3.1. *Geoscientific Model Development*, *11*(2), 713–723. https://doi.org/10.5194/gmd-11-713-2018

Roach, L. A., Dörr, J., Holmes, C. R., Massonnet, F., Blockley, E., Notz, D., Rackow, T., Raphael, M. N., O'Farrell, S., Bailey, D. H., & Bitz, C. M. (2020). Antarctic Sea Ice Area in CMIP6. *Geophysical Research Letters, 47*(9). https://doi.org/10.1029/2019gl086729

Roy, I., & Tedeschi, R. G. (2016). Influence of ENSO on Regional Indian Summer Monsoon Precipitation—Local Atmospheric Influences or Remote Influence from Pacific. *Atmosphere*, *7*(2), 25. https://doi.org/10.3390/atmos7020025

Ruddiman, W. (2008). *Earth's Climate: Past and Future*. WH Freeman.

Rudeva, I., Simmonds, I., Crock, D., & Boschat, G. (2019). Midlatitude Fronts and Variability in the Southern Hemisphere Tropical Width. *Journal of Climate*, *32*(23), 8243–8260. https://doi.org/10.1175/jcli-d-18-0782.1

Sabeerali, C. T., Ajayamohan, R. S., & Rao, S. A. (2019b). Loss of predictive skill of indian summer monsoon rainfall in NCEP CFSv2 due to misrepresentation of Atlantic zonal mode. *Climate Dynamics*, *52*(7–8), 4599–4619. https://doi.org/10.1007/s00382-018-4390-1.

Sabeerali, C. T., Ajayamohan, R. S., Bangalath, H. K., & Chen, N. (2019). Atlantic Zonal Mode: An Emerging Source of Indian Summer Monsoon Variability in a Warming World. *Geophysical Research Letters*, *46*(8), 4460–4467. https://doi.org/10.1029/2019gl082379

Saeed, S., Müller, W. H., Hagemann, S., & Jacob, D. (2011). Circumglobal wave train and the summer monsoon over northwestern India and Pakistan: the explicit role of the surface heat low. *Climate Dynamics*, *37*(5–6), 1045–1060. https://doi.org/10.1007/s00382-010-0888-x

Saji, N. H., Goswami, B. N., Vinayachandran, P. N., & Yamagata, T. (1999). A dipole mode in the tropical Indian Ocean. *Nature*, *401*(6751), 360–363. https://doi.org/10.1038/43854

Salunke, P., Jain, S., & Mishra, S. K. (2019). Performance of the CMIP5 models in the simulation of the Himalaya-Tibetan Plateau monsoon. *Theoretical and Applied Climatology, 137*(1–2), 909–928. https://doi.org/10.1007/s00704-018-2644-9

Sarthi, P. P., Dash, S., & Mamgain, A. (2012). Possible changes in the characteristics of Indian Summer Monsoon under warmer climate. *Global and Planetary Change*, *92–93*, 17–29. https://doi.org/10.1016/j.gloplacha.2012.03.006

Schlosser, E., Haumann, F. A., & Raphael, M. N. (2017). Atmospheric influences on the anomalous 2016 Antarctic sea ice decay. *The Cryosphere*, *12*(3), 1103–1119. https://doi.org/10.5194/tc-12-1103-2018

Schneider, D. J., Okumura, Y., & Deser, C. (2012). Observed Antarctic Interannual Climate Variability and Tropical Linkages. *Journal of Climate*, *25*(12), 4048–4066. https://doi.org/10.1175/jcli-d-11-00273.1

Schneider, T., & Bordoni, S. (2008). Eddy-Mediated Regime Transitions in the Seasonal Cycle of a Hadley Circulation and Implications for Monsoon Dynamics. *Journal of the Atmospheric Sciences,* *65*(3), 915–934. https://doi.org/10.1175/2007jas2415.1

Scott, M. (2009). Sea Ice and the Southern Oscillation. *Journal of Climate,* 8, 637 – 647.

Screen, J. A., Bracegirdle, T. J., & Simmonds, I. (2018). Polar Climate Change as Manifest in Atmospheric Circulation. *Current Climate Change Reports*, *4*(4), 383–395. https://doi.org/10.1007/s40641-018-0111-4

Servain, J., Wainer, I., Ayina, H. L., & Roquet, H. (2000). The relationship between the simulated climatic variability modes of the tropical Atlantic. *International Journal of Climatology*. https://doi.org/10.1002/1097-0088(200007)20:9

Shen, H., He, S., & Wang, H. (2019). Effect of Summer Arctic Sea Ice on the Reverse August Precipitation Anomaly in Eastern China between 1998 and 2016. *Journal of Climate, 32*(11), 3389–3407. https://doi.org/10.1175/jcli-d-17-0615.1

Shi, W., Wang, Q., Xiao, Z., Wang, Q., Duan, W., Cheng, W., Cheng, W., & Duan, W. (2021). Modulation of Atlantic Multidecadal Oscillation on the Interdecadal Variation of South Asian High and Somali Jet in Summer. *Frontiers in Earth Science*, 9. https://doi.org/10.3389/feart.2021.772202

Shi, W., Xiao, Z., & Sun, H. (2017). The Correlation of Somali Jet Strength with South Asia High on Interdecadal Timescale. *Chinese Journal* of Atmospheric Sciences, 41(3), 561 – 577. DOI:10.3878/j.issn.1006-9895.1609.16163

Shi, W., Xiao, Z., & Xue, J. (2016). Teleconnected influence of the boreal winter Antarctic Oscillation on the Somali Jet: Bridging role of sea surface temperature in southern high and middle latitudes. *Advances in Atmospheric Sciences*, *33*(1), 47–57. https://doi.org/10.1007/s00376-015-5094-7

Shu, Q., Wang, Q., Song, Z., Qiao, F., Zhao, J., Chu, M. K., & Li, X. (2020). Assessment of Sea Ice Extent in CMIP6 with Comparison to Observations and CMIP5. *Geophysical Research Letters*, *47*(9). https://doi.org/10.1029/2020gl087965

Sikka, D. R. (1980). Some aspects of the large scale fluctuations of summer monsoon rainfall over India in relation to fluctuations in the planetary and regional scale circulation parameters. *Journal of Earth System Science*, *89*(2), 179–195. https://doi.org/10.1007/bf02913749

Sikka, D. R., & Narasimha, R. (1995). Genesis of the monsoon trough boundary layer experiment (MONTBLEX). *Journal of Earth System Science, 104*(2), 157–187. https://doi.org/10.1007/bf02839270

Silvestri, G., & Vera, C. (2003). Antarctic Oscillation signal on precipitation anomalies over southeastern South America. *Geophysical Research Letters*, *30*(21). https://doi.org/10.1029/2003gl018277

Simmonds, I. (2003). Modes of atmospheric variability over the Southern Ocean. *Journal of Geophysical Research*, *108*(C4). https://doi.org/10.1029/2000jc000542

Simmonds, I. (2015). Comparing and contrasting the behaviour of Arctic and Antarctic sea ice over the 35 year period 1979-2013. *Annals of Glaciology*, *56*(69), 18–28. https://doi.org/10.3189/2015aog69a909

Simmonds, I., & Budd, W. F. (1991). Sensitivity of the southern hemisphere circulation to leads in the Antarctic pack ice. *Quarterly Journal of the Royal Meteorological Society*, *117*(501), 1003–1024. https://doi.org/10.1002/qj.49711750107

Simmonds, I., & Jacka, T. H. (1995). Relationships between the Interannual Variability of Antarctic Sea Ice and the Southern Oscillation. *Journal of Climate*, *8*(3), 637–647. https://doi.org/10.1175/1520-0442(1995)008.

Simmonds, I., & Li, M. (2021). Trends and variability in polar sea ice, global atmospheric circulations, and baroclinicity. *Annals of the New York Academy of Sciences*, *1504*(1), 167–186. https://doi.org/10.1111/nyas.14673.

Simmonds, I., & Wu, X. (1993). Cyclone behavior response to changes in winter Southern Hemisphere sea-ice concentration. *Quarterly Journal of the Royal Meteorological Society,* 119 (513), 1121–1148.

Simmons, A., Poli, P., Dee, D., Berrisford, P., Hersbach, H., Kobayashi, S., & Peubey, C. (2014). Estimating low-frequency variability and trends in atmospheric temperature using ERA-Interim. *Quarterly Journal of the Royal Meteorological Society*, *140*(679), 329–353. https://doi.org/10.1002/qj.2317

Simmons, A., Wallace, J. K., & Branstator, G. (1983). Barotropic Wave Propagation and Instability, and Atmospheric Teleconnection Patterns. *Journal of the Atmospheric Sciences*, *40*(6), 1363–1392. https://doi.org/10.1175/1520-0469(1983)040

Singh, P. (2017). Indian summer monsoon rainfall (ISMR) forecasting using time series data: A fuzzy-entropy-neuro based expert system. *Geoscience Frontiers*, *9*(4), 1243–1257. https://doi.org/10.1016/j.gsf.2017.07.011

Singh, R., Jaiswal, N., & Kishtawal, C. M. (2022). Rising surface pressure over Tibetan Plateau strengthens indian summer monsoon rainfall over northwestern India. *Scientific Reports, 12*(1). https://doi.org/10.1038/s41598-022-12523-8

Sinha, P., Mohanty, U. C., Kar, S., Dash, S., Robertson, A. I., & Tippett, M. K. (2013). Seasonal prediction of the Indian summer monsoon rainfall using canonical correlation analysis of the NCMRWF global model products. *International Journal of Climatology*, *33*(7), 1601–1614. https://doi.org/10.1002/joc.3536

Slingo, J. (1999). The Indian Summer Monsoon and its Variability. *In Springer eBooks* (pp. 103–118). https://doi.org/10.1007/978-3-642-58369-8_5

Smith, D. J., Dunstone, N., Scaife, A. A., Fiedler, E., Copsey, D., & Hardiman, S. C. (2017). Atmospheric Response to Arctic and Antarctic Sea Ice: The Importance of Ocean–Atmosphere Coupling and the Background State. *Journal of Climate*, *30*(12), 4547–4565. https://doi.org/10.1175/jcli-d-16-0564.1

Stammerjohn, S., Martinson, D. G., Smith, R. J. E., Yuan, X., & Rind, D. (2008). Trends in Antarctic annual sea ice retreat and advance and their relation to El Niño–Southern Oscillation and Southern Annular Mode variability. *Journal of Geophysical Research*, *113*(C3). https://doi.org/10.1029/2007jc004269

Stammerjohn, S., Massom, R. A., Rind, D., & Martinson, D. G. (2012). Regions of rapid sea ice change: An inter-hemispheric seasonal comparison. *Geophysical Research Letters*, *39*(6), n/a. https://doi.org/10.1029/2012gl050874

Stocker, T. F., Qin, D., Plattner, G., Tlgnor, M.,…& Midgley, P. M. (2013). Climate Change 2013 The Physical Science Basis. *Working Group I Contribution to the Fifth Assessment Report of the Intergovernmental Panel on Climate Change*, 1029-1136. Retrieved from chrome-extension://efaidnbmnnnibpcajpcglclefindmkaj/https://www.ipcc.ch/site/assets/uploads/2017/09/WG1AR5_Frontmatter_FINAL.pdf

Stroeve, J., Jenouvrier, S., Campbell, G. G., Barbraud, C., & Delord, K. (2016). Mapping and assessing variability in the Antarctic marginal ice zone, pack ice and coastal polynyas in two sea ice algorithms with implications on breeding success of snow

petrels. *The Cryosphere*, *10*(4), 1823–1843. https://doi.org/10.5194/tc-10-1823-2016.

Stroeve, J., Kattsov, V. M., Barrett, A. P., Serreze, M. C., Pavlova, T. V., Holland, M. M., & Meier, W. N. (2012). Trends in Arctic sea ice extent from CMIP5, CMIP3 and observations. *Geophysical Research Letters*, *39*(16). https://doi.org/10.1029/2012gl052676

Stuecker, M. F., Bitz, C. M., & Armour, K. C. (2017). Conditions leading to the unprecedented low Antarctic sea ice extent during the 2016 austral spring season. *Geophysical Research Letters*, *44*(17), 9008–9019. https://doi.org/10.1002/2017gl074691

Stuut, J. W., Crosta, X., Van Der Borg, K., & Schneider, R. R. (2004). Relationship between Antarctic sea ice and southwest African climate during the late Quaternary. *Geology*, *32*(10), 909. https://doi.org/10.1130/g20709.1.

Su, H., & Neelin, J. D. (2003). The Scatter in Tropical Average Precipitation Anomalies*. *Journal of Climate*, *16*(23), 3966–3977. https://doi.org/10.1175/1520-0442(2003)016.

Sun, J., Wang, H., & Yuan, W. (2009). A possible mechanism for the co-variability of the boreal spring Antarctic Oscillation and the Yangtze River valley summer rainfall. *International Journal of Climatology*, *29*(9), 1276–1284. https://doi.org/10.1002/joc.1773.

Sundaram, S., & Holland, D. M. (2022). A Physical Mechanism for the Indian Summer Monsoon—Arctic Sea-Ice Teleconnection. *Atmosphere, 13*(4), 566. https://doi.org/10.3390/atmos13040566

Tanaka, M. (1982). Interannual Fluctuations of the Tropical Easterly Jet and the Summer Monsoon in the Asian Region. *Journal of the Meteorological Society of Japan*, *60*(3), 865–875. https://doi.org/10.2151/jmsj1965.60.3_865

Tanaka, M. (1982). Interannual Fluctuations of the Tropical Easterly Jet and the Summer Monsoon in the Asian Region. Journal of the *Meteorological Society of Japan, 60*(3), 865–875. https://doi.org/10.2151/jmsj1965.60.3_865

Tang, B., Shrestha, B., Li, Z., Liu, G., Ouyang, H., Gurung, D. R., Giriraj, A., & Aung, K. S. (2013). Determination of snow cover from MODIS data for the Tibetan Plateau region. International *Journal of Applied Earth Observation and Geoinformation*, 21, 356–365. https://doi.org/10.1016/j.jag.2012.07.014

Tao, N. Q., & Sun, Z. B. (2007). Influence of Mascarene High on Meiyu Precipitation in Changjiang-Huaihe Basin. *Journal of Nanjing Institute of Meteorology*. http://en.cnki.com.cn/Article_en/CJFDTOTAL-NJQX200706008.htm

Taschetto, A. S., Gupta, A. S., Hendon, H. H., Ummenhofer, C. C., & England, M. H. (2011). The Contribution of Indian Ocean Sea Surface Temperature Anomalies on Australian Summer Rainfall during El Niño Events. *Journal of Climate*, 24(14), 3734–3747. https://doi.org/10.1175/2011jcli3885.1

Tattar, P. N., Ramaiah, S., & Manjunath, B. G. (2016). *A Course in Statistics with R*. John Wiley & Sons.

Taylor, K. E., Stouffer, R. J., & Meehl, G. A. (2012). An Overview of CMIP5 and the Experiment Design. *Bulletin of the American Meteorological Society*, *93*(4), 485–498. https://doi.org/10.1175/bams-d-11-00094.1.

Thompson, D. R., & Solomon, S. (2002). Interpretation of Recent Southern Hemisphere Climate Change. *Science, 296*(5569), 895–899. https://doi.org/10.1126/science.1069270

Trenberth, K. E., Fasullo, J. T., & Kiehl, J. T. (2009). Earth's Global Energy Budget. *Bulletin of the American Meteorological Society*, *90*(3), 311–324. https://doi.org/10.1175/2008bams2634.1.

Trenberth, K. E., Stepaniak, D. P., & Caron, J. M. (2000). The Global Monsoon as Seen through the Divergent Atmospheric Circulation. *Journal of Climate*, *13*(22), 3969–3993. https://doi.org/10.1175/1520-0442(2000)013.

Tsonis, A. A., Swanson, K. L., & Kravtsov, S. (2007). A new dynamical mechanism for major climate shifts. *Geophysical Research Letters*, *34*(13), n/a. https://doi.org/10.1029/2007gl030288.

Turner, A. D., & Annamalai, H. (2012). Climate change and the South Asian summer monsoon. *Nature Climate Change,* *2*(8), 587–595. https://doi.org/10.1038/nclimate1495

Turner, J. A. (2004). The El Niño-southern oscillation and Antarctica. *International Journal of Climatology*, *24*(1), 1–31. https://doi.org/10.1002/joc.965.

Turner, J. A., & Overland, J. (2009). Contrasting climate change in the two polar regions. *Polar Research*, *28*(2), 146–164. https://doi.org/10.1111/j.1751-8369.2009.00128.x

Turner, J. A., Bracegirdle, T. J., Phillips, T., Li, Z., & Hosking, J. S. (2013). An Initial Assessment of Antarctic Sea Ice Extent in the CMIP5 Models. *Journal of Climate*, *26*(5), 1473–1484. https://doi.org/10.1175/jcli-d-12-00068.1.

Turner, J. A., Comiso, J. C., Li, Z., Lachlan-Cope, T., Bracegirdle, T., Maksym, T., Meredith, M. P., Wang, Z., & Orr, A. (2009). Non-annular atmospheric circulation change induced by stratospheric ozone depletion and its role in the recent increase of Antarctic sea ice extent. *Geophysical Research Letters*, *36*(8). https://doi.org/10.1029/2009gl037524.

Turner, J. A., Hosking, J. S., Bracegirdle, T. J., Li, Z., & Phillips, T. (2015). Recent changes in Antarctic Sea Ice. *Philosophical Transactions of the Royal Society A*, *373*(2045), 20140163. https://doi.org/10.1098/rsta.2014.0163

Turner, J. A., Hosking, J. S., Li, Z., Phillips, T., & Bracegirdle, T. J. (2016). Antarctic sea ice increase consistent with intrinsic variability of the Amundsen Sea Low. *Climate Dynamics*, *46*(7–8), 2391–2402. https://doi.org/10.1007/s00382-015-2708-9.

Turner, J. A., Phillips, T., Li, Z., Hosking, J. S., Pope, J. M., Bracegirdle, T. J., & Deb, P. (2017). Unprecedented springtime retreat of Antarctic sea ice in 2016. *Geophysical Research Letters*, *44*(13), 6868–6875. https://doi.org/10.1002/2017gl073656.

Turner, J., & Marshall, G. J. (2011). *Climate Change in the Polar Regions*. Cambridge University Press.

Uotila, P., Holland, P. R., Vihma, T., Marsland, S. J., & Kimura, N. (2014). Is realistic Antarctic sea-ice extent in climate models the result of excessive ice drift? *Ocean Modelling*, *79*, 33–42. https://doi.org/10.1016/j.ocemod.2014.04.004.

Vidya, M. J., Ravichandran, M., Subeesh, M. P., Chatterjee, S., & Nuncio, M. (2020). Global warming hiatus contributed weakening of the Mascarene High in the Southern Indian Ocean. *Scientific Reports*, *10*(1). https://doi.org/10.1038/s41598-020-59964-7.

Vizy, E. K., & Cook, K. H. (2020). Interannual variability of East African rainfall: role of seasonal transitions of the low-level cross-equatorial flow. *Climate Dynamics, 54(*11–12), 4563–4587. https://doi.org/10.1007/s00382-020-05244-z

Wadhams, P. (2009). Sea Ice. Encyclopedia of Ocean Sciences (Second Edition), 141 – 158.

Walker, G. C. (1928). World weather. *Quarterly Journal of the Royal Meteorological Society*, *54*(226), 79–87. https://doi.org/10.1002/qj.49705422601.

Wallace, J. L., & Gutzler, D. S. (1981). Teleconnections in the Geopotential Height Field during the Northern Hemisphere Winter. *Monthly Weather Review*, *109*(4), 784–812. https://doi.org/10.1175/1520-0493(1981)109

Walsh, J.E. (1983). Role of sea ice in climate variability: Theories and evidence. *Atmospheric –Ocean*, *21*(3), 229–242.
Wang, B., & Ding, Q. (2008). Global monsoon: Dominant mode of annual variation in the tropics. *Dynamics of Atmospheres and Oceans*, *44*(3–4), 165–183. https://doi.org/10.1016/j.dynatmoce.2007.05.002.
Wang, B., Liu, J., Kim, H. S., Webster, P. J., & Yim, S. (2012). Recent change of the global monsoon precipitation (1979–2008). *Climate Dynamics*, *39*(5), 1123–1135. https://doi.org/10.1007/s00382-011-1266-z.
Wang, B., Wu, R., & Fu, X. (2000). Pacific–East Asian Teleconnection: How Does ENSO Affect East Asian Climate? *Journal of Climate*, *13*(9), 1517–1536. https://doi.org/10.1175/1520-0442(2000)013
Wang, B., Wu, R., & Lau, K. Y. (2001). Interannual Variability of the Asian Summer Monsoon: Contrasts between the Indian and the Western North Pacific–East Asian Monsoons*. *Journal of Climate*, *14*(20), 4073–4090. https://doi.org/10.1175/1520-0442(2001)014.
Wang, G., Hendon, H. H., Arblaster, J. M., Lim, E., Abhik, S., & Van Rensch, P. (2019). Compounding tropical and stratospheric forcing of the record low Antarctic sea-ice in 2016. *Nature Communications*, *10*(1). https://doi.org/10.1038/s41467-018-07689-7.
Wang, H., & Fan, K. L. (2006). Southern Hemisphere mean zonal wind in upper troposphere and East Asian summer monsoon circulation. *Science Bulletin*, *51*(12), 1508–1514. https://doi.org/10.1007/s11434-006-2009-0.
Wang, L., Xu, P., & Chowdary, J. S. (2021). Teleconnection along the Asian jet stream and its association with the Asian summer monsoon. In *Elsevier eBooks* (pp. 287–298). https://doi.org/10.1016/b978-0-12-822402-1.00009-0
Washington, R., & Preston, A. W. H. (2006). Extreme wet years over southern Africa: Role of Indian Ocean sea surface temperatures. *Journal of Geophysical Research, 111*(D15). https://doi.org/10.1029/2005jd006724
Watanabe, S., Hajima, T., Sudo, K., Nagashima, T., Takemura, T., Okajima, H., Nozawa, T., Kawase, H., Abe, M., Yokohata, T., Ise, T., Sato, H., Kato, E., Takata, K., Emori, S., & Kawamiya, M. (2011). MIROC-ESM 2010: model description and basic results of CMIP5-20c3m experiments. *Geoscientific Model Development*, *4*(4), 845–872. https://doi.org/10.5194/gmd-4-845-2011
Watterson, I., Hirst, A., & Rotstayn, L. D. (2013). A skill score based evaluation of simulated Australian climate. *Australian Meteorological and Oceanographic Journal*, *63*(1), 181–190. https://doi.org/10.22499/2.6301.011
Webster, P. J. (1987). The elementary monsoon, Wiley, New York.
Webster, P. J., & Yang, S. (1992). Monsoon and Enso: Selectively Interactive Systems. *Quarterly Journal of the Royal Meteorological Society*, *118*(507), 877–926. https://doi.org/10.1002/qj.49711850705.
Weeks, W. (2010). *On Sea Ice*. University of Alaska Press.
Wendler, G., & Nagashima, Y. (1987). Inter-Relations between the Arctic Sea Ice and the General Circulation of the Atmosphere. *Journal of Glaciology*, *33*(114), 173–176. https://doi.org/10.1017/s0022143000008662
White, W. B., & Peterson, R. D. (1996). An Antarctic circumpolar wave in surface pressure, wind, temperature and sea-ice extent. *Nature*, *380*(6576), 699–702. https://doi.org/10.1038/380699a0.
World Meteorological Organization (1989). Calculation of Monthly and Annual 30-year Standard Normals, WMO-TD/No. 341, Geneva.
World Meteorological Organization (2011). Guide to Climatological Practices, WMO-No. 100, 3rd Edition, Geneva.

World Meteorological Organization (2017). WMO Guidelines on the Calculation of Climate Normals, WMO-No. 1203, Geneva.

Wu, B., Zhang, R., & Wang, B. (2009). On the association between spring Arctic sea ice concentration and Chinese summer rainfall: A further study. *Advances in Atmospheric Sciences*, *26*(4), 666–678. https://doi.org/10.1007/s00376-009-9009-3.

Wu, B., Zhang, R., Wang, B., & D'Arrigo, R. (2009). On the association between spring Arctic sea ice concentration and Chinese summer rainfall. *Geophysical Research Letters*, *36*(9). https://doi.org/10.1029/2009gl037299.

Wu, G. X., Liu, Y., Dong, B., Liang, X., Duan, A., Bao, Q., & Yu, J. (2012). Revisiting Asian monsoon formation and change associated with Tibetan Plateau forcing: I. Formation. *Climate Dynamics, 39* (5), 1169–1181. DOI:10.1007/ s00382-012-1334-z.

Wu, Z., Dou, J., & Lin, H. (2015). Potential influence of the November–December Southern Hemisphere annular mode on the East Asian winter precipitation: a new mechanism. *Climate Dynamics*, *44*(5–6), 1215–1226. https://doi.org/10.1007/s00382-014-2241-2.

Xie, S., Kosaka, Y., Du, Y., Hu, K., Chowdary, J. S., & Huang, G. (2016). Indo-western Pacific ocean capacitor and coherent climate anomalies in post-ENSO summer: A review. *Advances in Atmospheric Sciences, 33*(4), 411–432. https://doi.org/10.1007/s00376-015-5192-6

Xue, F., Guo, P., & Yu, Z. (2003). Influence of Interannual Variability of Antarctic Sea-Ice on Summer Rainfall in Eastern China. *Advances in Atmospheric Sciences*, *20*(1), 97–102. https://doi.org/10.1007/bf03342053.

Xue, F., Wang, H., & He, J. (2004). Interannual Variability of Mascarene High and Australian High and Their Influences on East Asian Summer Monsoon. *Journal of the Meteorological Society of Japan*, *82*(4), 1173–1186. https://doi.org/10.2151/jmsj.2004.1173.

Xulu, N. G., Chikoore, H., Bopape, M. M., & Nethengwe, N. S. (2020). Climatology of the Mascarene High and Its Influence on Weather and Climate over Southern Africa. *Climate*, *8*(7), 86. https://doi.org/10.3390/cli8070086.

Yadav, J., Kumar, A., Srivastava, A., & Mohan, R. (2022). Sea ice variability and trends in the Indian Ocean sector of Antarctica: Interaction with ENSO and SAM. *Environmental Research,* 212, 113481. https://doi.org/10.1016/j.envres.2022.113481

Yadav, R. S., Srinivas, G., & Chowdary, J. S. (2018). Atlantic Niño modulation of the Indian summer monsoon through Asian jet. *Npj Climate and Atmospheric Science*, *1*(1). https://doi.org/10.1038/s41612-018-0029-5.

Yamazaki, K., & Nakamura, T. (2021). The stratospheric QBO affects antarctic sea ice through the tropical convection in early austral winter. *Polar Science*, 28, 100674. https://doi.org/10.1016/j.polar.2021.100674

Yanai, M., & Wu, G. (2006). *Effects of the Tibetan Plateau*. In Springer eBooks (pp. 513–549). https://doi.org/10.1007/3-540-37722-0_13

Yang, C., Liu, J., Hu, Y., Horton, R. M., Chen, L., & Cheng, X. (2016). Assessment of Arctic and Antarctic sea ice predictability in CMIP5 decadal hindcasts. *The Cryosphere*, *10*(5), 2429–2452. https://doi.org/10.5194/tc-10-2429-2016.

Yu, L., Zhong, S., Vihma, T., Sui, C., & Sun, B. (2022). The Impact of the Indian Ocean Basin Mode on Antarctic Sea Ice Concentration in Interannual Time Scales. *Geophysical Research Letters*, 49(11). https://doi.org/10.1029/2022gl097745

Yuan, N., Ding, M., Ludescher, J., & Bunde, A. (2017). Increase of the Antarctic Sea Ice Extent is highly significant only in the Ross Sea. *Scientific Reports*, *7*(1). https://doi.org/10.1038/srep41096.

Yuan, X. (2004). ENSO-related impacts on Antarctic sea ice: a synthesis of phenomenon and mechanisms. *Antarctic Science*, *16*(4), 415–425. https://doi.org/10.1017/s0954102004002238.

Yuan, X., & Martinson, D. G. (2000). Antarctic Sea Ice Extent Variability and Its Global Connectivity*. *Journal of Climate*, *13*(10), 1697–1717. https://doi.org/10.1175/1520-0442(2000)013

Yuan, X., & Martinson, D. G. (2001). The Antarctic dipole and its predictability. *Geophysical Research Letters*, *28*(18), 3609–3612. https://doi.org/10.1029/2001gl012969.

Yuan, Z., Qin, J., Li, S., Huang, S., & Mbululo, Y. (2021). Impact of Spring AAO on Summertime Precipitation in the North China Part: Observational Analysis. Asia-Pacific *Journal of Atmospheric Sciences, 57*(1), 1–16. https://doi.org/10.1007/s13143-019-00157-2

Zebiak, S. E. (1993). Air–Sea Interaction in the Equatorial Atlantic Region. *Journal of Climate*, *6*(8), 1567–1586. https://doi.org/10.1175/1520-0442(1993)006

Zhang, J. (2007). Increasing Antarctic Sea Ice under Warming Atmospheric and Oceanic Conditions. *Journal of Climate*, *20*(11), 2515–2529. https://doi.org/10.1175/jcli4136.1

Zhang, S., Meng, L., Zhao, Y., Yang, X., & Huang, A. (2022). The Influence of the Tibetan Plateau Monsoon on Summer Precipitation in Central Asia. *Frontiers in Earth Science*, 10. https://doi.org/10.3389/feart.2022.771104

Zhang, S., Zeng, G., Yang, X., Iyakaremye, V., & Hao, Z. (2021). Connection between interannual variation of spring precipitation in Northeast China and preceding winter sea ice over the Barents Sea. *International Journal of Climatology*, *42*(3), 1922–1936. https://doi.org/10.1002/joc.7343

Zhao, P., Zhang, X., Zhou, X., Ikeda, M., & Yin, Y. (2004). The Sea Ice Extent Anomaly in the North Pacific and Its Impact on the East Asian Summer Monsoon Rainfall. *Journal of Climate*, *17*(17), 3434–3447. https://doi.org/10.1175/1520-0442(2004)017

Zhao, X., Dong, B., & Lu, R. (2021). Interdecadal weakening of the cross-equatorial flows over the Maritime Continent during the boreal summer in the mid-1990s: drivers and physical processes. *Climate Dynamics*, *57*(1–2), 55–72. https://doi.org/10.1007/s00382-021-05692-1

Zhao, Y., Huang, A., Zhou, Y., and Yang, Q. (2016). The Impacts of the Summer Plateau Monsoon over the Tibetan Plateau on the Rainfall in the Tarim Basin, China. *Theor. Appl. Climatol., 126* (1-2), 265–272. doi:10.1007/s00704-015-1576-x

Zhao, Y., Huang, A., Zhou, Y., Huang, D., Yang, Q., Ma, Y., et al. (2014). Impact of the Middle and Upper Tropospheric Cooling over Central Asia on the Summer Rainfall in the Tarim Basin, China. *J. Clim., 27* (12), 4721–4732. doi:10.1175/jcli-d-13-00456.1

Zhao, Y., Yu, X., Yao, J., Dong, X., and Li, H. (2019). The Concurrent Effects of the South Asian Monsoon and the Plateau Monsoon over the Tibetan Plateau on Summer Rainfall in the Tarim Basin of China. *Int. J. Climatol, 39* (1), 74–88. doi:10.1002/joc.5783

Zheng, F., Li, J., & Ding, R. (2017). Influence of the preceding austral summer Southern Hemisphere annular mode on the amplitude of ENSO decay. *Advances in Atmospheric Sciences*, *34*(11), 1358–1379. https://doi.org/10.1007/s00376-017-6339-4

Zheng, F., Li, J., Clark, R. J. H., Ding, R., Li, F., & Wang, L. (2015). Influence of the boreal spring Southern Annular Mode on summer surface air temperature over northeast China. *Atmospheric Science Letters*, *16*(2), 155–161. https://doi.org/10.1002/asl2.541

Zhou, B., Xu, M., Sun, B., Han, T., & Cheng, Z. (2021). Possible role of Southern Hemispheric sea ice in the variability of West China autumn rain. *Atmospheric Research*, *249*, 105329. https://doi.org/10.1016/j.atmosres.2020.105329

Zunz, V., Goosse, H., & Massonnet, F. (2013). How does internal variability influence the ability of CMIP5 models to reproduce the recent trend in Southern Ocean sea ice extent? *The Cryosphere*, *7*(2), 451–468. https://doi.org/10.5194/tc-7-451-2013.

Zwally, H. J., Abdalati, W., Herring, T. A., Larson, K. M., Saba, J. L., & Steffen, K. (2002). Surface Melt-Induced Acceleration of Greenland Ice-Sheet Flow. *Science*, *297*(5579), 218–222. https://doi.org/10.1126/science.1072708